STRINGQFT

String-Theoretic Construction
of Quantum Field Theory

VOLUME II

Physical String Preliminaries

Xingyang Yu

StringQFT v1.0 / Source build candidate

Drafted with AI assistance under the supervision of the author.
Manuscript free to read. All rights reserved.

Contents

II.1 Worldsheet actions and quantization of the bosonic string 1

II.1.1 A vibrating string and its particle spectrum 1
II.1.2 The auxiliary metric turns area into a usable action 2
II.1.3 Conformal gauge leaves the physical constraints 3
II.1.4 Loops and endpoints select different modes 5
II.1.5 Oscillator algebra and stress modes 7
II.1.6 Transverse states, intercept and criticality 10
II.1.7 Mass shells and the first spacetime states 12
II.1.8 What this model supplies and where its proof stops 13
II.1.9 Exercises 14
II.1.10 Take-home message 15
Status and sources 15

II.2 Worldsheet CFT toolkit: OPE, state–operator map, current algebras 17

II.2.1 Why an insertion can describe a string state 17
II.2.2 A local insertion from a regulated free boson 18
II.2.3 Stress tensor and primary weights 20
II.2.4 States on a circle and the Virasoro extension 21
II.2.5 Currents, compact charge lattices and locality 24
II.2.6 Ghost systems and the BRST boundary 26
II.2.7 Limits of local CFT data 28
II.2.8 Exercises 29
II.2.9 Take-home message 29
Status and sources 30

II.3 Toroidal compactification, T-duality, and Narain moduli 31

II.3.1 A string can wrap a circle 31
II.3.2 Closed strings on a circle 32
II.3.3 Radius inversion and enhanced currents 33
II.3.4 Toroidal charge lattices and Narain moduli 35
II.3.5 Background fields and local Buscher rules 39
II.3.6 Localized sources and the limit of geometry 42
II.3.7 Exercises 43
II.3.8 Take-home message 44

Status and sources . . . 44

II.4 RNS superstrings, GSO projection, type IIA/IIB spectra 46
II.4.1 A fermion on the string . . . 46
II.4.2 Boundary signs make two fermion sectors . . . 47
II.4.3 Vacuum energies and first massless levels . . . 48
II.4.4 GSO selection and the physical Ramond spinor . . . 50
II.4.5 Tensoring the two sides into type IIA and IIB . . . 52
II.4.6 RR potentials and electric brane dimensions . . . 54
II.4.7 Exercises . . . 56
II.4.8 Take-home message . . . 57
Status and sources . . . 57

II.5 Heterotic strings and gauge enhancement 59
II.5.1 Two different halves of one string . . . 59
II.5.2 Asymmetric worldsheet sectors . . . 59
II.5.3 Even self-dual gauge lattices . . . 61
II.5.4 Gauge enhancement . . . 64
II.5.5 Wilson lines . . . 66
II.5.6 Compactification interface . . . 68
II.5.7 Exercises . . . 70
II.5.8 Take-home message . . . 71
Status and sources . . . 71

II.6 Orbifolds: twisted sectors, modular invariance, fixed-point spectra 73
II.6.1 A string can close only on the quotient . . . 73
II.6.2 Gauging a finite target symmetry . . . 74
II.6.3 Twisted oscillators . . . 76
II.6.4 Torus sectors and modular closure . . . 78
II.6.5 Open invariant states . . . 82
II.6.6 Discrete torsion . . . 84
II.6.7 Exercises . . . 86
II.6.8 Take-home message . . . 87
Status and sources . . . 87

II.7 Orientifolds and unoriented strings 89
II.7.1 An open string loses its arrow . . . 89
II.7.2 Parity as a gauged operation . . . 90
II.7.3 Chan-Paton projection . . . 91
II.7.4 Crosscaps and one-loop channels . . . 93
II.7.5 O-plane charge units . . . 96
II.7.6 Local and compact cancellation . . . 99
II.7.7 Exercises . . . 101
II.7.8 Take-home message . . . 102
Status and sources . . . 102

II.8 Supergravity limits and decoupling 104
II.8.1 What a charged brane leaves in the bulk . . . 104
II.8.2 Bulk actions and fields . . . 105
II.8.3 Branes as charged solutions . . . 107
II.8.4 Flux fixes a scale . . . 110
II.8.5 Reduction on a physical circle . . . 113
II.8.6 Decoupling versus control . . . 115
II.8.7 Exercises . . . 117
II.8.8 Take-home message . . . 118
Status and sources . . . 118

II.9 The duality web: S-, T-, U-duality and M-theory 120
II.9.1 Why a web needs typed links . . . 120
II.9.2 The perturbative circle link . . . 121
II.9.3 IIB charge doublets . . . 124
II.9.4 The IIA/M circle . . . 126
II.9.5 Heterotic duality interfaces . . . 128
II.9.6 Chains and their conditionality . . . 130
II.9.7 Exercises . . . 133
II.9.8 Take-home message . . . 133
Status and sources . . . 134

II.10 NS5-branes and other solitonic objects 136
II.10.1 A fivebrane seen from outside . . . 136
II.10.2 NS charge and a fivebrane throat . . . 137
II.10.3 Dilaton and near-source control . . . 139
II.10.4 A circle transverse to the source . . . 141
II.10.5 Fivebrane charges and holomorphic curves . . . 143
II.10.6 Interfaces to six-dimensional theories . . . 147
II.10.7 Exercises . . . 148
II.10.8 Take-home message . . . 149
Status and sources . . . 149

Chapter II.1

Worldsheet actions and quantization of the bosonic string

II.1.1 A vibrating string and its particle spectrum

A plucked string has many frequencies, but a string in spacetime poses a more surprising question. Which of its vibrations appear as particles to a spacetime observer? The answer needs more than a wave equation. Reparametrizing the two coordinates on the swept surface cannot change the particle, and the equations enforcing that redundancy remove oscillations that point along time or along the direction of propagation. The remaining frequencies give a sequence of masses and polarizations.

An embedding $X^\mu(\tau, \sigma)$ assigns a target-space position to each point of a worldsheet. The time coordinate τ orders the motion and σ runs along the string. For an open string $0 \leq \sigma \leq \pi$; for a closed string σ is periodic with period 2π. Figure II.1.1 shows these two surfaces and the same increasing-τ direction. We work in flat D-dimensional Minkowski target space with mostly-plus metric, and set $\hbar = c = 1$. The string tension is $T = 1/(2\pi\alpha')$ with $\alpha' > 0$.

By the end of this chapter the reader should be able to

- recover the area action from the auxiliary-metric action on its positive, nondegenerate classical branch and retain the stress constraints;
- normalize closed, NN and fixed-DD modes on their respective σ intervals, including the different momentum zero modes;
- derive transverse level counts and open/closed mass shells with the intercept and any DD stretching term in the right place;
- distinguish the regulated zero-point energy from the cited quantum consistency and no-ghost results.

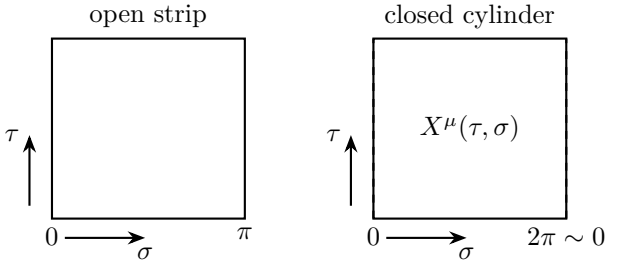


Figure II.1.1: An open string traces a strip with two endpoint histories; a closed string traces a cylinder whose $\sigma = 0$ and 2π edges are identified. Both diagrams orient τ upward. The drawings are coordinate surfaces, not target-space trajectories.

For example, an open string with free transverse endpoints can carry a shape proportional to $\cos(2\sigma)\cos(2\tau)$. The endpoint slope vanishes, and the frequency is two in the coordinates used here. Quantization turns that shape into an oscillator of level two. Only after the metric constraints are solved can we call its transverse excitation a physical state. The chapter derives that chain from area to constraints, modes, oscillator levels and mass shells. The boundary language passes to D-branes in Chapter III.1; the closed zero modes change on a circle in Chapter 3; worldsheet fermions change the spectrum in Chapter 4.

II.1.2 The auxiliary metric turns area into a usable action

What action measures the area swept by a string while still allowing us to solve for its waves? The tangent vectors $\partial_a X^\mu$, with $a, b \in \{\tau, \sigma\}$ and $\mu = 0, \ldots, D-1$, induce the metric $h_{ab} = \partial_a X^\mu \partial_b X_\mu$. The Nambu–Goto action is the Lorentzian area of a nondegenerate timelike patch,

$$h_{ab} = \partial_a X \cdot \partial_b X, \qquad S_{\mathrm{NG}} = -T \int d^2\xi \, \sqrt{-\det h}, \qquad \xi^a = (\tau, \sigma). \tag{II.1.1}$$

The square root couples the embedding coordinates nonlinearly. Introduce an independent Lorentzian worldsheet metric g_{ab} and instead consider

$$S_{\mathrm{P}} = -\frac{T}{2} \int d^2\xi \, \sqrt{-g}\, g^{ab} h_{ab}. \tag{II.1.2}$$

Figure II.1.2 separates the induced metric, which comes from the target embedding, from the auxiliary metric varied in this action.

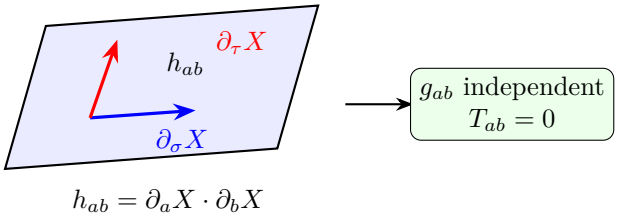


Figure II.1.2: The embedding tangents span a timelike worldsheet patch and form h_{ab}. The independent g_{ab} multiplies their contractions in the Polyakov action. Classical elimination uses a nondegenerate patch and the positive conformal branch.

The metric identity $\delta\sqrt{-g} = -\frac{1}{2}\sqrt{-g}\, g_{ab}\delta g^{ab}$ makes the variation explicit. With the variational normalization of the stress tensor we obtain

$$\delta_g S_{\rm P} = -\frac{T}{2}\int d^2\xi\sqrt{-g}\left(h_{ab} - \frac{1}{2}g_{ab}g^{cd}h_{cd}\right)\delta g^{ab}, \qquad T_{ab} = T\left(h_{ab} - \frac{1}{2}g_{ab}g^{cd}h_{cd}\right). \tag{II.1.3}$$

Thus g_{ab} imposes $T_{ab} = 0$. Its trace vanishes identically in two dimensions, while its traceless components give genuine equations. On a nondegenerate Lorentzian patch, the equation says that h and g are conformal. Choose the branch that preserves the shared causal orientation,

$$T_{ab} = 0 \quad \Longrightarrow \quad g_{ab} = e^{2\phi}h_{ab}, \qquad e^{2\phi} > 0. \tag{II.1.4}$$

On this branch $\sqrt{-g} = e^{2\phi}\sqrt{-h}$ and $g^{ab}h_{ab} = 2e^{-2\phi}$. Their product cancels the auxiliary factor,

$$S_{\rm P}\big|_{g=e^{2\phi}h} = -\frac{T}{2}\int d^2\xi\, e^{2\phi}\sqrt{-h}\,(2e^{-2\phi}) = S_{\rm NG}. \tag{II.1.5}$$

This is a classical local equivalence, not an equality of quantum path integrals. It does not eliminate the metric at degenerate folds.

A numerical patch exposes the branch condition. Take $h = \left(\begin{smallmatrix} -3 & 2 \\ 2 & 5 \end{smallmatrix}\right)$, so $\det h = -19$. At $e^{2\phi} = 2$, the auxiliary metric is $g = \left(\begin{smallmatrix} -6 & 4 \\ 4 & 10 \end{smallmatrix}\right)$, $\sqrt{-g} = 2\sqrt{19}$ and $g^{ab}h_{ab} = 1$; the density is therefore $-T\sqrt{19}$. The algebraic choice $g = -2h$ also makes the metric equation zero, but its inverse contraction is -1 while $\sqrt{-g} = 2\sqrt{19}$, giving $+T\sqrt{19}$. The positive branch is a real physical restriction, not an optional sign hidden in the square root. The next section uses the auxiliary metric before eliminating it. Chapter 2 will ask what survives when that metric and the coordinate symmetry are quantized.

II.1.3 Conformal gauge leaves the physical constraints

Locally on a Lorentzian worldsheet we can choose conformal coordinates $g_{ab} = e^{2\phi}\eta_{ab}$ with $\eta_{ab} = \mathrm{diag}(-1, 1)$. The Weyl factor cancels from $\sqrt{-g}g^{ab}$ in two dimensions. The

embedding then obeys a simple wave equation,

$$S_{\rm P} = \frac{T}{2}\int d\tau d\sigma\,(\dot{X}^2 - X'^2), \qquad \dot{X} = \partial_\tau X, \quad X' = \partial_\sigma X. \tag{II.1.6}$$

Varying X and integrating by parts in the interior gives

$$\delta_X S_{\rm P} = -T\int d^2\xi\,(\ddot{X} - X'')\cdot\delta X + \text{boundary term}, \qquad \ddot{X} - X'' = 0. \tag{II.1.7}$$

The boundary term will decide which open-string endpoint conditions are allowed. Gauge fixing before metric variation would lose the independent metric equations, so we retain $T_{ab} = 0$ from (II.1.3).

It is useful to see directly how the two descriptions of the wave equation fit together. Set $\xi^\pm = \tau \pm \sigma$ and define the coordinate derivatives $\partial_\pm = \frac{1}{2}(\partial_\tau \pm \partial_\sigma)$. Writing $X = X_R(\tau - \sigma) + X_L(\tau + \sigma)$ gives

$$(\partial_\tau^2 - \partial_\sigma^2)X = 4\partial_+\partial_- X = 0, \qquad \partial_- X = \frac{dX_R}{d(\tau-\sigma)}, \quad \partial_+ X = \frac{dX_L}{d(\tau+\sigma)}. \tag{II.1.8}$$

The wave equation only prevents one chiral function from depending on the other characteristic. The stress equations additionally demand that each chiral tangent be null in target space. A superposition of perfectly valid traveling waves need not meet that demand.

In this gauge the two independent stress components are

$$T_{\tau\tau} = T_{\sigma\sigma} = \frac{T}{2}(\dot{X}^2 + X'^2), \qquad T_{\tau\sigma} = T\dot{X}\cdot X'. \tag{II.1.9}$$

The same two equations are the null constraints

$$T_{++} = T(\partial_+ X)^2 = 0, \qquad T_{--} = T(\partial_- X)^2 = 0. \tag{II.1.10}$$

Figure II.1.3 shows why the two signs correspond to independent traveling waves. Residual changes $\xi^+ \mapsto f(\xi^+)$ and $\xi^- \mapsto k(\xi^-)$ preserve the local conformal form, subject to the global periodicity or endpoint restrictions. These residual symmetries are the reason for the constraints on states.

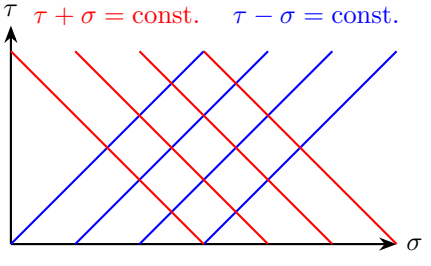


Figure II.1.3: In (τ, σ) coordinates the two null families have $\tau + \sigma$ or $\tau - \sigma$ constant. The wave equation carries both; the corresponding stress components must separately vanish. Arrows mark increasing τ.

For a concrete off-constraint configuration in a mostly-plus three-component target, set $\dot{X} = (2, 1, 0)$ and $X' = (0, 2, 1)$ at one point, and take $T = 2$. Their contractions are $\dot{X}^2 = -3$, $X'^2 = 5$ and $\dot{X} \cdot X' = 2$. Equation (II.1.9) therefore gives $T_{\tau\tau} = T_{\sigma\sigma} = 2$ and $T_{\tau\sigma} = 4$, while $\eta^{ab} T_{ab} = -2 + 2 = 0$. Tracelessness did not impose either constraint. For comparison, $X^\mu = k^\mu F(\tau - \sigma)$ with $k^2 = 0$ solves the wave equation and both stress constraints: $\partial_+ X = 0$ and $(\partial_- X)^2 = (kF')^2 = 0$. This local example is not a complete closed-string solution unless F also has the required periodicity. The distinction between the Weyl trace identity and the two residual constraints is essential when Chapter 2 introduces quantum stress tensors.

II.1.4 Loops and endpoints select different modes

The same wave equation gives different particles when its boundary data change. Its general local solution is a sum of functions of $\tau - \sigma$ and $\tau + \sigma$. For a nonwinding closed coordinate, $X(\tau, \sigma + 2\pi) = X(\tau, \sigma)$. A useful normalization is

$$\begin{aligned} X^\mu &= x^\mu + \alpha' p^\mu \tau + i\sqrt{\frac{\alpha'}{2}} \sum_{n \neq 0} \frac{1}{n} \left(\alpha_n^\mu e^{-in(\tau - \sigma)} + \widetilde{\alpha}_n^\mu e^{-in(\tau + \sigma)} \right), \\ \alpha_0^\mu &= \widetilde{\alpha}_0^\mu = \sqrt{\frac{\alpha'}{2}}\, p^\mu. \end{aligned} \tag{II.1.11}$$

The untilded family travels with $\tau - \sigma$, and the tilded family with $\tau + \sigma$. Each chiral zero mode contributes half of the total $\alpha' p \tau$ drift. This assignment will fix the two factors of four in the closed mass shell.

To derive the zero-mode split, write a linear chiral solution as $X_R = A_R(\tau - \sigma)$ and $X_L = A_L(\tau + \sigma)$. The nonwinding periodicity requires their σ slopes to cancel, so $A_R = A_L$ when the same target momentum is carried by both. The total momentum integral below fixes $A_R + A_L = \alpha' p$, hence

$$X_{R,0} = \frac{\alpha' p}{2}(\tau - \sigma), \qquad X_{L,0} = \frac{\alpha' p}{2}(\tau + \sigma), \qquad X_{R,0} + X_{L,0} = \alpha' p \tau. \tag{II.1.12}$$

This simple cancellation fails when a compact target coordinate admits winding. Chapter 3 will restore the distinct chiral zero-mode slopes in that case.

For an open string, the X variation has boundary contribution

$$\delta S_{\partial\Sigma} = -T \int d\tau \, [X' \cdot \delta X]_{\sigma=0}^{\sigma=\pi}. \tag{II.1.13}$$

It vanishes when an endpoint is free in a direction and $X' = 0$ (Neumann, N), or when that endpoint has fixed position and $\delta X = 0$ (Dirichlet, D). For NN data the cosine eigenfunctions have zero endpoint slope. The zero mode and oscillators are

$$X_{\mathrm{NN}}^\mu = x^\mu + 2\alpha' p^\mu \tau + i\sqrt{2\alpha'} \sum_{n \neq 0} \frac{\alpha_n^\mu}{n} e^{-in\tau} \cos(n\sigma), \qquad \alpha_0^\mu = \sqrt{2\alpha'}\, p^\mu. \tag{II.1.14}$$

Figure II.1.4 compares the $n = 2$ NN shape with the $n = 3$ fixed-endpoint shape on the same interval. The latter direction may have unequal fixed values y_0 and y_π. A compatible expansion is

$$X_{\rm DD} = y_0 + \frac{\Delta y}{\pi}\sigma - \sqrt{2\alpha'}\sum_{n\neq 0}\frac{\alpha_n}{n}e^{-in\tau}\sin(n\sigma), \qquad \Delta y = y_\pi - y_0. \tag{II.1.15}$$

The DD oscillator has a real overall coefficient. With $\alpha_n^\dagger = \alpha_{-n}$, replacing n by $-n$ in the adjoint of each term gives the same sum. Inserting the NN factor i instead would make the $n, -n$ sine pair anti-Hermitian. Fixed endpoints also remove the translational DD momentum zero mode; the linear slope remains.

The elementary modes make the endpoint rule visible without taking it on faith. For an NN wave $u_n = \cos(n\sigma)\cos(n\tau)$, the wave operator annihilates u_n and

$$u_n' = -n\sin(n\sigma)\cos(n\tau), \qquad u_n'(\tau,0) = u_n'(\tau,\pi) = 0 \quad (n \in \mathbb{Z}_{>0}). \tag{II.1.16}$$

For $n = 2$, the two endpoints move together at $\tau = 0$ while the midpoint moves oppositely. A DD fluctuation $v_n = \sin(n\sigma)\cos(n\tau)$ instead obeys

$$v_n(\tau,0) = v_n(\tau,\pi) = 0, \qquad (\partial_\tau^2 - \partial_\sigma^2)v_n = 0. \tag{II.1.17}$$

At $n = 3$ it has two interior nodes, while its endpoints stay fixed on the sloped line $y_0 + \Delta y\,\sigma/\pi$. A closed left mode at $n = 2$ and a right mode at $n = 3$ both return to their initial value under $\sigma \mapsto \sigma + 2\pi$. Their independent frequencies show why periodicity by itself does not impose level matching; the closed-string zero-mode constraints will do that.

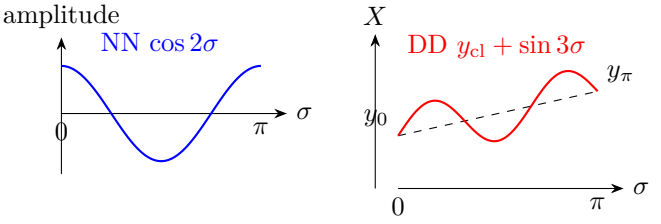


Figure II.1.4: On the shared interval $0 \le \sigma \le \pi$, a Neumann $\cos(2\sigma)$ mode has zero endpoint slope, while a Dirichlet $\sin(3\sigma)$ mode has zero endpoint displacement. The DD panel plots the total $X = y_{\rm cl} + \text{fluctuation}$ on one vertical axis; the dashed classical profile and red profile meet at y_0 and y_π. Vertical amplitudes are schematic.

Why are the two drifts different? The momentum density is $P^\mu = T\dot{X}^\mu$. The nonzero periodic closed modes and open NN cosine modes integrate to zero on their respective intervals. Thus, for closed coordinates and open NN directions respectively,

$$p^\mu_{\rm closed} = \int_0^{2\pi} d\sigma\, P^\mu = \frac{2\pi\alpha' p^\mu}{2\pi\alpha'} = p^\mu, \qquad p^\mu_{\rm open,NN} = \int_0^{\pi} d\sigma\, P^\mu = \frac{\pi(2\alpha' p^\mu)}{2\pi\alpha'} = p^\mu. \tag{II.1.18}$$

There is no conserved DD translation zero mode: fixed endpoints break translation in that direction and can exchange momentum with the string. This does not make the instantaneous integral of DD momentum density zero. For $X_{\rm DD} = y_{\rm cl} + \sin\sigma\cos\tau$, $\int_0^\pi d\sigma\, P_{\rm DD} = -\sin\tau/(\pi\alpha')$; its endpoint displacement is still zero. Its rate of change equals the net endpoint force $T[X'_{\rm DD}]_0^\pi = -\cos\tau/(\pi\alpha')$. The canonical brackets for the periodic and NN sectors reflect their interval choices. The periodic delta function has constant and nonzero coefficients $1/(2\pi)$, whereas the NN cosine resolution has constant $1/\pi$ and positive-mode coefficients $2/\pi$,

$$\delta_{2\pi}(\sigma-\sigma') = \frac{1}{2\pi}\sum_{n\in\mathbb{Z}} e^{in(\sigma-\sigma')}, \qquad \delta_{\rm NN}(\sigma,\sigma') = \frac{1}{\pi} + \frac{2}{\pi}\sum_{n\geq 1}\cos(n\sigma)\cos(n\sigma'). \tag{II.1.19}$$

This Fourier comparison tests the normalizations once the oscillator algebra is specified; it is not a proof of that algebra. Chapter III.1 will interpret NN directions as motion along a D-brane and DD directions as transverse positions. Chapter 3 will replace the closed nonwinding zero mode when a target direction is compact.

II.1.5 Oscillator algebra and stress modes

Quantization asks how the waves become a level count. Equal-time canonical brackets for an NN coordinate are

$$[X^\mu(\tau,\sigma), P_\nu(\tau,\sigma')] = i\delta^\mu{}_\nu\delta_{\rm NN}(\sigma,\sigma'), \qquad P_\nu = T\dot{X}_\nu. \tag{II.1.20}$$

Substituting the normalized expansion and comparing cosine coefficients gives $[x^\mu, p_\nu] = i\delta^\mu{}_\nu$ and

$$[\alpha_m^\mu, \alpha_n^\nu] = m\eta^{\mu\nu}\delta_{m+n,0}. \tag{II.1.21}$$

For a closed string the two families separately obey this relation and commute with each other. The minus sign of η^{00} creates negative-norm states in the unconstrained covariant Fock space. This is why the constraints cannot be replaced by the instruction to keep all embedding oscillators as particles. For $n > 0$, α_n^μ annihilates the momentum vacuum $|0;p\rangle$, while α_{-n}^μ creates a covariant excitation; the tilded closed family follows the same convention. Normal ordering moves these annihilators to the right. The vacuum is an algebraic starting point, not yet a physical state.

For example, a positive-frequency NN term has coordinate coefficient $i\sqrt{2\alpha'}\alpha_n/n$. Its momentum-density coefficient is $\alpha_n/(\pi\sqrt{2\alpha'})$. Pairing it with the $-n$ term in the commutator produces the coefficient

$$\frac{2i}{\pi}\sum_{n>0}\cos(n\sigma)\cos(n\sigma') + \frac{i}{\pi} = i\delta_{\rm NN}(\sigma,\sigma'). \tag{II.1.22}$$

The displayed equality uses $[\alpha_n, \alpha_{-n}] = n$ and the zero-mode bracket. It checks the coefficient of the oscillator expansion against the endpoint delta resolution; without the $\sqrt{2\alpha'}$ factor the canonical normalization would fail.

Consider the open string. Its chiral derivative can be expressed using the same oscillators, and the Fourier coefficients of the quadratic stress tensor define unshifted,

normally ordered modes. Indeed, the cosine and sine derivatives of (II.1.14) combine into one exponential,

$$\partial_- X = \frac{\dot{X} - X'}{2} = \sqrt{\frac{\alpha'}{2}} \sum_{n\in\mathbb{Z}} \alpha_n e^{-in(\tau-\sigma)}, \qquad T_{--} = \frac{1}{4\pi} \sum_{m,n\in\mathbb{Z}} \alpha_{m-n} \cdot \alpha_n e^{-im(\tau-\sigma)}. \tag{II.1.23}$$

The coefficient follows from $T = 1/(2\pi\alpha')$. With the stress-mode normalization $2\pi T_{--} = \sum_m L_m e^{-im(\tau-\sigma)}$, the quadratic sum becomes

$$L_m = \frac{1}{2} \sum_{n\in\mathbb{Z}} : \alpha_{m-n} \cdot \alpha_n : . \tag{II.1.24}$$

In particular, separate the $n = 0$ term from positive and negative oscillators, moving annihilators to the right,

$$L_0 = \frac{1}{2}\alpha_0^2 + N_{\rm cov}, \qquad N_{\rm cov} = \sum_{n>0} \alpha_{-n} \cdot \alpha_n. \tag{II.1.25}$$

The closed string has independent L_m and $\widetilde{L}_m$. For the covariant free-boson modes, the sourced unshifted Virasoro relation is

$$[L_m, L_n] = (m-n)L_{m+n} + \frac{D}{12}(m^3 - m)\delta_{m+n,0}. \tag{II.1.26}$$

The tilded closed copy obeys the same relation and commutes with the untilded copy. Physical covariant states obey $L_n|\text{phys}\rangle = 0$ for $n > 0$ and $(L_0 - a)|\text{phys}\rangle = 0$; closed states obey both sets of conditions, including $(\widetilde{L}_0 - a)|\text{phys}\rangle = 0$. We identify physical states differing by a physical null state. The positive-mode conditions avoid imposing all Virasoro modes as strong operator equations in the presence of the central term. The intercept is a physical-state condition, not a shift in the definition of the L_m above.

The same quadratic definition specifies how a stress mode changes an oscillator. Commuting the two factors in L_m with α_n gives two equal contributions, each supported where its mode index sums to $-n$. After the factor $1/2$ removes their duplication,

$$[L_m, \alpha_n^\mu] = -n\alpha_{m+n}^\mu, \qquad [L_0, \alpha_{-n}^\mu] = n\alpha_{-n}^\mu \quad (n > 0). \tag{II.1.27}$$

Thus one creation operator of frequency two raises L_0 by two, whereas two frequency-one operators also raise it by two. This operator relation explains the level partitions below rather than merely assigning their weights by name.

The zero modes obtained from the momentum integrals make the distinct kinetic terms immediate,

$$\frac{1}{2}\alpha_{0,\text{open}}^2 = \alpha' p^2, \qquad \frac{1}{2}\alpha_{0,\text{closed}}^2 = \frac{1}{2}\widetilde{\alpha}_{0,\text{closed}}^2 = \frac{\alpha' p^2}{4}. \tag{II.1.28}$$

This is the first place the open/closed factor of four enters. A cylinder vacuum-energy shift belongs to a different choice of stress modes and cannot silently replace the plane-mode definition above.

At open level one, let p^μ be nonzero target momentum and ϵ_μ a polarization vector. The state $|\epsilon;p\rangle = \epsilon_\mu \alpha_{-1}^\mu |0;p\rangle$ has $L_1|\epsilon;p\rangle = (\alpha_0\cdot\epsilon)|0;p\rangle$ by (II.1.27). Since $\alpha_0 = \sqrt{2\alpha'}p$, the positive-mode condition gives $p\cdot\epsilon = 0$. At the critical intercept $a = 1$, the zero-mode condition makes $p^2 = 0$. The state $L_{-1}|0;p\rangle = \alpha_0\cdot\alpha_{-1}|0;p\rangle$ is then physical and null. Indeed $L_1L_{-1}|0;p\rangle = 2L_0|0;p\rangle = 0$ at $p^2 = 0$; higher positive modes also annihilate this level-one state. Thus $\epsilon^\mu \sim \epsilon^\mu + cp^\mu$ for a scalar gauge parameter c. This sourced level-one quotient explains the massless vector; it is not an all-level no-ghost proof.

The free-scalar central term illustrates what normal ordering contributes. In (II.1.26) with $n = -m$ and $m > 0$, $[L_m, L_{-m}] = 2mL_0 + D(m^3 - m)/12$. The c-number comes from the double contraction of the two quadratic modes, a finite sum of D identical coordinate contributions,

$$\frac{D}{2}\sum_{k=1}^{m-1} k(m-k) = \frac{D}{2}\left[m\frac{m(m-1)}{2} - \frac{m(m-1)(2m-1)}{6}\right] = \frac{D}{12}(m^3 - m). \quad \text{(II.1.29)}$$

Here the identities for $\sum k$ and $\sum k^2$ prove the finite arithmetic step; the operator derivation and its ghost counterpart belong to Chapter 2. The covariant N_{cov} includes target indices with indefinite metric. Only after solving the constraints will N count $D - 2$ transverse families.

Within that physical free-oscillator premise, level counting is an elementary partition problem. Each transverse color can occupy any positive frequency n any nonnegative number r_n of times, adding nr_n to the level. For q colors,

$$\sum_{N\geq 0} d_N(q) z^N = \prod_{n\geq 1}\left(\sum_{r\geq 0} z^{nr}\right)^q = \prod_{n\geq 1}(1 - z^n)^{-q}. \quad \text{(II.1.30)}$$

Figure II.1.5 displays the two ways to make level two and the three ways to make level three before color choices. At level two, two frequency-one quanta have $q(q+1)/2$ symmetric color assignments, and one frequency-two quantum has q,

$$d_2(q) = \binom{q+1}{2} + q = \frac{q(q+3)}{2}. \quad \text{(II.1.31)}$$

At level three the partitions $1+1+1$, $2+1$ and 3 give

$$d_3(q) = \binom{q+2}{3} + q^2 + q. \quad \text{(II.1.32)}$$

For $q = 3$ these formulas yield $d_2 = 9$ and $d_3 = 22$. Truncation of the product at frequency N is exact for d_N because higher frequencies cannot enter. No no-ghost theorem follows from this combinatorial statement.

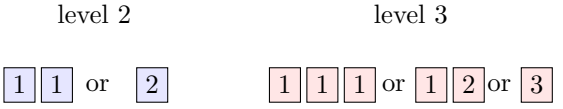


Figure II.1.5: Occupation partitions of levels two and three. A box labeled n contributes frequency n; each box also carries one of q transverse colors. Repeated frequency-one boxes are bosonic symmetric occupations.

II.1.6 Transverse states, intercept and criticality

Which of the covariant oscillators are physical? On a patch with $p^+ \neq 0$, choose light-cone coordinates $X^\pm = (X^0 \pm X^{D-1})/\sqrt{2}$ and fix X^+ proportional to τ. The constraints $(\partial_\pm X)^2 = 0$ then determine each $\partial_\pm X^-$ in terms of the transverse coordinates,

$$-2\partial_\pm X^+ \partial_\pm X^- + \partial_\pm X^i \partial_\pm X^i = 0, \qquad \partial_\pm X^- = \frac{\partial_\pm X^i \partial_\pm X^i}{2\partial_\pm X^+}, \quad i = 1, \ldots, D-2. \tag{II.1.33}$$

The two longitudinal coordinates do not provide independent oscillator families. For an open string the resulting transverse number operator is

$$N = \sum_{n>0} \alpha^i_{-n} \alpha^i_n, \qquad q = D - 2. \tag{II.1.34}$$

For a closed string we call the tilded $\tau + \sigma$ level N_L and the untilded $\tau - \sigma$ level N_R.

Each transverse boson has a formal zero-point contribution $\frac{1}{2}\sum_{n\geq 1} n$. It is a divergent sum, so assign a regulated value through the analytic continuation $\zeta(-1) = -1/12$. The result for one chiral sector is

$$E_0 \overset{\text{reg}}{=} \frac{D-2}{2}\zeta(-1) = -\frac{D-2}{24}, \qquad a = \frac{D-2}{24}. \tag{II.1.35}$$

The equality with the regulated value is not an ordinary summation of $1 + 2 + 3 + \cdots$, nor does this calculation establish the critical dimension. Figure II.1.6 distinguishes the intercept calculation from two quantum consistency questions.

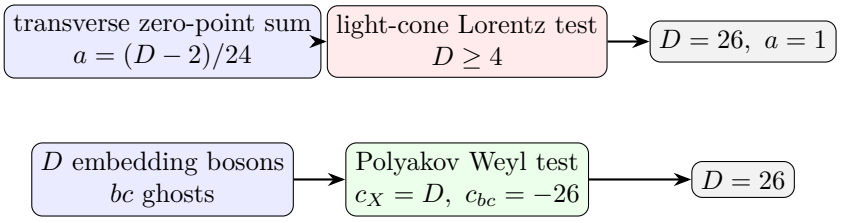


Figure II.1.6: The upper branch combines the regulated transverse zero-point energy with the sourced light-cone Lorentz-commutator test for $D \geq 4$. The lower branch independently tests Weyl consistency using D embedding bosons and bc ghosts. Both select $D = 26$; at that dimension the regulated sum gives $a = 1$. The arrows are not operator proofs.

In the light-cone calculation, the sourced commutator $[M^{i-}, M^{j-}]$ contains an antisymmetric transverse oscillator bilinear multiplied, mode by mode, by

$$C_n = \left(\frac{D-2}{24} - 1\right) n + \frac{a - (D-2)/24}{n}. \tag{II.1.36}$$

When $D \geq 4$, there are at least two distinct transverse indices, so the antisymmetric operator sector is nontrivial. Its independent mode coefficients must vanish. Writing $A = (D-2)/24 - 1$ and $B = a - (D-2)/24$, the conditions $C_2 = C_5 = 0$ give $4A + B = 0$ and $25A + B = 0$. Subtracting yields $21A = 0$ and then $B = 0$, hence

$$\frac{D-2}{24} - 1 = 0, \qquad a - \frac{D-2}{24} = 0, \qquad (D, a) = (26, 1). \tag{II.1.37}$$

The full quantum commutator is a cited result, not derived by this two-mode comparison. At $D = 3$ there is only one transverse index, so the antisymmetric i, j operator vanishes identically. That logical exception does not turn a three-dimensional light-cone Nambu–Goto construction into the standard anomaly-free Polyakov theory.

The comparison only has force when the antisymmetric operator it multiplies exists. The number of index pairs is $\binom{D-2}{2}$, equal to zero at $D = 3$ and positive at $D \geq 4$.

The conformal-gauge route instead counts central charge for D free flat embedding bosons and the reparametrization bc ghosts. For that specific matter and ghost content, the sourced ghost calculation gives $c_{bc} = -26$ per chiral sector, hence

$$c_X = D, \qquad c_{bc} = -26, \qquad c_{\text{total}} = D - 26. \tag{II.1.38}$$

Cancellation selects $D = 26$ for the standard flat Polyakov quantization. For a comparison, at $D = 27$ the regulated free-oscillator formula gives $a = 25/24$, while $c_{\text{total}} = 1$. An unstretched formal open level-one mass formula would give $\alpha' M^2 = 1 - 25/24 = -1/24$; it is not a consistent critical flat spectrum. The two routes test different quantum requirements, and neither follows merely from the regulated sum. Chapter 2 derives the CFT ingredients of the second route; Chapter 4 changes the matter content and therefore the criticality calculation.

II.1.7 Mass shells and the first spacetime states

The zero-mode coefficients in Section II.1.5 now turn a transverse level into a spacetime mass. Define $M^2 = -p^2$ for conserved flat target momentum. In the all-NN open sector, after the constraints are solved, the physical zero-mode equation becomes

$$\alpha' p^2 + N - a = 0, \qquad \alpha' M^2 = N - a. \tag{II.1.39}$$

For a nonwinding closed string there is one equation in each chiral sector,

$$\frac{\alpha' p^2}{4} + N_L - a = 0, \qquad \frac{\alpha' p^2}{4} + N_R - a = 0. \tag{II.1.40}$$

Subtracting them gives level matching, and solving either one gives

$$N_L = N_R, \qquad \alpha' M^2 = 4(N_L - a) = 4(N_R - a). \tag{II.1.41}$$

There is one intercept per chiral equation. Writing $N_L + N_R - 2a$ in one of them would double-count the shift. These are physical equations after constraint solving, not new definitions of the covariant L_0.

At $D = 26$, $a = 1$. For an unstretched open string, $N = 0$ has $M^2 = -1/\alpha'$, while $N = 1$ has $M^2 = 0$. In a space-filling NN sector and at nonzero null momentum, the level-one oscillator carries the 24 transverse polarizations of a massless vector. On a Dp-brane, the same excitations split into worldvolume vector components and transverse scalar components. For a nonwinding closed string, $(N_L, N_R) = (0, 0)$ has $M^2 = -4/\alpha'$, and $(1, 1)$ is massless. Figure II.1.7 keeps the two mass scales separate.

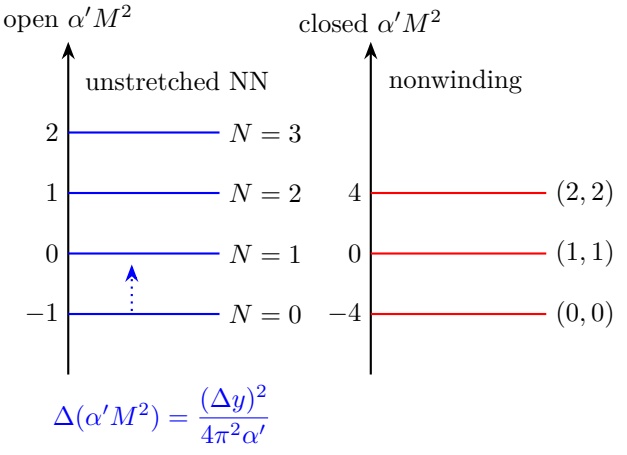


Figure II.1.7: Critical flat, unstretched open NN and nonwinding closed mass levels on separate $\alpha' M^2$ axes. Only matched closed pairs appear. The dotted open displacement illustrates a DD stretching contribution for parallel matching-brane boundary conditions; it is not another oscillator level.

At nonzero null momentum, the closed $(1,1)$ states are products of left and right transverse vectors. Their $24^2 = 576$ components split under $SO(24)$ into symmetric traceless, antisymmetric and trace parts,

$$24 \otimes 24 = \left(\frac{24 \cdot 25}{2} - 1\right) \oplus \frac{24 \cdot 23}{2} \oplus 1 = 299 \oplus 276 \oplus 1. \tag{II.1.42}$$

They are the linearized graviton, antisymmetric tensor and dilaton sectors. This free-state classification does not compute their interactions or establish stability of the tachyonic vacuum.

Fixed DD endpoints add a separate classical energy. For parallel branes with matching NN/DD assignments and no ND directions, set $X_{\rm cl} = y_0 + \Delta y\, \sigma/\pi$ in one spatial DD direction. The static contribution to the open worldsheet Hamiltonian is

$$H_{\rm stretch} = \frac{1}{4\pi\alpha'} \int_0^\pi d\sigma \left(\frac{\Delta y}{\pi}\right)^2 = \frac{(\Delta y)^2}{4\pi^2\alpha'}. \tag{II.1.43}$$

Dividing the zero-mode condition by α' yields the mass of the conserved brane momentum,

$$M^2 = \frac{N-a}{\alpha'} + \left(\frac{\Delta y}{2\pi\alpha'}\right)^2. \tag{II.1.44}$$

The independent classical check is $E = T|\Delta y| = |\Delta y|/(2\pi\alpha')$; its square matches the added term. Thus an open-string ground state stretched far enough need not retain the unstretched tachyonic mass. For $N = 0$ and $a = 1$, the threshold $M^2 = 0$ is

$$-\frac{1}{\alpha'} + \frac{(\Delta y)^2}{4\pi^2\alpha'^2} = 0 \quad \Longleftrightarrow \quad |\Delta y| = 2\pi\sqrt{\alpha'}. \tag{II.1.45}$$

This threshold uses the same flat parallel-brane assumptions as the mass formula. It is not a statement about the dynamics of brane separation or the stability of the entire bosonic background.

For a numerical example keep lengths fixed and set $\alpha' = 2$, $y_0 = -\pi$, $y_\pi = 3\pi$, $N = 3$ and $D = 26$. The DD slope is $\Delta y/\pi = 4$ and $\Delta y = 4\pi$. The oscillator contribution is $(3-1)/2 = 1$, while the stretching contribution is $(4\pi/(4\pi))^2 = 1$, so $M^2 = 2$. If we had set $\alpha' = 1$ prematurely, the denominator error would have been harder to see.

For a closed example at $\alpha' = 2$, the candidate $(N_L, N_R) = (2,1)$ fails level matching. The matched $(2,2)$ state has $M^2 = 4(2-1)/2 = 2$. Each 24-color chiral side has $d_2(24) = 24 \cdot 27/2 = 324$ states, so the product has $324^2 = 104976$ oscillator states before further spacetime interpretation. Counting only one side or squaring a level-one count would answer a different question. Toroidal momentum and winding in Chapter 3 alter these zero-mode and matching equations; Chapter III.1 uses the stretched formula as a distance-to-mass dictionary.

II.1.8 What this model supplies and where its proof stops

The bosonic string gives a controlled route from worldsheet action to free-state masses, but the tachyonic ground states show that flat bosonic perturbation theory is not a stable

vacuum model. It also has no spacetime fermions. The lesson for later constructions is more specific than an inventory of states. Boundary conditions determine available zero modes, residual constraints remove unphysical polarizations, and the remaining oscillator levels determine masses.

The cited no-ghost comparison between covariant and light-cone physical states requires the critical flat theory, nonzero target momentum, a light-cone patch with $p^+ \neq 0$, and the appropriate physical ghost-number or relative-cohomology sector. The theorem itself is not proved here. In the level-one example above, p is target momentum, ϵ is polarization and c parametrizes its null-state equivalence. At $p = 0$, $p \cdot \epsilon = 0$ and $\epsilon \sim \epsilon + cp$ lose both a constraint and a gauge direction. That exceptional sector cannot be counted using the nonzero-momentum polarization argument. The full BRST construction and ghost OPE belong to Chapter 2.

The three-dimensional exception is likewise a boundary on an inference. The antisymmetric light-cone Lorentz commutator cannot force a coefficient to vanish when only one transverse index exists. Known three-dimensional light-cone Nambu–Goto strings illustrate that point. The standard Weyl test for D embedding bosons and bc ghosts still has $c_{\text{total}} = D - 26$; the two premises must not be conflated. Compactification, Wilson lines, a background B field and superstring matter are outside the flat noncompact model used for the equations above.

II.1.9 Exercises

For Exercises 1–5, submit an `answer` object with the fields specified in the companion question file. Rational numbers may be exact fractions. The written explanations are part of the exercise even when only the numerical fields receive automatic grading. Exercises 1–5 reproduce parameters worked above; a correct submitted number alone does not test transfer to a new configuration.

1. In a mostly-plus three-component target, let $\dot{X} = (2, 1, 0)$, $X' = (0, 2, 1)$ and $T = 2$. Compute $T_{\tau\tau}$, $T_{\tau\sigma}$, $T_{\sigma\sigma}$ and $\eta^{ab}T_{ab}$ using the variational tensor in (II.1.3). Explain why vanishing trace does not impose the physical constraints.

2. For parallel matching-brane NN/DD data with no ND direction, take $y(0) = -\pi$, $y(\pi) = 3\pi$, $\alpha' = 2$, $D = 26$ and $N = 3$. Find the slope in $y_{\text{cl}} = y(0) + s\sigma$ and the full open M^2 of the conserved brane momentum. Keep endpoint separation fixed in length units. As an ungraded transfer variation, repeat the mass calculation at $\alpha' = 1$ with the same endpoints and level.

3. With three transverse colors, derive the numbers of open Fock states at levels two and three by listing oscillator partitions and their color multiplicities. Submit d_2 and d_3. As an ungraded variation, find d_2 for four transverse colors.

4. As formal flat free-field algebra, set $D = 27$, $\alpha' = 1$ and $N = 1$. Compute a, c_{total} and the formal open NN M^2. Explain why these numbers are not a consistent critical flat spectrum.

5. At $D = 26$ and $\alpha' = 2$, decide whether nonwinding closed levels $(N_L, N_R) = (2, 1)$ are allowed. Then find the mass squared and the two-sector oscillator degeneracy at $(2, 2)$.

6. Explain in writing how the light-cone Lorentz and conformal-gauge Weyl tests select the critical flat bosonic model. Include the $D \geq 4$ restriction of the antisymmetric Lorentz test, the $D = 3$ exception, the role of the regulated intercept, and the place of BRST cohomology and the no-ghost theorem. Identify the cited source sections supporting the quantum statements. This answer requires human reading.

II.1.10 Take-home message

Take-home message

The auxiliary worldsheet metric makes the embedding equations linear while preserving the area action on its positive nondegenerate classical branch. Its constraints remove longitudinal oscillators. Open and closed zero modes differ because their σ intervals differ; that difference produces $\alpha' M^2 = N - a$ and $\alpha' M^2 = 4(N_L - a) = 4(N_R - a)$. At critical flat bosonic content, $D = 26$ and $a = 1$, the first massless open and closed sectors carry vector and tensor states. Their tachyonic ground states and the separate quantum consistency theorems limit what this free-spectrum calculation establishes.

Status and sources

Sections 1–2. The action uses a flat, mostly-plus target metric, the displayed string tension, and the stated local coordinates and positive branch. The classical area action, auxiliary metric equation and positive-branch reduction are [WS] statements from Tong (2009, physical PDF pp. 25–26, eqs. (1.22)–(1.25)) and Polchinski (1994, physical PDF pp. 48–49, eqs. (2.2.1)–(2.2.3)). Classical elimination and the displayed non-diagonal patch are [MATH] on the stated nondegenerate positive branch. Quantum equivalence is not claimed.
Section 3. Gauge equations and stress constraints are scoped classical [WS] statements following Tong (2009, physical PDF pp. 29–31, eqs. (1.27), (1.31)–(1.34)). The stress-component fixture and trace comparison are [MATH]. Our variational T_{ab} includes T; Tong's eq. (1.32) divides by that factor. Residual global maps depend on the surface.
Section 4. Closed periodic and open NN/DD mode profiles are [WS] under their stated boundary conditions, following Tong (2009, physical PDF pp. 32–34 and 57–60, eqs. (1.35)–(1.41) and (3.1)–(3.5)). The unequal fixed-DD profile is on Tong (2009, physical PDF p. 66, Sec. 3.3, displays before (3.7)). The interval normalization, real DD sine Hermiticity, restricted closed/NN momentum integrals and Fourier coefficients are [MATH] within those sourced modes. DD endpoint forces permit a nonzero instantaneous integrated momentum density without a conserved DD zero mode. The brane interpretation used later is [GEO-E] for the standard parallel-brane setting.

Section 5. The oscillator algebra, vacuum convention, unshifted Virasoro relation and physical-mode conditions are sourced [WS] statements from Tong (2009, physical PDF pp. 36–38, eqs. (2.2)–(2.7), and p. 102, unnumbered Virasoro relation). The level-one transversality and physical-null quotient follow Polchinski (1994, physical PDF pp. 52–53, eqs. (2.3.10)–(2.3.13)) at nonzero null momentum and $a = 1$; they are [WS] in this scope. The finite central-term sum is [MATH] conditional on the sourced free-boson operator contraction, whose central-charge coefficient is [ANOM]. Colored partitions are [MATH] conditional on the physical transverse Fock premise. These finite steps do not prove the full Virasoro representation or no-ghost theorem. The unshifted modes and separate physical intercept use the normalizations defined above.
Section 6. Light-cone reduction and the regulated intercept are [WS] inputs from Tong (2009, physical PDF pp. 42–47, eqs. (2.17)–(2.26)). The full Lorentz commutator is a sourced [WS] result from Tong (2009, physical PDF pp. 53–55, Sec. 2.4); the $D \geq 4$ coefficient comparison is [MATH] conditional on that operator result. The $D = 3$ exception is described in Mezincescu and Townsend (2011, version 2, physical PDF p. 2, Introduction). The conformal-gauge ghost coefficient $c_{bc} = -26$ and matter coefficient $c_X = D$ are sourced [ANOM] inputs following Tong (2009, physical PDF pp. 123–124, Secs. 5.2–5.3) and Polchinski (1994, physical PDF p. 58, eq. (2.4.17)). The vanishing-Weyl-anomaly criterion for this field content is a sourced [ANOM] statement. The full quantum closure and ghost OPE are not local derivations; $D = 27$ is formal algebra only.
Sections 7–8. The free open/closed mass shells, nonzero-momentum vector/tensor interpretation and matched-level conditions are scoped [WS] claims following Tong (2009, physical PDF pp. 47–52 and 60–62) and Polchinski (1994, physical PDF pp. 52–54). The unequal-DD mass shift and threshold specifically follow Tong (2009, physical PDF p. 66, Sec. 3.3, displays before (3.7)) for parallel matching NN/DD endpoints. Mass-shell substitution, the stretch integral and $SO(24)$ counts are [MATH] in that sourced scope. The BRST construction is a sourced [WS] input, and the nonzero-momentum no-ghost comparison is a cited [MATH] theorem from Polchinski (1994, physical PDF pp. 61–65, eqs. (2.5.9)–(2.5.27)); the theorem is not proved here. The physical sector, nonzero p^+ patch and exceptional zero-momentum limitation are stated above. No compactification or superstring claim is admitted by these sections.

References

Mezincescu, L. and P. K. Townsend (2011). *Quantum 3D Superstrings*. Version 2, Introduction. arXiv: `1106.1374 [hep-th]`.

Polchinski, J. (1994). *What is String Theory?* Les Houches lectures, version 1 read; distinct from the 1998 book. arXiv: `hep-th/9411028 [hep-th]`.

Tong, D. (2009). *Lectures on String Theory*. Version 3 source locators are recorded in the chapter source list. arXiv: `0908.0333 [hep-th]`.

Chapter II.2

Worldsheet CFT toolkit: OPE, state–operator map, current algebras

II.2.1 Why an insertion can describe a string state

A string vibration was a mode of the embedding $X^\mu(\tau, \sigma)$ in Chapter 1. On a Euclidean worldsheet, the same excitation can be prepared by inserting an operator at a point. This change of viewpoint is useful because a small circle around the insertion measures its energy and charges. Bringing two insertions together then tells us which states can appear when they combine. The operator product expansion (OPE) is the local rule for that combination, rather than a list of formal singularities.

We will follow one free coordinate far enough to see the whole route. Its regulated two-point function fixes the OPE of momentum exponentials. The stress tensor reads their scale weights, a logarithmic map carries them to cylinder states, and a current contour reads their charge. A compact coordinate adds winding and a locality test. Finally, conformal gauge adds ghost fields; their central charges show when the standard critical BRST construction can be used. The explicit free-field calculations do not prove the general state–operator correspondence or the no-ghost theorem.

After this chapter, the reader should be able to

- calculate a free-boson bulk OPE and the weight of a momentum vertex;
- translate a plane primary into cylinder energy, angular momentum and an oscillator state in the conventions of Chapter 1;
- compute compact-boson charges, weights and full-bulk monodromy;
- separate matter, ghost and total central charges from the number of light-cone transverse coordinates;
- state the conditions under which the cited BRST and no-ghost results apply.

II.2.2 A local insertion from a regulated free boson

What singular product does the string action assign to nearby insertions? Use Euclidean coordinates $\sigma^1 = \tau_E$, $\sigma^2 = \sigma$ and $z = \sigma^1 + i\sigma^2$ on a bulk patch. We start with spacelike target coordinates X^i so their Gaussian integral is well defined. The continued time coordinate will enter only after the local calculation. The tension normalization of Chapter 1 gives

$$S_E = \frac{1}{4\pi\alpha'} \int d^2\sigma\, \partial_a X^i \partial_a X^i, \qquad \alpha' > 0. \tag{II.2.1}$$

The constant mode of X has no quadratic action. We remove it while inverting the Laplacian, choose a translation-invariant infrared prescription, and integrate it separately in momentum correlators. Thus a bare $\langle XX \rangle$ carries an additive infrared constant, whereas neutral products of consistently normalized vertices have a definite coordinate dependence.

Integration by parts puts the quadratic kernel at $-\Delta/(2\pi\alpha')$. Since $\Delta \ln|z-w|^2 = 4\pi\delta^{(2)}(z-w)$, its inverse has the local form

$$\langle X^i(z,\bar z) X^j(w,\bar w)\rangle_{\neq 0} = -\frac{\alpha'}{2}\delta^{ij}\ln|z-w|^2 + C\delta^{ij}, \qquad -\frac{\Delta}{2\pi\alpha'}G = \delta^{(2)}. \tag{II.2.2}$$

Here C records the infrared choice and $\neq 0$ indicates that the constant mode has been removed. Locally $X = X_L(z) + X_R(\bar z)$, with $X^i_L(z)X^j_L(w) \sim -\alpha'\delta^{ij}\ln(z-w)/2$. Differentiating first at w and then at z fixes the sign that is easy to miss,

$$\partial X^i_L(z)\partial X^j_L(w) \sim -\frac{\alpha'\delta^{ij}}{2(z-w)^2}, \qquad \partial X^i_L(z) X^j_L(w) \sim -\frac{\alpha'\delta^{ij}}{2(z-w)}. \tag{II.2.3}$$

The symbol $\sim$ retains singular terms as $z \to w$ inside a correlator with spectator insertions outside the small circle. Figure II.2.1 shows that scale ordering. A bulk holomorphic contraction is not yet an open-string boundary contraction. A boundary changes the Green function through its boundary condition, which Chapter III.2 will supply.

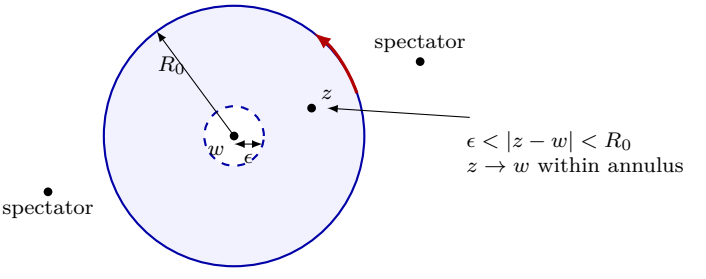


Figure II.2.1: A disk of radius ϵ surrounds the insertion at w; z lies in the annulus $\epsilon < |z-w| < R_0$, and spectator operators remain outside the outer contour. The OPE organizes the $z \to w$ limit after the same short-distance subtraction is used for each insertion. The arrows mark counterclockwise positive contours on the z plane.

Normal ordering subtracts the chosen self-contraction. Define the bulk momentum vertex $V_k =: e^{ik\cdot X} :$. Wick's theorem joins different insertions but leaves each exponential internally normal ordered. For spacelike k, q with zero time components, it gives

$$\begin{aligned} V_k(z,\bar{z})V_q(w,\bar{w}) \sim |z-w|^{\alpha' k\cdot q}\big[&V_{k+q}(w,\bar{w}) \\ &+ (z-w) : ik\cdot\partial X_L V_{k+q} : (w,\bar{w}) \\ &+ (\bar{z}-\bar{w}) : ik\cdot\bar{\partial} X_R V_{k+q} : (w,\bar{w}) + \cdots\big]. \end{aligned} \tag{II.2.4}$$

The factor follows directly from $\exp[-k\cdot q\langle X(z)X(w)\rangle]$; the displayed descendants come from expanding $X(z)$ about w. The exponent is therefore a calculated physical scale, not a convention assigned to the OPE.

The zero mode integral enforces $\sum_a k_a = 0$. In the same prescription, the nonzero-mode Gaussian gives

$$\left\langle \prod_{a=1}^{N} V_{k_a}(z_a,\bar{z}_a) \right\rangle \propto \delta\left(\sum_a k_a\right) \prod_{a<b} |z_a - z_b|^{\alpha' k_a\cdot k_b}. \tag{II.2.5}$$

The proportionality contains the common normalization and zero-mode measure. Shifting $G \mapsto G + C$ changes the product of vertex normalizations by $\exp[-C\sum_{a<b} k_a\cdot k_b] = \exp[(C/2)\sum_a k_a^2]$ under neutrality. A matched redefinition of each vertex absorbs it; the coordinate powers do not change.

Here is a four-insertion example with all momenta spacelike. The charges $(k,-k,q,-q)$ sit at $(0,x,1,\infty)$, respectively. The insertion at infinity means

$$V_{-q}(\infty) = \lim_{y\to\infty} |y|^{\alpha' q^2} V_{-q}(y). \tag{II.2.6}$$

Pairs involving y combine to precisely that scaling because the total charge is zero. The remaining variable pairs yield

$$\langle V_k(0)V_{-k}(x)V_q(1)V_{-q}(\infty)\rangle \propto |x|^{-\alpha' k^2}|1-x|^{-\alpha' k\cdot q}. \tag{II.2.7}$$

For example, with $\alpha' = 2$, $k = 1$ and $q = 2$ in one spacelike direction, the powers are -2 and -4. The $x \to 0$ behavior is exactly the $k, -k$ OPE into the identity channel. This is a Gaussian correlator, not a string scattering amplitude. An amplitude also needs the appropriate ghost insertions and moduli integration. Chapter 6 will use local products for twist fields, while Chapter 3 changes the allowed momenta.

The same example also shows how an OPE selects an intermediate charge. If instead $x \to 1$, the nearby charges are $-k$ and q; their combined vertex is V_{q-k} and their bulk singular power is $-\alpha' k\cdot q$. The two limits refer to distinct pairings of the same four insertions. No crossing equation was required to calculate either local limit, because the Gaussian correlator already fixed all pairwise contractions. In an interacting CFT, consistency between channels becomes a separate problem. This distinction will matter for the twist fields of Chapter 6, whose products are not given by one free exponential formula.

II.2.3 Stress tensor and primary weights

How can a small contour tell whether an insertion is a permissible worldsheet field? The holomorphic stress tensor measures the response to local coordinate changes. For the free coordinates it is

$$T(z) = -\frac{1}{\alpha'} : \partial X^i \partial X^i : (z). \tag{II.2.8}$$

An operator $\mathcal{O}$ is a holomorphic primary of weight h if its singular stress-tensor product is

$$T(z)\mathcal{O}(w) \sim \frac{h\mathcal{O}(w)}{(z-w)^2} + \frac{\partial\mathcal{O}(w)}{z-w}. \tag{II.2.9}$$

The antiholomorphic product independently defines $\tilde{h}$. A weight is a local transformation exponent; it becomes a cylinder energy in the next section. We first calculate it instead of assigning it by analogy.

One contraction of $\partial X^i(z)$ with the exponential gives

$$\partial X^i(z) V_k(w,\bar{w}) \sim -\frac{i\alpha' k^i}{2(z-w)} V_k(w,\bar{w}). \tag{II.2.10}$$

In TV_k, the two ways to make one contraction combine into $\partial V_k/(z-w)$. The double contraction produces the second-order pole. Explicitly,

$$T(z)V_k(w,\bar{w}) \sim \frac{\alpha' k^2}{4(z-w)^2} V_k(w,\bar{w}) + \frac{\partial V_k(w,\bar{w})}{z-w}, \qquad h = \tilde{h} = \frac{\alpha' k^2}{4}. \tag{II.2.11}$$

This also explains why normal ordering matters. If a self-contraction remained inside V_k, the supposed operator would depend on its own regulator rather than transform with a fixed weight.

The two terms in Eq. (II.2.11) have different jobs. The double pole measures the rescaling of an insertion, while the simple pole translates it along the local coordinate. A small contour weighted by a vector field $\varepsilon(z)$ therefore gives

$$\delta_\varepsilon V_k(w) = \oint_w \frac{dz}{2\pi i} \varepsilon(z) T(z) V_k(w) = \big(\varepsilon(w)\partial + h\partial\varepsilon(w)\big) V_k(w). \tag{II.2.12}$$

For a translation, $\partial\varepsilon = 0$ and the insertion moves. For a local dilation, the second term supplies its weight. The antiholomorphic contour acts in the same way with $\tilde{h}$.

The derivative field supplies a second check. Contracting one of the two factors in T with ∂X^i yields

$$T(z)\partial X^i(w) \sim \frac{\partial X^i(w)}{(z-w)^2} + \frac{\partial^2 X^i(w)}{z-w}. \tag{II.2.13}$$

Thus ∂X^i is primary with $h = 1$. Differentiating this OPE at w produces a third-order pole $2\partial X^i/(z-w)^3$ in $T(z)\partial^2 X^i(w)$. Although $\partial^2 X^i$ has scale weight two, the extra pole shows that it is a descendant, not a primary. Scale weight alone cannot distinguish those two statements.

To see the central charge, contract two stress tensors. There are two double pairings of the free fields, each contributing a fourth-order pole. The remaining single pairings reconstruct the stress tensor and its derivative,

$$T(z)T(w) \sim \frac{D/2}{(z-w)^4} + \frac{2T(w)}{(z-w)^2} + \frac{\partial T(w)}{z-w}. \tag{II.2.14}$$

The standard coefficient $c/2$ of the fourth pole therefore gives $c_m = D$ for D free matter coordinates. This is a chiral central charge, not a count of physical transverse oscillators.

Each double pairing of two copies of Eq. (II.2.3) contributes $\alpha'^2\delta^{ij}\delta^{ij}/[4(z-w)^4]$ before the two stress-tensor prefactors. The two pairings total $D/[2(z-w)^4]$. A single contraction leaves a normal-ordered pair of derivatives. Its zeroth Taylor term gives $2T/(z-w)^2$; the next gives $\partial T/(z-w)$. The fourth pole is thus a local count of free scalar contractions, rather than a count obtained by imposing target-space constraints.

Target time requires a separate physical step. Continue the spacelike calculation to the mostly-plus target metric $\eta_{\mu\nu}$, with a choice of contour for X^0 rather than a convergent real Euclidean Gaussian. Every single contraction replaces δ^{ij} by $\eta^{\mu\nu}$. The two contractions in the vertex weight therefore produce $k^2 = \eta^{\mu\nu}k_\mu k_\nu$, while the fourth pole of TT contains $\eta_{\mu\nu}\eta^{\mu\nu} = D$; the time sign is squared. The continued formula reads

$$h = \tilde{h} = \frac{\alpha'}{4}\eta^{\mu\nu}k_\mu k_\nu, \qquad c_m = D. \tag{II.2.15}$$

As a concrete mass-shell use, an unexcited closed momentum vertex in the standard flat critical bosonic construction needs $(h, \tilde{h}) = (1, 1)$. Equation (II.2.15) then gives

$$k^2 = \frac{4}{\alpha'}, \qquad M^2 = -k^2 = -\frac{4}{\alpha'}. \tag{II.2.16}$$

This reproduces the closed ground-state mass found from the oscillator constraints in Chapter 1. The weight condition is one ingredient of a physical vertex; it does not by itself establish BRST closure or a positive-norm spectrum. Chapter 4 will apply related tests to worldsheet fermions, and Chapter III.1 will apply them to open-string vertices with boundary normalization.

II.2.4 States on a circle and the Virasoro extension

Why does the weight in a small plane disk become energy? Quantize on concentric circles centered at the insertion. The path integral inside a circle prepares a state on that circle; a local operator at the origin prepares $|\mathcal{O}\rangle = \mathcal{O}(0)|0\rangle$. This state–operator correspondence is used here in the standard unitary Euclidean CFT setting. For noncompact momenta, fixed-k vertices give delta-normalized generalized states rather than normalizable vectors.

The logarithmic map turns radial distance into Euclidean time,

$$z = e^u, \qquad u = \tau_E + i\sigma, \qquad \sigma \sim \sigma + 2\pi. \tag{II.2.17}$$

An increase of τ_E moves outward, while increasing σ moves counterclockwise. Figure II.2.2 fixes these directions. The Laurent modes of the plane stress tensor are

$$L_n = \oint_0 \frac{dz}{2\pi i}\, z^{n+1} T(z), \qquad \tilde{L}_n = \oint_0 \frac{d\bar{z}}{2\pi i}\, \bar{z}^{n+1} \tilde{T}(\bar{z}). \tag{II.2.18}$$

Each contour is positively oriented in its own complex coordinate. A physical traversal in the $+\sigma$ direction is counterclockwise in z but clockwise in $\bar{z}$; it cannot serve as the positive contour for both residues. The primary OPE immediately gives $L_0|\mathcal{O}\rangle = h|\mathcal{O}\rangle$ and $L_{n>0}|\mathcal{O}\rangle = 0$ when the insertion at zero is primary. The same statement holds in the right sector.

To see why positive modes annihilate the primary state, surround the origin by a small contour in Eq. (II.2.18). The double pole in Eq. (II.2.9) contributes a derivative of z^{n+1} at zero, and the simple pole contributes its value there. Both vanish for $n > 0$; for $n = 0$ the derivative is one and yields h. Negative modes instead create descendants, such as $L_{-1}|\mathcal{O}\rangle$ corresponding to $\partial\mathcal{O}(0)|0\rangle$. The state language organizes all local derivatives of an insertion.

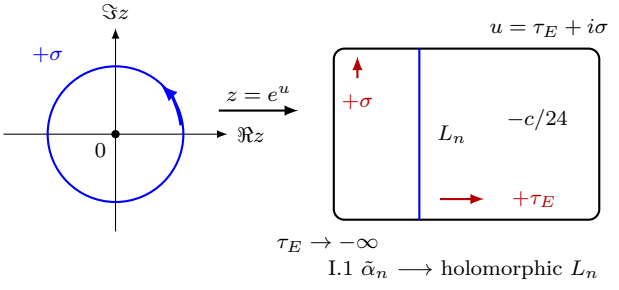


Figure II.2.2: The map $z = e^{\tau_E + i\sigma}$ sends circles around the origin to spatial slices of a cylinder. Positive σ is counterclockwise on the plane. The plane origin prepares an incoming state at $\tau_E \to -\infty$. With the Chapter 1 wave convention, its tilded oscillator is the holomorphic oscillator used by L_n here. The $-c/24$ label is the Schwarzian shift of one chiral sector.

The fourth pole of the TT OPE makes these modes a central extension. Radial ordering places the operator at larger $|z|$ to the left. Subtracting the two radial orderings in $[L_m, L_n]$ shrinks the difference of the outer z contours to a small positive circle around w. The singular TT OPE gives

$$[L_m, L_n] = \oint_0 \frac{dw}{2\pi i}\, w^{n+1} \operatorname*{Res}_{z=w} z^{m+1} \left[\frac{c/2}{(z-w)^4} + \frac{2T(w)}{(z-w)^2} + \frac{\partial T(w)}{z-w} \right].$$

The second and first poles contribute $2(m+1)w^m T(w) + w^{m+1}\partial T(w)$. Integrating the derivative term by parts on the closed w contour replaces it by $-(m+n+2)w^{m+n+1}T(w)$. Their coefficient is $2(m+1) - (m+n+2) = m - n$. The fourth-pole residue is $(c/12)(m+1)m(m-1)w^{m-2}$, so the remaining contour gives

$$[L_m, L_n] = (m-n)L_{m+n} + \frac{c}{12} m(m^2-1)\delta_{m+n,0}. \tag{II.2.19}$$

The central integrand is proportional to w^{m+n-1} and has a residue only if $m+n=0$. These are integer modes of an untwisted stress tensor. The polynomial can be evaluated formally elsewhere, but that evaluation is not a mode algebra for an arbitrary twisted sector.

For example, $m=1$, $n=-1$ leaves no central term because $m(m^2-1)=0$. The generators L_{-1}, L_0, L_1 close to the global conformal algebra. At $m=2$, $n=-2$ the central contribution is $c/2$, so the extension first appears beyond those global transformations. Knowing only the global transformation law does not determine a twisted sector's cylinder ground energy.

The stress tensor is not a primary under $z=e^u$. We import its finite transformation law, $T_{uu}=(dz/du)^2 T_{zz}+(c/12)\{z,u\}$, where the Schwarzian is $\{f,u\}=f'''/f'-(3/2)(f''/f')^2$. For $f=e^u$ all three derivatives equal e^u, hence $\{e^u,u\}=1-3/2=-1/2$. The same calculation in $\bar{u}$ gives the right-sector shift. Taking the spatial zero mode of each cylinder stress tensor yields

$$H_L=\frac{1}{2\pi}\int_0^{2\pi} d\sigma\, T_{uu}=L_0-\frac{c}{24}, \qquad H_R=\frac{1}{2\pi}\int_0^{2\pi} d\sigma\, \tilde{T}_{\bar{u}\bar{u}}=\tilde{L}_0-\frac{\tilde{c}}{24}. \tag{II.2.20}$$

Euclidean time translates both sectors, whereas positive σ rotates them oppositely. Adding and subtracting these two charges gives

$$H_{\text{cyl}}=L_0+\tilde{L}_0-\frac{c+\tilde{c}}{24}, \qquad P_{\text{cyl}}=L_0-\tilde{L}_0-\frac{c-\tilde{c}}{24}. \tag{II.2.21}$$

Both quantities are dimensionless for a circumference 2π. For $c=\tilde{c}=1$ and a state of $(h,\tilde{h})=(1/4,1/4)$, the energy is $1/4+1/4-2/24=5/12$, while the angular momentum is zero. The identity has energy $-2/24=-1/12$. A state with unequal weights has nonzero angular momentum; even equal weights can give a shift when $c\neq\tilde{c}$. The $-c/24$ term is a coordinate-transformation effect. It is distinct from the regulated light-cone intercept a in Chapter 1's physical L_0-a constraint.

There is a convention trap in carrying the oscillators from Chapter 1. There α_n multiplies a wave in $\tau-\sigma$ and $\tilde{\alpha}_n$ one in $\tau+\sigma$. After $\tau=-i\tau_E$, our $u=\tau_E+i\sigma$ is holomorphic in the latter combination. Consequently the plane L_n in this chapter is made from the Chapter 1 tilded oscillators,

$$L_n^{\text{plane}}=\frac{1}{2}\sum_{m\in\mathbb{Z}} :\tilde{\alpha}_{n-m}\cdot\tilde{\alpha}_m:_{\text{II.1}}, \qquad \tilde{L}_n^{\text{plane}}=\frac{1}{2}\sum_{m\in\mathbb{Z}} :\alpha_{n-m}\cdot\alpha_m:_{\text{II.1}}. \tag{II.2.22}$$

These plane zero modes are unshifted. In a compact direction their zero-mode entries are $\tilde{\alpha}_0=\sqrt{\alpha'/2}\,p_L$ and $\alpha_0=\sqrt{\alpha'/2}\,p_R$. The next section obtains p_L, p_R from momentum and winding. This map is needed whenever a cylinder character in Chapter 6 or a channel exchange in Chapter III.2 is translated back to a string oscillator state.

II.2.5 Currents, compact charge lattices and locality

When does a contour measure a conserved charge? For one compact spacelike boson define the normalized holomorphic current

$$J(z) = i\sqrt{\frac{2}{\alpha'}}\,\partial X_L(z), \qquad J(z)J(w) \sim \frac{1}{(z-w)^2}. \tag{II.2.23}$$

The factor i converts the negative derivative contraction in Eq. (II.2.3) into a positive double pole. We call this $U(1)$ level one in this chosen basis. Rescaling J changes the number on the right, so a numerical level has meaning only with a current normalization.

For a circle $X \equiv X + 2\pi R$, momentum is n/R and winding is the integer in $X(\sigma + 2\pi) - X(\sigma) = 2\pi w R$. The left and right momenta in our α' normalization are

$$p_L = \frac{n}{R} + \frac{wR}{\alpha'}, \qquad p_R = \frac{n}{R} - \frac{wR}{\alpha'}, \qquad n, w \in \mathbb{Z}. \tag{II.2.24}$$

The local vertex is $V_{n,w} =: e^{ip_L X_L + ip_R X_R} : C_{n,w}$. Here the exponential shifts the zero-mode charge, and $C_{n,w}$ acts on the incoming charge sector before that shift. Its action will be fixed below by the exchange calculation. Contracting with T and J gives

$$(h, \tilde{h}) = \left(\frac{\alpha' p_L^2}{4}, \frac{\alpha' p_R^2}{4}\right), \qquad J(z)V_{n,w}(0) \sim \frac{\sqrt{\alpha'/2}\,p_L}{z} V_{n,w}(0). \tag{II.2.25}$$

The contour $J_0 = \oint dz\, J(z)/(2\pi i)$ therefore measures $\sqrt{\alpha'/2}\,p_L$. It is a left charge, while target momentum n/R and winding w combine differently in the two sectors.

The difference of weights is particularly simple. The product $(p_L - p_R)(p_L + p_R)$ cancels R and α',

$$h - \tilde{h} = \frac{\alpha'}{4}(p_L^2 - p_R^2) = nw. \tag{II.2.26}$$

The sign of the angular momentum is the sign of nw in the $+\sigma$ convention of Eq. (II.2.21). Positive winding gives positive angular momentum when $n > 0$; for $n = -1, w = 1$ the angular momentum is instead -1. For two charges $a = (n, w)$ and $b = (n', w')$, taking one full bulk vertex around the other changes its phase by 2π times

$$\mathcal{M}(a, b) = \frac{\alpha'}{2}(p_{L,a}p_{L,b} - p_{R,a}p_{R,b}) = nw' + wn' \in \mathbb{Z}. \tag{II.2.27}$$

The full exponential is single-valued around another lattice vertex. A holomorphic factor alone can have a fractional power and need not be single-valued. Integer full monodromy also does not settle the sign of a half-exchange of bosonic fields.

The derivation of Eq. (II.2.27) can be seen without guessing an integral lattice. Substitute Eq. (II.2.24) into the left-minus-right pairing. The terms proportional to nn'/R^2 cancel, as do those proportional to $ww'R^2/\alpha'^2$. The surviving cross terms are

$$p_{L,a}p_{L,b} - p_{R,a}p_{R,b} = \frac{2}{\alpha'}(nw' + wn'). \tag{II.2.28}$$

The radius disappears. Locality of the full bulk exponentials is therefore stable as R varies, even though their weights change.

At $R = \sqrt{\alpha'}$, take $A = (1, 0)$ and $B = (0, 1)$. For A, Eq. (II.2.24) gives $(p_{L,A}, p_{R,A}) = (1, 1)/\sqrt{\alpha'}$. For B it gives $(p_{L,B}, p_{R,B}) = (1, -1)/\sqrt{\alpha'}$. Each square in Eq. (II.2.25) is therefore $1/\alpha'$, and its factor $\alpha'/4$ gives $1/4$. The signed pairing is $\alpha'[1/\alpha' - (-1/\alpha')]/2 = 1$. Thus $\mathcal{M}(A, B) = 1$. Adding the charges to obtain $(1, 1)$ adds the left momenta and cancels the right momenta. Its weight-one holomorphic vertex is a local input for the enhanced-current example in Chapter 3, whose global spectrum requires more than this one OPE. Figure II.2.3 marks these lattice points and the pairing.

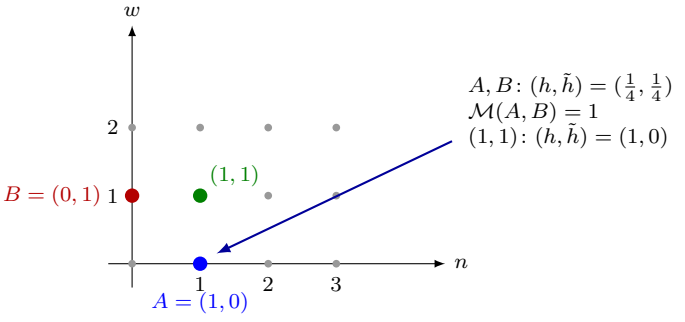


Figure II.2.3: A small part of the (n, w) lattice at $R = \sqrt{\alpha'}$. The points $A = (1, 0)$ and $B = (0, 1)$ have opposite right momenta and $\mathcal{M}(A, B) = 1$; their bare half-exchange is odd. The diagonal point $(1, 1)$ has $(h, \tilde{h}) = (1, 0)$. The axes count integers, rather than geometric distances in target space.

The chiral contractions make the bare product of charge a and b proportional to $(z - w)^{\alpha' p_{L,a} p_{L,b}/2} (\bar{z} - \bar{w})^{\alpha' p_{R,a} p_{R,b}/2}$. On a counterclockwise half-rotation, the second factor rotates in the opposite direction. The bare exchange phase is $\exp[i\pi \mathcal{M}(a, b)]$. It equals -1 for A, B. One local way to cancel that odd exchange is the bilinear cocycle

$$\epsilon(a, b) = (-1)^{wn'}, \qquad \frac{\epsilon(a, b)}{\epsilon(b, a)} = (-1)^{nw' + wn'}. \tag{II.2.29}$$

To connect this coefficient to the zero modes, let E_a be the charge shift inside the exponential, $E_a|b\rangle = |a + b\rangle$, and set $C_a|b\rangle = \epsilon(a, b)|b\rangle$. Thus the zero-mode action of $V_a = E_a C_a$ is $V_a|b\rangle = \epsilon(a, b)|a + b\rangle$. The leading local product, with oscillator contractions restored, is

$$V_a(z, \bar{z}) V_b(w, \bar{w}) \sim \epsilon(a, b)(z - w)^{\alpha' p_{L,a} p_{L,b}/2} (\bar{z} - \bar{w})^{\alpha' p_{R,a} p_{R,b}/2} \big[V_{a+b}(w, \bar{w}) + \cdots \big].$$

For A, B, $\epsilon(A, B)/\epsilon(B, A) = -1$ cancels the bare half-exchange sign, giving $+1$ for the full vertices. Bilinearity gives $\epsilon(a, b)\epsilon(a + b, c) = \epsilon(b, c)\epsilon(a, b + c)$, the associativity condition for this illustration. In particular, applying $E_a C_a E_b C_b$ to $|c\rangle$ and using this identity gives $\epsilon(a, b) E_{a+b} C_{a+b} |c\rangle$. This local construction is not a specification of every sector of a compact CFT. Chapter 3 develops the global momentum–winding and duality story.

If $c = (n'', w'')$, the exponent on the first product of cocycles is $wn' + (w + w')n''$, while the exponent on the second is $w'n'' + w(n' + n'')$. They are the same integer.

This verifies associativity for all three lattice charges, rather than only for A, B. It does not determine the complete vertex spectrum or modular invariance.

Nonabelian currents use a separate level symbol K and a declared positive invariant form κ^{ab}. Their OPE is

$$J^a(z)J^b(w) \sim \frac{K\kappa^{ab}}{(z-w)^2} + \frac{if^{ab}{}_c J^c(w)}{z-w}. \tag{II.2.30}$$

With $J^a_m = \oint dz\, z^m J^a(z)/(2\pi i)$, the two residues give

$$[J^a_m, J^b_n] = if^{ab}{}_c J^c_{m+n} + Km\kappa^{ab}\delta_{m+n,0}. \tag{II.2.31}$$

The m comes from $\partial_z z^m = mz^{m-1}$ in the double pole. This local algebra will help identify heterotic gauge currents in Chapter 5. It neither fixes a representation spectrum nor allows us to carry a numerical level from a source using another invariant-form normalization.

II.2.6 Ghost systems and the BRST boundary

Why does a theory with D embedding fields need fields with negative central charge? Conformal gauge removes coordinate redundancy only after its Faddeev–Popov determinant is included. The corresponding b, c pair is anticommuting. A first-order pair of weights $(h_b, h_c) = (\lambda, 1-\lambda)$ has a local bc OPE $b(z)c(w) \sim 1/(z-w)$. The commuting β, γ pair has the same weight pattern but different statistics and ordered OPE signs. It appears when local worldsheet supersymmetry is gauge fixed in the RNS construction of Chapter 4. We keep its vacuum and picture structure outside this chapter.

The difference can be displayed before computing a central charge. In the ordered products of the source convention,

$$\begin{aligned} b(z)c(w) &\sim \frac{1}{z-w}, \qquad c(z)b(w) \sim \frac{1}{z-w}, \\ \beta(z)\gamma(w) &\sim -\frac{1}{z-w}, \quad \gamma(z)\beta(w) \sim \frac{1}{z-w}. \end{aligned} \tag{II.2.32}$$

The similar first-order kinetic terms do not justify erasing these order and statistics signs. In each system the source stress tensor has the compact form

$$T_{uv} =: (\partial u)v : -\lambda : \partial(uv) :, \qquad (u,v) = (b,c) \text{ or } (\beta,\gamma), \tag{II.2.33}$$

with the normal order and contractions appropriate to that pair. Differentiating the two terms and applying Eq. (II.2.32) produces the fourth-pole coefficient below.

For either first-order kinetic term, the stress tensor is built from the weighted derivatives of the pair. In the TT product the two ordered double contractions have coefficients λ^2 and $(1-\lambda)^2$, and the cross terms total $-4\lambda(1-\lambda)$. Their sum is

$$\lambda^2 + (1-\lambda)^2 - 4\lambda(1-\lambda) = 6\lambda^2 - 6\lambda + 1. \tag{II.2.34}$$

For commuting fields this is the coefficient of the fourth pole; for anticommuting fields the Wick permutation reverses its sign. Since the fourth-pole coefficient is $c/2$, the local formulas are

$$\begin{aligned} c_{bc}(\lambda) &= -2(6\lambda^2 - 6\lambda + 1) = 1 - 3(2\lambda - 1)^2, \\ c_{\beta\gamma}(\lambda) &= 2(6\lambda^2 - 6\lambda + 1) = 3(2\lambda - 1)^2 - 1. \end{aligned} \tag{II.2.35}$$

At $\lambda = 1/2$ these give $+1$ and -1 respectively, a quick check that the two statistics must not be interchanged. These are local stress-tensor OPE results, not claims about global vacua or superghost pictures.

The reparametrization ghosts have $(h_b, h_c) = (2, -1)$, so $c_{bc} = -26$. The RNS superghosts have $(h_\beta, h_\gamma) = (3/2, -1/2)$, so $c_{\beta\gamma} = 11$. For D free bosons the matter charge is D; for the standard flat RNS matter system, D bosons and D real worldsheet fermions give $3D/2$. Thus the local central-charge sums are

$$c_{\text{tot}}^{\text{bos}} = D - 26, \qquad c_{\text{tot}}^{\text{RNS}} = \frac{3D}{2} - 26 + 11 = \frac{3D}{2} - 15. \tag{II.2.36}$$

The separate arithmetic makes the physical distinction explicit. For the bosonic system, $D - 26 = 0$ gives $D = 26$. In the RNS matter sector, each boson contributes one unit of chiral charge and each real fermion one half, so $D + D/2 = 3D/2$. Both ghost systems then give $3D/2 - 15 = 0$, hence $D = 10$. These equations concern covariant worldsheet field content. They do not arise by subtracting two longitudinal coordinates from the matter central charge. At $D = 26$, the bosonic entries are $(c_m, c_{bc}, c_{\text{tot}}) = (26, -26, 0)$. The number of light-cone transverse coordinates is $D - 2 = 24$. At $D = 10$, the RNS entries are $(c_m, c_{bc}, c_{\beta\gamma}, c_{\text{tot}}) = (15, -26, 11, 0)$, while there are eight transverse coordinates. Figure II.2.4 keeps the central charges and oscillator counts in separate rows.

flat bosonic, $D = 26$			
$c_m = 26$	$c_{bc} = -26$	$c_{\text{tot}} = 0$	
flat RNS, $D = 10$			
$c_m = 15$	$c_{bc} = -26$	$c_{\beta\gamma} = 11$	$c_{\text{tot}} = 0$
light-cone transverse coordinates		bosonic 24	RNS 8

Figure II.2.4: Chiral central-charge sums for the flat critical bosonic and RNS systems. The final row counts transverse target coordinates after light-cone constraints. In particular, 24 is not the bosonic total central charge and 8 is not the RNS total central charge.

The vanishing of the total anomaly is a condition for the standard critical conformal-gauge BRST charge Q_B to square to zero. In the bosonic construction at the stated critical field content, let $b(z) = \sum_n b_n z^{-n-2}$ be the weight-two antighost and b_0 its zero mode. Write $L_{0,\text{tot}} = L_{0,m} + L_{0,gh}$ for the plane matter-plus-bc zero mode, including the ghost normal-ordering constant. This differs from the unshifted matter L_0 used

in Eq. (II.2.22). With ghost number normalized so a matter primary multiplied by an unintegrated c has degree one, $\mathrm{gh}(c) = 1$, $\mathrm{gh}(b) = -1$, and Q_B raises degree by one. The critical BRST relations are

$$\begin{aligned} c_{\mathrm{tot}} = 0 \quad \text{in the standard critical construction} \quad &\Longrightarrow \quad Q_B^2 = 0, \\ \{Q_B, b_0\} &= L_{0,\mathrm{tot}}. \end{aligned} \tag{II.2.37}$$

The first implication is scoped to that construction. It is not a general theorem that an arbitrary system with $c_{\mathrm{tot}} = 0$ has a healthy physical Hilbert space. The second relation explains a subtle point about the relative complex. For an arbitrary $\psi \in \ker b_0$, before imposing $Q_B\psi = 0$, it says $b_0 Q_B \psi = L_{0,\mathrm{tot}}\psi$. Hence $Q_B\psi$ stays in $\ker b_0$ when $L_{0,\mathrm{tot}}\psi = 0$. Nilpotence and the anticommutator also give $[Q_B, L_{0,\mathrm{tot}}] = 0$, so Q_B preserves $\ker b_0 \cap \ker L_{0,\mathrm{tot}}$. For the standard open-string ghost-number-one sector, the relative physical space is consequently

$$H^1_{\mathrm{rel}}(Q_B) = \frac{\ker Q_B \cap \ker b_0 \cap \ker L_{0,\mathrm{tot}}\big|_{\mathrm{gh}=1}}{Q_B\big(\ker b_0 \cap \ker L_{0,\mathrm{tot}}\big|_{\mathrm{gh}=0}\big)}. \tag{II.2.38}$$

The numerator consists of degree-one closed states in this relative complex. The denominator identifies those differing by Q_B of a degree-zero state in the same domain. Exact representatives are thus taken within the same relative complex. Writing only $\ker Q_B$ would retain gauge-exact states; writing only $\ker b_0$ would not define a subcomplex.

Positive norm is a further statement. In the cited bosonic setting with one free time coordinate and a unitary spatial CFT of $c = 25$, with the appropriate relative physical sector and nonexceptional nonzero momentum, the no-ghost comparison identifies the physical cohomology with the positive light-cone spectrum. The exceptional $k = 0$ cohomology is not covered by that comparison. We use the result as a theorem from the source, not as a consequence of Eq. (II.2.36). Chapter 4 supplies the RNS sectors and GSO projection. Chapter 7 uses the unoriented closed-channel source dictionary, while Chapter III.2 introduces the ghost and superghost completion of boundary states, including the ordered pictures needed for its cylinder calculation.

II.2.7 Limits of local CFT data

The same short-distance contraction supplied several kinds of data. The TV double pole determined scale weight, the TT fourth pole determined central charge, and the JV simple pole determined charge. On the cylinder, weight became energy only after the state–operator map and Schwarzian term were supplied. On a circle, allowed charges formed an integral lattice, but local monodromy and the illustrative cocycle did not specify a complete compact CFT.

This distinction matters downstream. Orbifold sectors in Chapter 6 need their own twisted ground states; boundary states in Chapter III.2 need boundary gluing and normalization. A local OPE is a necessary input to those constructions, not their replacement. Likewise, the local condition $c_{\mathrm{tot}} = 0$ supports the critical BRST construction, while the comparison with a positive physical spectrum invokes the cited no-ghost theorem under its hypotheses.

II.2.8 Exercises

For the first five exercises, give the requested exact rational fields as JSON strings through the chapter's reader companion. Show the intermediate Wick contractions or substitutions in written working; the bounded grader checks the submitted numbers, not that explanation. Use the public IDs and schemas in `benchmark/tasks.json`; submit through `benchmark/PROTOCOL.md`. Submit the listed fields directly, without an `answer` envelope; the last task requires written review.

1. Set $\alpha' = 2$, $k = (1, 2)$ and $q = (-1, 1)$ in two orthonormal spacelike directions, with zero target-time components. Compute the full $|z - w|$ power in $V_k V_q$ and the holomorphic weights of V_k, V_q, V_{k+q}. Submit `bulk_ope_power`, `h_k`, `h_q` and `h_sum`.

2. For a neutral one-scalar correlator with $\alpha' = 2$, charges $(1, -1, 2, -2)$ at $(0, x, 1, \infty)$, compute the powers of $|x|$ and $|1 - x|$ after the standard infinity scaling. Submit `abs_x_power` and `abs_one_minus_x_power`.

3. A primary on a 2π cylinder has $(h, \tilde{h}) = (1/4, 1/4)$ and $c = \tilde{c} = 1$. Compute its dimensionless energy and momentum and the identity-vacuum energy. Submit `energy`, `momentum` and `vacuum_energy`.

4. Take $\alpha' = R = 1$ and charges $A = (1, 0)$, $B = (0, 1)$. Find $(h, \tilde{h})$ for both and their full-bulk mutual-monodromy exponent. Submit `h_a`, `htilde_a`, `h_b`, `htilde_b` and `mutual_monodromy`. Explain in writing why this integer does not alone settle the bare half-exchange.

5. For a bc pair at $\lambda = 2$ and a commuting $\beta\gamma$ pair at $\lambda = 3/2$, compute their separate central charges. Then compute total charges for flat bosonic $D = 26$ and RNS $D = 10$, and the respective transverse-coordinate counts. Submit `c_bc`, `c_beta_gamma`, `c_bosonic_total`, `c_rns_total`, `bosonic_transverse` and `rns_transverse`.

6. Explain in writing why $c_{\mathrm{tot}} = 0$ and $Q_B^2 = 0$ do not alone prove positive norm. State the relative ghost-number-one complex and the free-time, unitary-spatial-CFT and nonexceptional nonzero-momentum scope of the cited no-ghost comparison. Explain why exceptional $k = 0$ is outside the statement used here.

II.2.9 Take-home message

Take-home message

A regulated free-boson contraction determines the singular products that give a vertex its weight. Radial quantization turns that weight into cylinder energy, and current contours turn simple poles into charges. Compact momentum and winding make locality an integer-lattice condition, with a cocycle needed for the illustrated bosonic exchange. Ghost central charges test the critical BRST construction; the positive physical spectrum rests on a separate theorem with stated hypotheses.

Status and sources

Sections 2.2–2.3. The calculations use the stated Euclidean continuation, mostly-plus target metric, string scale, and bulk normal ordering. The Gaussian OPE uses Tong (2009, physical PDF pp. 74–75, 84–86, Secs. 4.1.3 and 4.3.1). Vertices, stress tensor and primary weights use Tong (2009, physical PDF pp. 87–89, Sec. 4.3.3). The Wick coefficients and four-point example are [MATH] under the Gaussian and infrared premises. Target time is analytically continued.
Section 2.4. The Schwarzian, Virasoro and state–operator map follow Tong (2009, physical PDF pp. 91–92, 99–102 and 106–110, Secs. 4.4–4.6). The oscillator and chirality translation is given above. The central residue and cylinder example are [MATH]; fixed noncompact momentum is delta normalized.
Section 2.5. Physical p_L, p_R use Tong (2009, physical PDF pp. 206–208, Sec. 8.2). The lattice locality and affine OPE use Ginsparg (1988, physical PDF pp. 54–57 and 69–70, Secs. 8.1 and 9.1), translated to this α' and current basis. Spin, monodromy and the cocycle identity are [MATH] locally. No full compact CFT or affine representation classification is claimed.
Section 2.6. The distinct first-order systems and ordered OPEs use Polchinski (1994, PDF pp. 25–29, Sec. 1.6); the *bc* and RNS charge fixtures also use Tong (2009, physical PDF pp. 121–125, Secs. 5.2–5.3) and Polchinski (1994, PDF p. 66, Sec. 2.6). The polynomial and arithmetic are [MATH] for those fields. BRST nilpotence, the relative complex and the nonexceptional no-ghost comparison are cited from Polchinski (1994, PDF pp. 60–65, Secs. 2.5–2.6). They are not proved by the central-charge calculation; exceptional zero-momentum cohomology and global superghost pictures are excluded.

References

Ginsparg, P. (1988). *Applied Conformal Field Theory.* arXiv: `hep-th/9108028`.
Polchinski, J. (1994). *What Is String Theory?* arXiv: `hep-th/9411028`.
Tong, D. (2009). *Lectures on String Theory.* arXiv: `0908.0333 [hep-th]`.

Chapter II.3

Toroidal compactification, T-duality, and Narain moduli

II.3.1 A string can wrap a circle

A particle moving around a circle has quantized momentum. A closed string has a second possibility: as its parameter σ goes once around the string, its image can go around the target circle several times. The string can carry momentum n and winding w at once. Their energies respond oppositely to the radius. This simple observation is the starting point for T-duality.

The distinction becomes useful when a compact direction is small. A particle with nonzero momentum becomes heavy as the radius shrinks. A wound string instead becomes light. The full string spectrum can therefore reorganize under an inverse radius, provided its chiral oscillators and integer charges are transformed together. On a flat torus the same idea acts on a lattice of momentum and winding charges. With an isometry it also acts locally on metric, antisymmetric tensor and dilaton fields. Each step needs a different argument.

We use the free closed-string conventions of Chapter 1 and the chiral operator normalization of Chapter 2. The target metric is mostly plus, $\alpha' > 0$, and the worldsheet coordinate obeys $0 \le \sigma < 2\pi$. A physical circle coordinate has circumference $2\pi R$. Later we use a dimensionless angle of period 2π; keeping these two coordinates distinct is essential for the background-field rules. Figure II.3.1 fixes the positive winding orientation.

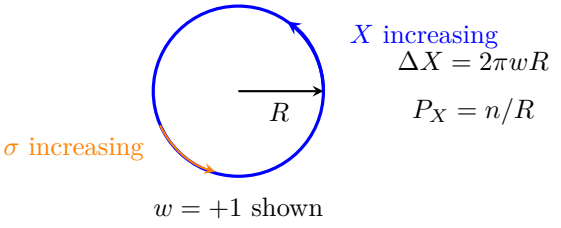


Figure II.3.1: The physical target coordinate $X \sim X + 2\pi R$ increases in the arrow's direction. Increasing worldsheet σ traces the image of the closed string. The drawing shows $w = +1$; n labels momentum along the same positive target direction and can have either sign. The target circle is not the worldsheet circle.

By the end of the chapter the reader can derive the two compact chiral momenta and their level-matching sign, match states under radius inversion, calculate a non-diagonal torus norm and its integer transformations, apply a local Buscher rule in physical units, and identify when the required circle isometry is absent. The brane boundary-condition dictionary of Chapter III.8 and later circle reductions use precisely these distinctions.

II.3.2 Closed strings on a circle

Why do momentum and winding enter different chiral sectors? Take a compact coordinate $X \sim X + 2\pi R$, and let $n, w \in \mathbb{Z}$. Momentum is quantized because wavefunctions on the target circle must be single-valued. Winding counts the change of a lifted coordinate on the target line when σ completes a period. With positive winding as in Figure II.3.1, the two integrals are

$$P_X = \frac{1}{2\pi\alpha'} \int_0^{2\pi} d\sigma\, \dot{X} = \frac{n}{R}, \qquad \int_0^{2\pi} d\sigma\, X' = 2\pi w R. \tag{II.3.1}$$

The kinetic action has coefficient $1/(4\pi\alpha')$, so the first integral is its canonical momentum. Oscillators integrate to zero in both expressions. Write the zero mode as $X_0 = x + v\tau + c\sigma$. The integrals determine its two slopes without a guess about chirality,

$$v = \frac{\alpha' n}{R}, \qquad c = wR, \qquad X_0 = x + \frac{\alpha' n}{R}\tau + wR\sigma. \tag{II.3.2}$$

The wave equation splits the field into functions of $\tau + \sigma$ and $\tau - \sigma$. Define p_L to multiply the former and p_R the latter,

$$X_0 = x + \frac{\alpha'}{2} p_L(\tau + \sigma) + \frac{\alpha'}{2} p_R(\tau - \sigma). \tag{II.3.3}$$

Comparing the τ and σ coefficients gives two simultaneous equations, $p_L + p_R = 2n/R$ and $p_L - p_R = 2wR/\alpha'$. Therefore

$$p_L = \frac{n}{R} + \frac{wR}{\alpha'}, \qquad p_R = \frac{n}{R} - \frac{wR}{\alpha'}, \qquad p_L^2 - p_R^2 = \frac{4nw}{\alpha'}. \tag{II.3.4}$$

The L and R labels here describe propagation directions, not the presence or absence of a tilde in another notation. In Chapter 1 the $\tau + \sigma$ oscillators are tilded. Thus $N_L = \widetilde{N}$ and $N_R = N$ in that chapter's mode expansion. Chapter 2's Euclidean map $z = e^{\tau_E + i\sigma}$ makes the same L sector holomorphic. This translation prevents a common sign error in level matching.

Let M^2 be the mass squared in the noncompact directions of the critical bosonic string. The two physical-state conditions, each with intercept one, read

$$M^2 = p_L^2 + \frac{4}{\alpha'}(N_L - 1) = p_R^2 + \frac{4}{\alpha'}(N_R - 1). \tag{II.3.5}$$

Subtracting the two sides and using (II.3.4) yields

$$N_R - N_L = nw. \tag{II.3.6}$$

Adding the two mass-shell expressions instead yields

$$M^2 = \frac{n^2}{R^2} + \frac{w^2 R^2}{\alpha'^2} + \frac{2}{\alpha'}(N_L + N_R - 2). \tag{II.3.7}$$

The two positive zero-mode terms have direct meanings. The first is the Kaluza–Klein momentum squared. The second is the mass squared of a wound string of length $2\pi|w|R$ and tension $1/(2\pi\alpha')$, before the oscillator and intercept contributions. The level equation is an additional constraint, so one must never choose levels independently of (n, w).

For a numerical state set $\alpha' = 2$, $R = 3$, $n = w = 1$, $N_R = 1$ and $N_L = 0$. Then

$$p_L = \frac{1}{3} + \frac{3}{2} = \frac{11}{6}, \qquad p_R = \frac{1}{3} - \frac{3}{2} = -\frac{7}{6}, \qquad N_R - N_L = nw = 1. \tag{II.3.8}$$

The left shell gives $121/36 - 2 = 49/36$; the right shell gives $49/36 + 0 = 49/36$. The equality of the two routes checks both the sign and the intercept. At fixed n a shrinking circle raises the first term in (II.3.7), while at fixed w it lowers the second. This is the physical reason to seek an exchange of the two charges in the next section. Exercise 1 asks for the same four independently submitted quantities.

II.3.3 Radius inversion and enhanced currents

Can a circle of radius R and a circle of a different radius describe the same string states? Exchange integer momentum and winding while setting

$$R' = \frac{\alpha'}{R}, \qquad n' = w, \qquad w' = n. \tag{II.3.9}$$

Substitution into (II.3.4) gives the chiral action

$$p'_L = \frac{w}{R'} + \frac{nR'}{\alpha'} = p_L, \qquad p'_R = \frac{w}{R'} - \frac{nR'}{\alpha'} = -p_R. \tag{II.3.10}$$

The map preserves nw and therefore preserves (II.3.6). It also preserves the two mass-shell equations when the oscillator levels are carried along unchanged. On the worldsheet it leaves one compact chiral field in place and reflects the other. The radius inversion is involutive, since applying it twice returns R, n, w. Figure II.3.2 depicts the same two charge families at reciprocal radii; the drawn circumferences alone do not establish their worldsheet equivalence.

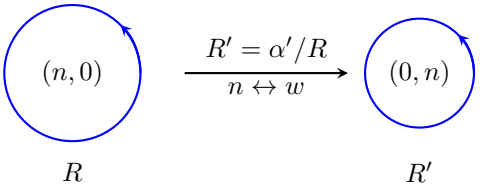


Figure II.3.2: Two physical target circles at R and $R' = \alpha'/R$. The momentum family $(n, 0)$ maps to the winding family $(0, n)$. The arrows give the positive charge convention on each circle; the right-moving compact field is reflected as in (II.3.10). The illustration compares charge families, not the sizes of their drawn loops.

The pure-momentum example makes the exchange visible. At $\alpha' = 2$, $R = 3$, $(n, w) = (1, 0)$ and $N_L = N_R = 1$, both chiral momenta equal $1/3$ and $M^2 = 1/9$. The dual radius is $2/3$ and the dual charge is $(0, 1)$. Its momenta are $p'_L = 1/3$ and $p'_R = -1/3$, while its wound contribution is $(R'/\alpha')^2 = 1/9$. In the mixed example of the previous section, the same transformation takes $(1, 1)$ to itself and changes $(11/6, -7/6)$ to $(11/6, 7/6)$. Both shells still give $49/36$. Exercise 2 isolates the pure-charge calculation.

At $R = \sqrt{\alpha'}$ the circle is fixed by inversion. This radius has more massless states in the critical bosonic theory. For $(n, w) = (1, 1)$,

$$p_L = \frac{2}{\sqrt{\alpha'}}, \qquad p_R = 0, \qquad (N_L, N_R) = (0, 1), \qquad M^2 = 0. \tag{II.3.11}$$

The compact left vertex $: e^{ip_L X_L} :$ has weight $h = \alpha' p_L^2/4 = 1$ in Chapter 2's normalization, while the right oscillator supplies the other unit of weight. The sign-reversed left charge gives the conjugate current. Charges with $n = -w$ instead give right chiral currents. Together with $i\partial X_L$ and $i\bar{\partial} X_R$, these are the chiral $SU(2)_L \times SU(2)_R$ currents of this bosonic compact CFT. Their spacetime vector states are additional to the generic-radius vectors.

The free-boson contraction from Chapter 2 shows why the new weight-one exponentials close with the derivative current. In one chiral coordinate, take $X_L(z)X_L(0) \sim -\alpha' \ln z/2$ and use the same normal ordering as for the momentum vertices. Then

$$: e^{2iX_L(z)/\sqrt{\alpha'}} :: e^{-2iX_L(0)/\sqrt{\alpha'}} : \sim \frac{1}{z^2}\left(1 + \frac{2iz}{\sqrt{\alpha'}}\partial X_L(0) + O(z^2)\right). \tag{II.3.12}$$

The leading power is z^{-2} because the two opposite charges have product $-4/\alpha'$ in the Gaussian contraction. The simple pole contains the derivative current. The same

contraction gives its charge action on either exponential:

$$\frac{i}{\sqrt{\alpha'}}\partial X_L(z) : e^{\pm 2iX_L(0)/\sqrt{\alpha'}} : \sim \pm\frac{1}{z} : e^{\pm 2iX_L(0)/\sqrt{\alpha'}} : . \tag{II.3.13}$$

The derivative current's own normalization is the same contraction,

$$\frac{i}{\sqrt{\alpha'}}\partial X_L(z)\,\frac{i}{\sqrt{\alpha'}}\partial X_L(0) \sim \frac{1}{2z^2}. \tag{II.3.14}$$

The right chiral sector repeats the calculation with X_R. These local OPEs explain the current enhancement at the self-dual radius; the extra spacetime vectors still require the critical bosonic physical-state conditions used in (II.3.11).

This enhancement belongs to the critical bosonic example with its intercept and tachyon. It is not a statement about the Type II spectrum; worldsheet fermions and projections enter in Chapter 4. Even for the bosonic theory, the explicit spectral map proves equality of these free state formulas, not the global identification of interacting backgrounds. The full compact-boson worldsheet argument also accounts for oscillator operators, winding sectors, periodic dual coordinates and holonomies. The bosonic vacuum genus sum is formal because of tachyon divergence. These conditions matter when the local transformation is used on curved backgrounds.

II.3.4 Toroidal charge lattices and Narain moduli

On a torus, how can a metric and an antisymmetric background change while integer string charges remain meaningful? Use angles $\theta^i \sim \theta^i + 2\pi$, $i = 1, \ldots, d$. In the angular coordinate frame G_{ij} and B_{ij} have units of length squared. Set $g = G/\alpha'$ and $b = B/\alpha'$, both dimensionless, with g symmetric positive and b antisymmetric. The integer winding column w is the σ slope of θ, while the momentum column n is the integrated canonical momentum.

The antisymmetric term changes that canonical momentum. For constant backgrounds the zero-mode relation is

$$n = g\dot{\theta}_0 + bw, \qquad \dot{\theta}_0 = g^{-1}(n - bw), \qquad \theta_0' = w. \tag{II.3.15}$$

Thus $n - bw$, rather than n alone, is the kinetic covector. Choose the unique symmetric positive square root $g^{1/2}$ to express momenta in an orthonormal frame. Splitting the zero mode into $\tau \pm \sigma$ gives

$$p_{L,R} = \frac{1}{\sqrt{\alpha'}}\left[g^{-1/2}(n - bw) \pm g^{1/2}w\right]. \tag{II.3.16}$$

The plus sign belongs to the $\tau + \sigma$ sector. Squaring the two vectors makes their sum independent of the cross term and their difference independent of g and b,

$$\frac{p_L^2 + p_R^2}{2} = \frac{(n - bw)^T g^{-1}(n - bw) + w^T g w}{\alpha'}, \qquad \frac{\alpha'}{2}(p_L^2 - p_R^2) = 2n^T w. \tag{II.3.17}$$

Indeed $w^T b w = 0$. The difference therefore retains the integer level-matching pairing even as the positive norm varies continuously. For $q = (n, w)^T$, write this relation with the split bilinear form

$$\eta = \begin{pmatrix} 0 & I_d \\ I_d & 0 \end{pmatrix}, \qquad q^T \eta q = 2 n^T w \in 2\mathbb{Z}. \tag{II.3.18}$$

The form is even. Its determinant has magnitude one, so it is unimodular as an integral form on $\mathbb{Z}^{2d}$. These are direct properties of this specified lattice, not a derivation of the general classification of toroidal CFTs.

The positive quadratic form can be made explicit in charge order (n, w),

$$\alpha' \frac{p_L^2 + p_R^2}{2} = q^T \mathcal{H}(g, b) q, \qquad \mathcal{H}(g, b) = \begin{pmatrix} g^{-1} & -g^{-1} b \\ b g^{-1} & g - b g^{-1} b \end{pmatrix}. \tag{II.3.19}$$

Its off-diagonal signs follow by expanding $(n - bw)^T g^{-1} (n - bw)$. This matrix will also fix the signs of a factorized duality on a non-diagonal torus. Merely matching a source's field symbols is unsafe unless its charge order and dual-coordinate orientation agree.

Take the positive, non-diagonal example

$$\alpha' = 2, \qquad g = \begin{pmatrix} 4 & 1 \\ 1 & 3 \end{pmatrix}, \qquad b = \begin{pmatrix} 0 & \frac{1}{2} \\ -\frac{1}{2} & 0 \end{pmatrix}, \qquad n = \begin{pmatrix} 2 \\ 1 \end{pmatrix}, \quad w = \begin{pmatrix} 1 \\ 2 \end{pmatrix}. \tag{II.3.20}$$

The leading principal minors 4 and 11 show $g > 0$. Here $bw = (1, -1/2)^T$, so $n - bw = (1, 3/2)^T$. Since $g^{-1} = \frac{1}{11} \left(\begin{smallmatrix} 3 & -1 \\ -1 & 4 \end{smallmatrix} \right)$, the two terms in the norm are

$$(n - bw)^T g^{-1} (n - bw) = \frac{9}{11}, \qquad w^T g w = 20, \qquad \frac{p_L^2 + p_R^2}{2} = \frac{229}{22}, \qquad n^T w = 4. \tag{II.3.21}$$

The nonzero b matters numerically: replacing $n - bw$ by n would change the first term. This is the state used in Exercise 3.

An integral antisymmetric matrix K acts by

$$b' = b + K, \qquad n' = n + Kw, \qquad w' = w. \tag{II.3.22}$$

The kinetic covector is unchanged, $n' - b'w' = n - bw$, and $n'^T w' = n^T w + w^T K^T w = n^T w$. The triangular charge matrix has determinant one and obeys $M_K^T \eta M_K = \eta$. With $K_{12} = 1$ in (II.3.20), $Kw = (2, -1)^T$, so $n' = (4, 0)^T$ and $b'_{12} = 3/2$. Both values in (II.3.21) stay fixed. For nonintegral K, the same real algebra can hold, but $n + Kw$ fails to be integral for some allowed w. It therefore fails as a map of the whole integer charge lattice. Figure II.3.3 marks this distinction.

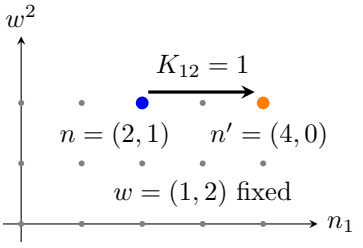


Figure II.3.3: The drawing projects the four-dimensional integer (n, w) charge lattice onto (n_1, w^2); the full shift also changes n_2. The full lattice carries the even pairing $q^T \eta q = 2n \cdot w$. An antisymmetric integral B shift shears the momentum labels by Kw while leaving w fixed. The displayed T^2 state changes $n = (2, 1)$ to $(4, 0)$ for $K_{12} = 1$. A real shear with a nonintegral entry would miss lattice points for some winding charges.

There is another kind of integral identification that changes the angular basis rather than the antisymmetric period. Let $U \in GL(d, \mathbb{Z})$ have determinant ± 1 and set $\theta' = U\theta$. An integer inverse is essential: it maps the full 2π-periodic angle lattice bijectively to itself. The winding and momentum columns transform oppositely because momentum is a covector,

$$w' = Uw, \quad n' = U^{-T} n, \quad g' = U^{-T} g U^{-1}, \quad b' = U^{-T} b U^{-1}. \tag{II.3.23}$$

Consequently

$$\begin{gathered} n' - b'w' = U^{-T}(n - bw), \\ (n' - b'w')^T (g')^{-1} (n' - b'w') = (n - bw)^T g^{-1} (n - bw), \\ (n')^T w' = n^T w. \end{gathered} \tag{II.3.24}$$

The winding norm is likewise unchanged. This is a coordinate relabelling of the same flat torus; its integrality is a stronger condition than invertibility over the real numbers.

For a concrete shear of the running T^2 example, choose $U = \left(\begin{smallmatrix} 1 & 1 \\ 0 & 1 \end{smallmatrix}\right)$. The transformed data are

$$g' = \begin{pmatrix} 4 & -3 \\ -3 & 5 \end{pmatrix}, \qquad b'_{12} = \frac{1}{2}, \qquad n' = \begin{pmatrix} 2 \\ -1 \end{pmatrix}, \qquad w' = \begin{pmatrix} 3 \\ 2 \end{pmatrix}. \tag{II.3.25}$$

Now $b'w' = (1, -3/2)^T$ and $n' - b'w' = (1, 1/2)^T$. The inverse metric is $\frac{1}{11}\left(\begin{smallmatrix} 5 & 3 \\ 3 & 4 \end{smallmatrix}\right)$, so the kinetic term is $9/11$. The winding term is still 20, and $(n')^T w' = 2 \cdot 3 - 1 \cdot 2 = 4$. This reproduces the norm $229/22$ by a transformation distinct from the B shift.

For the first-circle exchange in charge order (n, w), swap n_1 and w^1 with positive signs, leaving spectator charges in place. Requiring (II.3.19) to be invariant for every real charge determines the transformed fields. With $g = \left(\begin{smallmatrix} x & y \\ y & z \end{smallmatrix}\right)$, $b_{12} = t$ and $x > 0$, the result is

$$g'_{11} = \frac{1}{x}, \quad g'_{12} = -\frac{t}{x}, \quad g'_{22} = z - \frac{y^2 - t^2}{x}, \quad b'_{12} = -\frac{y}{x}. \tag{II.3.26}$$

The full momentum block, including the spectator momentum, is needed to recover g'. In a non-diagonal metric the coefficient of $(n_1')^2$ belongs to $(g')^{-1}$ and is generally not $1/g'_{11}$.

The coefficient comparison can be followed without a formal group action. Set $\Delta = xz - y^2 > 0$ and write the zero-mode numerator before dividing by α'. Direct inversion of g gives

$$\begin{aligned}\alpha' \frac{p_L^2 + p_R^2}{2} = {} & \frac{z(n_1 - tw^2)^2 - 2y(n_1 - tw^2)(n_2 + tw^1) + x(n_2 + tw^1)^2}{\Delta} \\ & + x(w^1)^2 + 2yw^1w^2 + z(w^2)^2.\end{aligned} \tag{II.3.27}$$

Exchange n_1 and w^1, leaving n_2, w^2 fixed. The terms quadratic in the new momentum column $n' = (n_1', n_2')^T$ give the entire inverse metric block,

$$(g')^{-1} = \frac{x}{\Delta}\begin{pmatrix} \Delta + t^2 & t \\ t & 1 \end{pmatrix}, \qquad g' = \frac{1}{x}\begin{pmatrix} 1 & -t \\ -t & \Delta + t^2 \end{pmatrix}. \tag{II.3.28}$$

Here the $x(n_1')^2$ winding term in (II.3.27) supplies the Δ in the first entry of $(g')^{-1}$. Inverting this full 2×2 block gives $g'_{11} = 1/x$, whereas $(g')^{-1}_{11} = x(\Delta + t^2)/\Delta$. To identify the antisymmetric field, write $b'_{12} = s$. The coefficient of $n_2'w'^1$ in the exchanged polynomial is $-2y/\Delta$; in $(n' - b'w')^T(g')^{-1}(n' - b'w')$ it is $2s(g')^{-1}_{22} = 2sx/\Delta$. Thus $s = -y/x$. The remaining quadratic coefficients then reproduce (II.3.26) for every charge. Since the exchanged full quadratic form is positive, its momentum block and the recovered g' remain positive.

For the numerical T^2 above,

$$g' = \begin{pmatrix} \frac{1}{4} & -\frac{1}{8} \\ -\frac{1}{8} & \frac{45}{16} \end{pmatrix}, \quad b'_{12} = -\tfrac{1}{4}, \qquad n' = \begin{pmatrix} 1 \\ 1 \end{pmatrix}, \quad w' = \begin{pmatrix} 2 \\ 2 \end{pmatrix}. \tag{II.3.29}$$

The positive exchange acts on the first entries of both charge columns. Substitution into (II.3.17) again gives 229/22 and $n'^T w' = 4$. Applying the transformation a second time restores the original fields and charges. The unreflected GPR chart instead has positive mixed components $g'_{12} = t/x$, $b'_{12} = y/x$. Its first dual output angle is opposite to the angle used here. Its first transformed momentum and winding are $-w^1$ and $-n_1$. Feeding our positive exchanged charges into those unreflected fields gives 163/22 for this example, which exposes the chart mismatch. Reflecting the first output angle changes both mixed components and both first charges, recovering (II.3.29). The local background-field version of this reflection appears in the next section.

For clarity, the transformed kinetic covector and inverse metric are

$$n' - b'w' = \begin{pmatrix} 3/2 \\ 1/2 \end{pmatrix}, \qquad (g')^{-1} = \frac{1}{11}\begin{pmatrix} 45 & 2 \\ 2 & 4 \end{pmatrix}. \tag{II.3.30}$$

Their quadratic product is 421/44, while $(w')^T g' w' = 45/4$. The sum is 229/11 before the factor $1/\alpha' = 1/2$. This independent evaluation matters because a mixed sign error can leave the radius inversion intact while breaking the non-diagonal example.

For positive Gaussian torus theories the continuous backgrounds form a local $O(d,d;\mathbb{R})/(O(d) \times O(d))$ parameter space. Integral B shifts, integer angular basis

changes and factorized exchanges provide discrete identifications in the full toroidal CFT classification. The positive-Gaussian lattice/coset classification is a sourced mathematical statement; the discrete full-worldsheet identification is separately sourced. Our finite examples establish only the displayed maps. Equality of the zero-mode norm is necessary for a CFT identification but cannot by itself identify all operators, amplitudes and global sectors. Chapter IV.4 develops the broader integral-lattice tools; no heterotic gauge-lattice classification is attempted here.

The parameter count explains why both g and b appear in this space. A symmetric $d\times d$ matrix has $d(d+1)/2$ independent entries, and an antisymmetric one has $d(d-1)/2$.

$$\frac{d(d+1)}{2}+\frac{d(d-1)}{2}=d^2. \tag{II.3.31}$$

For $d=2$ these are three metric entries and one antisymmetric entry. Positivity restricts the metric to an open region rather than removing a local parameter. The Gaussian torus classification identifies a local family with this dimension; obtaining its global quotient requires the discrete CFT identifications, beyond this count.

II.3.5 Background fields and local Buscher rules

What becomes of a circle that is fibered over another coordinate? First fix units. Let $\theta\sim\theta+2\pi$ be dimensionless and set the physical circumference coordinate $X=R\theta$, so $X\sim X+2\pi R$. The angular-frame component is $G_{\theta\theta}=R^2$ with units of length squared. A dual angle $\widetilde{\theta}$ also has period 2π; its physical coordinate is $\widetilde{X}=R'\widetilde{\theta}$, where $R'=\alpha'/R$ in the flat circle limit. Thus the angular dual metric is α'^2/R^2, while a formula written for length coordinates cannot be copied into it without the corresponding powers of α'.

Ordinary local gauging requires a circle Killing vector $k=\partial_\theta$. It must preserve the metric, the three-form $H=dB$, and the dilaton; locally $\mathcal{L}_kB$ may be a gauge-exact form. In a suitable local gauge these fields are independent of θ. The gauged worldsheet action replaces derivatives of θ by a gauge field and adds a periodic multiplier imposing its flatness. Integrating the multiplier or the gauge field gives different local descriptions. Their identification on a worldsheet with cycles also requires the multiplier period and gauge holonomies. The field components below are the local output, while the functional measure supplies a separate dilaton shift.

A flat worldsheet gauge field illustrates the global point without a curved target. On a worldsheet cylinder with periodic σ, set $a=a_\sigma d\sigma$ with constant a_σ. Its curvature is zero, yet

$$da=0,\qquad \oint_\sigma a=2\pi a_\sigma. \tag{II.3.32}$$

A single-valued small gauge transformation cannot remove an arbitrary holonomy. Integrating a nonperiodic multiplier would only impose the local flatness equation and would miss the correct sum over compact sectors. The worldsheet argument includes the multiplier period and the gauge-field holonomies; the component substitutions that follow do not reproduce that global step. This is why agreement of local metrics and spectra is not, by itself, an equality of complete worldsheet theories.

In the present Lorentzian convention the antisymmetric action gives canonical momentum $n = g\dot{\theta} + b\theta'$ for constant torus data. With $\tau = -i\tau_E$, its Euclidean antisymmetric term has negative i relative to the real integrand. The GPR chart $z = (\tau_E + i\sigma)/\sqrt{2}$ and $(g+b)\partial\theta\bar{\partial}\theta$ gives the opposite i sign. Conjugating that complex chart transposes $g + b$, and the multiplier orientation must change with the output dual coordinate. The convention used here chooses positive charge exchange $\widetilde{n}_\theta = w^\theta$ and $\widetilde{w}^\theta = n_\theta$. It is the reflected output coordinate $\widetilde{\theta}_{\text{book}} = -\widetilde{\theta}_{\text{GPR}}$. Consequently the unreflected GPR positive mixed-field signs pair with negative first exchanged charges, as the numerical T^2 check showed. This is a coordinate and charge translation, not a physical disagreement between the rules.

For a circle index θ and a base index a, the book-chart local relations in angular length-squared units include

$$\widetilde{G}_{\theta\theta} = \frac{\alpha'^2}{G_{\theta\theta}}, \qquad \widetilde{G}_{\theta a} = -\frac{\alpha' B_{\theta a}}{G_{\theta\theta}}, \qquad \widetilde{B}_{\theta a} = -\frac{\alpha' G_{\theta a}}{G_{\theta\theta}}. \tag{II.3.33}$$

The first formula reproduces $R' = \alpha'/R$. The second and third are the reflected versions that implement positive first-charge exchange. For $B_{\theta a} = 0$, the remaining base metric is the Schur complement

$$\widetilde{G}_{ab} = G_{ab} - \frac{G_{\theta a} G_{\theta b}}{G_{\theta\theta}}. \tag{II.3.34}$$

These equations are local field relations, with gauge choices and patching still to be specified if the fibration is global.

Take one base coordinate x, $h > 0$, and a circle fibration with θ-independent R, A, h,

$$ds^2 = R^2(d\theta + A\,dx)^2 + h\,dx^2, \qquad B = 0, \qquad (G_{\theta\theta}, G_{\theta x}, G_{xx}) = (R^2, R^2 A, R^2 A^2 + h). \tag{II.3.35}$$

The base component contains a square of the connection. Substituting these three entries into (II.3.33) and (II.3.34) cancels it,

$$\widetilde{G}_{\theta\theta} = \frac{\alpha'^2}{R^2}, \quad \widetilde{G}_{\theta x} = 0, \quad \widetilde{G}_{xx} = R^2 A^2 + h - \frac{(R^2 A)^2}{R^2} = h, \quad \widetilde{B}_{\theta x} = -\alpha' A. \tag{II.3.36}$$

The geometric connection has become an antisymmetric potential. In this one-coordinate base, $A(x)\,dx$ has zero exterior derivative for any smooth $A(x)$, since $dx \wedge dx = 0$. Thus the local dual $\widetilde{H} = d\widetilde{B}$ also vanishes in this two-coordinate example. On a base with at least two coordinates and a connection one-form $A = A_i(x)dx^i$, the same local rule gives $\widetilde{B} = -\alpha' d\widetilde{\theta} \wedge A$ and hence

$$\widetilde{H} = d\widetilde{B} = \alpha' d\widetilde{\theta} \wedge dA. \tag{II.3.37}$$

Only a nonzero connection curvature dA gives this local three-form contribution. A constant A gives a locally constant $\widetilde{B}$ and $\widetilde{H} = 0$; possible flat holonomy is global information, not local flux. Figure II.3.4 shows the exchange of mixed components with the orientation fixed.

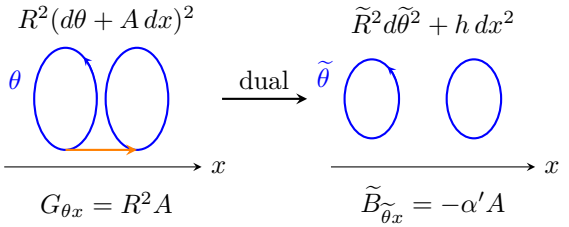


Figure II.3.4: Locally the physical circle $X = R\theta$ is fibered over x with connection $A\,dx$. In the reflected book output chart the dual angle has period 2π, the mixed metric vanishes and $\widetilde{B}_{\widetilde{\theta}x} = -\alpha' A$. For constant A the drawing does not represent H flux. Increasing θ in the input and increasing $\widetilde{\theta}$ in the output point upward; x increases rightward in both.

The dilaton changes because the gauge-field integral has a measure. Writing the physical dilaton coupling as $+\Phi R^{(2)}/(4\pi)$ and GPR's curvature coupling as $-\phi R^{(2)}/(8\pi)$ gives $\phi = -2\Phi$. Its logarithm uses the dimensionless angular component $g_{\theta\theta} = R^2/\alpha'$. The resulting physical shift is

$$\widetilde{\Phi} = \Phi - \frac{1}{2}\ln\frac{R^2}{\alpha'} = \Phi - \ln\frac{R}{\sqrt{\alpha'}}, \qquad \frac{\widetilde{g}_s}{g_s} = \frac{\sqrt{\alpha'}}{R}. \tag{II.3.38}$$

Hamiltonian covariance alone does not derive this functional-measure statement. The logarithm cannot contain R without a reference length. Its argument is the dimensionless ratio fixed by the angular metric.

For $\alpha' = 2$, $R = 3$, $A = 1/2$ and $h = 5$, the original angular metric has entries $(9, 9/2, 29/4)$ and determinant $9(29/4) - (9/2)^2 = 45$. The dual entries and determinant are

$$(\widetilde{G}_{\theta\theta}, \widetilde{G}_{\theta x}, \widetilde{G}_{xx}, \widetilde{B}_{\theta x}) = \left(\frac{4}{9}, 0, 5, -1\right), \qquad \det\widetilde{G} = \frac{20}{9}, \qquad \frac{\widetilde{g}_s}{g_s} = \frac{\sqrt{2}}{3}. \tag{II.3.39}$$

Both metrics are positive. The constant dual B has zero local three-form strength. Exercise 4 asks for each component, the determinant and the coupling ratio. The D-brane map of Chapter III.8 uses this circle operation on boundary conditions; it requires more than these closed-string field components.

Two neighboring inputs test the orientation and the role of the connection. If $A = 0$ with the same R, h, α', the original metric is diagonal, and the dual has the same diagonal entries $(4/9, 5)$ as above but $\widetilde{B}_{\theta x} = 0$. Changing only the sign to $A = -1/2$ changes the original mixed metric component to $-9/2$ while leaving $G_{xx} = 29/4$. The dual metric stays diagonal with entries $(4/9, 5)$, and

$$A = 0: \ \widetilde{B}_{\theta x} = 0, \qquad A = +\tfrac{1}{2}: \ \widetilde{B}_{\theta x} = -1, \qquad A = -\tfrac{1}{2}: \ \widetilde{B}_{\theta x} = +1. \tag{II.3.40}$$

The sign follows the reflected output coordinate, whereas the base Schur complement depends on A^2 and is insensitive to that reversal. These three backgrounds fix the local sign relation; they do not establish global equivalence for a nontrivial circle bundle.

II.3.6 Localized sources and the limit of geometry

When is the local circle rule unavailable? A circle coordinate can be periodic without generating a symmetry of the background. The gauging step requires $\mathcal{L}_k G = 0$, $\mathcal{L}_k H = 0$ and $k^\mu \partial_\mu \Phi = 0$ for $k = \partial_\theta$, with the stated local B gauge condition. A localized source can retain explicit θ dependence, even if the transverse topology includes a circle. Then k is not a Killing vector of that field configuration.

An illustrative pair of functions makes this premise test concrete. Let $r > 0$, $R > 0$, $h_0 > 0$, $Q \geq 0$, and take $|\epsilon|$ small enough that both profiles remain positive,

$$H_s(r) = h_0 + \frac{Q}{r}, \qquad H_\ell(r,\theta) = H_s(r) + \epsilon e^{-r/R}\cos\theta. \tag{II.3.41}$$

The first function has no angular dependence. The second satisfies

$$\partial_\theta H_s = 0, \qquad \partial_\theta H_\ell = -\epsilon e^{-r/R}\sin\theta. \tag{II.3.42}$$

For nonzero ϵ, the latter derivative is nonzero at generic angles. If such a function controls a metric or flux component, the corresponding Lie derivative also fails to vanish. Averaging over the circle gives

$$\frac{1}{2\pi}\int_0^{2\pi} H_\ell(r,\theta)d\theta = H_s(r), \tag{II.3.43}$$

which deletes the angular harmonic rather than dualizing it. This is why a smeared zero-mode approximation can admit an ordinary Buscher description while the localized background does not admit the same gauging step. The functions in (II.3.41) are only a transparent symmetry example. They are not an exact localized NS5 solution and do not exclude every other notion of duality.

To see which tensor premise fails, use either positive function merely as the coefficient of dr^2 in a local illustrative metric. For $k = \partial_\theta$, the radial component of its Lie derivative is

$$G_{rr} = H_\ell(r,\theta) \quad \Longrightarrow \quad (\mathcal{L}_k G)_{rr} = \partial_\theta G_{rr} = -\epsilon e^{-r/R}\sin\theta. \tag{II.3.44}$$

The same construction with $G_{rr} = H_s(r)$ has a vanishing radial Lie derivative. No coordinate periodicity can set the nonzero expression in (II.3.44) to zero. Figure II.3.5 draws both profiles at the same fixed r. In the right panel the angular average is still H_s, but the values at $\theta = 0$ and $\theta = \pi$ differ by $2\epsilon e^{-r/R}$; the missing information is precisely the angular harmonic removed by smearing.

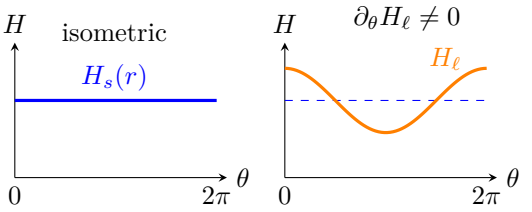


Figure II.3.5: At the same fixed r, the left angular profile is constant and admits the displayed $k = \partial_\theta$ symmetry. The right profile differs by $\epsilon e^{-r/R}\cos\theta$, so a shift of θ changes it for $\epsilon \neq 0$. Both horizontal axes run through one period $0 \leq \theta < 2\pi$. The curves illustrate a symmetry premise, not exact NS5 solutions.

The distinction persists even when an angular average matches a coefficient in an effective geometry. An average is a map from functions of (r, θ) to functions of r; it has a nontrivial kernel containing the $\cos\theta$ harmonic. A Buscher transformation of the averaged background therefore cannot reconstruct the original angle-dependent coefficient. One may use the averaged isometric background as a controlled approximation, but its dual describes the approximating input.

For an actual NS5 or KK configuration, global patching, quantized flux, circle fixed points and the string worldsheet are additional questions. The local rules above do not determine those data. This boundary matters in later fivebrane constructions: using an isometric zero mode can give a controlled geometric dictionary, while restoring localized angular data requires a separate analysis. Chapter 8 introduces the supergravity approximation; Chapter 10 applies it to the NS5 exterior and its limits. Chapter III.8 develops the brane boundary dictionary under T-duality. Exercise 5 asks for a written explanation of the failed premise rather than a numerical answer.

II.3.7 Exercises

The first four questions have exact numerical submissions in the chapter's reader companion. Use numerical JSON values for fractions and the declared field names. These submissions check the numbers; the requested explanations are written work and are not numerically graded. The fifth question calls for a written physical argument.

1. At $\alpha' = 2$, $R = 3$, $n = w = 1$ and $N_R = 1, N_L = 0$, derive p_L, p_R from the momentum and winding integrals. Calculate M^2 from both chiral shells and submit the level defect $N_R - N_L - nw$. Explain which sign would fail if the left sector were identified with the wrong chiral coordinate.

2. At $\alpha' = 2$, $R = 3$, $(n, w) = (1, 0)$ and $N_R = N_L = 1$, perform the positive charge exchange. Submit the dual radius, both integer dual charges, both dual chiral momenta and the dual mass squared. Explain why the right chiral momentum changes sign.

3. For $\alpha' = 2$ and the T^2 background $g = \left(\begin{smallmatrix} 4 & 1 \\ 1 & 3 \end{smallmatrix}\right)$, $b_{12} = 1/2$, $n = (2, 1)$, $w = (1, 2)$, calculate $(p_L^2 + p_R^2)/2$ and $n \cdot w$. Then apply the integer shift $b_{12} \mapsto b_{12} + 1$.

Submit the shifted n, new b_{12} and both invariants. Show the intermediate kinetic covector.

4. Let θ, x each have period 2π, $\alpha' = 2$, and $ds^2 = 9(d\theta + \frac{1}{2}dx)^2 + 5dx^2$ with $B = 0$. In the book dual chart with positive $n_\theta \leftrightarrow w^\theta$, submit the angular components $\widetilde{G}_{\theta\theta}, \widetilde{G}_{\theta x}, \widetilde{G}_{xx}, \widetilde{B}_{\theta x}$, the ratio $\widetilde{g}_s/g_s$, and $\det \widetilde{G}$. Explain why constant $\widetilde{B}$ is not nonzero H flux.

5. Consider an NS5 background whose transverse fields depend explicitly on an angular coordinate θ. State which condition needed for ordinary circle gauging fails. Explain what the angular average retains and loses, and why a local smeared calculation does not establish an exact localized dual. Give a written answer; this question has no numerical grading contract.

II.3.8 Take-home message

Take-home message

A closed string carries integer momentum and winding. Their chiral combination fixes the level equation $N_R - N_L = nw$, and exchanging the charges at $R' = \alpha'/R$ preserves the free spectrum while reflecting the right-moving compact field. On a flat torus the kinetic momentum is $n - bw$; integral transformations preserve its lattice and positive norm. A local isometric circle fibration trades its mixed metric for a B potential and shifts the dilaton through the worldsheet measure. The full toroidal CFT identification and the local Buscher procedure have global and source-dependent hypotheses. Periodicity of a coordinate alone does not provide the isometry required to gauge it.

Status and sources

Section 1. The distinction between the physical target circle and the closed worldsheet circle, and the opposite radius dependence of momentum and winding, are introductory [WS] statements following Tong (2009, physical PDF pp. 207–208, printed pp. 200–201, Sec. 8.2). The target metric is mostly plus, and the tension is as defined in the chapter.
Section 2. The compact chirality and positive-winding conventions are the physical circle and charge conventions stated above. Momentum and winding integrals, the two shell equations and their level sign are [WS] statements in the critical bosonic free theory, with Tong (2009, physical PDF pp. 207–208, printed pp. 200–201, Sec. 8.2, eqs. (8.4)–(8.6)) and Polchinski (1994, physical PDF pp. 82–84, printed pp. 82–84, Sec. 3.2). The $\alpha' = 2$ substitution is [MATH] under those conditions. The mode-label translation follows the chapter conventions of II.1 and II.2; it does not identify chiral sectors by typography alone.
Section 3. The radius map and self-dual bosonic currents are [WS] at the free critical-bosonic scope, following Tong (2009, physical PDF pp. 210–214, printed pp. 203–207, Secs. 8.2.3–8.3), Johnson (2000, physical PDF pp. 52–53, printed pp. 52–53, Sec. 3.3) and Polchinski (1994, physical PDF p. 84, printed p. 84, Sec. 3.2, eqs. (3.2.11)–(3.2.12), and

physical PDF pp. 85–87, printed pp. 85–87, Sec. 3.3). The finite state comparisons and local free-boson OPE are [MATH]; the full operator and global-holonomy identification is sourced [WS], not obtained from those comparisons. The genus statement is formal in the bosonic theory because its tachyon makes the vacuum expression divergent Giveon et al. (1994, physical PDF p. 18, printed p. 18, discussion before Sec. 2.4). No Type II enhancement is inferred.

Section 4. The positive Gaussian torus, dimensionless angular g, b, canonical momentum and lattice/coset statements follow Giveon et al. (1994, physical PDF pp. 18–24, printed pp. 18–24, Sec. 2.4, eqs. (2.4.1)–(2.4.29)) and the charge-order translation. The displayed norm, even unimodular form, integral shift, integer-basis shear and two-torus arithmetic are [MATH] in that scope. The general local lattice/coset classification is sourced [MATH] under the positive Gaussian hypotheses. The discrete identification of full toroidal worldsheet CFTs is separately sourced [WS]. Neither statement is established by the finite checks.

Section 5. Local Abelian gauging requires the Killing, H/B gauge, dilaton, period and holonomy conditions described by Giveon et al. (1994, physical PDF pp. 87–90, printed pp. 87–90, Sec. 4.1, eqs. (4.1.1)–(4.1.15)) and Tong (2009, physical PDF pp. 212–214, printed pp. 205–207, Sec. 8.3). The reflected mixed-component chart and physical/angular conversion are the [MATH] translation of Giveon et al. (1994, physical PDF pp. 88–89, printed pp. 88–89, eqs. (4.1.9)–(4.1.10)) and Johnson (2000, physical PDF p. 54, printed p. 54, eqs. (139)–(140)). The measure-induced dilaton shift is sourced [WS]; Hamiltonian algebra does not prove it. The flat-cylinder holonomy, numerical fibration, $A = 0$ and sign-reversal cases, and local $d\widetilde{B} = \alpha' d\widetilde{\theta} \wedge dA$ relation are [MATH] under the stated hypotheses. The original Buscher journal articles were not read; no claim is attributed to their pages.

Section 6. The local isometry premise follows Giveon et al. (1994, physical PDF pp. 87–88, printed pp. 87–88, Sec. 4.1, eqs. (4.1.3)–(4.1.6)). Differentiation and angular averaging of the illustrative functions are [MATH]. They are not an exact localized NS5 background or a general obstruction theorem.

Section 7. Exercises 1–4 ask for [MATH] consequences of the scoped [WS] inputs in Sections 2–5; Exercise 5 asks for written interpretation of the sourced isometry premise in Section 6. Numerical grading does not certify a physical premise.

Section 8. The take-home message summarizes the scoped [WS] and [MATH] statements above. The original Narain journal article was not read; the general torus statement is attributed only to the author review cited in Section 4.

References

Giveon, A., M. Porrati, and E. Rabinovici (1994). "Target Space Duality in String Theory". In: *Physics Reports* 244, pp. 77–202. arXiv: `hep-th/9401139`.

Johnson, C. V. (2000). *D-Brane Primer*. v3. arXiv: `hep-th/0007170`.

Polchinski, J. (1994). *What is String Theory?* v1. arXiv: `hep-th/9411028`.

Tong, D. (2009). *Lectures on String Theory*. v3. arXiv: `0908.0333`.

Chapter II.4

RNS superstrings, GSO projection, type IIA/IIB spectra

II.4.1 A fermion on the string

The bosonic string of Chapter 1 has transverse oscillations but no spacetime fermions. Its open-string ground state is also tachyonic. Adding a fermion to the two-dimensional worldsheet changes both features: its boundary condition determines whether a target-space spinor can appear, and its vacuum energy shifts the first physical level. We will follow one open string from boundary signs to its first vector and spinor, then tensor two chiral copies to obtain the massless type-II fields. The resulting Ramond–Ramond fields supply the potentials to which the branes of Chapter III.1 couple.

The setting is the flat critical RNS string in ten-dimensional mostly-plus Minkowski space. We use the open strip $0 \le \sigma \le \pi$, with time τ, and the same α' and oscillator mass normalization as Chapter 1. A light-cone count uses eight transverse bosons and eight transverse real fermions. This physical-state reduction is an input of the critical RNS theory; counting these oscillators does not establish the full no-ghost theorem. The Ramond spinor argument below always has a *nonzero* null momentum.

By the end of the chapter the reader can derive NS and R mode sets and vacuum energies, implement the specified first-level GSO selection, translate a covariant Dirac condition into a transverse chirality, count the massless IIA and IIB sectors, and map RR form degree to electric source dimension. Chapter 5 will combine chiral sectors differently; Chapter 8 and Chapter III.1 use the bulk fields and brane couplings obtained here.

II.4.2 Boundary signs make two fermion sectors

How can a field living on a strip know whether its ground state is a spinor? Introduce the real worldsheet fermions ψ_+^μ and ψ_-^μ. Their free equations propagate in opposite worldsheet directions, while the boundary term in the first-order action requires the two to agree up to a sign at an endpoint. Choose the sign at $\sigma = 0$ to be plus; its simultaneous reversal at both ends is a field redefinition. The remaining relative sign $\eta = \pm 1$ is physical:

$$\psi_+^\mu(\tau, 0) = \psi_-^\mu(\tau, 0), \qquad \psi_+^\mu(\tau, \pi) = \eta\, \psi_-^\mu(\tau, \pi). \tag{II.4.1}$$

The flat RNS matter action contains a first-order fermion kinetic term. Suppressing an overall normalization that does not affect the mode lattice, its structure is

$$S_F \propto \int d\tau\, d\sigma \left(i\psi_- \cdot \partial_+ \psi_- + i\psi_+ \cdot \partial_- \psi_+ \right), \qquad \partial_\pm = \partial_\tau \pm \partial_\sigma. \tag{II.4.2}$$

The equations $\partial_+ \psi_- = 0$ and $\partial_- \psi_+ = 0$ give $\psi_-^\mu(\tau, \sigma) = f^\mu(\tau - \sigma)$ and $\psi_+^\mu(\tau, \sigma) = g^\mu(\tau + \sigma)$. At $\sigma = 0$, $f^\mu(t) = g^\mu(t)$; at $\sigma = \pi$, $g^\mu(t + \pi) = \eta f^\mu(t - \pi)$. Substituting the first relation into the second, with $u = t - \pi$, gives $g^\mu(u + 2\pi) = \eta g^\mu(u)$. Thus the two endpoint conditions determine the monodromy of one chiral wave, rather than imposing periodicity on either strip field separately.

To display the reflection, let s run from 0 to 2π at fixed τ, and set $u = \tau + s$. Define the doubled wave by $\Psi^\mu(\tau + s) = \psi_+^\mu(\tau, s)$ for $0 \le s \le \pi$ and $\Psi^\mu(\tau + s) = \eta \psi_-^\mu(\tau, 2\pi - s)$ for $\pi \le s \le 2\pi$. The two branches agree at $s = \pi$ by the second endpoint condition. At $s = 2\pi$ the first endpoint condition gives $\Psi^\mu(u + 2\pi) = \eta \Psi^\mu(u)$, or

$$\Psi^\mu(u + 2\pi) = \eta\, \Psi^\mu(u), \qquad \eta = +1 \text{ (R)}, \quad \eta = -1 \text{ (NS)}. \tag{II.4.3}$$

The Ramond sector is periodic on the *doubled open strip*; the Neveu–Schwarz sector is antiperiodic there. Closed strings instead have independent left and right spin-structure choices. Figure II.4.1 shows the reflected segment and its endpoint identifications.

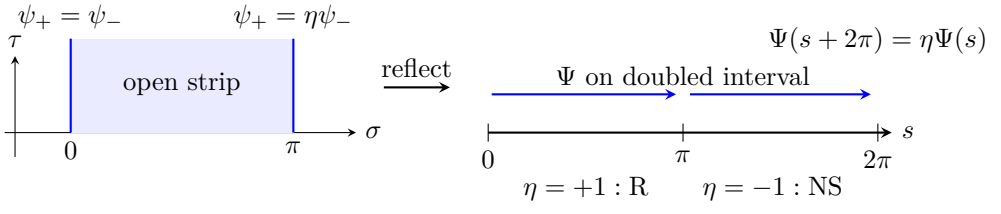


Figure II.4.1: The open strip has time τ upward and σ to the right. The signs at 0 and π identify the two chiral fermions. Reflection across the endpoints gives one doubled coordinate $s \in [0, 2\pi]$; $\eta = +1$ closes the fermion periodically (R), whereas $\eta = -1$ reverses it (NS). This is a worldsheet boundary statement, not a claim about every closed-string sector.

A Fourier wave in the chiral argument $u = \tau + s$ transported around the doubled interval acquires $e^{-2\pi i r} = \eta$. Thus periodic and antiperiodic boundary data give different mode lattices:

$$\Psi^\mu(u) = \sum_r \psi_r^\mu e^{-iru}, \qquad r \in \mathbb{Z}\ (\mathrm{R}), \qquad r \in \mathbb{Z} + \tfrac{1}{2}\ (\mathrm{NS}). \tag{II.4.4}$$

With the standard free-field normalization the modes obey

$$\{\psi_r^\mu, \psi_s^\nu\} = \eta^{\mu\nu}\delta_{r+s,0}, \qquad \{\psi_0^\mu, \psi_0^\nu\} = \eta^{\mu\nu} \quad (\mathrm{R}). \tag{II.4.5}$$

The NS set begins at $|r| = 1/2$, so its vacuum has no fermionic zero-mode degeneracy. The R set includes $r = 0$. Identifying $\psi_0^\mu = \Gamma^\mu/\sqrt{2}$ turns its zero-mode algebra into $\{\Gamma^\mu, \Gamma^\nu\} = 2\eta^{\mu\nu}$, the ten-dimensional Clifford algebra. A target spinor is therefore already present before one excites a positive-energy oscillator. For a concrete comparison, the first NS creation modes are $\psi^i_{-1/2}$, each raising the transverse level by $1/2$, whereas the first nonzero R creation modes ψ^i_{-1} raise it by 1. The R zero modes change the ground-state spin index without changing its level.

For $r > 0$, the vacuum condition is $\psi_r^i|0\rangle = 0$. A negative mode creates a quantum; applying the same component twice vanishes because $\{\psi^i_{-r}, \psi^i_{-r}\} = 0$ for $r \neq 0$. The R zero modes instead form a nondegenerate Clifford algebra. In ten dimensions its covariant complex Dirac module and chiral halves have

$$\dim S_{10} = 2^{10/2} = 32, \qquad \dim S_{10}^{\pm} = 16. \tag{II.4.6}$$

These numbers precede the massless physical equation. Neither sixteen-dimensional chirality space should be identified with the final eight polarizations until the null Dirac reduction is performed.

This step connects the chiral free-field language of Chapter 2 to target spin. Periodicity by itself gives a Clifford module; the physical Dirac condition and GSO choice will reduce it. In particular, reading "periodic" as a guarantee that all 32 covariant spinor components propagate would miss both reductions.

II.4.3 Vacuum energies and first massless levels

Which level can be massless after adding eight fermions? The answer must use the zero-point contribution of the same transverse modes whose excitations we count. Let E_0 be that regularized oscillator energy and define the intercept $a = -E_0$ in the unstretched open-string equation

$$\alpha' M^2 = N - a = N + E_0. \tag{II.4.7}$$

This definition fixes the sign. A negative NS vacuum energy means a positive intercept, even if a source uses a different shorthand for its normal-ordering constant. We use zeta regularization of the oscillator sums, not a claim that their unregulated sums converge.

For one transverse boson the ground energy is one half of the positive integer frequency sum. For one real NS fermion, anticommutation reverses the zero-point sign

and its frequencies are positive half-integers. The Hurwitz values $\zeta(-1) = -1/12$ and $\zeta(-1, 1/2) = 1/24$ give

$$E_B = \frac{1}{2}\sum_{n=1}^{\infty} n \mathrel{\widehat{=}} -\frac{1}{24}, \qquad E_{F,\mathrm{NS}} = -\frac{1}{2}\sum_{r=1/2,3/2,\ldots} r \mathrel{\widehat{=}} -\frac{1}{48}. \tag{II.4.8}$$

The hat marks regulated equality. In the R sector the positive fermionic frequencies are integers; the zero modes contribute no frequency. Hence

$$E_{F,\mathrm{R}} = -\frac{1}{2}\sum_{n=1}^{\infty} n \mathrel{\widehat{=}} +\frac{1}{24}, \qquad E_{B+F,\mathrm{NS}} = -\frac{1}{16}, \quad E_{B+F,\mathrm{R}} = 0. \tag{II.4.9}$$

The cancellation in the R pair is mode by mode after the compatible regularization; it is not obtained by inserting the bosonic-string intercept from Chapter 1.

The half-integer sum can be recovered from the Hurwitz relation $\zeta(s, 1/2) = (2^s - 1)\zeta(s)$. At $s = -1$ it yields

$$\zeta(-1, 1/2) = \left(\frac{1}{2} - 1\right)\left(-\frac{1}{12}\right) = \frac{1}{24}, \qquad E_{F,\mathrm{NS}} = -\frac{1}{2}\zeta(-1, 1/2). \tag{II.4.10}$$

This is analytic continuation of the oscillator sum. Rearranging an ordinary divergent series would not establish it. The NS and R results differ because their positive mode lattices differ, while their fermionic zero-point sign is the same.

There are $D - 2$ physical pairs in this light-cone count. Multiplication by eight in the critical $D = 10$ theory gives

$$E_{0,\mathrm{NS}} = -\frac{8}{16} = -\frac{1}{2}, \quad a_{\mathrm{NS}} = +\frac{1}{2}; \qquad E_{0,\mathrm{R}} = 0, \quad a_{\mathrm{R}} = 0. \tag{II.4.11}$$

Thus the bare NS ground state has $\alpha' M^2 = -1/2$ and the first $\psi^i_{-1/2}$ state has $N = 1/2$ and $M^2 = 0$. The R ground state has $N = 0$ and is also massless. It is still subject to its Dirac condition. Figure II.4.2 keeps levels and masses distinct so that discarding a state cannot be mistaken for shifting its mass.

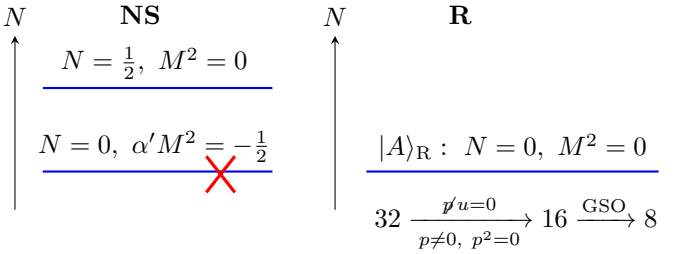


Figure II.4.2: First open-string levels at ten-dimensional criticality. The NS bare vacuum has $N = 0$ and $\alpha' M^2 = -1/2$; the one-fermion state has $N = 1/2$ and $M^2 = 0$. The R ground state has $N = M^2 = 0$. Crossing out the NS vacuum depicts the stated GSO parity choice, not a change of its intercept. For nonzero null p, $\not{p}$ is a nonzero rank-16 operator and $\not{p}\, u = 0$ leaves a 16-state kernel. The R GSO arrow then selects one chirality from that kernel.

As a check that the number $-1/2$ has a physical origin, repeat the calculation with four transverse pairs. The same sums give

$$E_{0,\mathrm{NS}}(4) = 4\left(-\frac{1}{24} - \frac{1}{48}\right) = -\frac{1}{4}, \quad a_{\mathrm{NS}}(4) = \frac{1}{4}, \qquad E_{0,\mathrm{R}}(4) = 0. \tag{II.4.12}$$

At that pair count, the first half-integer excitation would have $\alpha' M^2 = 1/2 - 1/4 = 1/4$, not zero. This arithmetic is a diagnostic of the ten-dimensional balance; it does not define a consistent critical four-pair RNS theory. Exercise 1 repeats the actual critical calculation with submitted values. The massless NS vector and R spinor can now be compared only after specifying which states survive the projection.

The critical dimension has an independent worldsheet diagnostic. A free boson contributes chiral central charge one, and a real Majorana fermion contributes one half. The reparametrization and superconformal ghosts contribute -26 and $+11$. Thus

$$c_{\mathrm{tot}} = D + \frac{D}{2} - 26 + 11 = \frac{3}{2}(D - 10). \tag{II.4.13}$$

At $D = 10$ this anomaly vanishes. This connects the eight-pair light-cone calculation to Chapter 2's conformal central-charge count. It does not prove all physical-state and modular properties. The four-pair arithmetic example also changes this anomaly and so is not a second critical model.

II.4.4 GSO selection and the physical Ramond spinor

How do we retain the first NS vector without retaining its tachyonic vacuum? Assign the NS bare vacuum $(-1)^F = -1$ and let every fermionic creation oscillator flip that sign. Projecting onto $(-1)^F = +1$ gives

$$(-1)^F|0\rangle_{\mathrm{NS}} = -|0\rangle_{\mathrm{NS}}, \qquad (-1)^F\psi^i_{-1/2}|0\rangle_{\mathrm{NS}} = +\psi^i_{-1/2}|0\rangle_{\mathrm{NS}}. \tag{II.4.14}$$

Two fermionic creation operators restore the odd sign. The first retained NS level therefore has eight transverse vector polarizations, 8_v. The higher spectrum needs its own physical constraints; the first-level parity test is only a local part of the GSO construction.

The R ground state begins with a 32-component covariant Dirac module. Its physical zero-mode condition is a massless Dirac equation. The index placement matters: with mostly-plus metric choose the native *contravariant* nonzero null ray

$$\begin{aligned} p^\mu &= (E, -E, 0, \ldots, 0), \quad E \neq 0, \\ p_\mu &= (-E, -E, 0, \ldots, 0), \\ \not{p} &= p_\mu\Gamma^\mu = -E(\Gamma^0 + \Gamma^1). \end{aligned} \tag{II.4.15}$$

Multiplication by Γ^0 converts the kernel equation into an eigenvalue equation. Since $(\Gamma^0)^2 = -1$ and $(\Gamma^1)^2 = +1$,

$$\not{p}|u\rangle = 0 \iff (1 - \Gamma^0\Gamma^1)|u\rangle = 0, \qquad P_{\mathrm{phys}} = \frac{1 + \Gamma^0\Gamma^1}{2}. \tag{II.4.16}$$

The involution $\Gamma^0\Gamma^1$ has equally large positive and negative eigenspaces, so this nonzero-momentum kernel is 16-dimensional. At $p = 0$ the Dirac operator vanishes and its kernel is 32-dimensional; the above rank argument must not be reused there. This is a state-count at generic massless momentum, not a statement about a zero-momentum gauge or collective mode.

One can verify the rank without choosing explicit gamma matrices. The Clifford algebra gives $(\Gamma^0\Gamma^1)^2 = 1$, and conjugation by Γ^0 changes the sign of $\Gamma^0\Gamma^1$, so its trace vanishes. Therefore

$$P_{\text{phys}}^2 = P_{\text{phys}}, \qquad \operatorname{tr} P_{\text{phys}} = \frac{1}{2}\operatorname{tr} 1 = 16. \tag{II.4.17}$$

This confirms the physical kernel dimension for $E \neq 0$. At $E = 0$ the operator $\not{p}$ vanishes, and the displayed projector is no longer equivalent to the Dirac equation.

To relate the sixteen states to ten-dimensional chirality, order the transverse planes as $(2,3),(4,5),(6,7),(8,9)$ and define their spin weights by

$$2S_i = -i\Gamma^{2i}\Gamma^{2i+1} \quad (i = 1,2,3,4), \qquad 2S_i = \pm 1, \qquad W = \prod_{i=1}^{4}(2S_i). \tag{II.4.18}$$

Using the ten-dimensional ordered Clifford product, rather than just the names 8_s and 8_c, yields

$$\Gamma_{11} = \Gamma^0\Gamma^1\cdots\Gamma^9 = (\Gamma^0\Gamma^1)W, \qquad \Gamma_{11}\big|_{P_{\text{phys}}} = W. \tag{II.4.19}$$

There are $\binom{4}{0} + \binom{4}{2} + \binom{4}{4} = 8$ weight assignments with an even number of minus signs, $W = +1$, and $\binom{4}{1} + \binom{4}{3} = 8$ with $W = -1$. In this local naming they are 8_s and 8_c. On our selected ray the even-minus 8_s has positive ten-dimensional chirality. A Ramond GSO chirality choice retains one of these eight-dimensional physical spaces. The usual positive choice therefore pairs with the eight NS vector states at this massless level.

For example, $(+,+,+,+)$, $(-,-,+,+)$ and $(-,-,-,-)$ all have $W = +1$, whereas $(-,+,+,+)$ has $W = -1$. Flipping one chosen sign pairs every even-minus assignment with an odd-minus assignment. In the native frame the physical sequence of dimensions is

$$32 \xrightarrow{\not{p}u=0,\ E\neq 0} 16 = 8_s \oplus 8_c \xrightarrow{\Gamma_{11}=+1} 8_s. \tag{II.4.20}$$

The first arrow imposes the massless physical-state equation; the second chooses one chirality. This order exposes the connection between transverse weights and ten-dimensional chirality.

The opposite null ray provides a useful sign control. For $p^\mu = (E,E,0,\ldots)$ one has $p_\mu = (-E,E,0,\ldots)$ and $\not{p} = E(-\Gamma^0 + \Gamma^1)$, which selects $\Gamma^0\Gamma^1 = -1$. A source using this ray may instead write $\Gamma_0\Gamma_1 = +1$: indeed $\Gamma_0 = -\Gamma^0$ and $\Gamma_1 = \Gamma^1$. Then $\Gamma_{11} = -W$ on that ray. The label 8_s alone cannot determine ten-dimensional chirality until the ray, index placement and ordered planes are fixed. It also cannot determine the sign of an RR Hodge constraint.

The two rays give a compact sign control:

p^μ	$\Gamma^0\Gamma^1$ on ker $\not{p}$	Γ_{11} on ker $\not{p}$
$(E,-E,0,\ldots)$	$+1$	W
$(E,E,0,\ldots)$	-1	$-W$

$(E \neq 0)$. (II.4.21)

An apparent mismatch between spinor tables can therefore arise just from transferring an upper-index gamma product across opposite rays. The momentum must first be lowered with the metric.

Exercise 2 tests the projection using actual state counts. Removing the tachyon while keeping both R chiralities would leave sixteen R polarizations against eight NS polarizations at the first massless level; it would not give the stated vector–spinor matching. Conversely, obtaining $8+8$ does not prove the all-level spacetime supercharge construction, modular invariance or a no-ghost theorem. Those are physical inputs of the critical RNS/GSO theory, not consequences of these finite calculations. The spinor selected on each side now determines which closed type-II spectrum we obtain.

II.4.5 Tensoring the two sides into type IIA and IIB

What changes when two copies of the massless open-sector building blocks form a closed string? A closed state has independent left and right movers, subject to their own physical conditions and level matching. At the first massless level the allowed choices are NS–NS, R–R, NS–R and R–NS. We write 8_v for an NS vector and one eight-dimensional chiral spinor for each R side. Their tensor-product dimensions are $8 \times 8 = 64$ in every sector. The two Ramond ten-dimensional chiralities are opposite for IIA and equal for IIB; the common positive-Majorana–Weyl choice in IIB is our orientation convention, not a consequence of an unlabeled $SO(8)$ character.

At the massless level each chiral side contributes zero to its own physical oscillator mass. In the notation of the open building blocks, this statement is level matching of the two zero contributions:

$$N_L - a_L = N_R - a_R = 0, \qquad (N-a)_{\mathrm{NS}} = \tfrac{1}{2} - \tfrac{1}{2} = 0, \quad (N-a)_{\mathrm{R}} = 0 - 0 = 0. \tag{II.4.22}$$

The equation compares levels only; the closed-string mass normalization is not the open formula $\alpha' M^2 = N - a$. It shows concretely why a mixed NS–R state can be level matched despite different ground energies.

The NS–NS product is shared. The tensor of two vectors splits into a trace, an antisymmetric tensor and a symmetric traceless tensor:

$$8_v \otimes 8_v = 1 \oplus 28 \oplus 35_v, \qquad 1 + \binom{8}{2} + \left[\frac{8 \cdot 9}{2} - 1\right] = 64. \tag{II.4.23}$$

These are the dilaton, two-form B_2 and graviton polarizations. The number 35 is a transverse, on-shell count, not the number of components of an unconstrained ten-dimensional symmetric tensor. For example, $8 \cdot 9/2 = 36$ counts symmetric transverse matrices and subtracting the one trace leaves 35. This is the exact reason the three familiar bulk fields fit in one 64-state sector.

The Ramond tensor product depends on chirality. The sourced spinor-to-form correspondence gives the transverse decompositions

$$\text{IIA}: \quad 8_s \otimes 8_c = 8_v \oplus 56_v, \qquad \text{IIB}: \quad 8_s \otimes 8_s = 1 \oplus 28 \oplus 35_+. \tag{II.4.24}$$

For IIA, the independent C_1 and C_3 potentials have $\binom{8}{1} = 8$ and $\binom{8}{3} = 56$ physical polarizations. For IIB, C_0 gives one, C_2 gives $\binom{8}{2} = 28$, and the constrained C_4 sector

gives half of $\binom{8}{4} = 70$, namely 35. The half-count arises from self-duality of the associated five-form *field strength*. A ten-dimensional four-form potential itself is not being equated to its Hodge dual. Figure II.4.3 displays the four-sector count without silently adding an independent copy of a dual potential.

The representation dimensions and the spacetime field identification play distinct roles. Opposite transverse spinor chiralities give the $8 + 56$ decomposition; equal chiralities give $1 + 28 + 35$ after the middle-form constraint. These products fix the on-shell sizes. The sourced RR bispinor dictionary identifies the pieces with ten-dimensional strengths and potentials. The finite $SO(8)$ tensor product alone does not establish the nonlinear field equations of those potentials.

Upper row: bosons $64 + 64 = 128$

NS–NS $8_v \otimes 8_v = 1 + 28 + 35_v$ $\phi, B_2, g:\ 64$	**R–R** IIA: $8_s \otimes 8_c = 8 + 56$ IIB: $8_s \otimes 8_s = 1 + 28 + 35_+$ 64 in either case
NS–R $8_v \otimes 8_{s/c} = 8 + 56 = 64$	**R–NS** $8_{s/c} \otimes 8_v = 8 + 56 = 64$

Lower row: fermions $64 + 64 = 128$

Figure II.4.3: Massless closed-string sectors. Each box has 64 on-shell polarizations. The NS–NS and mixed-sector totals are common; the RR box distinguishes opposite IIA and equal IIB ten-dimensional R chiralities. The 35_+ in IIB records the five-form field-strength constraint, not a self-duality equation for C_4.

The mixed sectors contain a transverse vector-spinor ψ_i with $i = 2, \ldots, 9$. Write S_s, S_c for the two transverse spinor spaces. Gamma contraction is the map $T : S_s \otimes 8_v \to S_c$ given by $T(\psi) = \Gamma^i \psi_i$, and likewise with s and c exchanged. It flips chirality since each transverse Γ^i anticommutes with the transverse chirality operator. For any χ of the target chirality, $\psi_i = \Gamma_i \chi/8$ is a right inverse, because the transverse Clifford relation gives

$$T\left(\left\{\frac{\Gamma_i \chi}{8}\right\}\right) = \frac{1}{8}\sum_{i=2}^{9} \Gamma^i \Gamma_i \chi = \chi. \tag{II.4.25}$$

Hence the trace has rank eight and its gamma-traceless kernel has dimension $64 - 8 = 56$:

$$8_v \otimes 8_s = 8_c \oplus 56_s, \qquad 8_v \otimes 8_c = 8_s \oplus 56_c. \tag{II.4.26}$$

The trace image supplies the spin-1/2 polarizations; the gamma-traceless 56_s or 56_c supplies gravitino polarizations. With the left R factor named 8_s as above, IIB uses 8_s on the right too: NS–R and R–NS each give $8_c \oplus 56_s$. IIA uses 8_c on the right: NS–R gives $8_s \oplus 56_c$ while R–NS gives $8_c \oplus 56_s$. Thus their dimensions agree although the

two IIA gravitinos have opposite chiralities and the IIB pair have the same chirality. This remains an on-shell transverse count; it does not replace the covariant gauge and field equations. Summing sectors gives

$$\begin{aligned} N_{\text{bos}} &= N_{\text{NSNS}} + N_{\text{RR}} = 64 + 64 = 128, \\ N_{\text{ferm}} &= N_{\text{NSR}} + N_{\text{RNS}} = 64 + 64 = 128. \end{aligned} \tag{II.4.27}$$

For a numerical combinatorial check in IIB, the bosonic side is (1+28+35)+(1+28+35) = 128 and the fermionic side is $(8 + 56) + (8 + 56) = 128$. IIA replaces only the second parenthesis by $8 + 56$, leaving the same total. Exercise 3 asks for the component counts, including the constrained 35.

These are linearized on-shell massless spectra of the flat critical theories. They explain which fields Chapter 8 and Chapter III.1 can use; they do not derive nonlinear supergravity interactions from the first oscillator level. In particular, one must not apply the open-string mass equation of the previous section separately to each closed chiral sector: closed-string normalization and level matching are independent inputs. The RR form degrees next turn the spectrum into a brane coupling dictionary.

II.4.6 RR potentials and electric brane dimensions

Which bulk field can an electrically charged Dp-brane source? The Ramond spin fields form a bispinor. The physical RR identification decomposes that bispinor into differential-form *field strengths*: even ranks in IIA and odd ranks in IIB. This identification is a sourced physical premise, rather than a theorem obtained solely from the $SO(8)$ dimensions. Write C_q for a q-form potential and, at the free linearized level, $F_{q+1} = dC_q$. Taking one derivative reverses the parity of the potential rank relative to the strength rank:

	$\deg F$	$\deg C = \deg F - 1$
IIA	$2, 4, 6, 8$	$1, 3, 5, 7$
IIB	$1, 3, 5, 7, 9$	$0, 2, 4, 6, 8$

(II.4.28)

The full lists are democratic descriptions. The independent local massless degrees can be represented by C_1, C_3 in IIA and by C_0, C_2 together with a C_4 whose five-form strength obeys its constraint in IIB. Magnetic dual partners in the remaining entries describe the same on-shell quanta.

The rank relation can be read in both directions. An IIA strength of rank four comes from C_3 and couples electrically to a $D2$. Its dual strength has rank six and can be represented by C_5, which couples electrically to a $D4$. The two potentials are presentations of the same free field:

$$F_{q+1} = dC_q, \qquad *F_{q+1} \sim F_{9-q} = dC_{8-q}, \qquad q \longleftrightarrow 8 - q. \tag{II.4.29}$$

The symbol $\sim$ leaves action-dependent normalization and signs unstated; the oscillator count does not prove a duality equation. The equality of complementary ranks explains the braces in Figure II.4.4.

An electric source fills a $(p+1)$-dimensional worldvolume W_{p+1}. The minimal rank-matching coupling has the form

$$S_{\text{electric}} \supset \mu_p \int_{W_{p+1}} C_{p+1}, \qquad q = p+1, \qquad p = q-1. \tag{II.4.30}$$

The integral requires the potential degree to equal the worldvolume dimension. It does not determine μ_p, its minimal quantum, or the existence of a consistent brane boundary state by dimensional degree matching alone. For $q = 0$, $p = -1$ names the Euclidean $D(-1)$ instanton coupling to the scalar C_0; it is not a negative-dimensional Lorentzian worldvolume. The mapping and its dual identifications are laid out in Figure II.4.4.

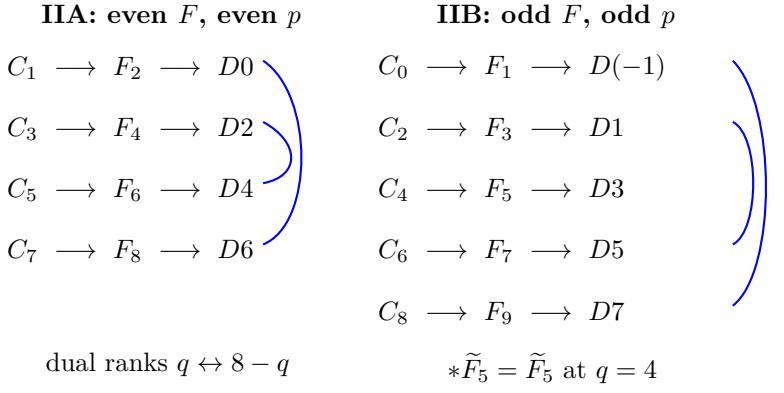


Figure II.4.4: The massless RR rank sequence. Each line reads $C_q \longrightarrow F_{q+1} \longrightarrow D(q-1)$, where the last entry is the electric source dimension. Braces connect Hodge-dual descriptions q and $8-q$; they do not indicate extra propagating polarizations. The IIB C_4 line is constrained by $*\widetilde{F}_5 = \widetilde{F}_5$. The displayed rank sequence excludes the separate massive-IIA $D8$ and top-form $D9$ extensions.

Take IIB as a worked example. C_0, C_2, C_4 lead to F_1, F_3, F_5 and to $D(-1), D1, D3$ electric couplings. Their independent transverse counts are $1, 28, 35$, summing to 64. The democratic C_6 and C_8 supply magnetic dual descriptions of the C_2 and C_0 data, often phrased as $D5$ and $D7$ electric couplings to those dual potentials. In IIA, C_1, C_3 produce F_2, F_4 and $D0, D2$, with $8 + 56 = 64$ states; C_5, C_7 describe their $D4, D6$ dual couplings. Exercise 4 asks the reader to reconstruct the full IIA rank list rather than memorize the names.

The degree counts can be checked without adding particles. A free q-form potential in ten dimensions has $\binom{8}{q}$ transverse polarizations at its propagating massless level. In a dual pair, $\binom{8}{q} = \binom{8}{8-q}$, so counting both would double the same data.

The identity follows by choosing occupied or complementary unoccupied directions among eight transverse directions. In IIA it gives

$$\binom{8}{1} = \binom{8}{7} = 8, \qquad \binom{8}{3} = \binom{8}{5} = 56, \qquad 8 + 56 = 64. \tag{II.4.31}$$

The C_7 description repeats the C_1 eight and C_5 repeats the C_3 fifty-six. Counting all four democratic entries independently would incorrectly give 128 RR bosonic states before even adding the NS–NS sector. The middle IIB case has $q = 4$: $\binom{8}{4} = 70$, and the self-dual five-form halves it to 35. On oriented transverse $\mathbb{R}^8$, the Hodge star pairs each four-index subset with its complementary subset. Its plus and minus eigenspaces therefore have equal dimension:

$$\Lambda^4(\mathbb{R}^8) = \Lambda^4_+ \oplus \Lambda^4_-, \qquad 70 = 35 + 35. \tag{II.4.32}$$

The two halves are transverse polarization spaces. The selected half is fixed by the ten-dimensional strength constraint together with the spacetime orientation, not by a free choice to delete half the components of C_4. Write $H_3 = dB_2$ and the bare RR strengths $F_3 = dC_2$ and $F_5 = dC_4$. These are the strengths used in the free linearized count. In the interacting IIB convention it is the modified strength $\widetilde{F}_5$, rather than the bare F_5, that obeys $*\widetilde{F}_5 = \widetilde{F}_5$, with

$$\widetilde{F}_5 = F_5 - \frac{1}{2} C_2 \wedge H_3 + \frac{1}{2} B_2 \wedge F_3. \tag{II.4.33}$$

The free-field counting uses its linearization. The sign of the interacting Hodge equation is part of the spacetime convention; it is not inferred from calling a transverse spinor 8_s.

This rank map is the prerequisite for a later dynamical question: why the relevant boundary conditions and worldvolume fields produce D-branes. That construction belongs to Chapter III.1. The massless rank sequence here also does not infer the Romans mass and $D8$ of massive IIA, or a $D9$/top-form extension in IIB. Their existence requires additional premises beyond propagating massless RR states. Similarly, the sourced RR coupling establishes the type of charge, while charge normalization and quantization require more than the rank map.

II.4.7 Exercises

The reader companion grades the exact submitted fields for Exercises 1–4 through the chapter's public JSON interface. Show intermediate steps in written work; those steps and the interpretation in Exercise 5 need reading beyond the numerical result.

1. In the ten-dimensional flat RNS light-cone theory, evaluate the regulated boson, NS fermion and R fermion vacuum contributions for eight pairs. Submit D, E_{NS}, E_{R}, a_{NS} and the first surviving NS level. Explain why the unstretched open-string mass equation demands $a = -E_0$.

2. With an odd NS bare vacuum and positive projected parity, determine whether zero, one and two fermion creation operators survive. Give the first NS vector count and the Ramond physical counts before and after one chirality choice at nonzero null momentum. Derive the physical projector for the native contravariant ray before interpreting the counts.

3. Tensor the IIB massless left and right spaces. Submit the NS–NS scalar, two-form and traceless-symmetric counts; the RR C_0, C_2 and constrained C_4 counts; the

two mixed-sector totals; and the final boson and fermion totals. Explain in writing why the middle RR contribution is 35 and identify the field to which the self-duality equation applies.

4. Starting from even RR field-strength parity in massless IIA, submit the independent potential ranks, the full democratic potential ranks, their field-strength ranks and the electric Dp values in matching order. Explain why listing a dual potential does not add another propagating state. Do not add the massive-IIA $D8$ extension to this massless list.

5. A student removes the bare NS tachyon and announces that the full type-II theory is supersymmetric and modular invariant. State precisely what the first-level calculation establishes. Identify the additional physical-state, all-level GSO and spacetime charge premises needed for the stronger claim. Give a written argument; this question has no numerical score.

II.4.8 Take-home message

Take-home message

Open-string endpoint signs give integer Ramond modes or half-integer Neveu–Schwarz modes. Eight transverse boson–fermion pairs produce $E_{0,\mathrm{NS}} = -1/2$ and $E_{0,\mathrm{R}} = 0$, so the specified GSO choice retains the NS massless vector and one physical Ramond eight-spinor. At nonzero null momentum, the covariant Dirac equation must be reduced before relating $SO(8)$ weights to ten-dimensional chirality. Tensoring two chiral copies gives the shared NS–NS sector and distinct IIA/IIB RR forms, with 128 bosonic and 128 fermionic on-shell states. A q-form RR potential couples electrically to a $D(q-1)$ source; democratic dual potentials do not double those states. The IIB self-duality condition constrains $\widetilde{F}_5$, not C_4.

Status and sources

Section 1. The critical RNS physical-state and light-cone eight-pair frame is sourced [WS] from Johnson (2000, physical PDF pp. 85–87, Sec. 5.1) and Polchinski (1994, physical PDF p. 66, eqs. (2.6.2)–(2.6.6)). The target metric is mostly plus and the Clifford convention is the one stated above; the chiral plane/cylinder naming uses the II.2 convention.
Section 2. Endpoint signs, doubling, mode sets and zero-mode Clifford algebra are [WS] at the free RNS scope, anchored to Johnson (2000, physical PDF pp. 85–86, eqs. (224)–(227)). The Fourier consequence of the sign is [MATH]. The diagram depicts the open doubled strip only.
Section 3. The transverse zero-point sums and physical mass formula are [WS] inputs from Johnson (2000, physical PDF p. 87, eqs. (231)–(233)). Our explicitly defined $a = -E_0$ gives $a_{\mathrm{NS}} = +1/2$ in the subtractive equation; the source's nearby prose uses the opposite shorthand sign. The zeta values, pair sums and four-pair check are [MATH]

under that regularization. Criticality and the light-cone reduction remain sourced rather than proved by these sums.

Section 4. The NS vacuum parity, first retained vector, Ramond Dirac condition and eight-state chirality selection are sourced [WS] from Johnson (2000, physical PDF pp. 88–90, eqs. (234)–(243)). The explicit native-ray covariant contraction, projector and ordered weight count are [MATH] under the stated Clifford convention and the local conventions. Johnson physical p. 89 uses the opposite contravariant ray and lower-index gamma product in eq. (241); its spinor names cannot be transferred without that translation. The all-level GSO, no-ghost, modular-consistency and spacetime-charge statements are source-level physical premises, not consequences of the finite count. The original Gliozzi–Scherk–Olive article was not read or used as a page anchor.

Section 5. The NS–NS, RR and mixed-sector representation identifications are sourced [WS] from Johnson (2000, physical PDF pp. 90–93, eqs. (243)–(250) and Insert 9). Binomial dimensions and the $128 + 128$ sum are [MATH] given those identifications. The C_4 count uses self-duality of its five-form strength, with the displayed Clifford convention; the transverse label alone does not set the signed Hodge equation.

Section 6. RR strength parity and the bispinor reading are sourced [WS] from Johnson (2000, physical PDF pp. 92–93, eqs. (248)–(250)). Potential parity and electric brane coupling are separately sourced by Polchinski (1995, physical PDF pp. 2–4, eqs. (1)–(7), and p. 6, eqs. (12)–(15)). The $q \mapsto q + 1 \mapsto q - 1$ rank map and binomial comparisons are [MATH]. The original RR source leaves potential normalization arbitrary at physical p. 6 and discusses a historical normalization comparison at physical p. 7; neither the coefficient nor its charge quantum follows from this chapter. Massive/top-form extensions and nonlinear RR dynamics are outside this massless count. The interacting $\widetilde{F}_5$ sign uses the stated chirality and orientation conventions.

Section 7. Exercises 1–4 request [MATH] consequences of the sourced flat-spectrum and RR-identification premises. The submitted fields test finite results; the written steps and Exercise 5 ask for physical interpretation, without certifying the source premises.

Section 8. The take-home message summarizes the section-scoped [WS] inputs and [MATH] reductions above.

References

Johnson, C. V. (2000). *D-Brane Primer*. arXiv: `hep-th/0007170v3`.

Polchinski, J. (1994). *What is String Theory?* arXiv: `hep-th/9411028v1`.

Polchinski, J. (1995). *Dirichlet-Branes and Ramond-Ramond Charges*. arXiv: `hep-th/9510017v3`.

Chapter II.5

Heterotic strings and gauge enhancement

II.5.1 Two different halves of one string

A closed string has two waves that travel in opposite directions. In the bosonic string of Chapter 1 they carry the same sort of oscillator. In the superstring of Chapter 4 each wave can carry a worldsheet fermion. The heterotic string makes another choice: one wave has the bosonic string's internal degrees of freedom, while the other has those of a superstring. Its first surprising feature is that the asymmetry is compatible with a single ten-dimensional spacetime. Its practical payoff is a gauge sector whose roots are momenta of the bosonic wave.

We call the wave depending on $\tau + \sigma$ *left* and the one depending on $\tau - \sigma$ *right*. The left side contains ten spacetime coordinates X^μ and sixteen internal chiral bosons Y^I; the right side contains ten X^μ and their ten real RNS partners ψ^μ. The two sets of X^μ are the two chiral parts of the *same* spacetime field. There are ten target coordinates, not twenty. Figure II.5.1 fixes the directions and the ingredients.

The chapter follows five questions. Why do the two chiral conformal theories each meet their own criticality condition? Which internal momenta produce gauge currents? When do momentum and winding produce new massless vectors? How does a circle holonomy remove some of those vectors? Finally, which part of this charge story can be carried into a comparison with K3? By the end, the reader should be able to perform the chiral charge count, distinguish evenness from self-duality, solve a heterotic circle mass shell, enumerate roots surviving a specified holonomy, and translate a T^4 charge convention between two sources.

II.5.2 Asymmetric worldsheet sectors

The immediate puzzle is whether two different critical strings can be joined without a worldsheet conformal anomaly. Criticality is imposed separately on the chiral stress

tensors. A free real boson contributes $c = 1$ to its chiral matter theory and a free real fermion contributes $c = 1/2$. The bosonic reparametrization ghosts bc contribute -26 on each side. The right RNS superconformal ghosts $\beta\gamma$ contribute $+11$; there is no corresponding superghost on the left. Therefore

$$c_L^{\text{matter}} = 10 + 16 = 26, \qquad c_R^{\text{matter}} = 10 + 10\left(\frac{1}{2}\right) = 15. \tag{II.5.1}$$

Adding the ghost components separately gives

$$c_L^{\text{ghost}} = -26, \qquad c_R^{\text{ghost}} = -26 + 11 = -15, \tag{II.5.2}$$

and hence

$$c_L^{\text{total}} = 26 - 26 = 0, \qquad c_R^{\text{total}} = 15 - 26 + 11 = 0. \tag{II.5.3}$$

The ghost numbers can also be recovered from their conformal weights, instead of memorizing the final totals. A fermionic first-order pair of weights $(\lambda, 1-\lambda)$ has $c = -2(6\lambda^2 - 6\lambda + 1)$; its bosonic counterpart has the opposite sign. Reparametrization gives $\lambda = 2$, whereas the RNS superghost has $\lambda = 3/2$. Substitution yields

$$c_{bc} = -2(24 - 12 + 1) = -26, \qquad c_{\beta\gamma} = 2\big(6 \cdot \tfrac{9}{4} - 9 + 1\big) = 11. \tag{II.5.4}$$

The right superghost cancels part of the bc contribution; it is not an extra right matter fermion. This distinction will reappear in the right mass-shell intercept, which is a physical-state condition rather than a central-charge contribution. This is the reason that the chiral mismatch works at the level of local central charges. The sixteen Y^I supply exactly the left charge missing from ten bosons; the ten right fermions supply the right charge. The picture in Figure II.5.1 displays two separate sums, not a cancellation between left and right anomalies.

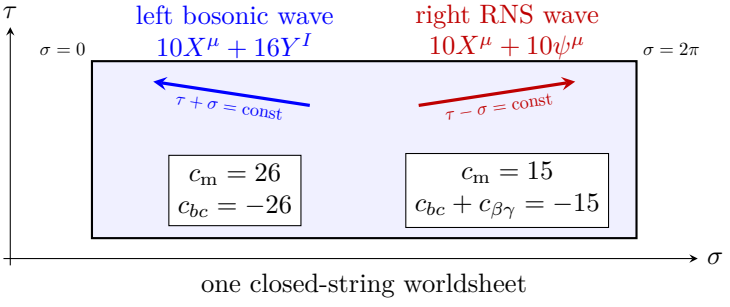


Figure II.5.1: The same closed-string cylinder carries a left wave along constant $\tau + \sigma$ and a right wave along constant $\tau - \sigma$. The edges $\sigma = 0$ and $\sigma = 2\pi$ are identified. The left $16Y^I$ and the right $10\psi^\mu$ supply different matter charges. Each sector cancels its own ghosts. The arrows label propagation conventions, not two different target spaces.

The arithmetic is sensitive to every ingredient. If one removed one internal boson while retaining the same ghosts, the left side would have

$$c_L^{\text{matter}}(15) = 10 + 15 = 25, \qquad c_L^{\text{total}}(15) = 25 - 26 = -1, \qquad c_R^{\text{total}} = 0. \tag{II.5.5}$$

The failure cannot be repaired by adding the right total: the two chiral stress tensors impose independent constraints. Conversely, $c_L = c_R = 0$ alone does not select the internal momentum lattice, the spin-structure sum, or a modular-invariant interacting theory. Those conditions are physical inputs to the heterotic construction, rather than consequences of the four sums above.

There is another useful way to see why the number sixteen belongs to the left sector. If the target dimension is held at ten and the left-moving internal count is k, then

$$c_L^{\text{total}}(k) = 10 + k - 26 = k - 16, \qquad c_R^{\text{total}} = 10 + \frac{10}{2} - 26 + 11 = 0. \tag{II.5.6}$$

The local condition has the unique solution $k = 16$ in this free-field setup. This statement does not choose between the two allowed rank-sixteen momentum lattices. Central charge sees a number of fields; the lattice choice supplies further information about the vertex operators and their pairings. That is the question of the next section.

The oscillator intercept is a second place where the two halves must be kept distinct. We write the left bosonic intercept as $a_L = 1$. In the right RNS description, $a_R = 1/2$ in the NS sector and $a_R = 0$ in the R sector. The right massless NS vector starts with a fermion oscillator of level $N_R = 1/2$; a right R ground state has $N_R = 0$. These are the physical levels after the appropriate GSO choices of Chapter 4. The original light-cone Green–Schwarz description of the right side uses a zero-intercept level N_{GS}. For a state compared at the same mass shell, its level translates as

$$N_{\text{GS}} = N_R - \frac{1}{2} \quad \text{(NS)}, \qquad N_{\text{GS}} = N_R \quad \text{(R)}. \tag{II.5.7}$$

Thus the Green–Schwarz right ground with $N_{\text{GS}} = 0$ corresponds to the RNS massless NS level $N_R = 1/2$, or to the R ground $N_R = 0$, according to its spacetime representation. It is not the NS bare vacuum at $N_R = 0$. In the source convention $\alpha' = 1/2$; here α' remains a length squared, so later momenta have inverse-length units. This translation will matter when we put a left lattice root beside a right vector oscillator.

II.5.3 Even self-dual gauge lattices

The sixteen internal bosons can carry quantized left momentum. Which momenta are allowed, and why do some become gauge fields? Write their dimensionless positive Euclidean momentum as $P \in \Lambda_{16}$. For a lattice Λ, three properties must be distinguished. It is *integral* if $P \cdot Q \in \mathbb{Z}$ for every $P, Q \in \Lambda$. It is *even* if $P^2 \in 2\mathbb{Z}$ for every $P \in \Lambda$. Its dual is

$$\Lambda^* = \{v \in \Lambda \otimes \mathbb{R} : \ v \cdot P \in \mathbb{Z} \text{ for all } P \in \Lambda\}. \tag{II.5.8}$$

It is *unimodular*, or self-dual, when $\Lambda = \Lambda^*$. For an integral lattice with a basis Gram matrix $G_{ij} = b_i \cdot b_j$, this is equivalent to $|\det G| = 1$. Evenness implies integrality by polarization, since

$$2P \cdot Q = (P + Q)^2 - P^2 - Q^2. \tag{II.5.9}$$

The converse fails: the standard $\mathbb{Z}^{16}$ has integral pairings and determinant one, but each unit basis vector has odd squared norm.

The source construction selects a positive even unimodular rank-sixteen gauge lattice. Its two possibilities, $E_8 \oplus E_8$ and D_{16}^+, are a classification result cited here, not obtained by the finite examples below. A compact internal free-boson exponential of momentum P has left conformal weight

$$h_{\text{int}} = \frac{\alpha' P_{\text{phys}}^2}{4} = \frac{P^2}{2}, \qquad P = \sqrt{\frac{\alpha'}{2}}\, P_{\text{phys}}. \tag{II.5.10}$$

The chosen dimensionless normalization makes $P^2 = 2$ a weight-one operator. Along with the right massless vector oscillator and the physical-state constraints, that is the internal ingredient of a non-Cartan gauge vector. The sixteen internal derivatives supply the Cartan currents. A root list describes a Lie algebra; it does not yet say which representations or global quotient are present.

The normalization in equation (II.5.10) has a direct dimensional check. P_{phys} has units of inverse length, so $\alpha' P_{\text{phys}}^2$ is dimensionless and can appear in a conformal weight. If the internal momentum is written as $P_{\text{phys}} = \sqrt{2/\alpha'}P$, then one unit of squared lattice norm contributes one half unit of left weight. For $P^2 = 2$, a left state with no extra oscillator has

$$h_{\text{int}} = 1, \qquad N_L = 0, \qquad h_{\text{int}} + N_L - a_L = 1 + 0 - 1 = 0. \tag{II.5.11}$$

This matches the left physical condition. The right massless vector condition is $N_R - a_R = 1/2 - 1/2 = 0$. Their joint vanishing explains why the norm-two lattice momentum can label a spacetime vector, given the sourced heterotic physical-state construction. Merely drawing an arrow of squared length two without checking its weight would not make that link.

Before accepting a rank-sixteen lattice, it helps to calculate a small root lattice by hand. In an orthonormal $\mathbb{R}^4$ basis e_i, take

$$\alpha_1 = e_1 - e_2, \quad \alpha_2 = e_2 - e_3, \quad \alpha_3 = e_3 - e_4, \quad \alpha_4 = e_3 + e_4. \tag{II.5.12}$$

Their Gram matrix and determinant are

$$G_{D_4} = \begin{pmatrix} 2 & -1 & 0 & 0 \\ -1 & 2 & -1 & -1 \\ 0 & -1 & 2 & 0 \\ 0 & -1 & 0 & 2 \end{pmatrix}, \qquad \det G_{D_4} = 4. \tag{II.5.13}$$

Every integer combination is integral and has even norm: diagonal terms contribute multiples of two and off-diagonal terms appear twice. But determinant four means the lattice generated by these roots is not unimodular. For instance

$$\alpha_1^2 = 2, \qquad (\alpha_1 + \alpha_2)^2 = (e_1 - e_3)^2 = 2, \qquad \alpha_1 \cdot \alpha_2 = -1. \tag{II.5.14}$$

There are $\binom{4}{2}$ pairs (i, j) and four independent signs for $\pm e_i \pm e_j$, hence $6 \cdot 4 = 24$ norm-two roots. Figure II.5.2 shows one plane slice and labels why its root pattern alone cannot tell us whether a full lattice equals its dual.

One can exhibit the missing dual points explicitly. The vector $v = e_1$ pairs integrally with every $x \in D_4$ because all coordinates of x are integers, yet $v \notin D_4$ because its

coordinate sum is odd. Therefore $D_4 \subsetneq D_4^*$. The determinant gives the size of the finite quotient: $|D_4^*/D_4| = 4$. This concrete witness is stronger than a visual impression of an evenly spaced root diagram. It also shows why the conditions have separate jobs. Evenness tests norm parity inside a proposed lattice; unimodularity asks whether every vector that pairs integrally with it is already included.

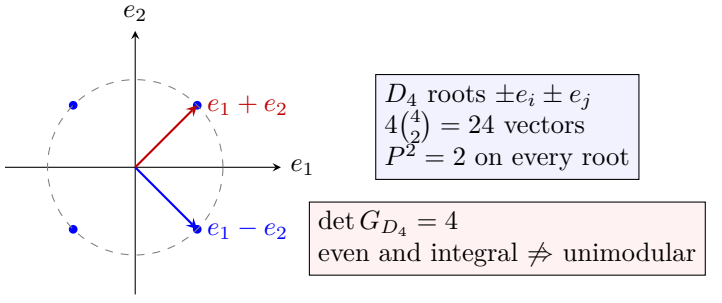


Figure II.5.2: A two-coordinate slice through the D_4 root set. Arrows $e_1 - e_2$ and $e_1 + e_2$ end at norm-two vectors; the full D_4 set contains twenty-four such vectors. The displayed slice and even norms do not imply self-duality: its full simple-root Gram determinant is four.

The glue in the two rank-sixteen examples repairs precisely this sort of missing dual-lattice information. Let

$$D_n = \{x \in \mathbb{Z}^n : \textstyle\sum_i x_i \in 2\mathbb{Z}\}. \tag{II.5.15}$$

The coordinate-sum parity map $\mathbb{Z}^n \to \mathbb{Z}_2$ has kernel D_n. Thus D_n has index two in $\mathbb{Z}^n$: its fundamental cell has volume two, and its Gram determinant, the square of that volume, is four. The integral vectors $\pm e_i \pm e_j$ have norm two. For $n = 8$, a spinor coset represented by $s_8 = (1/2, \ldots, 1/2)$ joins D_8 to form $E_8 = D_8 \cup (D_8 + s_8)$. The representative has $s_8^2 = 8/4 = 2$ and $s_8 \cdot x = (\sum_i x_i)/2 \in \mathbb{Z}$ for $x \in D_8$. For $n = 8, 16$, $s_n \notin D_n$ but $2s_n = (1, \ldots, 1) \in D_n$. Adding two vectors from the new coset therefore returns to D_n: the two-coset union closes under addition. For $x \in D_n$, $(x + s_n)^2 = x^2 + 2x \cdot s_n + s_n^2$ is even because x^2 and s_n^2 are even and $x \cdot s_n$ is integral. The larger lattice has half the D_n cell volume. Since the Gram determinant is the squared cell volume, the new determinant is

$$\det G_{E_8} = \frac{\det G_{D_8}}{2^2} = 1. \tag{II.5.16}$$

The coset has $2^7 = 128$ sign vectors of norm two, with the parity condition on minus signs. Together with $2 \cdot 8 \cdot 7 = 112$ integer roots, this gives 240 roots. Two independent copies give $E_8 \oplus E_8$ and 480 roots.

To see the sign count rather than simply quote it, a shortest half-integral vector has eight coordinates of magnitude $1/2$. There are 2^8 sign choices, and the $D_8 + s_8$ parity condition keeps half:

$$P^2 = 8\left(\frac{1}{2}\right)^2 = 2, \qquad N_{\text{half}} = \frac{2^8}{2} = 128, \qquad N_{E_8}^{P^2=2} = 112 + 128 = 240. \tag{II.5.17}$$

In contrast, sixteen half-unit coordinates have minimum norm four. The same gluing operation can therefore repair unimodularity in both ranks while changing the norm-two list only in rank eight. This is why the D_{16}^+ root count can agree with the D_{16} root count even though the two lattices are different.

For $n = 16$, the analogous extension is

$$D_{16}^+ = D_{16} \cup (D_{16} + s_{16}), \qquad s_{16} = (\tfrac{1}{2}, \ldots, \tfrac{1}{2}), \qquad s_{16}^2 = 4. \tag{II.5.18}$$

Again the index-two extension turns determinant four into one, and $s_{16} \cdot D_{16}$ is integral. A half-integral vector in this coset has norm at least four, so it supplies no new norm-two roots. The roots are exactly $\pm e_i \pm e_j$, now numbering

$$N_{D_{16}^+}^{P^2=2} = 4\binom{16}{2} = 480, \qquad 480 + 16 = 496 \tag{II.5.19}$$

including the Cartan directions in the second count. The extension is the D_{16}^+ lattice, not the unextended D_{16} root lattice. These gluing calculations illustrate parity, norm and volume; they do not prove that there are only two rank-sixteen even unimodular lattices, nor do they construct the full modular-invariant string by themselves.

The D_{16} roots have Lie algebra $\mathfrak{so}(32)$. The global heterotic gauge group is a separate question about the allowed weight and charge lattice, including the spinor coset. The sourced global form is commonly written $\mathrm{Spin}(32)/\mathbb{Z}_2$, with the relevant choice of the central subgroup. It cannot be replaced by $\mathrm{SO}(32)$ merely because both have the same Lie algebra. That distinction becomes visible again when we ask which Wilson-line shifts are genuine periods.

II.5.4 Gauge enhancement

At a generic circle radius the compact coordinate gives an abelian vector. Can a state with both momentum and winding turn into an additional massless gauge boson? Work in the no-Wilson sector and set internal gauge momentum $P = 0$. For integer momentum n and winding w, radius $R > 0$, and α' of dimension length squared, the book convention from Chapter 3 is

$$p_L = \frac{n}{R} + \frac{wR}{\alpha'}, \qquad p_R = \frac{n}{R} - \frac{wR}{\alpha'}. \tag{II.5.20}$$

The left bosonic level N_L and right RNS level N_R obey separate mass equations,

$$M_L^2 = p_L^2 + \frac{4}{\alpha'}(N_L - 1), \qquad M_R^2 = p_R^2 + \frac{4}{\alpha'}(N_R - a_R). \tag{II.5.21}$$

For a right NS vector oscillator we use $N_R = a_R = 1/2$. The mass on the two sides must agree. Subtracting the equations before setting either mass to zero and using $p_L^2 - p_R^2 = 4nw/\alpha'$ gives

$$\frac{\alpha'}{4}(M_L^2 - M_R^2) = nw + N_L - N_R - 1 + a_R = 0. \tag{II.5.22}$$

This is level matching in the chosen circle slice. It controls equality of the two shells, not their common value.

Take the left ground oscillator level $N_L = 0$ and the right NS vector level $N_R = 1/2$. The residual becomes $nw - 1 = 0$. To make the right shell massless, $p_R = 0$; to make the left shell massless, $p_L^2 = 4/\alpha'$. Thus

$$nw = 1, \qquad \frac{n}{R} = \frac{wR}{\alpha'}, \qquad p_L^2 = \frac{4}{\alpha'}. \tag{II.5.23}$$

With integer charges the elementary solutions are $(n, w) = (1, 1)$ and $(-1, -1)$ at $R^2 = \alpha'$. At that point

$$p_R = 0, \qquad p_L = \pm\frac{2}{\sqrt{\alpha'}}, \qquad M^2 = 0. \tag{II.5.24}$$

The two opposite charges supply the raising and lowering roots that join the circle Cartan current into an $\mathfrak{su}(2)$ algebra in this slice. More general charge lattices can have additional special loci. A root and its algebra alone do not identify the global group.

The condition $p_R = 0$ can be solved without guessing the radius. For n, w of the same nonzero sign it gives

$$\frac{n}{R} = \frac{wR}{\alpha'} \quad \Longrightarrow \quad R^2 = \alpha' \frac{n}{w}, \qquad p_L = \frac{2n}{R}. \tag{II.5.25}$$

The left massless condition then becomes $4n^2/R^2 = 4/\alpha'$, or $nw = 1$ after substituting the radius. Integer charges therefore force the two elementary sign-related solutions. This two-step derivation makes clear that $p_R = 0$ alone would give a candidate radius for many rational ratios n/w; the left shell removes them for the oscillator levels under discussion. Changing oscillator levels changes the question and may produce other loci. We have solved only the specified vector slice.

The dimensions matter. At $\alpha' = 3$ in length-squared units, the self-dual radius is $R = \sqrt{3}$ in length units. For $(n, w) = (1, 1)$,

$$p_L = \frac{2}{\sqrt{3}}, \quad p_R = 0, \quad p_L^2 = \frac{4}{3}, \quad M_L^2 = \frac{4}{3} - \frac{4}{3} = 0 = M_R^2. \tag{II.5.26}$$

Move to $R^2 = 12$ while keeping the same charges and levels. Then

$$p_L = \frac{1}{\sqrt{12}} + \frac{\sqrt{12}}{3} = \frac{5}{2\sqrt{3}}, \qquad p_R = \frac{1}{\sqrt{12}} - \frac{\sqrt{12}}{3} = -\frac{3}{2\sqrt{3}}, \tag{II.5.27}$$

so that

$$M_L^2 = \frac{25}{12} - \frac{4}{3} = \frac{3}{4}, \qquad M_R^2 = \frac{3}{4}, \qquad \frac{\alpha'}{4}(M_L^2 - M_R^2) = 0. \tag{II.5.28}$$

The state remains level matched but is no longer massless. This is the distinction drawn in Figure II.5.3: a zero of p_R and the left intercept condition meet at one radius, while equality of the two massive shells persists along the charge path.

For the same fixed state, the entire radius dependence can be written as a nonnegative square. With $n = w = 1$ and $N_R = 1/2$,

$$M^2 = M_R^2 = \left(\frac{1}{R} - \frac{R}{\alpha'}\right)^2, \qquad M_L^2 - M_R^2 = 0. \tag{II.5.29}$$

The first expression vanishes only at $R^2 = \alpha'$ for $R > 0$; the second vanishes at every radius. At $R^2 = 4\alpha'$ the common mass is $9/(4\alpha')$, which becomes $3/4$ when $\alpha' = 3$. The function explains the picture without hiding the left-shell check: its equality with the right expression follows from the level-matching residual, not from an independent positive-square ansatz.

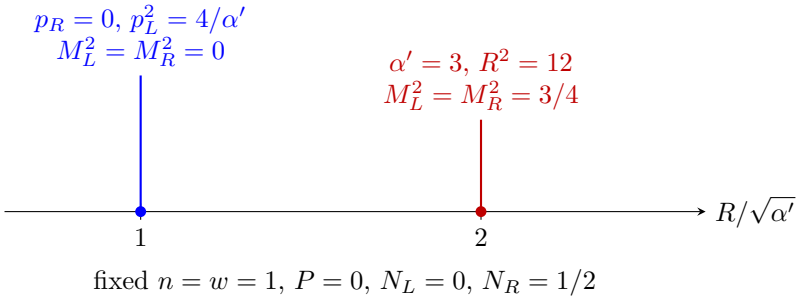


Figure II.5.3: For the fixed charges $n = w = 1$, $P = 0$, and levels $(N_L, N_R) = (0, 1/2)$, the radius $R^2 = \alpha'$ gives $p_R = 0$ and $p_L^2 = 4/\alpha'$. At the displayed off-radius point $R^2 = 4\alpha'$ both mass shells remain equal but their common M^2 is positive. The axis is $R/\sqrt{\alpha'}$; changing radius does not change the charges or oscillator levels.

The heterotic left intercept is essential. If one wrongly substituted $a_L = 1/2$ into the self-dual example, the left result would be

$$M^2_{L,\,a_L=1/2} = \frac{4}{3} + \frac{4}{3}(0 - \tfrac{1}{2}) = \frac{2}{3}, \tag{II.5.30}$$

which fails the massless level match with the right. In ten dimensions there is another instructive limit: with $n = w = 0$ and a gauge momentum $P^2 = 2$, equation (II.5.10) makes a left weight-one state at $N_L = 0$. The right NS vector oscillator supplies the other massless side. This is the gauge-root vector underlying the counts in the previous section; it is distinct from the circle root with $P = 0$. Chapter 3 supplied the momentum-winding kinematics, while this chapter's asymmetric intercepts decide which of those states become vectors.

II.5.5 Wilson lines

A gauge root may be massless before compactification but disappear from the zero-winding massless spectrum after a Cartan holonomy is turned on. Let A be a dimensionless Cartan holonomy around a circle of circumference $2\pi R$. A state with lattice

charge P acquires phase $\exp(2\pi i P\cdot A)$ after one traversal. In a local gauge where the connection is constant, the covariant circle derivative shifts the Fourier momentum. With integer Fourier label n we obtain

$$D_y=\partial_y-\frac{iP\cdot A}{R},\qquad D_y e^{iny/R}=\frac{i}{R}(n-P\cdot A)e^{iny/R}. \tag{II.5.31}$$

The sign of A depends on the covariant-derivative convention, but the zero condition is invariant under $A\mapsto -A$. For a zero-winding gauge root the compact momentum can vanish precisely when

$$n=P\cdot A\in\mathbb{Z},\qquad \exp(2\pi i P\cdot A)=1. \tag{II.5.32}$$

The integer n may change with the root. Insisting that the same $n=0$ work for every root would miss roots with integral nonzero holonomy. The equation tests the survival of pre-existing gauge roots in the $w=0$ sector. Winding and Wilson charge mix in the full compactified spectrum, so this equation cannot enumerate every massless state at a special radius.

The zero-mode criterion may equivalently be read as periodicity after parallel transport. In a gauge with periodic charged fields, the covariant derivative in equation (II.5.31) acts on $e^{iny/R}$ with shifted momentum $q=(n-P\cdot A)/R$. Gauging away the local connection instead gives a twisted boundary condition with the same spectrum. A covariantly constant mode requires $q=0$. When $P\cdot A=1$, the ordinary Fourier label is $n=1$; this state is covariantly constant although its local expression has an $e^{iy/R}$ factor. Calling it broken because $n\neq 0$ would confuse ordinary with covariant momentum.

We can do a complete finite count of these roots in D_{16}^{+}. Its norm-two roots are $P=\pm e_i\pm e_j$, $i<j$, giving 480 before the holonomy. Set

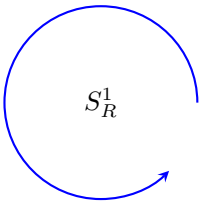
$$A=(\tfrac{1}{2},\tfrac{1}{2},0^{14}). \tag{II.5.33}$$

For the pair $(1,2)$ the four sign choices have dot products $1,0,0,-1$, all integral. A pair entirely among indices 3 through 16 also gives four integral zero products. A cross pair with exactly one index in $\{1,2\}$ gives $\pm 1/2$ and is broken. The count is

$$N_{\text{survive}}=4\binom{2}{2}+4\binom{14}{2}=4+364=368,\qquad N_{\text{broken}}=480-368=112. \tag{II.5.34}$$

For a visible pair of tests, $(e_1+e_2)\cdot A=1$ survives with $n=1$, whereas $(e_1+e_3)\cdot A=1/2$ does not. Figure II.5.4 shows the circle phase and the three pair types used in the count.

The cross-pair arithmetic is also explicit. There are $2\cdot 14=28$ choices of a pair with one index in each block, and each pair carries four sign choices. Every such root has a half-integral pairing with A, giving $28\cdot 4=112$ broken roots. The surviving pair counts sum to $1+\binom{14}{2}=92$ pairs, again with four signs each. Checking both $368+112=480$ and the partition into pair types is a useful guard against treating the two signs as only two roots per pair.



root pair for $A = (\frac{1}{2}, \frac{1}{2}, 0^{14})$
$(1, 2)$: 4 survive
$\{3, \ldots, 16\}$: 364 survive
cross pairs: 112 broken

Figure II.5.4: Left: a zero-winding root P transported around the circle acquires $e^{2\pi i P\cdot A}$. Right: for $A = (1/2, 1/2, 0^{14})$, the four roots on pair $(1, 2)$ and the 364 roots on pairs in $3, \ldots, 16$ survive, while 112 cross-pair roots do not. The table concerns root zero modes, not winding-mixed states or the global gauge group.

The origin $A = 0$ gives all 480 roots. A different half shift, $A' = (1/2, 0^{15})$, retains only pairs among indices 2 through 16:

$$N_{\text{survive}}(A') = 4\binom{15}{2} = 420, \qquad N_{\text{broken}}(A') = 60. \tag{II.5.35}$$

This is a useful counterexample to treating any half-unit shift as an invisible period. A genuine Wilson-line period must pair integrally with the charges of all allowed representations of the declared global group. A root-survival count alone sees the adjoint algebra and cannot determine that charge lattice or the quotient of Spin(32). Nor can it exclude extra vectors from nonzero winding. The full compactification conditions belong to the broader toroidal charge problem introduced in Chapter 3; the restricted calculation here tells us exactly which original gauge roots remain on this circle slice.

Even in the restricted example, the surviving roots have a visible algebraic pattern. The four roots using only indices $1, 2$ form the D_2 root set, while the 364 roots using indices $3, \ldots, 16$ form D_{14}. The sixteen Cartan currents remain Cartan currents, so the zero-winding adjoint root algebra has the local pattern $\mathfrak{so}(4) \oplus \mathfrak{so}(28)$ at this holonomy. This is a statement about Lie algebra roots in the chosen sector. It does not by itself state the compact group, all charged matter, or whether additional winding states enhance the algebra at the same background. The one-half shift A' gives a different finite pattern, with D_{15} roots and the remaining Cartan direction.

II.5.6 Compactification interface

The circle calculation suggests a more general question. Which part of its charge geometry remains useful when four heterotic directions are compactified and compared with a K3 construction? For a d-torus the book's signature convention assigns $16 + d$ positive directions to the bosonic left charge projection and d negative directions to the supersymmetric right projection. At $d = 4$ the count is

$$\Gamma^{20,4}_{\text{book}}: \quad (16 + 4)_{L,+} + 4_{R,-} = (20, 4). \tag{II.5.36}$$

This indefinite toroidal charge lattice is not the positive Euclidean Λ_{16} used for ten-dimensional internal gauge momenta. Its moduli and all of its charge vectors require the full toroidal construction, which is beyond the circle slice calculated here.

Aspinwall's K3 discussion writes the same signature as $\Gamma^{4,20}$. The notation reverses both the sector names and the sign convention used here: its *left* side is supersymmetric, its *right* side bosonic, and the latter has negative norm. Thus an enhancement root described there by

$$p_{L,\,\mathrm{source}} = 0, \qquad p^2_{R,\,\mathrm{source}} = -2 \tag{II.5.37}$$

becomes, in dimensionless book charge units,

$$p_{R,\,\mathrm{book}} = 0, \qquad p^2_{L,\,\mathrm{book}} = +2. \tag{II.5.38}$$

The change of sign is part of the quadratic-form convention, not an exchange of a physical spacelike state for a timelike one. The change of letter is a sector-name translation. Equations (II.5.37) and (II.5.38) describe one root criterion in two notations, and the latter has the familiar left weight one of equation (II.5.10).

At a generic T^4 point, the abelian rank can be read as

$$\underbrace{16}_{\text{internal Cartan}} + \underbrace{4}_{\text{metric vectors}} + \underbrace{4}_{\text{two-form vectors}} = 24. \tag{II.5.39}$$

For example, choose a book-frame charge vector with right projection zero and left norm two. It is orthogonal to the right four-plane and lies on an enhancement condition, so it can contribute a non-Cartan root if the physical state and moduli conditions are satisfied. Away from that special locus the same integral charge generally has a nonzero right projection, just as the circle state acquired positive mass away from $R^2 = \alpha'$. This comparison relates a root hyperplane and a generic rank count. It does not determine a K3 singularity, a map of background fields, or an equivalence of full spectra.

The $16 + 4 + 4$ decomposition has a direct field interpretation. The sixteen Cartan gauge fields descend from the ten-dimensional gauge sector. Reducing the metric with one index along each of four circle directions produces four Kaluza–Klein vectors. Reducing the antisymmetric two-form with one internal index gives another four. The total is rank twenty-four at a generic point, before special roots become massless. This count is a statement about generic abelian gauge fields; it does not assert that their individual couplings or charge normalizations are identical.

The norm condition is also more precise than saying that a lattice has roots somewhere. A vector v in the fixed integral lattice has projections v_L and v_R that depend on the chosen background plane. Its lattice norm is fixed, while its projections move:

$$(v,v)_{\mathrm{book}} = v_L^2 - v_R^2, \qquad (v,v)_{\mathrm{book}} = 2,\ v_R = 0 \implies v_L^2 = 2. \tag{II.5.40}$$

The root condition therefore selects both an integral charge of the right norm and a locus where its right projection vanishes. A norm-two charge at a generic plane need not produce a massless vector. The zero right projection alone does not select a root: at zero Wilson line, $v = 2(e_1 - e_2)$ in the internal D_{16} lattice has $v_R = 0$ but $v_L^2 = (v,v)_{\mathrm{book}} = 8$. The circle calculation provided a one-parameter version of exactly

this distinction. Here the cited toroidal and K3 discussion supplies the larger charge setting; our calculation is only this projection translation.

The future K3 discussion in Part III can use the signature and the root-plane condition as explicit questions: which integral charge lattice is identified, how is its positive or negative plane mapped, and which singular geometry produces the same extra states? A duality claim also needs the moduli and B field, physical-state mapping, global and discrete charge information, and a controlled regime in which both descriptions can be compared. None follows from matching the number 24 or the norm-two condition. The analogous F-theory and model-building uses later in the monograph demand their own geometric and physical arguments.

II.5.7 Exercises

Exercises 1–4 use the public exact-answer fields associated with this chapter. Submit the indicated numbers and Boolean choices, and show the intermediate argument in written work. Exercise 5 is a written interpretation task. In particular, a submitted finite count checks its arithmetic under the stated hypotheses; it does not certify a source theorem or a full compactified spectrum.

1. Take ten spacetime bosons on each side, ten right real fermions and sixteen left internal bosons. Find both matter central charges, both ghost charges and both totals. Repeat the left total with fifteen internal bosons. State why the right cancellation cannot compensate for a nonzero left total.

2. Use the four D_4 simple roots in equation (II.5.12). Count all roots $\pm e_i \pm e_j$, compute α_1^2 and $(\alpha_1 + \alpha_2)^2$, and find the simple-root Gram determinant. Is the generated lattice unimodular? Explain why your answer cannot classify the two rank-sixteen lattices.

3. Set $\alpha' = 3$, $R^2 = 3$, $P = 0$, $n = w = 1$, $N_L = 0$, $N_R = a_R = 1/2$, and $a_L = 1$. Calculate p_L^2, p_R^2, M_L^2, M_R^2 and nw. If a_L were incorrectly changed to $1/2$, what would the left mass squared become? Explain why level matching and masslessness are separate tests.

4. For zero-winding D_{16}^+ roots $P = \pm e_i \pm e_j$, take $A = (1/2, 1/2, 0^{14})$. Find total, surviving and broken root numbers. Decide whether $e_1 + e_2$ and $e_1 + e_3$ survive, using an integer Fourier mode when possible. Repeat the survivor count for $A' = (1/2, 0^{15})$. Explain why A' is not an invisible period of this zero-winding root test.

5. Translate Aspinwall's $\Gamma^{4,20}$ and his negative norm-two enhancement condition into the book's left/right and sign convention. Give the generic abelian rank in the T^4 comparison. Then list the additional physical information required to turn a root or rank match into a heterotic/K3 duality argument. This is a written task without an automatic numerical score.

II.5.8 Take-home message

Take-home message

The heterotic string joins a left critical bosonic sector to a right critical superstring sector in one ten-dimensional target. Sixteen left chiral bosons complete the left central charge and carry an even unimodular gauge lattice. Its norm-two vectors provide weight-one currents, but roots alone do not fix the global gauge group. With the heterotic intercepts, a circle state of charges $n = w = \pm 1$ becomes an extra massless root at $R^2 = \alpha'$. A Cartan holonomy removes precisely those zero-winding gauge roots with nonintegral $P \cdot A$ (holonomy phase unequal to one). On T^4, signature and root conditions supply a precise interface to K3; a duality needs further physical identifications.

Status and sources

Sections 1–2. The asymmetric ten-dimensional free heterotic construction is [WS] from Gross et al. (1985, physical PDF pp. 4–5, printed pp. 256–257, Sec. 2.1, p. 5 states $T_0 = 1/(2\pi\alpha') = 1/\pi$). The separate matter and ghost sums are [MATH] using the critical worldsheet values established in Chapters 2 and 4. The original right light-cone GS level and left intercept are [WS] from Gross et al. (1985, physical PDF p. 7, printed p. 259, eqs. (2.17)–(2.19)). The stated NS/R level translation uses the book's RNS intercepts. Central-charge arithmetic does not establish the spin-structure sum, no-ghost theorem, modular invariance or interacting consistency.

Section 3. The heterotic consistency requirements of evenness, integrality and self-duality are [WS] at the source construction scope in Gross et al. (1985, physical PDF pp. 11–13, printed pp. 263–265, eqs. (2.36)–(2.40)). The classification into two positive-definite even unimodular lattices of rank sixteen is a separate [MATH] input, cited from physical PDF p. 12, printed p. 264, rather than proved here. The D_4 Gram determinant, root enumeration, E_8 and D_{16}^+ glue calculations and weight conversion are [MATH] under the declared free-boson normalization. They illustrate the cited classification but do not prove it. The D_{16}^+ root count and massless discussion are anchored at physical PDF pp. 13–14, printed pp. 265–266, including eqs. (2.40)–(2.42). The global $\mathrm{Spin}(32)/\mathbb{Z}_2$ distinction is [WS] at GHMR physical p. 13, printed p. 265, and Witten (1998, physical PDF p. 2, printed p. 1); the Lie-algebra roots alone do not determine the quotient.

Section 4. The heterotic mass-level construction is [WS] from Gross et al. (1985, physical PDF pp. 7, 14, printed pp. 259, 266, eqs. (2.17)–(2.19), (2.42)). The circle momentum convention uses the book's Chapter 3 result. Residual, masslessness and off-radius arithmetic are [MATH] in the stated no-Wilson, $P = 0$, right NS slice. The GSO and physical-state premises are sourced rather than established by the finite shell test.

Section 5. The circle Wilson-line background and charge shifts are [WS] from Aspinwall (1996, physical PDF p. 36, printed p. 35, eqs. (79)–(84)). Equations (II.5.31)–(II.5.32) are the local Fourier-mode derivation under that sourced background premise, not formulas quoted from Aspinwall. The D_{16}^+ roots used in the count are [WS] from GHMR physical p. 13, printed p. 265. The 368 and 420 counts are [MATH] for zero-winding

gauge roots only. Gauge-period and global-group caution is [WS] from Witten (1998, physical PDF p. 2, printed p. 1). No full winding-mixed spectrum or allowed period lattice is deduced.

Section 6. The toroidal charge signature and rank premises are [WS] from Aspinwall (1996, physical PDF p. 35, printed p. 34, eqs. (77)–(78), and physical pp. 43–44, printed pp. 42–43, eq. (95)). The sector-name, sign and finite-rank translations are [MATH] under the book convention. The cited discussion of heterotic/IIA on K3 is not a duality proof here. The original Narain article was not read and supports no claim in this chapter. The full one-loop modular argument cited by GHMR lies outside the pages used here.

Section 7. Exercises 1–4 ask for [MATH] consequences of the declared physical premises. Exercise 5 is a written comparison and requires assessment of its physical argument.

References

Aspinwall, P. S. (1996). *K3 Surfaces and String Duality*. arXiv: hep-th/9611137v5.

Gross, D. J. et al. (1985). "Heterotic String Theory (I): The Free Heterotic String". In: *Nuclear Physics B* 256, pp. 253–284. DOI: 10.1016/0550-3213(85)90394-3.

Witten, E. (1998). "Toroidal Compactification Without Vector Structure". In: *Journal of High Energy Physics* 1998.02, p. 006. DOI: 10.1088/1126-6708/1998/02/006. arXiv: hep-th/9712028v1.

Chapter II.6

Orbifolds: twisted sectors, modular invariance, fixed-point spectra

II.6.1 A string can close only on the quotient

A point on a quotient target has several images in its covering space. A closed string can therefore return to an image of its starting point after one circuit of its spatial coordinate. Such a string is closed on the quotient even though its lifted path is not closed on the cover. The new boundary conditions are the first physical difference between an orbifold string and a theory obtained by retaining only invariant parent states. When a D-brane is placed at the fixed locus, an open string has endpoint labels on image branes. Projecting those labels is a second construction, acting on a different Hilbert space. Figure II.6.1 keeps the two strings separate.

We will answer five questions. Which closed sectors does a finite quotient require? How does a twist change spatial oscillators? What does changing the cycles of a worldsheet torus demand? Which open fields survive the endpoint projection? Finally, how can a discrete phase alter the torus sum and the open endpoint algebra? The answers are finite calculations inside a consistent parent string theory. They do not by themselves construct every possible orbifold CFT or determine every massless state.

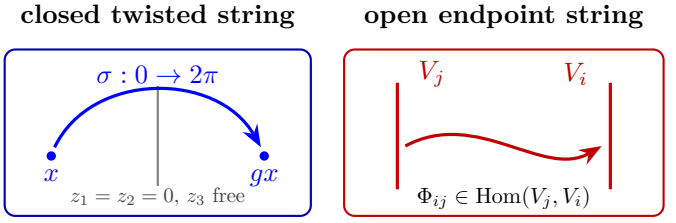


Figure II.6.1: Left: a lifted closed string runs from x to gx during one spatial circuit $\sigma \sim \sigma + 2\pi$. Its transverse displacement vanishes on the fixed line $z_1 = z_2 = 0$, along which z_3 is free. Right: an open string joins image-brane endpoint spaces V_j and V_i; its matrix is in $\mathrm{Hom}(V_j, V_i)$. The pictures represent different Hilbert spaces, even when both are supported near the same fixed locus.

II.6.2 Gauging a finite target symmetry

Why does a finite quotient need new closed states? Let Γ be a finite symmetry of the complete parent worldsheet theory. Its action must include fermions and any internal or gauge degrees of freedom, not just the visible target coordinates. For each $g \in \Gamma$ there is a space $\mathcal{H}_g$ of states quantized with spatial boundary condition

$$X(\tau, \sigma + 2\pi) = g \cdot X(\tau, \sigma). \tag{II.6.1}$$

The identity sector $\mathcal{H}_e$ contains ordinary closed strings. Retaining $\mathcal{H}_e^\Gamma$ alone would miss strings obeying (II.6.1) for $g \neq e$. For the ordinary orbifold without discrete torsion, the quotient closed state space has one sector per conjugacy class,

$$\mathcal{H}_{\mathrm{orb}} = \bigoplus_{[g]} \mathcal{H}_g^{C_\Gamma(g)}, \qquad C_\Gamma(g) = \{h \in \Gamma : hg = gh\}. \tag{II.6.2}$$

Conjugation changes the chosen lift of the same quotient string: $u\mathcal{H}_g = \mathcal{H}_{ugu^{-1}}$. Only elements of the centralizer act within a fixed g sector. The projection in that sector is

$$P_g = \frac{1}{|C_\Gamma(g)|} \sum_{h \in C_\Gamma(g)} h, \qquad P_g^2 = P_g. \tag{II.6.3}$$

The last equality follows because each element k occurs exactly $|C_\Gamma(g)|$ times in the double sum $\sum_{h,h'} hh'$. The class sum already accounts for conjugate lifts; adding a separate unweighted projected copy for every element would overcount them.

For this ordinary projection, an equivalent trace sum makes the normalization transparent. Denote by $Z[g, h]$ the trace in spatial sector g with temporal insertion h, defined explicitly in Section II.6.4. Instead of choosing one class representative, sum over each spatial element and allowed temporal insertion with one group average:

$$\frac{1}{|\Gamma|} \sum_{\substack{g,h \in \Gamma \\ gh = hg}} Z[g, h] = \sum_{[g]} \frac{1}{|C_\Gamma(g)|} \sum_{h \in C_\Gamma(g)} Z[g, h]. \tag{II.6.4}$$

For a class of size $|\Gamma|/|C_\Gamma(g)|$, every conjugate representative contributes the same trace after relabeling states. Multiplying that class size by $1/|\Gamma|$ gives $1/|C_\Gamma(g)|$. The finite sum has one projected sector per class. Its algebra alone does not specify how the individual traces transform when the torus cycles change.

The simplest fixed-set calculation makes the geometry visible. Let $\omega = e^{2\pi i/3}$ and let g act on $\mathbb{C}^3$ with weights $(1, -1, 0)$,

$$g(z_1, z_2, z_3) = (\omega z_1, \omega^{-1} z_2, z_3), \qquad 1 - 1 = 0 \pmod 3. \tag{II.6.5}$$

The nontrivial action on (z_1, z_2) lies in $SU(2)$; z_3 is a spectator. A fixed point of g must solve

$$(\omega - 1)z_1 = 0, \quad (\omega^{-1} - 1)z_2 = 0, \quad z_3 = z_3, \qquad M^g = \{(0, 0, z_3) : z_3 \in \mathbb{C}\}. \tag{II.6.6}$$

Since ω^2 and ω^{-2} are also nontrivial, g^2 has the same fixed complex line. This line can support localized twisted motion transverse to it, while a string may propagate along it. In this noncompact example a fixed-line equation is not a count of normalizable massless particles. The compact $T^6/\mathbb{Z}_3$ example used below has a different action and 27 isolated fixed points. Neither number can be transferred to the other geometry.

The coordinate test works for any power of a diagonal cyclic action. If a generator has weights $(a_1, \ldots, a_m)$ modulo n, then its pth power fixes coordinate z_α without forcing it to vanish exactly when

$$(\omega^{pa_\alpha} - 1)z_\alpha = 0, \qquad z_\alpha \text{ free iff } pa_\alpha = 0 \pmod n. \tag{II.6.7}$$

For $p = 1$ or 2 and weights $(1, -1, 0)$, only the third coordinate is free. For $p = 0$, all three are free and the identity fixes the parent. This is geometric input to a fixed-set index, not a Hilbert-space projection. The centralizer must still act on the states associated with that geometry.

For a nonabelian control, consider S_3. Its three conjugacy classes are the identity, the three transpositions, and the two three-cycles. Their centralizers have sizes 6, 2, and 3, respectively. The class-size relation can be checked without character theory:

$$|[g]|\,|C_{S_3}(g)| = 6, \qquad (|[g]|, |C(g)|) = (1, 6), (3, 2), (2, 3). \tag{II.6.8}$$

Thus the identity sector receives an S_3 projection, a representative transposition sector receives a two-element projection, and a representative three-cycle sector receives a three-element projection. Writing $t = (12)$ and $c = (123)$ makes these operations explicit:

$$P_e = \frac{1}{6}\sum_{u \in S_3} u, \qquad P_t = \frac{1}{2}(e + t), \qquad P_c = \frac{1}{3}(e + c + c^2). \tag{II.6.9}$$

The identity in P_t and P_c acts on their respective twisted spaces. Replacing these two averages by P_e would be invalid: an element outside the centralizer sends the selected twisted space to a conjugate one. In the abelian $\mathbb{Z}_3$ example every element centralizes every other, so each twisted sector instead uses a three-element average. The same numbers count commuting ordered pairs:

$$\#\{(g, h) \in S_3^2 : gh = hg\} = 1 \cdot 6 + 3 \cdot 2 + 2 \cdot 3 = 18. \tag{II.6.10}$$

A transposition commutes only with itself and the identity; a three-cycle commutes with both three-cycles and the identity. Thus one reconstructs 18 without listing all 36 ordered pairs. Calling these "18 sectors" would be wrong. Eighteen counts torus labels before averaging, whereas (II.6.2) has one projected Hilbert space per class, hence three in this example. The temporal insertion h in a torus trace must commute with its spatial twist g, so this finite count will recur in the torus calculation. It also shows why an unrestricted h sum inside each twisted sector is incorrect. Chapter 2 supplies the state and operator language behind the sectors; Part III develops the group action and geometry further.

II.6.3 Twisted oscillators

What does the boundary condition do to a coordinate before any GSO or mass-shell analysis? Take a complex coordinate Z with a twist $e^{2\pi i\theta}$, where $0 \le \theta < 1$. If g^p acts on a cyclic weight a in $\mathbb{Z}_n$, the fractional part of pa/n is θ. At fixed worldsheet time expand Z into spatial Fourier waves $e^{ik\sigma}$. The boundary condition demands

$$e^{ik(\sigma+2\pi)} = e^{2\pi i\theta}e^{ik\sigma} \quad \Longrightarrow \quad e^{2\pi i(k-\theta)} = 1 \quad \Longrightarrow \quad k \in \mathbb{Z} + \theta. \tag{II.6.11}$$

Conjugating the boundary equation gives a different set for $\bar{Z}$,

$$\bar{Z}(\sigma + 2\pi) = e^{-2\pi i\theta}\bar{Z}(\sigma), \qquad k_{\bar{Z}} \in \mathbb{Z} - \theta. \tag{II.6.12}$$

These k are exponents of spatial waves. Assigning left- and right-moving creation operators needs the full time-dependent field expansion and the chosen worldsheet fermion formulation. The two sets above are not, by themselves, a physical-state spectrum.

A real target plane contains two real coordinate functions, packaged as $Z = X^1 + iX^2$ and $\bar{Z} = X^1 - iX^2$. The group rotates the plane through $2\pi\theta$, so conjugation reverses the rotation. A single integer label m therefore appears as $m + \theta$ in one complex combination and $m - \theta$ in the other. Assigning both combinations $m + \theta$ would give the wrong boundary behavior when reconstructing X^1 and X^2. At $\theta = 0$ the two shifted sets coincide, as ordinary periodic coordinates require.

The fate of the coordinate zero mode follows immediately. A spatially constant term has $k = 0$. For $0 < \theta < 1$, neither shifted integer set contains zero. In the untwisted case $\theta = 0$, both do:

$$k = 0 \in \mathbb{Z} + \theta \iff \theta = 0, \qquad Z_{\text{constant}} \text{ is absent when } 0 < \theta < 1. \tag{II.6.13}$$

This is why a twisted string cannot translate freely in the rotated plane. Translation along a spectator fixed direction, such as z_3 in (II.6.6), remains available. The distinction between transverse and tangent motion is a useful way to read Figure II.6.1.

The zero-mode test also has a geometric form. A constant Z_0 would obey $Z_0 = e^{2\pi i\theta}Z_0$. For a nontrivial phase only $Z_0 = 0$ works. This is the fixed-coordinate equation applied to the string's center in that plane. Oscillator modes still fluctuate around that center, so an absent coordinate zero mode does not mean an empty twisted Hilbert

space. It means the transverse center cannot be moved away from the fixed set while retaining that boundary condition.

For an explicit numerical calculation, take $n = 5$, weight $a = 2$, and $p = 1$. Then $\theta = 2/5$. The positive shifted labels are obtained by listing integers, rather than by guessing a fractional frequency:

$$\begin{aligned} k_Z &= m + \tfrac{2}{5} \quad (m = 0, 1, \ldots) \quad &&= \tfrac{2}{5}, \tfrac{7}{5}, \tfrac{12}{5}, \ldots, \\ k_{\bar{Z}} &= m - \tfrac{2}{5} \quad (m = 1, 2, \ldots) \quad &&= \tfrac{3}{5}, \tfrac{8}{5}, \tfrac{13}{5}, \ldots. \end{aligned} \tag{II.6.14}$$

Figure II.6.2 places the two positive sets on the same k axis. The distinct first dots are the observable arithmetic consequence of complex conjugation; neither row has a dot at zero.

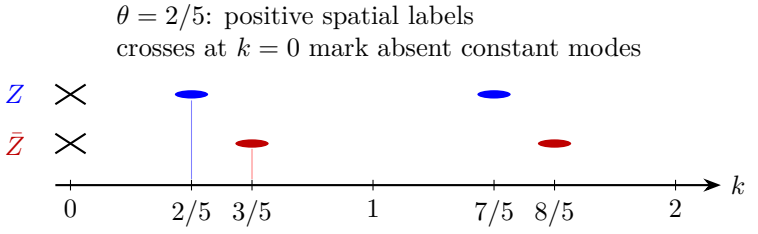


Figure II.6.2: First positive spatial Fourier exponents for a $2/5$ twist. Blue marks $\mathbb{Z} + 2/5$ for Z and red marks the positive part of $\mathbb{Z} - 2/5$ for $\bar{Z}$. Crosses mark the absent constant terms. The dots label spatial waves, not physical oscillator states after GSO and mass-shell conditions.

For $p = 0$, both sets become integers and their first two strictly positive labels are $1, 2$, in addition to the constant mode. If the chosen group element is g^2 instead, the fractional part is $4/5$; its positive Z labels begin $4/5, 9/5$ and its conjugate labels begin $1/5, 6/5$. Thus the shift tracks the actual element, not merely the abstract cyclic group.

$$\theta(g^2) = \tfrac{4}{5}, \qquad k_Z^+(g^2) = \{\tfrac{4}{5}, \tfrac{9}{5}, \ldots\}, \qquad k_{\bar{Z}}^+(g^2) = \{\tfrac{1}{5}, \tfrac{6}{5}, \ldots\}. \tag{II.6.15}$$

The superscript $+$ selects positive exponents; it is not a new chirality or a creation-operator convention.

The sign of a spatial exponent matters even when only positive labels are requested. For the $2/5$ twist, $-2/5$ belongs to $\mathbb{Z} - 2/5$ and is a valid conjugate exponent, while the first *positive* one is $3/5$. The first positive label follows by choosing the least integer m with $m - \theta > 0$. Interchanging Z and $\bar{Z}$ changes this answer from $2/5$ to $3/5$. Exercise 1 uses that distinction.

The original $T^6/\mathbb{Z}_3$ heterotic construction gives a useful example of how much more is needed for masslessness. Its specified light-cone Green–Schwarz twist has oscillator shifts $\pm 1/3$. Its particular spin action, E_8 gauge embedding, and physical-state projection yield nine untwisted and 27 fixed-point twisted positive-chirality **27** multiplets of E_6, hence

$$N_{\mathbf{27}}^{\text{untwisted}} = 9, \qquad N_{\mathbf{27}}^{\text{twisted}} = 27, \qquad N_{\mathbf{27}}^{\text{total}} = 36. \tag{II.6.16}$$

The lift in this example is concrete. The geometric order-three rotation lies in $SU(3)$ and the source selects an $E_6 \times SU(3)$ subgroup of the first E_8. The group generator acts through the center of this gauge $SU(3)$, together with the specified action on spacetime fermions that has order three. This choice leaves $E_6 \times SU(3) \times E_8$ unbroken in the stated model. In the untwisted quantization, its projection retains three copies of $(\mathbf{27}, \mathbf{3})$ under $E_6 \times SU(3)$. Ignoring the latter flavor label only after this step gives $3 \cdot 3 = 9$ positive-chirality E_6 multiplets.

$$3(\mathbf{27}, \mathbf{3}, \mathbf{1}) \quad \longrightarrow \quad 3 \cdot \dim(\mathbf{3}) = 9 \text{ copies of } \mathbf{27}_{E_6}. \tag{II.6.17}$$

This is a representation count within the specified lift, not a character decomposition of every heterotic orbifold.

In a nontrivial twisted sector, the compact coordinate oscillators carry shifts $+1/3$ or $-1/3$, while the two uncompactified transverse coordinates remain integrally moded. The source uses a light-cone Green–Schwarz description. Only its two unshifted spacetime fermions have zero modes, giving the needed right-moving helicity doublet. On the gauge side, the paper realizes an $O(16) \times O(16)$ subgroup with 32 fermions. Its chosen twist reduces the first factor through $O(10) \times SU(3)$; the ten unshifted fermions provide a spinor that the complete gauge-sector construction fills into an E_6 **27**. This source-specific state construction supplies one positive-chirality **27** at each of the 27 isolated fixed points. The inverse-twist sector contains the corresponding antiparticles. These facts explain the terms in (II.6.16); they are not conclusions of the simple spatial Fourier calculation or a generic rule for $SU(3)$ orbifolds. Here the 27 is a model-specific physical spectrum result, not the general rule "one massless multiplet per fixed point." The Fourier calculation in (II.6.11) knows neither a fermion zero-mode projection nor a gauge embedding. Chapter 4 supplies GSO language, while Chapter 5 shows why internal gauge data matter in a heterotic model. The next question is how these spatial twists are organized when the worldsheet itself is a torus.

II.6.4 Torus sectors and modular closure

A torus has two independent cycles, so a twisted partition function needs two ordered holonomies. Write its covering plane as $\mathbb{C}/(\mathbb{Z} + \tau\mathbb{Z})$, with the spatial A cycle of period 1 and the temporal B cycle of period τ, $\operatorname{Im}\tau > 0$. Let g act on A and h on B. Traversing the boundary of a fundamental parallelogram in two orders gives gh and hg; consistency requires

$$(g, h) \in \Gamma^2, \qquad gh = hg. \tag{II.6.18}$$

In operator language, h is an insertion in the g-twisted trace. For a consistent lift and a chosen insertion phase, we denote it by

$$Z[g, h](\tau) = \operatorname{Tr}_{\mathcal{H}_g}\left(h\, q^{L_0 - c/24} \bar{q}^{\bar{L}_0 - \bar{c}/24}\right), \qquad q = e^{2\pi i \tau}. \tag{II.6.19}$$

Summing over $h \in C_\Gamma(g)$ in this trace gives the centralizer projector of (II.6.3). Summing over spatial twists supplies the other sectors. This gives a second view of the class decomposition and explains why the pair count in (II.6.10) is relevant to the torus.

For S_3, the 18 commuting pairs contribute to the three class projectors in distinct proportions. The identity spatial twist has six temporal insertions. Each of the three transposition twists has two, and each of the two three-cycle twists has three. Dividing the all-element sum by six gives exactly the class-weighted sum in (II.6.4). A temporal element that fails to commute with a selected spatial transposition would take its Hilbert space to a different conjugate sector, so it cannot be inserted in the trace over that single sector. This gives an operator explanation of the commuting-pair restriction, independent of the torus picture.

To see which pairs must accompany one another, change the oriented cycle basis by an integer row matrix of determinant one,

$$\begin{pmatrix} A' \\ B' \end{pmatrix} = \begin{pmatrix} k & l \\ m & n \end{pmatrix} \begin{pmatrix} A \\ B \end{pmatrix}, \qquad kn - lm = 1. \tag{II.6.20}$$

Because g and h commute, transport along $kA + lB$ has holonomy $g^k h^l$, and similarly for B'. The two new geometric periods are $k + l\tau$ and $m + n\tau$. Normalizing the first to one gives

$$(g', h') = (g^k h^l, g^m h^n), \qquad \tau' = \frac{m + n\tau}{k + l\tau}. \tag{II.6.21}$$

The period ratio is part of the transformation; a formula for pairs alone is not enough to identify a modular operation. Figure II.6.3 shows the row conventions and the ordinary trace T.

The determinant condition in (II.6.20) keeps the new cycles as an oriented integral basis. It is the reason the new parallelogram is another fundamental torus domain rather than a multiple cover. If one supplied only a pair map such as $(g, h) \mapsto (gh, h)$, the map could be associated with the upper shear U but would not determine which normalized complex period is being called τ'. Computing periods before writing a trace identity prevents this ambiguity.

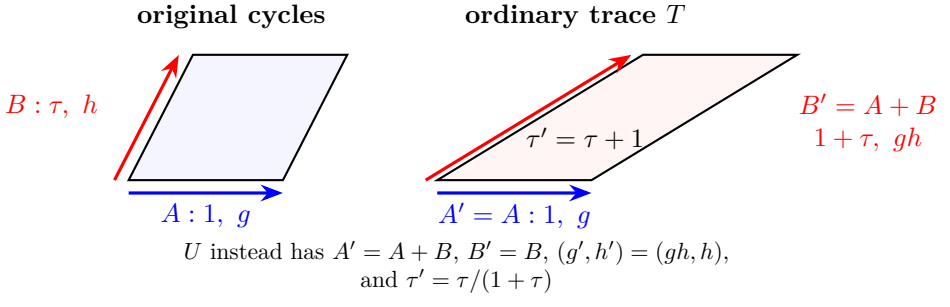


Figure II.6.3: The A cycle is spatial with period 1 and twist g; B is temporal with period τ and insertion h. The ordinary trace T keeps A and replaces B by $A + B$, so $\tau \mapsto \tau + 1$ and $(g, h) \mapsto (g, gh)$. The distinct upper shear U replaces A by $A + B$, giving (gh, h) and $\tau/(1 + \tau)$. Arrowheads define the positive cycle orientations.

The generators and a commonly confused shear are obtained by direct substitution:

	(A', B')	(g', h')	τ'
S	$(-B, A)$	(h^{-1}, g)	$-1/\tau$
T	$(A, A+B)$	(g, gh)	$\tau+1$
U	$(A+B, B)$	(gh, h)	$\tau/(1+\tau)$

(II.6.22)

The T in a trace is the lower shear shown here. Calling the upper shear T transposes which cycle carries the twist. The inverse of S or a passive pullback changes the written formula again, so every cycle statement needs its declared convention.

There is also an operator condition behind the T entry. Directly replacing τ by $\tau+1$ in (II.6.19) inserts the full phase

$$\exp\left[2\pi i\left(L_0 - \bar{L}_0 - \frac{c-\bar{c}}{24}\right)\right]$$

in the g-twisted trace. Thus a state of spin $s = L_0 - \bar{L}_0$ carries $e^{2\pi i[s-(c-\bar{c})/24]}$, not automatically $e^{2\pi i s}$. The spin-only form applies if the relevant total trace has a trivial vacuum phase, for example when its total $c-\bar{c}$ vanishes modulo 24. If the trace is a matter contribution with a nontrivial vacuum phase, the remaining sectors and their lift must supply its compensating phase; no such compensation follows from the matter trace alone. With a complete, anomaly-free lift and level matching for which the full insertion acts as the declared spatial action g on $\mathcal{H}_g$, and with compatible temporal insertion phases, one obtains the conditional trace relation

$$Z[g,h](\tau+1) = Z[g,hg](\tau). \tag{II.6.23}$$

Finite closure of the pairs does not establish this operator condition, the required spin-structure sum, or absence of an orbifold anomaly.

The cyclic $\mathbb{Z}_3$ case gives a complete finite example. Write $g = \omega^a$ and $h = \omega^b$, with $a, b \in \mathbb{F}_3$. Then the pair actions are

$$S(a,b) = (-b, a), \qquad T(a,b) = (a, a+b) \pmod 3. \tag{II.6.24}$$

Starting at $(0,1)$, the successive S and T images reach $(2,0), (0,2), (1,0)$ and then all pairs with both entries nonzero. An explicit enumeration avoids hiding the orbit size:

$$\mathcal{O}_{(0,1)} = \{(0,1),(0,2),(1,0),(2,0),(1,1),(1,2),(2,1),(2,2)\}, \qquad |\mathcal{O}_{(0,1)}| = 8. \tag{II.6.25}$$

The zero pair $(0,0)$ is fixed and forms its own orbit. A sum that included $(0,1)$ but omitted $(2,0)$ would fail even the finite S closure test. A sum over these nine pairs passes that test; its actual partition functions still need the CFT consistency conditions just described. Figure II.6.4 makes both statements visible without assigning a partition-function value to a vertex.

It is possible to verify the orbit without trusting a drawing. S takes $(0,1)$ to $(2,0)$, then to $(0,2)$ and $(1,0)$; applying T to $(1,0)$ gives $(1,1)$ and $(1,2)$. The S image of $(1,2)$ is $(1,1)$ modulo three, while the S image of $(1,1)$ is $(2,1)$. Applying T to $(2,1)$ gives $(2,0)$ and then $(2,2)$ in successive steps, completing the eight nonzero pairs. Each

image is nonzero because an invertible integer cycle change remains invertible modulo three. The zero pair consequently cannot join this orbit.

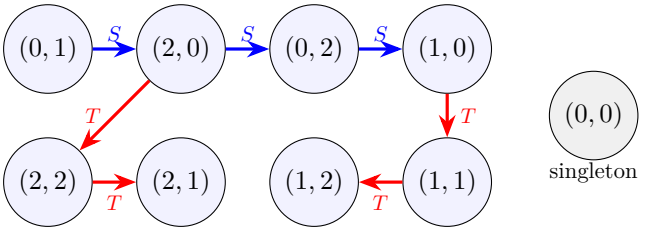


Figure II.6.4: The eight nonzero ordered $\mathbb{Z}_3$ pairs form one orbit under the indicated S and ordinary trace T actions; $(0,0)$ is a singleton. The vertices are sector labels, not values of $Z[g,h]$. The leftmost S arrow takes $(0,1)$ to $(2,0)$.

Let M be the smooth compact parent of a suitable supersymmetric sigma model. With a well-defined Euler index, a consistent group lift, and fixed-set Euler characteristics for every commuting pair, the orbifold index is given by the fixed-set sum

$$\chi_{\mathrm{orb}} = \frac{1}{|\Gamma|} \sum_{\substack{g,h\in\Gamma \\ gh=hg}} \chi(M^{g,h}), \qquad M^{g,h} = M^g \cap M^h. \tag{II.6.26}$$

This is an index statement supplied by the supersymmetric orbifold construction, not a formula derived from the finite orbit table. In the specified compact $T^6/\mathbb{Z}_3$ example, the identity-pair term has Euler characteristic zero, while each of the eight nonzero pairs has the 27 common fixed points of that action. Substitution gives

$$\chi_{\mathrm{orb}} = \frac{0 + 8(27)}{3} = 72. \tag{II.6.27}$$

The factor 27 can itself be understood in that compact model's hexagonal two-torus geometry. For one complex torus $\mathbb{C}/\Lambda$ with $\Lambda = \mathbb{Z} + \omega\mathbb{Z}$, a point fixed by multiplication by ω obeys $\omega z = z + \lambda$ for some $\lambda \in \Lambda$. Shifting the representative z by a lattice vector changes λ by an element of $(1-\omega)\Lambda$. Fixed points are counted by

$$\Lambda/(1-\omega)\Lambda, \qquad [1-\omega]_{(1,\omega)} = \begin{pmatrix} 1 & 1 \\ -1 & 2 \end{pmatrix}, \qquad |\det[1-\omega]| = 3. \tag{II.6.28}$$

There are three fixed classes per complex torus and hence $3^3 = 27$ on the product of three such factors. This belongs to the specified compact geometry, rather than every order-three action. For a nonidentity pair (g^a, g^b) here, at least one power is nontrivial and their common fixed set is those same 27 points. That accounts for the eight equal terms in (II.6.27). Connecting this index to the 36 heterotic families of (II.6.16) requires that particular spin and gauge lift; the geometric sum by itself does not provide it. Likewise, an Euler count for a suitable compact model does not assert that every noncompact fixed set has a normalizable massless mode or that every quotient has a crepant resolution. The next section adds D-branes and therefore a different projection.

II.6.5 Open invariant states

An open string ending on image branes carries Chan–Paton labels at its two ends. Write their total endpoint space as $V = \mathbb{C}^K = \bigoplus_i V_i$, where $V_i \simeq \mathbb{C}^{N_i}$ and $K = \sum_i N_i$. The labels transform in a unitary representation $\gamma\colon \Gamma \to U(K)$. The open gauge field A_μ transforms only through its labels, while a transverse scalar Φ_α also transforms under the geometric action R on its coordinate. In a basis that diagonalizes the cyclic target action on these scalar species, $R_\alpha(g)$ is the scalar eigenvalue for Φ_α. Their invariant-field equations are

$$A_\mu = \gamma(g) A_\mu \gamma(g)^{-1}, \qquad \Phi_\alpha = R_\alpha(g)\gamma(g)\Phi_\alpha\gamma(g)^{-1}. \tag{II.6.29}$$

These are projections on the open-string vector space. They do not identify Φ_α with a closed g-twisted state in $\mathcal{H}_g$. The latter has a twisted spatial boundary condition; the former has two endpoints and a matrix of endpoint labels.

For example, the closed sector of the local $SU(2)$ quotient in Section II.6.2 has a string whose lifted coordinate closes only after the action of g. A brane placed on the fixed line instead permits an open string starting on one image-brane space and ending on another. Its endpoints need not be identified around a closed spatial worldsheet circle. The orbifold acts on both systems, but on the open string it acts by simultaneous rotation of an oscillator and conjugation of endpoint labels. This is why the two projections have different formulas.

Use $\omega = e^{2\pi i/3}$ and take the $\mathbb{C}^3/\mathbb{Z}_3$ action with weights $(1,1,1)$,

$$(z_1, z_2, z_3) \longmapsto (\omega z_1, \omega z_2, \omega z_3), \qquad 1+1+1 = 0 \pmod 3. \tag{II.6.30}$$

The action is in $SU(3)$. Decompose the Chan–Paton space into γ eigenspaces $V_i \simeq \mathbb{C}^{N_i}$, $i = 0, 1, 2$, with

$$V = V_0 \oplus V_1 \oplus V_2, \qquad \gamma(g) = \operatorname{diag}(\mathbf{1}_{N_0}, \omega\mathbf{1}_{N_1}, \omega^2\mathbf{1}_{N_2}). \tag{II.6.31}$$

Let row i label the target space V_i and column j the source space V_j of a matrix block. Thus $A_{ij}, \Phi_{ij} \in \operatorname{Hom}(V_j, V_i)$, with dimensions $N_i \times N_j$. Conjugation by γ multiplies this block by ω^{i-j}:

$$\big(\gamma(g) M \gamma(g)^{-1}\big)_{ij} = \omega^{i-j} M_{ij}. \tag{II.6.32}$$

The gauge field has geometric weight zero, so its block survives iff $i = j$ modulo three. Each of the three transverse scalars has weight one, so its block survives iff

$$A_{ij} \neq 0 \implies j = i, \qquad \Phi^\alpha_{ij} \neq 0 \implies 1 + i - j = 0 \pmod 3, \quad \text{or } j = i+1. \tag{II.6.33}$$

Here a nonzero symbol denotes an allowed block, not a claim that its vacuum expectation value is nonzero. The directed book edges are $0 \to 1$, $1 \to 2$, and $2 \to 0$, with three scalar species on each edge. One can check a block directly. For Φ_{01}, $R(g)\gamma_0(g)\gamma_1(g)^{-1} = \omega \cdot 1 \cdot \omega^{-1} = 1$, so every one of its $N_0 N_1$ matrix entries survives. For Φ_{02} the same factor is $\omega \cdot 1 \cdot \omega^{-2} = \omega^{-1} \neq 1$, so that block is removed. This pair of calculations fixes the arrow orientation without appealing to a memorized quiver picture. Repeating it

at $i = 1, 2$ gives the other two directed edges. The projection can be read as a sparse block matrix. In row and column order $(0, 1, 2)$, each scalar species has

$$A_\mu = \begin{pmatrix} A_{00} & 0 & 0 \\ 0 & A_{11} & 0 \\ 0 & 0 & A_{22} \end{pmatrix}, \qquad \Phi_\alpha = \begin{pmatrix} 0 & \Phi^\alpha_{01} & 0 \\ 0 & 0 & \Phi^\alpha_{12} \\ \Phi^\alpha_{20} & 0 & 0 \end{pmatrix}. \tag{II.6.34}$$

A nonzero entry in row 2 and column 0 is a map $V_0 \to V_2$; the book calls its field X_{20} and draws the arrow $2 \to 0$. The drawn direction follows the representation carried by the matrix, not the direction of the linear map. In the book convention $i \to j$ denotes $X_{ij} \in \mathrm{Hom}(V_j, V_i)$, transforming as $(\mathbf{N}_i, \overline{\mathbf{N}}_j)$. The mathematical quiver map convention instead draws an arrow for $V_i \to V_j$; translating from that convention reverses the drawn arrow for the same matrix. Figure II.6.5 labels the book arrows and dimensions.

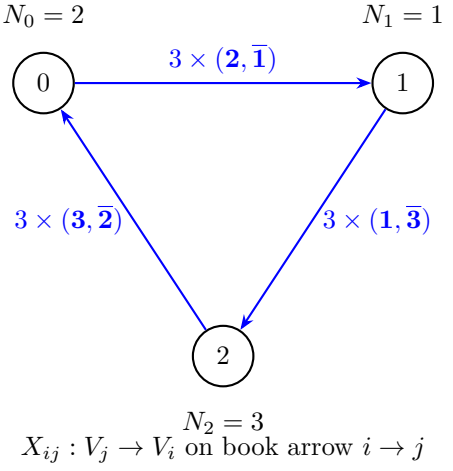


Figure II.6.5: Invariant open scalar blocks for weights $(1, 1, 1)$. Three species sit on each book arrow $i \to i + 1$; the associated matrix maps V_{i+1} into V_i. Circles show chosen ranks $(2, 1, 3)$, rather than ranks forced by a regular-brane representation.

Choose $(N_0, N_1, N_2) = (2, 1, 3)$. The invariant gauge blocks have complexified matrix-entry counts

$$\dim_{\mathbb{C}} \bigoplus_i \mathrm{End}(V_i) = N_0^2 + N_1^2 + N_2^2 = 4 + 1 + 9 = 14. \tag{II.6.35}$$

The three scalar species have rectangular block sizes $N_0 N_1 = 2$, $N_1 N_2 = 3$, and $N_2 N_0 = 6$ per species. Therefore

$$\dim_{\mathbb{C}} \bigoplus_{\alpha=1}^{3} \bigoplus_{i=0}^{2} \mathrm{Hom}(V_{i+1}, V_i) = 3(2 + 3 + 6) = 33. \tag{II.6.36}$$

The gauge-field count uses the complexification of its matrix blocks; Hermiticity gives the real gauge-field condition afterward. The projected worldvolume gauge product at

this stage is $U(2) \times U(1) \times U(3)$. A regular representation with N copies would instead have (N, N, N); the chosen ranks are an arbitrary local mixture for illustrating the vector-space projection. Neither 14 nor 33 proves cancellation of 4D gauge anomalies or compact-model tadpoles. Those questions need interactions and the full brane setup.

For arbitrary nonnegative ranks the vector-space result has a closed form. If three complex coordinates have cyclic weights a_1, a_2, a_3, scalar species α has an allowed block exactly when $j = i + a_\alpha$ modulo three. Thus the complex dimensions before constraints are

$$d_A = \sum_{i=0}^{2} N_i^2, \qquad d_\Phi = \sum_{\alpha=1}^{3} \sum_{i=0}^{2} N_i N_{i+a_\alpha}. \tag{II.6.37}$$

For weights $(1, 1, 1)$ this becomes $3 \sum_i N_i N_{i+1}$, which reproduces 33 at $(2, 1, 3)$. If a rank vanishes, its rectangular blocks vanish because of the rank product; the expression still gives the projected vector space without dividing by a zero rank. It does not decide which interactions survive or which ranks admit a consistent compact realization.

The rank distinction matters physically. A single regular $\mathbb{Z}_3$ representation contains one copy of each one-dimensional irrep, so the multiplicities are $(1, 1, 1)$. Taking N such copies produces N at every node. The vector $(2, 1, 3)$ cannot be written that way; it records extra fractional-brane multiplicities at selected nodes. Equation (II.6.29) remains a valid local matrix projection for this representation, but statements about a complete 4D daughter require additional model data. The same finite block algebra is useful in Volume VI precisely because it can be combined there with interactions and consistency conditions.

Replacing all three weights by -1 makes the scalar condition $j = i - 1$ and reverses every book arrow, although for this rank vector the aggregate matrix-entry count remains 33. Aggregate counting thus misses the representation orientation. Chapter III.1 develops open endpoints, Chapter III.2 develops boundary-state normalization, and Volume VI uses these blocks in full probe constructions.

II.6.6 Discrete torsion

Torus sectors can carry phases invisible in the geometric fixed set. Take $\Gamma = \mathbb{Z}_2 \times \mathbb{Z}_2$ with $g = (a, b)$ and $h = (c, d)$, all entries modulo two. Endpoint matrices may multiply projectively,

$$\gamma(g)\gamma(h) = \alpha(g, h)\gamma(g + h), \qquad \alpha(g, h) \in U(1). \tag{II.6.38}$$

Associativity forces the cocycle equation

$$\alpha(g, h)\alpha(g + h, k) = \alpha(h, k)\alpha(g, h + k). \tag{II.6.39}$$

For $\alpha(g, h) = (-1)^{ad}$ and $k = (e, f)$, both sides have exponent $ad + af + cf$ modulo two:

$$ad + (a + c)f = ad + af + cf = cf + a(d + f) \pmod 2. \tag{II.6.40}$$

This verifies this finite representative, not a classification of all discrete-torsion classes.

The equation is easiest to understand by multiplying three endpoint matrices in two orders. $(\gamma(g)\gamma(h))\gamma(k)$ first produces $\alpha(g, h)$ and then $\alpha(g + h, k)$. The other

bracketing first produces $\alpha(h,k)$ and then $\alpha(g,h+k)$. Since actual matrices multiply associatively, the two products must agree. For the displayed sign, the common exponent $ad+af+cf$ is an elementary finite check of that requirement. The normalization $\alpha(0,g)=\alpha(g,0)=1$ also follows directly because a zero coordinate makes each exponent vanish.

Changing matrix phases changes the raw cocycle. If $\gamma'(g)=\lambda(g)\gamma(g)$, then

$$\alpha'(g,h)=\alpha(g,h)\,\delta\lambda(g,h),\qquad \delta\lambda(g,h)=\frac{\lambda(g)\lambda(h)}{\lambda(g+h)}. \tag{II.6.41}$$

For $\lambda(a,b)=(-1)^{ab}$, addition modulo two gives $\delta\lambda(g,h)=(-1)^{ad+bc}$, hence

$$\alpha'(g,h)=(-1)^{bc}. \tag{II.6.42}$$

The multiplication tables differ, yet their commuting-pair phase is the same. For this abelian group define

$$\beta(g,h)=\frac{\alpha(g,h)}{\alpha(h,g)}=(-1)^{ad-bc},\qquad \beta'(g,h)=\beta(g,h). \tag{II.6.43}$$

The coboundary cancels in the ratio since $g+h=h+g$. β weights the corresponding closed torus pair and appears in the twisted-sector projection. It is not a continuously adjustable size of a fixed locus.

In this abelian example set $x=(1,0)$ and $y=(0,1)$. Every element commutes with a selected spatial twist. For $g=x$ the phase against $h=(c,d)$ is $\beta(x,h)=(-1)^d$. The phase-weighted sum over temporal insertions therefore has the explicit form

$$P_x^{\beta}=\frac{1}{4}\big(\mathbf{1}+x-y-(x+y)\big), \tag{II.6.44}$$

where the group symbols denote their actions on $\mathcal{H}_x$. The signs are $+,+,-,-$ for $h=0,x,y,x+y$. This shows in a single sector how a discrete torus phase changes which states survive a temporal sum. The formula assumes the consistent twisted-sector action supplied by the orbifold CFT; the four-sign arithmetic alone does not construct that action.

The exponent $ad-bc$ is the determinant of the two vectors in $\mathbb{F}_2^2$; modulo two, subtraction and addition agree. It vanishes if the pair is linearly dependent, and it is one for an ordered basis such as (x,y). Thus the phase is $+1$ on parallel twists and -1 on a pair that spans the group. Reversing the cycles exchanges g and h and sends β to its inverse; here the inverse of -1 is again -1. This check links the phase to the ordered torus cycles of Section II.6.4 without assigning it a geometric displacement.

The ordered pair $x=(1,0)$, $y=(0,1)$ exposes the distinction between raw representatives and the invariant phase. Direct substitution gives

	$\alpha(x,y)$	$\alpha(y,x)$	$\beta(x,y)$
$\alpha=(-1)^{ad}$	-1	$+1$	-1
$\alpha'=(-1)^{bc}$	$+1$	-1	-1

(II.6.45)

Comparing only $\alpha(x,y)$ between two papers can mistake a matrix rephasing for a different physical class.

The rephasing can be followed at the four group elements. The function $\lambda(a,b) = (-1)^{ab}$ equals -1 only at $(1,1)$ and $+1$ at $(0,0)$, x, and y. Consequently $\delta\lambda(x,y) = \lambda(x)\lambda(y)/\lambda(x+y) = -1$. It flips $\alpha(x,y)$ from -1 to $+1$. The same coboundary flips the reversed raw multiplier, so the quotient of the two does not move. This small table is a concrete reason to report β when comparing discrete-torsion choices.

Pauli matrices furnish a representative. Choose $\sigma_1\sigma_2 = i\sigma_3$ and

$$\gamma(a,b) = \sigma_2^b\sigma_1^a, \quad \gamma(x) = \sigma_1, \quad \gamma(y) = \sigma_2, \quad \gamma(x+y) = \sigma_2\sigma_1 = -i\sigma_3. \tag{II.6.46}$$

Then $\gamma(x)\gamma(y) = i\sigma_3 = -\gamma(x+y)$ and $\gamma(y)\gamma(x) = -i\sigma_3 = \gamma(x+y)$, reproducing the first row of (II.6.45). Another Pauli section sets $\gamma_D(x) = \sigma_1$, $\gamma_D(y) = \sigma_2$ and $\gamma_D(x+y) = \sigma_3$. Rephasing only the last matrix by $\lambda_D(x+y) = i$ gives its ordered multipliers

$$\alpha_D(x,y) = i, \qquad \alpha_D(y,x) = -i, \qquad \frac{\alpha_D(x,y)}{\alpha_D(y,x)} = -1. \tag{II.6.47}$$

The raw values depend on the section; the ratio agrees. This finite comparison does not require a general group-cohomology classification.

The Pauli calculation also shows why the raw values in this section are not constrained to be real. The matrices square to the identity at x and y, but the chosen product at $x+y$ can be $-i\sigma_3$ or σ_3. Both are legitimate projective sections; their multiplication phases compensate for the different choices. The physical ratio -1 records the anticommutation of the two generators. No continuous change of the phase choice is needed to move between these two representatives of the same discrete class.

Discrete torsion and a blow-up parameter answer different questions. $\beta(x,y) = -1$ is a finite torus-sector choice. A Fayet–Iliopoulos level, when available in a brane gauge theory, varies continuously and can affect a vacuum quotient. Rephasing projective matrices does not vary such a level. Volume VI returns to their interaction in specific probes. The closed torus phase and projective open endpoint algebra remain constructions on distinct string sectors.

II.6.7 Exercises

The first four exercises ask for exact finite answers. The fifth asks for a written physical comparison and is ungraded.

1. Let $Z(\sigma + 2\pi) = e^{2\pi i(2/5)}Z(\sigma)$. Derive the two shifted integer sets and give θ, the first two positive spatial Fourier labels of Z and $\bar{Z}$, and whether a constant coordinate mode exists. Submit the fields `theta`, `Z_modes`, `Zbar_modes`, and `constant_mode` using the public question schema. As an ungraded part, explain in words why these labels do not settle the GSO projection.

2. With A spatial and B temporal, use the S and ordinary trace T of (II.6.24). Enumerate every pair in the orbit of $(0,1)$ modulo three and give its size. Submit `orbit` and `orbit_size`. As an ungraded part, state why closure of this set is weaker than modular invariance of the partition function.

3. For $\mathbb{C}^3/\mathbb{Z}_3$ with weights $(1,1,1)$, $\gamma_i = \omega^i \mathbf{1}_{N_i}$, and ranks $(2,1,3)$, derive the invariant gauge blocks and book arrows with scalar-species multiplicities. Count complex matrix entries in the gauge and scalar block spaces before imposing reality or interactions. Submit `gauge_blocks`, `arrows`, `gauge_complex_components` and `scalar_complex_components`. As an ungraded part, explain why these counts do not establish an anomaly-free daughter.

4. For $x = (1,0)$ and $y = (0,1)$ in $\mathbb{Z}_2^2$, compare $\alpha((a,b),(c,d)) = (-1)^{ad}$ and $\alpha' = (-1)^{bc}$. Submit both ordered raw values, $\beta(x,y)$, and whether the representatives are cohomologous. Use the fields `alpha_gh`, `alpha_hg`, `alpha_prime_gh`, `alpha_prime_hg`, `beta_gh` and `same_class`. As an ungraded part, show the rephasing that supports your last answer.

5. Explain why a closed twisted state localized near a fixed locus is not an open quiver bifundamental. Explain why $\beta(x,y) = -1$ cannot be varied as an FI blow-up level. Name one physical premise needed before using a fixed-point count to infer massless states. Submit a written response in the `written_response` field; the interpretation is assessed by a reader rather than the finite-answer grader.

II.6.8 Take-home message

Take-home message

A finite quotient adds closed sectors with spatially twisted boundary conditions and centralizer projections. The twist produces shifted spatial Fourier labels and can remove a transverse coordinate zero mode. A torus traces over commuting spatial and temporal holonomies; changing its cycles constrains their set, while full consistency also needs the physical worldsheet lift and level matching. D-branes add a separate projection on open endpoint matrices, giving oriented quiver blocks. Discrete torsion is visible in a commuting-pair phase that survives rephasing of projective matrices. A fixed set, an index, and a physical massless spectrum answer different questions.

Status and sources

Sections 1–2. Closed twisted sectors, projection and centralizers are [WS] in Dixon et al. (1985, physical PDF pp. 3, 8, printed pp. 680, 685). The fixed-line and S_3 calculations are [MATH] under the stated actions. The noncompact line gives no massless-spectrum count.
Section 3. Fractional spatial Fourier sets and the zero-mode statement are [MATH] from the boundary condition. The model's $\pm 1/3$ shifts and its nine untwisted plus 27 twisted E_6 **27** multiplets are [WS] in Dixon et al. (1985, physical PDF pp. 4–6, printed pp. 681–683). Those counts require that model's gauge and spin lift.
Section 4. Commuting torus twists, cycle changes and the compact supersymmetric sigma-model Euler formula are [WS] at Dixon et al. (1985, physical PDF pp. 6–8, printed pp. 683–685, eq. (4)). The row-basis, $S/T/U$, S_3 pair and $\mathbb{Z}_3$ orbit calculations are

[MATH] under the declared cycles. The trace T equality additionally assumes the stated lift, level matching and insertion phases. Finite orbit and Euler arithmetic do not prove full modular invariance or a resolution.

Section 5. Gauge and transverse-scalar Chan–Paton transformations are [WS] from Douglas and Moore (1996, physical PDF pp. 8–9, 13–14, printed pp. 7–8, 12–13, eqs. (3.2)–(3.3), (4.3)–(4.6)). The $\mathbb{C}^3/\mathbb{Z}_3$ arrows and 14/33 counts are [MATH] applications of those transformations and the book's matrix convention. The source's mathematical map arrows run opposite the book's displayed matrix arrows. No full interacting or anomaly-free daughter follows from the projection.

Section 6. Torus phase and twisted projector are [WS] from Vafa and Witten (1994, physical PDF pp. 5–6, printed pp. 4–5, eqs. (2.1)–(2.4)). Projective endpoint matrices are [WS] from Douglas (1998, physical PDF p. 3, printed p. 2, eqs. (2.1)–(2.3)). The Pauli section is on Douglas (1998, physical PDF p. 5, printed p. 4, eq. (3.3)). Cocycle, coboundary and ratio arithmetic are [MATH] for the displayed representatives. They do not classify all classes or identify a discrete phase with an FI level.

Section 7. Exercises 1–4 ask for [MATH] consequences of the stated inputs. Exercise 5 is written physical reasoning and needs human assessment.

References

Dixon, L. et al. (1985). "Strings on Orbifolds". In: *Nuclear Physics B* 261, pp. 678–686.

Douglas, M. R. (1998). *D-branes and Discrete Torsion*. arXiv: `hep-th/9807235`.

Douglas, M. R. and G. Moore (1996). *D-branes, Quivers, and ALE Instantons*. arXiv: `hep-th/9603167`.

Vafa, C. and E. Witten (1994). *On Orbifolds with Discrete Torsion*. arXiv: `hep-th/9409188`.

Chapter II.7

Orientifolds and unoriented strings

II.7.1 An open string loses its arrow

An open string ending on a stack of D-branes has an ordered pair of endpoint labels. If one follows the string from $\sigma = 0$ to $\sigma = \pi$, the first label is i and the second is j. Worldsheet orientation reversal follows the same string in the opposite direction. It exchanges the labels. Gauging this operation changes the open-string states that survive, and it also allows nonorientable worldsheet surfaces. These two consequences lead, respectively, to orthogonal or symplectic gauge algebras and to crosscap contributions to Ramond–Ramond (RR) charge.

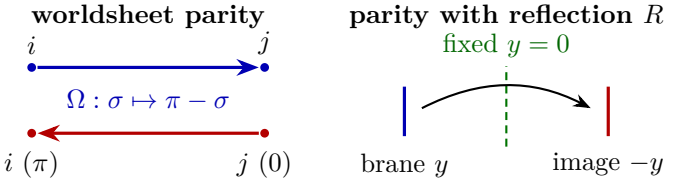


Figure II.7.1: Left: Ω reverses the orientation of an open segment and exchanges its ordered Chan–Paton endpoints. The arrow marks increasing σ, not a spacetime velocity. Right: when parity is combined with a target reflection R, a brane at y has an image at $-y$ and the fixed locus $y = 0$ supports an orientifold plane. Pure Type I Ω has no transverse reflection or separated image pair.

The Type I orientifold of Type IIB by worldsheet parity is our running example. We will first work out what happens to an individual endpoint matrix and a massless vector. We then view the one-loop surfaces as exchanges between boundaries and crosscaps. Finally, T-dual O7 and O3 examples show why a charge equation needs an explicit cover or quotient unit. The local projection and the global charge condition answer

different questions. Figure II.7.1 fixes the two geometric operations before any matrix calculation.

II.7.2 Parity as a gauged operation

What becomes of the ordered string when its orientation is gauged? Let Ω act on the open-string coordinate by $\sigma \mapsto \pi - \sigma$. A basis state $|\psi, ij\rangle$ has a worldsheet oscillator state $|\psi\rangle$ and endpoints in an N-dimensional Chan–Paton space V. The endpoint coefficient can be collected into $\lambda \in \mathrm{End}(V)$. In a basis in which Ω acts on endpoints through an invertible matrix γ_Ω, the operation on a component with oscillator parity η_ψ is

$$\Omega : |\psi, ij\rangle \longmapsto \eta_\psi (\gamma_\Omega)_{ii'} |\psi, j'i'\rangle (\gamma_\Omega^{-1})_{j'j}. \tag{II.7.1}$$

Thus the operation on the coefficient matrix is a transpose followed by a change of endpoint basis:

$$\lambda \longmapsto \eta_\psi \gamma_\Omega \lambda^{\mathsf{T}} \gamma_\Omega^{-1}. \tag{II.7.2}$$

The transpose is the algebraic record of exchanging the two endpoints. It is not a Hermitian conjugation. In particular, λ_{ij} and λ_{ji} label the two opposite orientations before the quotient.

The operation can also be seen on the matrix units E_{ij}, which have a single nonzero entry in row i and column j. With $\gamma_\Omega = I_N$, a parity-even oscillator maps E_{ij} to E_{ji}. The two-dimensional span of E_{ij} and E_{ji} therefore has one even and one odd eigenvector when $i \neq j$:

$$E_{ij}^{(+)} = E_{ij} + E_{ji}, \qquad E_{ij}^{(-)} = E_{ij} - E_{ji}, \qquad (E_{ij}^{(\pm)})^{\mathsf{T}} = \pm E_{ij}^{(\pm)}. \tag{II.7.3}$$

For $i = j$, the matrix unit is fixed by transposition; its survival still depends on the oscillator parity. This finite eigenspace calculation is the simplest way to see why an endpoint exchange does not just divide the number of states by two in every sector. The diagonal and off-diagonal pieces behave differently.

The orientifold group may contain Ωh, where h is a symmetry of the complete target and worldsheet theory. If $h = 1$, the Type I operation is pure parity: there is no target-space reflection whose fixed set could be drawn as a lower-dimensional plane. If $h = R$ reflects transverse coordinates, the fixed set of R is the orientifold locus. A D-brane away from it is accompanied by an image. This geometric distinction matters when we count branes later. The right panel of Figure II.7.1 illustrates a reflection in one coordinate y; the label $y = 0$ is a fixed locus only in that panel.

For the simple order-two diagonal sector, apply (II.7.2) twice. Suppressing an oscillator phase whose square is one, direct matrix multiplication gives

$$\lambda \overset{\Omega^2}{\longmapsto} (\gamma_\Omega \gamma_\Omega^{-\mathsf{T}}) \lambda (\gamma_\Omega^{\mathsf{T}} \gamma_\Omega^{-1}). \tag{II.7.4}$$

The complete algebra $\mathrm{End}(V)$ includes all pairs of endpoints. If (II.7.4) acts as the identity on every such matrix, its left factor is central. After an irrelevant overall phase choice and the order-two condition, the familiar possibilities are

$$\gamma_\Omega^{\mathsf{T}} = \epsilon_\Omega \gamma_\Omega, \qquad \epsilon_\Omega = +1 \text{ or } -1. \tag{II.7.5}$$

The antisymmetric choice requires even N. The closure argument uses the complete endpoint algebra and the specified sector. It must not be copied unchanged into a mixed Neumann–Dirichlet sector, where worldsheet phases can differ.

One can see why the complete algebra matters. If Ω^2 acts through $K\lambda K^{-1}$ for every $\lambda \in \mathrm{End}(V)$, then K commutes with each E_{ij}. Commuting with all diagonal E_{ii} makes K diagonal; commuting with every off-diagonal E_{ij} makes all its diagonal entries equal. Hence K is proportional to the identity. If only a block-diagonal subalgebra were present, independent scalar factors could remain on its blocks. The full endpoint spectrum removes that ambiguity in this simple sector.

A two-label example makes the state projection tangible. Set $\gamma_\Omega = I_2$ and take an oscillator with $\eta_\psi = +1$. The invariant state built from two different endpoints is

$$|\psi, 12\rangle_+ = \frac{|\psi, 12\rangle + |\psi, 21\rangle}{\sqrt{2}}, \qquad \Omega|\psi, 12\rangle_+ = |\psi, 12\rangle_+. \tag{II.7.6}$$

For a parity-odd oscillator, the invariant combination instead has a minus sign between the ordered states. The spacetime field associated with the oscillator therefore determines which endpoint matrix survives. An orientifold is a quotient of the string state space, not merely a quotient of points in spacetime. Chapter 2 supplies the state/operator language; Chapter 6 introduces open endpoints at orbifold images. The same endpoint operation will later project quiver nodes in Volume V.

For the massless vector, the parity sign has a worldsheet origin. Orient the strip by $d\tau \wedge d\sigma$ and use the outward-normal rule at its edges. At $\sigma = 0$ the outward normal is $-\partial_\sigma$ and the induced boundary tangent is $+\partial_\tau$; at $\sigma = \pi$ they are $+\partial_\sigma$ and $-\partial_\tau$. The map $\sigma \mapsto \pi - \sigma$ exchanges the edges while keeping τ fixed, so it sends the first induced tangent to the negative of the second. The oriented vector boundary insertion, schematically $A_\mu(X)\,\partial_{\text{tangent}} X^\mu$, uses this tangent and acquires the odd parity of the standard massless vector vertex, including its superstring completion. By contrast, differentiating $X(\tau, \pi - \sigma)$ with respect to the fixed coordinate τ produces no chain-rule minus sign. A bosonic Neumann–Neumann cosine expansion checks its mode-coordinate transformation but alone does not determine a superstring NS-state phase. With the sourced vector parity, the invariant state uses the antisymmetric endpoint combination. A transverse scalar or a string between branes with different boundary conditions can carry a different sign; the vector result cannot be used as a universal projection rule for every open field.

II.7.3 Chan-Paton projection

Why does the parity sign distinguish orthogonal and symplectic vector algebras? The massless open vector oscillator has Ω parity -1. Its Chan–Paton matrix A therefore obeys the invariant-state equation

$$A = -\gamma_\Omega A^{\mathsf{T}} \gamma_\Omega^{-1}. \tag{II.7.7}$$

We work in an orthonormal Chan–Paton basis, so the compact gauge generators are also anti-Hermitian, $A^\dagger = -A$. The matrix γ_Ω is unitary in this basis. Both statements are needed before a complex transpose equation can be called a compact real Lie algebra.

First choose the symmetric unitary form and bring it to $\gamma_\Omega = I_N$. Equation (II.7.7) becomes $A = -A^{\mathsf{T}}$. For each unordered pair $i < j$, one independent real antisymmetric generator has entries $A_{ij} = 1$ and $A_{ji} = -1$. The diagonal vanishes. Hence

$$\dim_{\mathbb{R}} \mathfrak{so}(N) = \binom{N}{2} = \frac{N(N-1)}{2}. \tag{II.7.8}$$

For $N = 6$ there are five entries above the first diagonal position, four above the second, and then three, two, one:

$$5 + 4 + 3 + 2 + 1 = 15, \qquad T_{12} = E_{12} - E_{21}, \quad T_{12}^{\mathsf{T}} = -T_{12}. \tag{II.7.9}$$

Since T_{12} is real antisymmetric, it also satisfies $T_{12}^{\dagger} = -T_{12}$. This is a count of independent vector generators, not the rank of a group.

The closure under commutators is visible without invoking a group classification theorem. If $A^{\mathsf{T}} = -A$ and $B^{\mathsf{T}} = -B$, then

$$[A, B]^{\mathsf{T}} = (AB - BA)^{\mathsf{T}} = B^{\mathsf{T}}A^{\mathsf{T}} - A^{\mathsf{T}}B^{\mathsf{T}} = -[A, B]. \tag{II.7.10}$$

Anti-Hermiticity is likewise preserved by commutators. For a small control, $N = 2$ leaves only $E_{12} - E_{21}$, a one-dimensional algebra. Increasing N adds one generator for every new unordered pair of labels. This is why the $N = 6$ calculation is a combinatorial count rather than a memorized dimension formula.

For the antisymmetric unitary form, let $N = 2k$ and choose a real symplectic representative

$$J = \begin{pmatrix} 0 & I_k \\ -I_k & 0 \end{pmatrix}, \qquad J^{\mathsf{T}} = -J, \quad J^{-1} = -J. \tag{II.7.11}$$

Multiplying the projection equation by J^{-1} shows that it is equivalent to $A^{\mathsf{T}}J + JA = 0$. This is the complex symplectic Lie-algebra equation. To see its independent entries, write A in $k \times k$ blocks and multiply explicitly:

$$A = \begin{pmatrix} P & Q \\ R & S \end{pmatrix}, \qquad A^{\mathsf{T}}J + JA = 0 \quad \Longleftrightarrow \quad S = -P^{\mathsf{T}}, \quad Q = Q^{\mathsf{T}}, \quad R = R^{\mathsf{T}}. \tag{II.7.12}$$

There are k^2 complex entries in P and $k(k+1)/2$ in each symmetric block. Intersecting this complex solution space with $A^{\dagger} = -A$ gives the compact real form with the same numerical dimension:

$$\dim_{\mathbb{R}} \mathfrak{usp}(2k) = k^2 + 2\frac{k(k+1)}{2} = k(2k+1). \tag{II.7.13}$$

Here the equality of the real dimension with that complex count depends on the unitary, orthonormal setup. It is not a property of an arbitrary invertible γ.

To make the real count explicit, insert $S = -P^{\mathsf{T}}$ into $A^{\dagger} = -A$. The top-left block gives $P^{\dagger} = -P$, so P has k^2 real parameters. The off-diagonal blocks give $R = -Q^{\dagger}$. Because $Q = Q^{\mathsf{T}}$, it has $k(k+1)/2$ complex entries, or $k(k+1)$ real parameters. Thus

$$\#(P, Q, R)_{\text{real}} = k^2 + k(k+1) = k(2k+1). \tag{II.7.14}$$

The reality condition has paired Q and R; it has not simply halved the complex entries in each block. The same compact constraints close under commutators because both $A^{\mathsf{T}}J + JA = 0$ and $A^{\dagger} = -A$ are preserved by taking commutators.

For $N = 4$, set $k = 2$. The blocks contribute four entries from P and three from each of Q, R, so the answer is ten. A concrete anti-Hermitian generator is

$$A_0 = \begin{pmatrix} iI_2 & 0 \\ 0 & -iI_2 \end{pmatrix}, \qquad A_0^{\dagger} = -A_0, \qquad A_0^{\mathsf{T}}J + JA_0 = 0. \tag{II.7.15}$$

The compact vector algebra is $\mathfrak{usp}(4)$, also denoted $\mathfrak{sp}(2)$ in a convention where the argument is quaternionic rank. The book's USp(N) uses the even Chan–Paton dimension N. The choice of algebra does not by itself fix the global gauge group, its quotient by a center, or the matter content.

The two $N = 4$ choices make the distinction particularly sharp. A symmetric γ gives $4(4-1)/2 = 6$ vector generators. An antisymmetric J_4 gives $2(2 \cdot 2+1) = 10$. The same number of endpoint labels therefore yields different vector spectra after gauging parity. Conversely, observing a ten-dimensional vector algebra does not determine which scalar or mixed-string states survive. Those sectors must be projected with their own worldsheet parity and endpoint action.

There is a useful failure test for the unitary premise. Take $\gamma = \mathrm{diag}(1, 2)$ and solve only $A = -\gamma A^{\mathsf{T}}\gamma^{-1}$. The diagonal entries vanish, while the off-diagonal entries obey

$$A_{12} = -\tfrac{1}{2}A_{21}, \qquad A_{21} = -2A_{12}. \tag{II.7.16}$$

Thus the complex solution space has dimension one. If we also require anti-Hermiticity relative to the unchanged identity metric, $A_{21} = -\overline{A}_{12}$. Combining this with (II.7.16) forces $A_{12} = 0$. A nonunitary basis transformation would also transform the Hermitian metric; keeping that metric fixed changes the real-form problem. This example explains why a computational rank count cannot classify compact orientifold vector algebras without its physical premises. Volume VI will use the unitary projection at local nodes, while distinct scalar and mixed-string sectors must carry their own parity signs.

II.7.4 Crosscaps and one-loop channels

How does a surface without an orientation boundary contribute RR charge? In the open-string loop description, the annulus, Möbius strip and Klein bottle are distinct vacuum surfaces. After exchanging the role of worldsheet time and space, each is a cylinder carrying a closed string between two ends. An ordinary boundary defines a boundary state $|B\rangle$; a crosscap is the end obtained by identifying opposite points with an orientation reversal and defines $|C\rangle$. Figure II.7.2 follows the two ends of each channel.

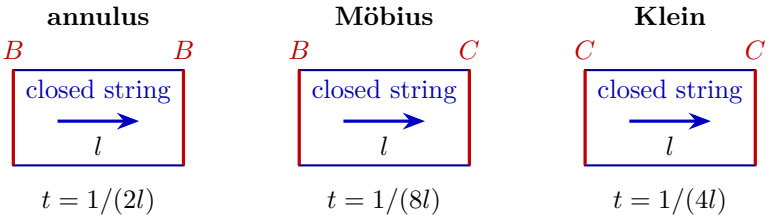


Figure II.7.2: Closed-channel views of the annulus, Möbius strip and Klein bottle. The cylinder runs in the indicated l direction; B denotes a D-brane boundary and C a crosscap. Its endpoints are BB, BC and CC, respectively. The drawing determines which sources can exchange a closed mode, but it does not determine the amplitude normalization or the crosscap sign.

The endpoint dictionary can be read directly from the surfaces. The annulus has two boundaries. The Möbius strip has one boundary and one crosscap. The Klein bottle has two crosscaps. If $\mathcal{D}(l)$ denotes propagation of closed modes over length l, their schematic terms are

$$\mathcal{A}_{\rm A} \sim \langle B|\mathcal{D}(l)|B\rangle, \qquad \mathcal{A}_{\rm M} \sim \langle B|\mathcal{D}(l)|C\rangle, \qquad \mathcal{A}_{\rm K} \sim \langle C|\mathcal{D}(l)|C\rangle. \tag{II.7.17}$$

These are channel labels. Their oscillator, ghost and projection factors remain part of the actual worldsheet amplitude. A crosscap is not an extra open-string Hilbert space; it is a closed-channel source associated with an unoriented surface.

The modulus relation illustrates why even the simplest diagram requires conventions. In the selected normalization, let t be the dimensionless loop modulus and l the length coordinate used for the closed cylinder. The same paper's transformation gives three different relations:

$$t_{\rm A} = \frac{1}{2l}, \qquad t_{\rm M} = \frac{1}{8l}, \qquad t_{\rm K} = \frac{1}{4l}. \tag{II.7.18}$$

For example, at $l = 3/2$ the three loop moduli are $1/3$, $1/12$ and $1/6$. Thus one cannot use a single bare replacement $t = 1/l$ for every surface. The factors in (II.7.18) belong to this coordinate and amplitude normalization; they are not topological invariants of the pictures.

The large-l limit probes the $t \to 0$ limit in each loop, but at different rates. If one inserted the annulus relation into the Klein bottle integral, one would assign the wrong measure and could spoil the relative source normalization. The three relations in (II.7.18) are therefore part of the amplitude calculation. The example $l = 3/2$ makes the distinction numerical: the Möbius loop modulus is one quarter of the annulus value, while the Klein value is one half of it.

At large l, the exchange can be dominated by massless closed RR modes. Write their boundary and crosscap source coefficients as q_B and q_C. With their relative amplitude weights included, the three channels have the familiar square structure

$$q_B^2 + 2q_Bq_C + q_C^2 = (q_B + q_C)^2. \tag{II.7.19}$$

Topology explains the three types of pairings but does not fix q_C/q_B or the coefficient of the mixed term in the fully normalized amplitude. Those numbers must be read

from a worldsheet calculation. In particular, the number 32 in the Type I example does not follow by counting crosscaps in Figure II.7.2.

The square is useful because each term has a channel interpretation. A brane boundary can exchange with another boundary, a boundary can exchange with a crosscap, and two crosscaps can exchange with each other. If the closed RR massless coefficient is normalized to a common propagator, the three contributions can be compared. This is a factorization statement about the sourced amplitude. It is stronger than the bare topology, since the crosscap can carry a sign and the worldsheet calculation chooses the normalization.

There are two complementary ways to see the Type I D9 condition. The ten-form coupling to n D9-branes and the orientifold source has the linear form

$$S_{\text{source}} = i\mu_9(n-32)\int_{M_{10}} A_{10}. \tag{II.7.20}$$

Here μ_9 is the chosen D9 charge unit and A_{10} is a ten-form potential. It has no propagating local degrees of freedom in ten dimensions. Variation with respect to it imposes the source condition $n-32=0$. The absence of a propagating ten-form particle is why the closed-channel language of a ten-form tadpole should be read as a consistency condition, not a literal on-shell particle emitted into a transverse direction.

The independent channel calculation supplies a quadratic control. In the untwisted nine-brane term of a larger Type I K3 orientifold amplitude, the relevant bracket is

$$\mathcal{B}_9 = 32^2 - 64\,\mathrm{Tr}(\gamma_{\Omega,9}^{-1}\gamma_{\Omega,9}^{\mathsf{T}}) + \big(\mathrm{Tr}\,\gamma_{1,9}\big)^2. \tag{II.7.21}$$

This term carries its source's overall volume and modular factors. It is one term of that amplitude, which also has five-brane and twisted-sector terms. In the Type I nine-brane control choose the symmetric $\gamma_{\Omega,9}$ and $\gamma_{1,9}=I_n$. The two traces in (II.7.21) are then n and n, giving

$$\mathcal{B}_9 = 32^2 - 64n + n^2 = (n-32)^2. \tag{II.7.22}$$

At $n=32$ the bracket vanishes. At $n=16$ it is 256, so the O9 source has not been canceled by merely counting sixteen cover D9 labels. The source amplitude carries a formal $(1-1)$ from NSNS and RR exchange; the two divergent coefficients must vanish separately. Their algebraic subtraction is not a physical cancellation. The linear source in (II.7.20) and the square in (II.7.22) test the same stated D9 normalization in different calculations. Neither equation alone establishes the full Type I worldsheet construction.

One can formulate the separate-cancellation requirement without assigning a spurious value to $1-1$. If C_{NSNS} and C_{RR} denote the two large-cylinder coefficients in a fixed channel, consistency requires

$$C_{\text{NSNS}} = 0, \qquad C_{\text{RR}} = 0, \qquad \text{rather than only } C_{\text{NSNS}} - C_{\text{RR}} = 0. \tag{II.7.23}$$

The displayed source bracket supplies the RR source test at the stated scope. Supersymmetric equality of two opposite divergences cannot substitute for the two conditions.

The source bracket also exposes the three coefficients. Under the stated trace substitutions, it reads

$$\underbrace{n^2}_{BB}+\underbrace{(-64n)}_{BC}+\underbrace{32^2}_{CC}. \tag{II.7.24}$$

The mixed coefficient equals $2(n)(-32)$, as required for a square of total source. For $n=24$, the three numbers are 576, -1536 and 1024. Their sum is $64=(24-32)^2$. At $n=32$, they are 1024, -2048 and 1024 and sum to zero. The signs here are those of the cited RR bracket in its model and normalization. They are not obtained by drawing the three surfaces.

The linear and quadratic formulas answer related but different questions. Equation (II.7.20) is linear because it is a coupling in the spacetime action. Equation (II.7.22) is quadratic because a two-ended cylinder factorizes into a source at each end. The square makes neutrality manifest, while varying the linear coupling states the field equation directly. The ten-form's lack of propagating degrees of freedom limits the particle interpretation of the long-cylinder picture; it does not remove the source condition.

The annulus channel in Chapter VI.7 will probe a twisted RR source rather than only this untwisted D9 one. The procedure is the same: identify the channel, specify its projection and normalization, and only then read the long-cylinder coefficient. The presence of a crosscap or of a vanishing total vacuum energy does not replace those steps.

II.7.5 O-plane charge units

What changes when a T-dual charge equation is written on the covering space or on the quotient? An ordinary Op^- plane has negative charge in this book's convention and gives the orthogonal projection when a Dp stack lies on it. In units where a covering Dp-brane contributes $+1$, its charge is

$$Q_{\text{cover}}(\text{O}p^-)=-2^{p-4}. \tag{II.7.25}$$

The charge-based superscript is important: a historical source used the opposite O^+ name for the negative-charge, orthogonal O7 plane. The reliable translation is its charge and endpoint projection, not the printed sign alone.

Start with the O9/D9 equation. There is one space-filling ordinary O9$^-$ source and 32 covering D9 units. Equation (II.7.25) gives $-2^{9-4}=-32$, so

$$Q_{\text{cover}}(\text{O9}^-)+Q_{\text{cover}}(32\text{D9})=-32+32=0. \tag{II.7.26}$$

This is also the $n=32$ condition in the previous section. The Chan–Paton vector space has dimension 32, and its unitary symmetric projection gives $\mathfrak{so}(32)$. A translation of the complete charge equation halves the complete cover equation to $-16+16=0$, but the O9 involution has no separated transverse image positions. The quotient number 16 in that line is not the Chan–Paton dimension and does not mean sixteen separated D9 pairs.

Now T-dualize two compact directions along the original D9 worldvolume. Their Neumann boundary conditions become Dirichlet conditions, so these directions are

transverse to the resulting D7/O7 system. Reflection on the dual two-torus has four fixed points because each circle has two points invariant under $x \mapsto -x$ modulo its period. In coordinates with periods $2\pi R_a$, the fixed-point equation is

$$x_a \equiv -x_a \pmod{2\pi R_a} \quad \Longleftrightarrow \quad x_a \in \{0, \pi R_a\}, \qquad a = 1, 2. \tag{II.7.27}$$

The ordered pairs $(0,0)$, $(0,\pi R_2)$, $(\pi R_1, 0)$ and $(\pi R_1, \pi R_2)$ give the four loci. Their existence is geometric; the charge -8 is additional orientifold input. Each ordinary O7$^-$ has cover charge $-2^{7-4} = -8$. The total charge is therefore

$$4Q_{\text{cover}}(\text{O7}^-) + N_{7,\text{cover}} = 4(-8) + 32 = 0. \tag{II.7.28}$$

Away from a fixed point, one physical D7 object on the quotient is represented by a brane and its image on the cover. Hence 32 cover labels correspond to 16 mobile quotient objects. If they are distributed uniformly, each fixed point is assigned eight cover labels, or four quotient objects. This distribution is an example, not a requirement of the total charge equation. Moving branes changes local gauge enhancement while preserving the global total.

In that uniform arrangement, the quotient charge count at each locus is especially transparent. The local O7 entry is -4 and the assigned four quotient D7 objects contribute $+4$. The same integrated total can be obtained with a nonuniform assignment, for example $(q_1, q_2, q_3, q_4) = (16, 0, 0, 0)$ quotient objects, because

$$\sum_{a=1}^{4} (q_a - 4) = 0 \quad \Longleftrightarrow \quad \sum_{a=1}^{4} q_a = 16. \tag{II.7.29}$$

The first distribution has four zero local entries; the second has one $+12$ and three -4 entries. The equation records integrated charge only. It does not certify that every such placement satisfies all local or dynamical consistency conditions.

For six compact reflected directions, there are $2^6 = 64$ fixed loci. Applying the ordinary O3$^-$ row gives $-2^{3-4} = -1/2$ per locus in cover D3 units. Its total is again -32:

$$64Q_{\text{cover}}(\text{O3}^-) + N_{3,\text{cover}} = 64\left(-\frac{1}{2}\right) + 32 = 0. \tag{II.7.30}$$

This is T-dual charge arithmetic for the ordinary row. It is not a direct computation of an O3 crosscap amplitude and does not specify every O3 variant.

The six-dimensional fixed-point count uses the same one-circle equation as (II.7.27). Each of six coordinates has two choices, so the ordered coordinate tuple has $2^6 = 64$ choices. A single O3 charge is a half-unit in the cover, and 64 such half-units make -32. This is why an individual fractional-looking O3 entry is compatible with an integral total. It does not turn a single mobile D3 object into a fractional brane.

The quotient convention halves both terms of a given covering equation. Thus a fixed O-plane entry is written as half its covering charge and the 32 covering Dp units as 16 quotient objects. The three examples can be displayed without silently changing

the unit midway:

$$\begin{aligned} \text{O9}: &\quad -16+16=0, \\ 4\,\text{O7}: &\quad 4(-4)+16=0, \\ 64\,\text{O3}: &\quad 64\left(-\frac{1}{4}\right)+16=0. \end{aligned} \tag{II.7.31}$$

Figure II.7.3 places these entries beside the covering equations. The factor of two is a translation of the whole source equation. Halving only the O-plane term or only the brane term would give a spurious tadpole. For O7 and O3 a mobile brane-image pair makes the quotient object count geometric. Stuck and fractional objects have different local charge counting and must be specified separately.

The distinction between a Chan–Paton dimension and a quotient object count is clearest at O9. The 32-dimensional endpoint space enters the vector projection and the trace in (II.7.21). The number 16 is what the full source equation reads after division by two. Replacing $n=32$ by $n=16$ in the source bracket would change the amplitude, as the explicit 256 residual showed. For O7, the same 32 cover labels can be grouped into sixteen mobile image pairs. These are two uses of a factor of two, connected by T-duality but geometrically different.

ordinary locus	**cover Dp units**	**quotient units**
one O9$^-$	$-32+32=0$	$-16+16=0$
four O7$^-$	$4(-8)+32=0$	$4(-4)+16=0$
64 O3$^-$	$64(-1/2)+32=0$	$64(-1/4)+16=0$

Figure II.7.3: The same ordinary minus-plane charge equations in covering Dp units and quotient units. Every source term is halved in the right column. The 16 on the O9 quotient line is only a translated count; it is not a set of separated image pairs. O3 entries apply to the ordinary untwisted row.

A historical naming trap occurs precisely in the O7 example. The source that discusses the standard $T^2/\mathbb{Z}_2$ orientifold calls each negative-charge O7 plane O^+ and states its charge as -8; it counts sixteen seven-brane pairs. In this book that same physical row is called O7$^-$. Its four planes contribute $4(-8)=-32$, while sixteen cover pairs contribute $+32$. The source's O^- instead denotes a positive-charge plane. We do not transfer its superscript into (II.7.25); we transfer the charge and the SO/Sp projection. This translation is enough for the ordinary charge equation and does not import the source's separate compactification without vector structure.

The O3 sign has an additional limit. The O3-associated construction has two independent mod-two discrete choices, one for the NS two-form and one for the RR two-form. Denote them $(\theta_{\mathrm{NS}},\theta_{\mathrm{RR}})\in\mathbb{Z}_2^2$. There are four choices of this pair:

$$(0,0),\quad (1,0),\quad (0,1),\quad (1,1). \tag{II.7.32}$$

An SO/USp projection sign alone is therefore not a complete variant label. Equations (II.7.30) and (II.7.31) use only the ordinary O3$^-$ charge row. We do not infer the

charges or global gauge groups of the other three choices from this finite table. Later O7 constructions, including the Sen limit, use the cover/quotient distinction; their dynamics require additional input beyond this charge equation.

II.7.6 Local and compact cancellation

When does a projected gauge theory satisfy the string charge condition? A local parity projection answers which open vectors can exist at a chosen stack. It supplies an algebra such as $\mathfrak{so}(N)$ or $\mathfrak{usp}(2k)$. An RR field equation answers a different question: can the total source be supported on the specified transverse space? To see the latter, write a schematic sourced equation for an RR field strength F as

$$d{*}F = j_{\text{brane}} + j_{\text{O}} + j_{\text{extra}}. \tag{II.7.33}$$

The last term stands for specified flux, curvature, gauge Chern–Simons or other sources when they occur. On a closed transverse cycle Σ of the appropriate dimension, Stokes' theorem gives

$$0 = \int_\Sigma d{*}F = \int_\Sigma j_{\text{brane}} + \int_\Sigma j_{\text{O}} + \int_\Sigma j_{\text{extra}}. \tag{II.7.34}$$

The simple O7 and O3 charge equations set the last integral to zero and assume ordinary minus planes in the indicated T-dual compact setup. Without those assumptions, their 32-unit answer is not a universal local rule. A noncompact transverse space may also permit boundary flux; then the same integral argument requires its boundary term.

To isolate the role of compactness, remove a small ball around each source and integrate over the remaining region U. Stokes' theorem now reads

$$\int_U d{*}F = \int_{\partial U} {*}F. \tag{II.7.35}$$

On a compact space the source fluxes across the small spheres must sum to zero after all other terms are included, since there is no outer boundary. On a noncompact space an outer boundary can carry flux. This is a statement about the chosen RR field and transverse geometry, not a license to discard a source equation. The Type I ten-form illustrates precisely why: its field equation has no transverse flux channel in which to use this escape.

For a noncompact region U_R enclosing the sources and cut off at radius R, let $\partial_{\text{out}}U_R$ be its outer boundary. The balance is

$$Q_{\text{source}}(U_R) = \int_{\partial_{\text{out}}U_R} {*}F. \tag{II.7.36}$$

The right side is absent for a closed compact transverse cycle. It may be nonzero in a noncompact geometry, subject to the actual boundary conditions. Equation (II.7.36) is schematic because the form degree and orientation depend on the RR field under study.

The D9 ten-form is a special boundary of this reasoning. It has no transverse spatial direction through which field lines can escape, even in flat noncompact ten-dimensional spacetime. Varying its coupling gives the zero-cycle constraint directly:

$$\delta_{A_{10}} S \propto (n_9 - 32) = 0. \tag{II.7.37}$$

It would be wrong to dismiss this condition just because the Type I spacetime is noncompact. It would also be wrong to model the ten-form as an ordinary propagating closed particle whose flux disperses to infinity. The field equation and the long-cylinder coefficient encode the same source requirement in their stated contexts.

Consider the local projected vector examples from Section II.7.3. The $N = 6$ symmetric case has fifteen vector generators, and the $N = 4$ antisymmetric case has ten. Neither number enters (II.7.37) as n_9. A local dimension count supplies no information about distant branes or O-planes. Conversely, satisfying the Type I $n_9 = 32$ source equation does not by itself specify a four-dimensional chiral spectrum after compactification. The gauge anomaly of such a local theory depends on chiral representations and possible inflow or Green–Schwarz terms, schematically

$$\mathcal{A}_{\text{local}} = \mathcal{A}_{\text{chiral matter}} + \mathcal{A}_{\text{inflow/GS}}. \tag{II.7.38}$$

The two equations may be linked by the dynamics of a particular model. They are still distinct calculations with distinct input data. A numerical crosscap charge is not a cubic anomaly coefficient.

For a concrete logical test, keep the local $N = 6$ symmetric endpoint sector fixed. Its vector count remains 15 whether a distant compact completion contains enough D-branes to satisfy an O7 charge equation or is missing one quotient object. In the latter toy charge equation the integrated charge would be $-16 + 15 = -1$ in quotient units; the local $\mathfrak{so}(6)$ count has not changed. Conversely, add the missing distant object and the global sum becomes zero without determining whether any four-dimensional chiral matter at the local node has an anomaly. The comparison concerns inputs, not two complete string vacua. It shows what a vector-algebra calculation lacks.

A compact O7 example shows the distinction without a general theorem. Put all sixteen quotient D7 objects near one of the four ordinary O7 loci. The global source sum remains

$$Q_{7,\text{total}} = 4(-4) + 16 = 0 \qquad \text{in quotient units.} \tag{II.7.39}$$

The local source at the populated point differs from the source at each unpopulated point. Gauge enhancement at that stack is a local open-string question, whereas (II.7.39) sums all four fixed loci. The full closed and open sectors determine allowed compact configurations. The equation alone is only a necessary charge condition under its assumptions.

The same warning applies to the quadratic channel bracket. Its untwisted nine-brane line can vanish while a different twisted RR source remains. In the K3 example from which (II.7.21) was extracted, the amplitude has additional five-brane and fixed-point terms. Solving one square therefore does not solve the entire model. Likewise, a four-dimensional local anomaly may receive inflow or Green–Schwarz contributions that are absent from a vector count. The appropriate comparison in a specific compactification is between its full set of RR field equations and its full spectrum and anomaly-cancellation mechanism.

This is the practical route into the later construction chapters. Volume VI.7 will track twisted RR contributions that the untwisted source sum omits. Volume VI.8 will use the transpose rule at a local node. Neither chapter can replace its model-specific source and anomaly calculations with a bare SO/USp label. The practical rule is to

declare the parity sector, the RR field and cycle, and the charge unit before comparing local and global statements.

II.7.7 Exercises

The first four tasks accept exact structured answers through the companion grader. Show the intermediate calculation on paper before submitting the named fields. The last two require written physical reasoning.

1. For a massless vector satisfying $A = -\gamma A^{\mathsf{T}} \gamma^{-1}$ and $A^{\dagger} = -A$ in an orthonormal Chan–Paton basis, find the compact real Lie-algebra dimensions for $\gamma = I_6$ and $\gamma = J_4$, where J_4 is the $k = 2$ matrix in (II.7.11). Submit the integer fields `so6_dimension` and `usp4_dimension`. Explain how the block count avoids confusing group rank with algebra dimension.

2. On the ordinary $T^2/\mathbb{Z}_2$ orientifold with four O7$^-$ planes, each of charge -8 in covering D7 units, assume no extra sources. Give the total O7 covering charge, the required D7 covering count, the quotient physical count, and the quotient count per plane for a uniform placement. Submit `o7_cover_total`, `d7_cover_required`, `d7_physical_required`, and `d7_physical_per_plane`. Explain why uniform placement is stronger than total neutrality.

3. Use $Q_{\mathrm{cover}}(\mathrm{O}p^-) = -2^{p-4}$ to find one O3 and one O9 charge in cover and quotient units. Submit `o3_cover` and `o3_quotient` as exact rational strings, and `o9_cover` and `o9_quotient` as integers. State why the O9 quotient line is a translated count rather than a count of separated image pairs.

4. Give the two closed-channel endpoint types for the annulus, Möbius strip and Klein bottle. Submit `annulus`, `mobius`, and `klein`, each as a two-element array of the strings `boundary` or `crosscap`. Explain in words why these six endpoint labels do not fix the number 32 in the Type I RR source.

5. A local projected quiver node has a well-defined SO or USp vector algebra. Explain why its four-dimensional anomaly calculation and the compact RR tadpole equation require different information. Name one additional source or term that may enter the integrated RR equation, and state what data a comparison in a specified compactification would require.

6. A colleague specifies an O3 model only as "O3-plus." Explain which NS and RR discrete choices must be given to identify a full variant. Explain why the SO/USp projection sign is insufficient, without constructing a charge table for the variants.

II.7.8 Take-home message

Take-home message

Worldsheet parity reverses the ordered endpoints of an open string. Its action on the massless vector matrix gives compact orthogonal or symplectic algebras when the Chan–Paton form is unitary in an orthonormal basis. The annulus, Möbius strip and Klein bottle become boundary–boundary, boundary–crosscap and crosscap–crosscap exchanges. Their actual RR coefficients come from the worldsheet amplitude; in Type I the D9 ten-form source fixes $n_9 = 32$. O9, O7 and ordinary O3 charge equations agree under T-duality when cover and quotient terms are translated together. Local vector content, RR neutrality and anomaly cancellation are related only through the full data of a specified model.

Status and sources

Section 1. The physical parity route is [WS] from Gimon and Polchinski (1996, physical PDF pp. 3–4, sec. 2). Pure Ω has no transverse fixed locus; ΩR includes a target reflection.
Section 2. Endpoint exchange and order-two closure are [WS] from Gimon and Polchinski (1996, physical PDF pp. 4–6, eqs. (2.2), (2.6)–(2.8)). The two-label eigenspace and complete-matrix argument are [MATH] under the stated sector assumptions.
Section 3. Vector parity and SO/USp projections are [WS] from Gimon and Polchinski (1996, physical PDF pp. 5–6, eqs. (2.7)–(2.8)). The compact block counts are [MATH] under a unitary Chan–Paton form and anti-Hermitian reality. The deliberately nonunitary $\gamma = \mathrm{diag}(1, 2)$ example is a separate [MATH] counterexample: it compares the complex transpose solution with its anti-Hermitian intersection at a fixed identity metric. The real J is the symplectic form used in the Chan–Paton projection. Witten (1998a, physical PDF p. 8) writes $\mathrm{Sp}(k)$ for this book's $\mathrm{USp}(2k)$. Global group form is not fixed.
Section 4. Channel ends and local moduli are [WS] from Gimon and Polchinski (1996, physical PDF pp. 9–12, eq. (3.8)). The linear nonpropagating ten-form source is [WS] from Polchinski (1995, physical PDF pp. 8–9, eq. (20)). The nine-brane bracket and separate NSNS/RR conditions are [WS] from Gimon and Polchinski (1996, physical PDF pp. 19–20, eqs. (3.30), (4.1)). The square and sample values are [MATH]; the bracket is one K3 amplitude term.
Section 5. The ordinary charge sign and cover units use the orientifold charge and covering-space conventions stated above at [WS] scope. O9/O7 normalization and historical sign translation are [WS] from Polchinski (1995, physical PDF p. 9, eq. (20)) and Witten (1998b, physical PDF pp. 4, 12–13). O3 fixed-point and unit arithmetic are [MATH] under T-duality, not a direct O3 amplitude. The twisted-cohomology result $H^3(\mathbb{RP}^5, \widetilde{\mathbb{Z}}) = \mathbb{Z}_2$ is a cited [MATH] input from Witten (1998a, physical PDF pp. 12–14, eqs. (3.4)–(3.7)); the integral local system reverses sign around the nontrivial loop. Identifying one such class for each quantized NS and RR two-form is a separate sourced physical premise, with primary evidence classification pending. The source couples

these fields to fundamental-string and D-string surfaces, respectively; the joint two-bit statement is not a perturbative fundamental-worldsheet derivation. No variant charge table or global gauge group follows.

Section 6. Integrated RR equations and extra curvature/gauge terms are [WS] from Gimon and Polchinski (1996, physical PDF p. 8, eqs. (3.1)–(3.2)); the D9 zero-cycle condition is [WS] from Polchinski (1995, physical PDF pp. 8–9). Cycle integration and the distinction from local anomaly data are [MATH] under stated assumptions. No universal anomaly equivalence or complete CFT is established.

Section 7. Exercises 1–4 ask [MATH] consequences; Exercises 5–6 require written physical interpretation.

Section 8. The take-home message summarizes the scoped claims above and makes no additional claim.

References

Gimon, E. G. and J. Polchinski (1996). "Consistency Conditions for Orientifolds and D-Manifolds". In: *Phys. Rev. D* 54, pp. 1667–1676. DOI: 10.1103/PhysRevD.54.1667. arXiv: hep-th/9601038.

Polchinski, J. (1995). "Dirichlet-Branes and Ramond-Ramond Charges". In: *Phys. Rev. Lett.* 75, pp. 4724–4727. DOI: 10.1103/PhysRevLett.75.4724. arXiv: hep-th/9510017.

Witten, E. (1998a). "Baryons and Branes in Anti de Sitter Space". In: *JHEP* 07, p. 006. DOI: 10.1088/1126-6708/1998/07/006. arXiv: hep-th/9805112.

Witten, E. (1998b). "Toroidal Compactification Without Vector Structure". In: *JHEP* 02, p. 006. DOI: 10.1088/1126-6708/1998/02/006. arXiv: hep-th/9712028.

Chapter II.8

Supergravity limits and decoupling

II.8.1 What a charged brane leaves in the bulk

A stack of D3-branes has two descriptions that are useful at different distances. Open strings ending on the stack give a four-dimensional gauge theory at low energy. Far from the stack, its charge and energy appear through ten-dimensional bulk fields. The latter description can become a curved throat. The immediate question is which parts of this relation follow from field equations and units, and which parts require a physical input about branes.

This chapter follows a deliberately small set of fields. The D3 uses a metric and a self-dual five-form in Type IIB theory. The M2 uses an eleven-dimensional metric and an electric four-form. Their radial functions have different powers because their transverse spaces have different dimensions. A flux integral then gives the classical M2 geometric scale. Finally, wrapping the membrane on a physical circle fixes the IIA string and gravitational units. Figure II.8.1 keeps these operations in their causal order.

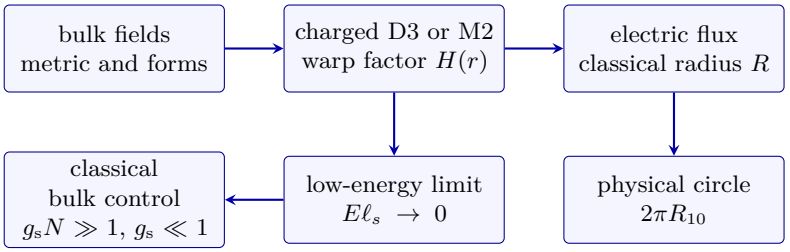


Figure II.8.1: The route through the chapter. A bulk action identifies fields and their coupling weights. A sourced charged-brane solution then selects a warp factor; its radial exponent can be checked away from the source. Flux fixes a classical geometric scale. Circle reduction compares physical lengths and tensions. The low-energy limit and the additional conditions for a classical bulk approximation are separate final tests. Arrows denote uses of information, not equivalences proved by the diagram.

The companion calculations can be reproduced with elementary differentiation and dimensional analysis. The full supersymmetric solutions, their source normalizations, and the existence of the corresponding branes are physical inputs. We will keep those inputs beside the calculations that use them. Chapter 4 supplied the massless string fields; the later D3 and M2 construction chapters will need the resulting scale and limit dictionary.

II.8.2 Bulk actions and fields

Which massless bulk field can carry a brane charge, and what changes when we describe the same physics in another metric frame? The NS sector of a ten-dimensional Type II theory contains a string-frame metric $g^{(s)}_{MN}$, the total dilaton Φ, and a two-form B_2 with $H_3 = dB_2$. Its leading bosonic terms are

$$S_{\rm NS} \sim \int d^{10}x\, \sqrt{-\det g^{(s)}}\, e^{-2\Phi} \left(R[g^{(s)}] + 4(\partial\Phi)^2 - \frac{1}{12} H_{MNP} H^{MNP}_{(s)} \right). \qquad \text{(II.8.1)}$$

The scalar $g_{\rm s} = e^{\Phi_\infty}$ below denotes the asymptotic string coupling and must not be confused with the string-frame tensor $g^{(s)}$. Johnson's Type IIA and IIB actions give the exact relative coefficients $+4$ and $-1/12$ in this leading bosonic NS sector. Here $H_{MNP}H^{MNP}_{(s)}$ is the raw contraction, whereas $|H_3|^2_s := H_{MNP}H^{MNP}_{(s)}/3!$; thus the last term is also $-\frac{1}{2}|H_3|^2_s$. More generally, $|F_p|^2 := F_{M_1\ldots M_p}F^{M_1\ldots M_p}/p!$, including the eleven-dimensional form below. Equation (II.8.1) suppresses only the common action normalization and the other fields and higher-order terms; it is not the complete Type II action. Johnson's G is our $g^{(s)}$, and his Φ is our total dilaton. His Einstein metric $\widetilde{G} = e^{(\Phi_\infty - \Phi)/2} G$ differs from the book metric $g^{(E)} = e^{-\Phi/2} g^{(s)}$ by the constant factor $\widetilde{G} = e^{\Phi_\infty/2} g^{(E)}$. This frame translation does not redefine the physical circle radius used later. The physical asymptotic gravitational coefficient κ_{10} is defined there by circle reduction. Changing frame in a curvature term also produces derivatives of Φ and a possible boundary term.

The Einstein-frame metric is defined in ten dimensions by $g^{(E)}_{MN} = e^{-\Phi/2} g^{(s)}_{MN}$. Thus a constant local Weyl factor acts on the measure and every inverse metric separately:

$$g^{(s)}_{MN} = e^{\Phi/2} g^{(E)}_{MN}, \qquad \sqrt{-\det g^{(s)}} = e^{5\Phi/2}\sqrt{-\det g^{(E)}}, \qquad g^{MN}_{(s)} = e^{-\Phi/2} g^{MN}_{(E)}. \tag{II.8.2}$$

The first factor in the measure uses all ten metric directions. A three-form norm contracts three inverse metrics. Consequently its density is

$$\sqrt{-\det g^{(s)}}\, e^{-2\Phi} |H_3|^2_s = \sqrt{-\det g^{(E)}}\, e^{(5/2-2-3/2)\Phi} |H_3|^2_E = \sqrt{-\det g^{(E)}}\, e^{-\Phi} |H_3|^2_E. \tag{II.8.3}$$

This is a density identity for the same three-form components. It does not require Φ to be constant. For example, take $y = x^1$ and $\Phi(y) = \Phi_0 + ay$ on a patch. The closed field $H_3 = h(x^1)\, dx^1 \wedge dx^2 \wedge dx^3$ has a local potential $B_2 = \big(\int^{x^1} h(t)\, dt\big) dx^2 \wedge dx^3$. In a locally diagonal metric, the Einstein-frame coefficient of its contracted norm at y and $y + \delta y$ changes by

$$\frac{e^{-\Phi(y+\delta y)}}{e^{-\Phi(y)}} = e^{-a\delta y}. \tag{II.8.4}$$

The example concerns the density coefficient, not a solution of the dilaton and three-form equations. If one transformed the full $R[g^{(s)}]$ term by using only the algebra in (II.8.3), one would miss the derivatives of the local Weyl factor.

It is useful to do that distinct curvature calculation once. Use $R^P{}_{QMN} = \partial_M \Gamma^P_{NQ} - \partial_N \Gamma^P_{MQ} + \Gamma^P_{MR}\Gamma^R_{NQ} - \Gamma^P_{NR}\Gamma^R_{MQ}$ and $R_{QN} = R^P{}_{QPN}$. For $g'_{MN} = e^{2\omega} g_{MN}$, the connection difference is $C^P{}_{MN} = \delta^P_M \partial_N \omega + \delta^P_N \partial_M \omega - g_{MN} \partial^P \omega$. Substituting $\Gamma' = \Gamma + C$ into the Ricci tensor gives $R'_{MN} = R_{MN} - (D-2)\nabla_M \partial_N \omega - g_{MN} \nabla^2 \omega + (D-2)[\partial_M \omega \partial_N \omega - g_{MN} (\partial\omega)^2]$. Contracting with $g'^{MN} = e^{-2\omega} g^{MN}$ yields $-(D-2) - D = -2(D-1)$ for $\nabla^2 \omega$ and $(D-2)(1-D) = -(D-1)(D-2)$ for $(\partial\omega)^2$:

$$R[g'] = e^{-2\omega} \left[R[g] - 2(D-1)\nabla^2 \omega - (D-1)(D-2)(\partial\omega)^2 \right]. \tag{II.8.5}$$

Set $D = 10$ and $\omega = \Phi/4$, with $g' = g^{(s)}$ and $g = g^{(E)}$. The measure and explicit NS dilaton factor cancel the leading $e^{-\Phi/2}$ from the curvature, leaving

$$\sqrt{-\det g^{(s)}}\, e^{-2\Phi} R[g^{(s)}] = \sqrt{-\det g^{(E)}} \left[R[g^{(E)}] - \frac{9}{2} \nabla^2_E \Phi - \frac{9}{2} (\partial\Phi)^2_E \right]. \tag{II.8.6}$$

The original $4(\partial\Phi)^2_s$ term contributes $4(\partial\Phi)^2_E$ to the same density. On a patch where the integrated Laplacian has no boundary contribution, their sum is therefore

$$\sqrt{-\det g^{(E)}} \left[R[g^{(E)}] - \frac{1}{2} (\partial\Phi)^2_E \right]. \tag{II.8.7}$$

The coefficient $-1/2$ depends on keeping both pieces. When a boundary is present, the discarded Laplacian must be paired with the appropriate boundary action. The three-form calculation in (II.8.3) was algebraic; the Ricci calculation is a transformation of derivatives of the metric. This distinction is a reusable diagnostic when a lower-dimensional effective action is written in a different frame.

In Type IIB the Ramond–Ramond (RR) sector includes C_0, C_2, and C_4. The five-form relevant to a D3 is a gauge-invariant combination $\widetilde{F}_5$ of dC_4 and lower-form terms. Its physical field strength obeys

$$\widetilde{F}_5 = *_{10}\widetilde{F}_5. \tag{II.8.8}$$

The familiar compact bosonic formula with a $|\widetilde{F}_5|^2$ term is a pseudo-action: its variations are accompanied by (II.8.8). This is a property of that conventional presentation. A covariant bosonic action with an auxiliary field also exists, so it would be false to infer that Type IIB has no covariant action. The distinction matters whenever a field equation or stress tensor is taken from a displayed five-form term.

The eleven-dimensional low-energy bosons are a metric g_{11} and a three-form potential C_3, with $F_4 = dC_3$. Its bosonic action contains an Einstein term, a four-form kinetic term, and a $C_3 \wedge F_4 \wedge F_4$ coupling. Schematically, in the common length convention used below,

$$S_{11} \sim \frac{1}{2\kappa_{11}^2}\int \sqrt{-g_{11}}\big(R_{11} - \tfrac{1}{2}|F_4|^2\big) \;+\; \text{a } C_3 \wedge F_4 \wedge F_4 \text{ term.} \tag{II.8.9}$$

We leave the last coefficient schematic because it is not needed for the electric branch calculated here. A membrane couples electrically to C_3. These field names tell us what a charged solution can excite. They do not derive its full projector, the fermionic completion, or the membrane worldvolume action. The next section uses sourced D3 and M2 solutions and asks what their radial dependence implies.

The eleven-dimensional three-form supplies two types of ten-dimensional potential. On a circle product patch, its components with all legs in ten dimensions form a three-form. Components with one leg on the circle form a two-form. The latter becomes the IIA NS field after the physical circle and field normalization are translated.

In a general Kaluza–Klein reduction, the invariant circle one-form includes the Kaluza–Klein vector. The ten-dimensional RR four-form also acquires a corresponding mixing. This component count identifies the fields, not their full reduced action. It explains one difference between wrapped and unwrapped membranes. The wrapped worldvolume samples the two-form component; an unwrapped membrane couples to the three-form component.

The sectors in this section have different evidential roles. The Weyl factors are tensor algebra once the frame map is chosen. The existence and field content of the supergravity theories are physical inputs. The pseudo-action rule is needed to read the Type IIB five-form consistently. None of those facts alone says that a particular D3 or M2 field configuration solves every equation. That extra input arrives with the explicit sourced solutions, after which their radial geometry can be checked directly. Figure II.8.1 places this field inventory before the sourced solutions. The frame change describes the same bulk fields and does not create a second theory.

II.8.3 Branes as charged solutions

Why do the D3 and M2 harmonic functions fall with the fourth and sixth powers of distance? Let r be a physical radius in a flat Euclidean transverse space, measured

away from the brane at $r = 0$. We start with the standard positive D3 solution in Type IIB string frame. Its dilaton is constant, and its metric and harmonic function are

$$\begin{aligned} ds^2_{10,s} &= H_3^{-1/2} ds^2(\mathbb{R}^{1,3}) + H_3^{1/2}(dr^2 + r^2 d\Omega_5^2), \\ H_3(r) &= 1 + \frac{L^4}{r^4}, \qquad L^4 = 4\pi g_{\rm s} N (\alpha')^2. \end{aligned} \tag{II.8.10}$$

The solution also carries an appropriate self-dual five-form. The coefficient L^4 and the BPS solution are sourced physical inputs. In the book's component-trace convention, $g^2_{\rm YM} = 4\pi g_{\rm s}$ for the D3 theory; a source using $2\pi g_{\rm s}$ has a different gauge-action normalization. We do not derive the bulk coefficient by inserting one source's gauge coupling into another convention. Here $H_3(r)$ is the scalar D3 harmonic function, distinct from the NS three-form $H_3 = dB_2$ used above.

For a radial function on punctured flat $\mathbb{R}^d$, the angular derivatives vanish and the Laplacian reduces to

$$\Delta_d H = \frac{1}{r^{d-1}} \frac{d}{dr}\left(r^{d-1} \frac{dH}{dr} \right), \qquad r > 0. \tag{II.8.11}$$

Integrating the homogeneous equation once gives $r^{d-1} H' = c$. If $d > 2$, one more integration gives the full radial family

$$H(r) = A + B r^{2-d}, \qquad d > 2. \tag{II.8.12}$$

The additive constant may be fixed to one by the asymptotic flat-space normalization. The $d = 2$ branch is logarithmic and cannot be obtained by simply setting $d = 2$ in (II.8.12). Nor does this punctured-space equation determine a distributional source at $r = 0$.

The missing source coefficient can be seen without assigning it a brane charge. For the radial function in (II.8.12), the outward derivative flux through a sphere of radius r is

$$\int_{S_r^{d-1}} \partial_r H \, dA = (2-d) B r^{1-d} \, \Omega_{d-1} r^{d-1} = -(d-2)\Omega_{d-1} B. \tag{II.8.13}$$

Here Ω_{d-1} is the area of the unit $(d-1)$-sphere. If a chosen Poisson equation had source $\Delta H = -Q\delta^{(d)}(x)$, integrating it over a small ball would set $B = Q/[(d-2)\Omega_{d-1}]$. That conditional mathematical statement still leaves the physical value of Q to the field normalization and brane source action. In a supergravity solution even the effective Poisson equation follows from the full ansatz; (II.8.13) alone cannot certify it. This is why the sourced coefficient in (II.8.10) remains an input.

An explicit power test shows what information harmonicity does contain. Write $H = 1 + A r^{-a}$. Direct differentiation gives

$$H' = -aAr^{-a-1}, \qquad \Delta_d H = a(a+2-d) A r^{-a-2}. \tag{II.8.14}$$

For a nonconstant decaying branch $a > 0$, the residual vanishes precisely when $a = d-2$. A D3 has six transverse spatial coordinates, so $a = 4$. Substituting $d = 6$ and $a = 4$ yields $4(4+2-6)Ar^{-6} = 0$. If we instead tried $a = 5$, the residual would be $5Ar^{-7}$,

which is nonzero. This simple counterexample keeps the local equation distinct from a guess based on dimensional appearance.

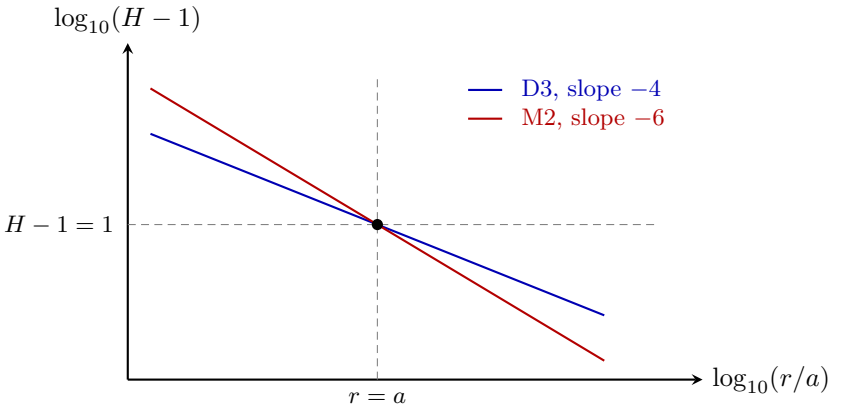


Figure II.8.2: The charge terms of the two sourced radial functions on dimensionless logarithmic axes. For the D3 take $a = L$ and $H - 1 = (r/a)^{-4}$; for the M2 take $a = R$ and $H - 1 = (r/a)^{-6}$. The slopes are the punctured-space harmonic exponents. The curves meet at $r = a$ by definition of each scale; the plot does not compare D3 and M2 charge units or show the source point $r = 0$.

Figure II.8.2 turns the exponent calculation into a direct comparison. The M2 charge term rises faster as one moves inward in its own radius units. The graph does not fix either radius; that requires the sourced coefficient or a flux integral.

An M2 has eight transverse spatial coordinates. Its sourced eleven-dimensional metric uses different warp powers,

$$ds_{11}^2 = H_2^{-2/3} ds^2(\mathbb{R}^{1,2}) + H_2^{1/3}(dr^2 + r^2 d\Omega_7^2), \qquad H_2(r) = 1 + \frac{R^6}{r^6}. \tag{II.8.15}$$

Now (II.8.14) gives $6(6 + 2 - 8)R^6 r^{-8} = 0$ for $r > 0$. The flat $k = 1$ source fixes $R^6 = 32\pi^2 N \ell_p^6$ in its classical normalization. The exponent six follows from eight transverse dimensions; the coefficient and the warp exponents do not follow from this one radial calculation. A full solution also requires the form-field equation, Einstein equation, source convention, and supersymmetry conditions.

The two sourced metrics have useful near-horizon limits. For the D3, $r \ll L$ permits $H_3 \simeq L^4/r^4$. The coefficient of the parallel metric becomes $H_3^{-1/2} = r^2/L^2$, while the transverse radial coefficient becomes $H_3^{1/2} = L^2/r^2$. Hence

$$ds_{10,s}^2 \simeq \frac{r^2}{L^2} ds^2(\mathbb{R}^{1,3}) + \frac{L^2}{r^2} dr^2 + L^2 d\Omega_5^2. \tag{II.8.16}$$

With $z = L^2/r$, the first two terms become $(L^2/z^2)[ds^2(\mathbb{R}^{1,3}) + dz^2]$. This identifies the local product geometry as a Poincaré patch of $\mathrm{AdS}_5 \times S^5$ with common radius L.

The coordinate change, rather than the label alone, tells the reader which radial end is the Poincaré horizon.

One should keep track of where this approximation is taken. The original H_3 approaches one for $r \gg L$, and the metric there approaches flat ten-dimensional space. Near $r = 0$, the constant one is negligible but the transverse sphere remains of radius L rather than shrinking with the coordinate r. The radial proper distance is logarithmic:

$$\int_{r_1}^{r_2} \sqrt{g_{rr}}\, dr = L \int_{r_1}^{r_2} \frac{dr}{r} = L \log \frac{r_2}{r_1} \qquad (r_1, r_2 \ll L). \tag{II.8.17}$$

The coordinate origin lies at infinite proper distance within this limiting metric. This explains why the radial limit creates a throat rather than simply a small flat ball. It does not decide which excitations of the throat are described by a particular boundary theory.

For the M2, $r \ll R$ gives $H_2 \simeq R^6/r^6$, and its parallel and radial factors become r^4/R^4 and R^2/r^2. Define a new positive coordinate z by

$$z = \frac{R^3}{2r^2}, \qquad \frac{r^4}{R^4} = \frac{R^2}{4z^2}, \qquad \frac{R^2}{r^2} dr^2 = \frac{R^2}{4z^2} dz^2. \tag{II.8.18}$$

The last identity follows from $dz/dr = -R^3/r^3$: inserting $dr = -(r^3/R^3)dz$ and $r^4 = R^6/(4z^2)$ gives exactly the displayed factor. The metric is therefore

$$ds_{11}^2 \simeq \frac{(R/2)^2}{z^2} \left[ds^2(\mathbb{R}^{1,2}) + dz^2 \right] + R^2 d\Omega_7^2, \qquad R_{\mathrm{AdS}_4} = \frac{R_{S^7}}{2}. \tag{II.8.19}$$

The coordinate z has units of length, so no hidden dimensionless rescaling of the M2 worldvolume coordinates is needed. The factor of two is fixed by the actual radial change. The full supersymmetric interpretation of these sourced backgrounds is a separate physical result. Here their local geometry prepares the flux calculation and the later M2 discussion.

The additive one in either harmonic function also sets an accuracy question for the near-horizon approximation. At $r = L/3$ for the D3, the charge term is $L^4/r^4 = 81$, so the ratio of the discarded one to that term is $1/81$. At $r = R/2$ for the M2, the corresponding ratio is $1/64$. At $r = L$ or $r = R$, by contrast, the charge term equals one and the approximation is not sharp. These ratios compare terms inside a sourced classical metric; they do not test whether string or quantum corrections are small. The latter depend on radius in fundamental units and will be treated separately in the last section.

II.8.4 Flux fixes a scale

What sets the radius R when the M2 transverse sphere is replaced by a free quotient? We use the common-phase action of $\mathbb{Z}_k$ on $S^7 \subset \mathbb{C}^4$, with positive integer k. On the sphere this action is free. The unit-radius angular space $Y_7 = S^7/\mathbb{Z}_k$ has a k-fold covering and volume

$$\mathrm{Vol}(S^7) = \frac{\pi^4}{3}, \qquad \mathrm{Vol}(Y_7) = \frac{\pi^4}{3k}. \tag{II.8.20}$$

The covering radius R is also the physical radius multiplying the quotient metric locally. Quotienting divides the angular integral by k; it does not divide the local curvature radius by k.

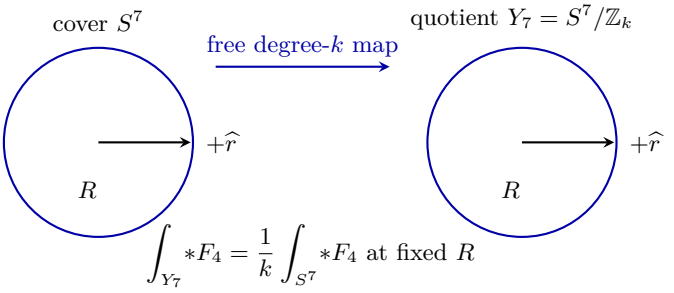


Figure II.8.3: Angular covering and quotient at the same local radius R. Each circle is a schematic section of the seven-dimensional angular geometry, not its topology or area. The radial arrows mark the positive outward orientation used for the electric dual flux. The free covering map has degree k, so integrating the same locally defined $*F_4$ over the quotient gives $1/k$ of the covering integral.

Figure II.8.3 separates the unchanged local radius from the changed integral. The radial arrows fix the positive angular orientation; the flux calculation below specifies its normalization.

For completeness, the unit volume in (II.8.20) can be recovered without memorizing a sphere formula. Evaluate the same Gaussian integral on $\mathbb{R}^8$ in Cartesian and polar coordinates:

$$\int_{\mathbb{R}^8} e^{-|x|^2} d^8x = \pi^4 = \Omega_7 \int_0^\infty e^{-r^2} r^7 dr = 3\Omega_7. \tag{II.8.21}$$

Thus $\Omega_7 = \pi^4/3$. The free quotient identifies k points in each generic orbit, so the angular measure of one fundamental domain is Ω_7/k. The fixed origin of the ambient cone is not on the unit sphere and does not change this volume division. A quotient with fixed points on the angular sphere would require more care; the free common-phase action avoids that issue in the calculation here.

Choose an orthonormal four-volume v_4 on the AdS_4 factor and an orthonormal seven-volume v_7 on the angular factor. We adopt the orientation $\mathrm{vol}_{11} = -v_4 \wedge v_7$, so $*v_4 = +v_7$ and $*v_7 = -v_4$. The positive classical electric branch has

$$F_4 = \frac{6}{R} v_4, \qquad *F_4 = \frac{6}{R} v_7 = 6R^6\, \widehat{\mathrm{vol}}_{Y_7}. \tag{II.8.22}$$

The hat denotes the volume form of the unit-radius quotient. Its factor R^7 has been shown explicitly in the last equality. On the angular section of this pure electric branch, the $C_3 \wedge F_4$ contribution to the classical Page form vanishes. We can therefore evaluate the classical electric integral through the angular seven-cycle without using that term.

The membrane unit and eleven-dimensional gravitational coefficient are fixed in one asymptotic length convention,

$$T_{\mathrm{M2}} = \frac{1}{(2\pi)^2 \ell_p^3}, \qquad 2\kappa_{11}^2 = (2\pi)^8 \ell_p^9, \qquad 2\kappa_{11}^2 T_{\mathrm{M2}} = (2\pi)^6 \ell_p^6. \tag{II.8.23}$$

The last equality is multiplication, not a derivation of the minimal membrane unit from a classical solution. Using (II.8.20) and (II.8.22), the positive classical count is

$$N_{\mathrm{cl}} := \frac{1}{2\kappa_{11}^2 T_{\mathrm{M2}}} \int_{Y_7} *F_4 = \frac{6R^6}{(2\pi)^6 \ell_p^6} \frac{\pi^4}{3k} = \frac{R^6}{32\pi^2 k \ell_p^6}. \tag{II.8.24}$$

Thus $R^6 = 32\pi^2 k N_{\mathrm{cl}} \ell_p^6$. At $k = 1$ this reproduces the flat M2 classical coefficient in (II.8.15). This is a useful known-object comparison, not an independent proof that the quotient supports every desired global state.

For a numerical geometric example, take $k = 2$ and $N_{\mathrm{cl}} = 3$. The quotient has volume $\pi^4/6$, which is half the covering volume. The radius relation gives

$$\frac{R^6}{\ell_p^6} = 32\pi^2(2)(3) = 192\pi^2, \qquad \frac{R}{\ell_p} = (192\pi^2)^{1/6}. \tag{II.8.25}$$

If the same classical electric count were placed on the unquotiented sphere, the sixth power would be $96\pi^2$, since the full sphere has twice the angular volume. The quotient example demonstrates why the k factor belongs in the integral before any radius is inferred. Neither example supplies a quantitative finite-N error estimate for supergravity.

The orientation is as important as the volume. Reversing the orientation of the angular integration cycle while keeping $F_4 = (6/R)v_4$ fixed reverses the sign of the integral. That operation does not describe the same positive-charge branch with a harmless relabeling. Alternatively, reversing the electric field as well restores the positive count but changes the charge sector. The formula $R^6 \propto kN_{\mathrm{cl}}$ assumes the positive branch and positive k. Its sign convention is an input to the calculation, just as the covering volume is.

The same radius formula offers a limited approximation check. In the eleven-dimensional covering geometry, a large ratio R/ℓ_p asks for $32\pi^2 k N_{\mathrm{cl}}$ to be parametrically large. It is useful to write

$$\left(\frac{\ell_p}{R}\right)^6 = \frac{1}{32\pi^2 k N_{\mathrm{cl}}}. \tag{II.8.26}$$

This only compares a local curvature scale with the Planck length. It is not a criterion for an exact quantum charge, nor does large k alone validate every region of an IIA reduction. The size of a reduced circle is a different geometric question, developed in the next section.

There is a separate global quantization statement for magnetic four-form flux. On the appropriate smooth spin M-theory space, in the normalization of (II.8.23), the shifted cohomology class obeys

$$\left[\frac{T_{\mathrm{M2}} F_4}{2\pi}\right] - \frac{p_1}{4} = \left[\frac{F_4}{(2\pi\ell_p)^3}\right] - \frac{p_1}{4} \in H^4(X, \mathbb{Z}). \tag{II.8.27}$$

Here p_1 is the first Pontryagin class of the eleven-dimensional spin geometry, with the cohomological normalization shown. The square brackets denote a de Rham class and the displayed integral condition is the sourced shifted law. It concerns magnetic four-cycles. Equation (II.8.24) instead integrates an electric dual over a seven-cycle. One cannot replace N_{cl} by an exact quantum Page charge or field-theory rank merely by quoting (II.8.27). Torsion and higher-derivative contributions require their own global treatment. This classical geometric scale will be used in the M2 construction chapters, while the topology chapters provide the tools for global flux questions.

II.8.5 Reduction on a physical circle

When does an M2 wrapping the eleventh circle become a fundamental IIA string? Let X^{10} be a physical length coordinate, with $X^{10} \sim X^{10} + 2\pi R_{10}$. Equivalently, write $X^{10} = R_{10}\theta_{10}$ with $\theta_{10} \sim \theta_{10} + 2\pi$. Figure II.8.4 displays the spatial slice of a once-wrapped membrane.

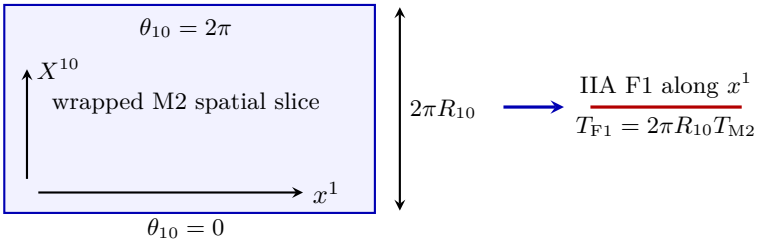


Figure II.8.4: Spatial slice of an M2 wrapped once on the physical X^{10} circle. The rectangle's upper and lower edges at $\theta_{10} = 2\pi$ and 0 are identified, making the vertical physical length $2\pi R_{10}$. Time is common and suppressed. Multiplying membrane tension by that length gives the string tension of the line along x^1. The drawing assumes an unwarped circle in the common asymptotic frame.

In the unwarped asymptotic frame used for all tensions below, the effective string tension is

$$T_{\mathrm{wrapped}} = (2\pi R_{10}) T_{\mathrm{M2}} = \frac{R_{10}}{2\pi \ell_p^3}. \tag{II.8.28}$$

This follows directly by taking a membrane worldvolume of area $(2\pi R_{10})$ times an unwrapped string worldsheet area. It is not a claim that every warped circle has the same proper circumference at every point.

The fundamental IIA string has $T_{\mathrm{F1}} = 1/(2\pi\alpha')$, and $\ell_s^2 = \alpha'$. Equating it to (II.8.28) fixes

$$\ell_p^3 = R_{10}\alpha', \qquad R_{10} = g_{\mathrm{s}}\ell_s, \qquad \ell_p = g_{\mathrm{s}}^{1/3}\ell_s. \tag{II.8.29}$$

The second equality is the physical IIA/M-theory circle relation in this asymptotic frame. Its source may use a differently rescaled eleven-dimensional metric and radius. Such a coordinate radius should not be set equal to R_{10} before the frame is translated.

The first and third equalities also show a useful dimension check: ℓ_p^3, $R_{10}\alpha'$, and $g_s\ell_s^3$ all have length cubed.

The same circumference appears in the gravitational action. Restrict to circle-independent zero modes on an unwarped product patch. Integrating the eleven-dimensional Einstein coefficient over X^{10} gives

$$\frac{1}{2\kappa_{10}^2} = \frac{2\pi R_{10}}{2\kappa_{11}^2}, \qquad 2\kappa_{10}^2 = \frac{2\kappa_{11}^2}{2\pi R_{10}}. \tag{II.8.30}$$

Substitute (II.8.23) and (II.8.29), retaining every power of the physical length:

$$2\kappa_{10}^2 = (2\pi)^7 \frac{\ell_p^9}{R_{10}} = (2\pi)^7 R_{10}^2 (\alpha')^3 = (2\pi)^7 g_s^2 (\alpha')^4. \tag{II.8.31}$$

Here κ_{10} is the asymptotic gravitational coupling in the stated ten-dimensional normalization. A full reduction with a varying circle and dilaton includes field-dependent Weyl factors; (II.8.30) is its simple constant-radius coefficient comparison.

Take the asymmetric example $R_{10} = 3\ell_s$. Then $g_s = 3$, $\ell_p^3 = 3\ell_s^3$, and $T_{\mathrm{M2}} = 1/[3(2\pi)^2\ell_s^3]$. Multiplying by the full circumference yields

$$(2\pi\, 3\ell_s)\frac{1}{3(2\pi)^2\ell_s^3} = \frac{1}{2\pi\ell_s^2} = T_{\mathrm{F1}}, \qquad 2\kappa_{10}^2 = 9(2\pi)^7\ell_s^8. \tag{II.8.32}$$

Using R_{10} instead of $2\pi R_{10}$ in the first multiplication would leave an erroneous $1/(2\pi)$ factor. Using the angle θ_{10} as though it had units of length would cause the same mistake in the gravity reduction. This dictionary supplies the physical units later used for circle lifts and Hopf-circle limits; it does not identify a general massive-IIA background with an eleven-dimensional product.

A second circle radius tests whether the relation is really about length rather than a convenient numerical choice. Take $R_{10} = \ell_s/8$, so $g_s = 1/8$ and $\ell_p^3 = \ell_s^3/8$. The wrapped membrane calculation now gives

$$(2\pi\ell_s/8)\frac{8}{(2\pi)^2\ell_s^3} = \frac{1}{2\pi\ell_s^2}, \qquad 2\kappa_{10}^2 = \frac{(2\pi)^7}{64}\ell_s^8. \tag{II.8.33}$$

The same fundamental string tension emerges although the eleven-dimensional circle and the ten-dimensional gravitational strength differ from the preceding example. In the first example $g_s = 3$, so a weakly coupled IIA perturbation series is not available merely because the algebra of wrapped tensions works. In this second example the asymptotic IIA coupling is smaller. Matching units is an exact dictionary within its assumptions, not a claim that one perturbative description works at every radius.

There is also a simple spectral meaning to the physical circumference. A field periodic in X^{10} has Fourier modes $e^{inX^{10}/R_{10}}$, with integer n. On an unwarped product background its Kaluza–Klein momentum is

$$p_{10} = \frac{n}{R_{10}}, \qquad M_n = \frac{|n|}{R_{10}} \quad \text{for a mode massless before compactification.} \tag{II.8.34}$$

The denominator is R_{10} because the angular period is 2π; the full $2\pi R_{10}$ entered the integrated action and the wrapped membrane tension. Confusing these two appearances of 2π is a common source of unit errors. The relation presumes the same unwarped circle used in (II.8.30); a varying circle requires its local proper radius.

II.8.6 Decoupling versus control

Can a low-energy D3 theory decouple from gravity while the corresponding curved bulk geometry is poorly approximated by classical supergravity? Yes. The low-energy limit holds the D3 count N, finite $g_{\rm s}$, a finite field-theory energy E, and $U = r/\alpha'$ fixed while $\alpha' \to 0$. The string length $\ell_s = \sqrt{\alpha'}$ then goes to zero. Massive strings have energy of order $1/\ell_s$, so

$$E\ell_s = E\sqrt{\alpha'} \longrightarrow 0. \tag{II.8.35}$$

The dimensionless ten-dimensional gravitational interaction at energy E scales as $\kappa_{10}^2 E^8$. Equation (II.8.31) makes its limit explicit:

$$\kappa_{10}^2 E^8 \;\propto\; g_{\rm s}^2(\alpha')^4 E^8 = g_{\rm s}^2 (E\ell_s)^8 \longrightarrow 0. \tag{II.8.36}$$

This is the fixed-energy decoupling argument in flat space. It suppresses exchange with ordinary bulk gravity while retaining a finite D3 gauge coupling in the chosen component convention. It does not make the dimensionless product $g_{\rm s}N$ large.

To see the curved throat at fixed U, divide the sourced D3 scale by string units:

$$\frac{L^4}{\ell_s^4} = \frac{L^4}{(\alpha')^2} = 4\pi g_{\rm s} N, \qquad \frac{L}{\ell_s} = (4\pi g_{\rm s} N)^{1/4}. \tag{II.8.37}$$

The ratio stays finite as $\alpha' \to 0$ at fixed $g_{\rm s}$ and N. For a parametrically small string-scale curvature, one needs $g_{\rm s}N \gg 1$. To suppress perturbative closed-string loops in the constant-dilaton D3 region, one separately needs $g_{\rm s} \ll 1$. Both can hold in a large-N regime, but neither is a logical consequence of (II.8.35). Figure II.8.5 keeps the two control axes distinct.

The fixed-U limit can also be read directly from the D3 metric rather than only from the radius ratio. Substitute $r = \alpha' U$ into (II.8.10). In the region that survives the low-energy scaling, $H_3 \simeq 4\pi g_{\rm s}N/[\alpha'^2 U^4]$. If $\lambda := 4\pi g_{\rm s}N$, the metric divided by α' becomes

$$\frac{ds_{10,s}^2}{\alpha'} = \frac{U^2}{\sqrt{\lambda}} ds^2(\mathbb{R}^{1,3}) + \sqrt{\lambda}\left(\frac{dU^2}{U^2} + d\Omega_5^2\right), \qquad \lambda = 4\pi g_{\rm s}N. \tag{II.8.38}$$

For example, at $U = U_0$ and $U = 2U_0$, the parallel metric coefficient increases by a factor of four while the angular sphere coefficient stays $\sqrt{\lambda}$. The ratio $L/\ell_s = \lambda^{1/4}$ controls the curvature in these string units. The overall α' of the dimensional metric vanishes, but the geometry measured in string units remains finite. Inferring "only zero modes" from that overall factor would miss the role of the redshift and the fixed U scaling.

The redshift can be made explicit for a static local excitation. At fixed U, the time component of the original metric satisfies $\sqrt{-g_{tt}} = \sqrt{\alpha'}\, U/\lambda^{1/4}$ if t is the asymptotic time coordinate used in (II.8.38). A mode whose conserved asymptotic energy is E has local proper energy $E_{\rm proper} = E/\sqrt{-g_{tt}}$. Therefore

$$E_{\rm proper}\ell_s = \frac{E\sqrt{\alpha'}}{\sqrt{-g_{tt}}} = \frac{E\lambda^{1/4}}{U}. \tag{II.8.39}$$

At fixed E and U, this ratio is finite even though $E\ell_s \to 0$ for an excitation measured at infinity. The calculation explains how finite local string-scale dynamics can coexist with decoupling of ordinary asymptotic massive strings. It uses the sourced D3 metric and a specified static observer; it does not construct the full spectrum of the throat or a duality map.

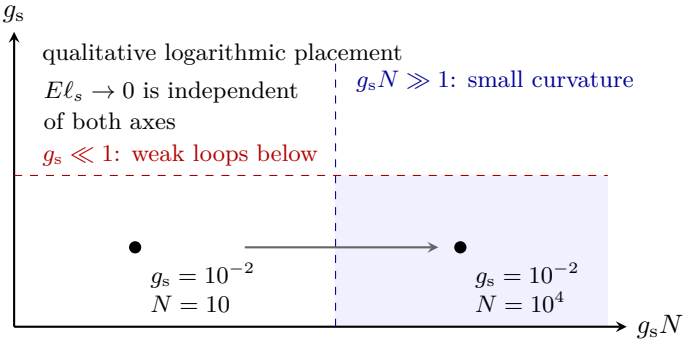


Figure II.8.5: Qualitative parameter plane for the D3 limit. The horizontal coordinate is g_sN and the vertical coordinate is g_s; logarithmic placement only illustrates parametric inequalities and marks no numerical cutoff. Rightward motion makes L/ℓ_s parametrically large. Downward motion weakens string loops. The low-energy condition $E\ell_s \to 0$ is an independent limiting operation and can be imposed at either marked point. The points show $g_s = 10^{-2}$ with $N = 10$ and $N = 10^4$.

For the first marked example, $g_s = 10^{-2}$ and $N = 10$. Then $g_sN = 0.1$ and $L/\ell_s = (0.4\pi)^{1/4}$, of order one. At any fixed finite E, (II.8.35) and (II.8.36) still tend to zero. String loops are weak in the stated asymptotic coupling, yet the curvature is not parametrically small. The symbol $\gg 1$ is essential: a value only just greater than one would not establish a controlled expansion.

Keep the same $g_s = 10^{-2}$ but set $N = 10^4$. Now $g_sN = 100$ and $L/\ell_s = (400\pi)^{1/4}$. This moves substantially toward a weak-curvature region while the loop parameter stays 10^{-2}. The latter is a finite illustrative value, not an asymptotic proof of negligible every correction. If one wanted parametric control, one could take a sequence with $g_s \to 0$, $N \to \infty$, and $g_sN \to \infty$. For example $g_s = m^{-1}$ and $N = m^3$ give

$$g_s \to 0, \qquad g_sN = m^2 \to \infty, \qquad \frac{L}{\ell_s} = (4\pi m^2)^{1/4} \to \infty \quad (m \to \infty). \tag{II.8.40}$$

The fixed-N low-energy limit and this separate parameter family answer different questions. The first isolates low-energy degrees of freedom; the second makes a particular classical bulk expansion reliable. General Dp backgrounds have position-dependent curvature and dilaton, so these D3 inequalities should not be copied unchanged to every brane. The later D3-probe chapter uses this distinction before comparing a brane field theory to a gravity region. Neither the two limits nor the local metric algebra proves a complete holographic equivalence.

For a converse finite example, take $g_{\mathrm{s}} = 2$ and $N = 10^4$. Then $g_{\mathrm{s}}N = 2 \times 10^4$, so the radius in string units is large, but perturbative string loops are not weak. The fixed-energy $\alpha' \to 0$ argument again removes ordinary massive strings and bulk gravity. These three examples occupy different parts of the same parameter plane; none changes the definition of the low-energy limit. In particular, replacing $g_{\mathrm{s}} \ll 1$ by $g_{\mathrm{s}}N \gg 1$ would incorrectly call this third case a controlled perturbative Type IIB solution.

II.8.7 Exercises

Work the intermediate steps before submitting the exact fields named below to the companion grader. The task IDs are `I08-E1` through `I08-E6`; the first five have bounded answers and the sixth asks for written interpretation. For public submissions, follow `benchmark/PROTOCOL.md`.

1. Convert $\sqrt{-\det g^{(s)}}\, e^{-2\Phi} |H_3|_s^2$ to Einstein frame in ten dimensions, using $g^{(E)} = e^{-\Phi/2} g^{(s)}$. Submit the integer field `einstein_dilaton_exponent`. Explain on paper why three inverse metrics appear.

2. Solve the punctured radial harmonic equation for $H = 1 + A/r^a$ on flat transverse $\mathbb{R}^6$ and $\mathbb{R}^8$. Submit integer fields `d3_power` and `m2_power`. Show the nonzero residual if the D3 power is increased by one.

3. Use the positive classical M2 electric branch $F_4 = (6/R)v_4$ and $2\kappa_{11}^2 T_{\mathrm{M2}} = (2\pi)^6 \ell_p^6$. On the free quotient $S^7/\mathbb{Z}_2$ with unit volume $\pi^4/6$, take $N_{\mathrm{cl}} = 3$. Write $R^6/\ell_p^6 = C\pi^p$. Submit integer fields `radius_six_coefficient` and `pi_power`, and the exact rational string `quotient_volume_ratio` for $\mathrm{Vol}(Y_7)/\mathrm{Vol}(S^7)$.

4. Take $R_{10} = 3\ell_s$, $T_{\mathrm{M2}} = 1/[(2\pi)^2 \ell_p^3]$, $T_{\mathrm{F1}} = 1/(2\pi\alpha')$, and $2\kappa_{11}^2 = (2\pi)^8 \ell_p^9$. Submit the exact rational string `lp_cubed_over_alpha_prime_over_ell_s` for $\ell_p^3/(\alpha' \ell_s)$ and the integer `gravity_coefficient` in $2\kappa_{10}^2 = (2\pi)^7 C \ell_s^8$. State which circumference enters both steps.

5. Let $g_{\mathrm{s}} = 1/100$, $N = 10$, and E be finite while $\alpha' \to 0$. Submit Boolean fields `gravity_decouples`, `small_curvature`, and `weak_loops`, using the separate criteria $E\ell_s \to 0$, $g_{\mathrm{s}}N \gg 1$, and $g_{\mathrm{s}} \ll 1$. In writing, repeat the analysis for $N = 10^4$ and distinguish a finite example from a parametric limit.

6. Explain in writing why the classical electric integral over $S^7/\mathbb{Z}_k$ cannot alone be identified with an exact finite-N Page or rank charge. Name one missing global or quantum ingredient, and distinguish it from the shifted magnetic cohomology condition.

II.8.8 Take-home message

Take-home message

The massless bulk fields admit charged D3 and M2 solutions whose sourced warp factors become curved throats. Away from a source, radial harmonicity fixes the powers r^{-4} and r^{-6}, while source and flux data fix their coefficients. A positive classical M2 electric integral on $S^7/\mathbb{Z}_k$ gives $R^6 = 32\pi^2 k N_{\rm cl} \ell_p^6$ and $R_{\mathrm{AdS}_4} = R/2$. Wrapping an M2 on the full physical circle gives $\ell_p^3 = R_{10}\alpha'$ and the ten-dimensional gravitational coefficient. At fixed finite $g_{\rm s}$ and N, low-energy D3 gravity decoupling does not require a large classical throat. Small curvature and weak string loops are additional, independent conditions.

The reader should now be able to change frame for a form density, solve a punctured radial warp-factor equation, compute a classical quotient flux scale, translate membrane and string units, and test decoupling separately from approximation control. Source-normalized brane solutions and the sourced flux-quantization law are used at their stated scope. The full projector, complete worldvolume action, quantum charge completion, and a holographic equivalence require further input.

Status and sources

Section 1. The D3/M2 route is an orientation to the sourced solutions below. It makes no independent equivalence claim. Chapter 4 supplies the massless field prerequisites.
Section 2. The eleven-dimensional metric and three-form content is [SUGRA] from Witten (1995, physical PDF pp. 11–12, sec. 2, eqs. (2.9)–(2.13)); the displayed eleven-dimensional form terms remain schematic. The exact relative $+4$ dilaton and $-1/12$ raw three-form coefficients in the leading bosonic Type II NS action are an additional [SUGRA] premise from Johnson (2000, physical PDF p. 95, eqs. (251)–(252)). Johnson's G and total Φ are translated to $g^{(s)}$ and Φ; his $\widetilde{G} = e^{\Phi_\infty/2} g^{(E)}$ has an extra constant factor, as his physical PDF pp. 47 and 95, eqs. (114) and (253), show. The NS three-form Weyl density is [MATH] under a smooth positive frame factor and the stated factorial norm. The connection-difference contraction derives the curvature transformation, and combining it with the sourced $+4$ term gives the $-1/2$ Einstein-frame dilaton coefficient, [MATH] when the integrated Laplacian has no boundary contribution. The IIB five-form constraint and distinction from the auxiliary-field action are [SUGRA] from Dall'Agata et al. (1997, physical PDF pp. 1–3, eqs. (1)–(4)). The metric, string units and form notation are as stated above.
Section 3. The flat D3 ansatz, coefficient and five-form content are [SUGRA] from Maldacena (1997, physical PDF pp. 3–4, sec. 2, eqs. (2.1)–(2.4)). The flat M2 ansatz, coefficient and electric field are [SUGRA] from Maldacena (1997, physical PDF p. 11, sec. 3.2, eq. (3.3)). Their BPS interpretation is sourced. The punctured radial solution is [MATH] for a radial twice-differentiable function in $d > 2$. The residuals, near-horizon coordinate changes and throat metrics are [MATH] under the sourced ansatze. The source's gauge coupling is translated to the gauge-coupling normalization given above; its displayed coefficient is not an independent book coupling definition.

Section 4. The positive electric orientation and minimal membrane and gravitational units are fixed above. The free quotient volume and classical electric integral are [MATH] under that physical normalization. The $k = 1$ coefficient agrees with Maldacena (1997, physical PDF p. 11, sec. 3.2). The shifted spin-manifold magnetic class is [ANOM] from Witten (1996, physical PDF p. 2, eq. (1.2), and pp. 6–7, Section 2.2). Its cited membrane fermion-sign mechanism fixes one mod-two flux-period condition; no anomaly calculation is reproduced here. It is distinct from the electric count. The membrane unit is input, with Lu (1997, physical PDF p. 3, eq. (1.5)) only a normalization cross-check.
Section 5. The physical-circle $R_{10} = g_s \ell_s$ and membrane/gravity units are as defined above. The once-wrapped M2/F1 tension relation is [MATH] in the common unwarped asymptotic frame. The reduced gravitational coefficient is [MATH] for circle-independent zero modes in that frame. Witten (1995, physical PDF pp. 11–12, sec. 2) gives a circle reduction in its own frame; Itzhaki et al. (1998, physical PDF p. 4, eq. (1) and footnote 1) records the IIA/M units after translation. No equality of differently framed source radii is assumed.
Section 6. The fixed-$U = r/\alpha'$ D3 decoupling limit as $\alpha' \to 0$ is a [DEC] assumption; the radius is a cited [SUGRA] input from Maldacena (1997, physical PDF pp. 3–4, sec. 2, eqs. (2.1)–(2.4)). The suppression of massive asymptotic strings and ten-dimensional gravity at fixed finite g_s, N and E follows mathematically under those inputs [MATH]. The separate small-curvature and weak-loop test is [MATH] under the sourced radius and constant dilaton. Curvature and dilaton control are kept distinct as in Itzhaki et al. (1998, physical PDF pp. 4–5, sec. 2, eqs. (1), (5)). Neither calculation establishes a full holographic duality.
Section 7. Exercises 1–5 test bounded calculations; Exercise 6 is written-only.
Section 8. The conclusion adds no new physical claim.

References

Dall'Agata, G., K. Lechner, and D. Sorokin (1997). *Covariant Actions for the Bosonic Sector of D=10 IIB Supergravity*. v1, PDF pp. 1–3. arXiv: `hep-th/9707044`.

Itzhaki, N. et al. (1998). *Supergravity and the Large N Limit of Theories with Sixteen Supercharges*. v2, PDF pp. 4–5. arXiv: `hep-th/9802042`.

Johnson, C. V. (2000). *D-Brane Primer*. v3, physical PDF pp. 47, 95–96, eqs. (114)–(116), (251)–(254). arXiv: `hep-th/0007170`.

Lu, J. X. (1997). *Remarks on M-Theory Coupling Constants and M-Brane Tension Quantizations*. v1, PDF p. 3. arXiv: `hep-th/9711014`.

Maldacena, J. M. (1997). *The Large N Limit of Superconformal Field Theories and Supergravity*. v3, PDF pp. 3–4 and 11. arXiv: `hep-th/9711200`.

Witten, E. (1995). *String Theory Dynamics in Various Dimensions*. v2, PDF pp. 11–12, sec. 2. arXiv: `hep-th/9503124`.

Witten, E. (1996). *On Flux Quantization in M-Theory and the Effective Action*. v2, PDF pp. 1–2 and 6–7. arXiv: `hep-th/9609122`.

Chapter II.9

The duality web: S-, T-, U-duality and M-theory

II.9.1 Why a web needs typed links

A closed string can wind around a spatial circle while carrying momentum along it. A D0-brane can carry the same integer label as momentum around a proposed eleventh circle. In Type IIB, a string can carry two integral charges. These facts invite a web of descriptions, but the links do different jobs. A free-circle calculation transports worldsheet zero modes. A strong-coupling identification supplies new physical states. A geometric change of coordinates only rewrites an existing configuration. A brane motion can require a further assumption about what persists in the infrared.

We will build the web in that order. The circle calculation gives an exact algebraic test and a separate measure condition. Electric Type IIB charges give an integral lattice test, with source and fivebrane axes kept distinct. The IIA/M dictionary makes the circle units physical. Two heterotic comparisons show how much low-energy agreement can establish. Finally, two selected construction paths show which assumptions remain after their steps are composed. Figure II.9.1 locates the three basic dictionaries and their later uses.

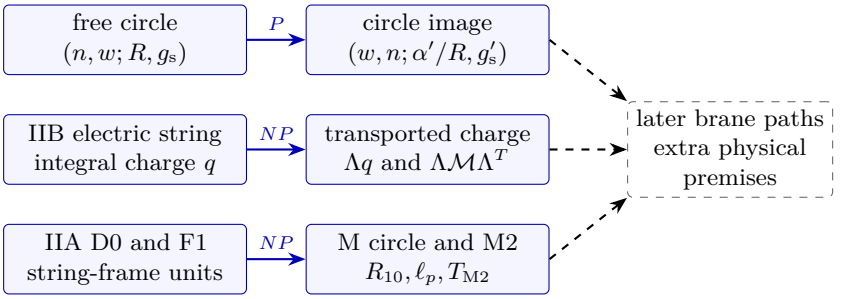


Figure II.9.1: Three interfaces used in this chapter. The top arrow is the free-circle transformation of momentum and winding under an isometry. The middle arrow is the proposed Type IIB nonperturbative transport of electric string charges. The lower arrow is the IIA/M strong-coupling circle dictionary. Dashed arrows point to later brane constructions and do not assert their dynamics.

Chapter 3 derived the compact-boson spectrum, while Chapter 8 fixed the asymptotic metric and membrane units. Chapter 10 will discuss NS5-branes themselves. Here we use an outward fivebrane charge only to track a selected mirror construction, not to infer an NS5 dynamics from a closed-string circle spectrum.

II.9.2 The perturbative circle link

How can a string with momentum on one circle be read as a winding string on another? Let $X \sim X + 2\pi R$ be a free spatial coordinate in the asymptotic string frame. Set $\ell_s^2 = \alpha' > 0$. An oriented closed string has momentum number $n \in \mathbb{Z}$ and winding number $w \in \mathbb{Z}$. In the book normalization its left- and right-moving zero-mode momenta are

$$p_L = \frac{n}{R} + \frac{wR}{\alpha'}, \qquad p_R = \frac{n}{R} - \frac{wR}{\alpha'}. \tag{II.9.1}$$

The first term comes from the periodic wavefunction $e^{inX/R}$. The second measures the displacement $2\pi wR$ of the embedding around the spatial worldsheet cycle. The signs say that winding contributes oppositely to the two chiral sectors. A change of the orientation chosen for the worldsheet or circle changes the corresponding sign assignments together.

For positive R, define the transformed data by

$$R' = \frac{\alpha'}{R}, \qquad (n', w') = (w, n). \tag{II.9.2}$$

Inserting these into the same formula, without relabelling just one sector, gives

$$p'_L = \frac{w}{R'} + \frac{nR'}{\alpha'} = \frac{wR}{\alpha'} + \frac{n}{R} = p_L, \qquad p'_R = \frac{wR}{\alpha'} - \frac{n}{R} = -p_R. \tag{II.9.3}$$

Thus one chirality is unchanged while the other is reflected. The transformation is an involution on these data. Applying it twice returns R and exchanges the integers twice. The fixed radius is $R = \sqrt{\alpha'}$; the map still acts nontrivially on states at that radius.

The zero modes enter both physical-state equations. With N_L, N_R the oscillator levels and a_L, a_R the appropriate intercepts in a specified string sector, write the common spacetime mass as

$$M^2 = p_L^2 + \frac{4}{\alpha'}(N_L - a_L) = p_R^2 + \frac{4}{\alpha'}(N_R - a_R). \tag{II.9.4}$$

Equivalently, their difference imposes level matching:

$$0 = \alpha'(p_L^2 - p_R^2)/4 + N_L - N_R - a_L + a_R = nw + N_L - N_R - a_L + a_R. \tag{II.9.5}$$

Equations (II.9.3)–(II.9.5) show why the two shells have the same numerical zero-mode contributions after the transformation. The rest of a physical spectrum still requires the oscillator, sector, and projection map. This calculation alone is not a theorem about every compact conformal field theory.

The one-loop measure adds information that a mass formula cannot supply. Gauging an isometric circle and integrating the worldsheet gauge field changes the dilaton contribution to the path-integral measure. In the present normalization it gives

$$\Phi' = \Phi - \log \frac{R}{\sqrt{\alpha'}}, \qquad g_{\rm s}' = g_{\rm s}\frac{\sqrt{\alpha'}}{R}. \tag{II.9.6}$$

The relation assumes a circle isometry and the corresponding holonomy and measure treatment; it is not obtained by squaring p_L or p_R. To see its role in the low-energy density, a constant-circle reduction weights a ten-dimensional string-frame NS term by the circle circumference and $e^{-2\Phi}$:

$$(2\pi R)e^{-2\Phi} \quad \longmapsto \quad (2\pi R')e^{-2\Phi'} = (2\pi R)e^{-2\Phi}. \tag{II.9.7}$$

The final equality follows by substituting $R' = \alpha'/R$ and $e^{-2\Phi'} = e^{-2\Phi}R^2/\alpha'$. It is a useful dimensional check on the measure shift, not an independent derivation of the gauged path integral. The source's curvature dilaton is -2Φ in our notation, and its dimensionless chiral momenta are $\sqrt{\alpha'/2}\,p_{L,R}$.

The same measure condition can be seen at arbitrary genus in the free-circle model, subject to the source's treatment of worldsheet periods. Put $\rho = R/\sqrt{\alpha'}$ and let $Z_h(\rho)$ denote the circle contribution at genus h. Its transformation in those dimensionless units is

$$Z_h(1/\rho) = \rho^{2h-2} Z_h(\rho). \tag{II.9.8}$$

The Euler-characteristic weight of a constant book dilaton is $g_{\rm s}^{2h-2}$. If $g_{\rm s}' = g_{\rm s}/\rho$, the transformed term becomes

$$(g_{\rm s}')^{2h-2} Z_h(1/\rho) = \left(\frac{g_{\rm s}}{\rho}\right)^{2h-2} \rho^{2h-2} Z_h(\rho) = g_{\rm s}^{2h-2} Z_h(\rho). \tag{II.9.9}$$

At genus one the exponent vanishes, so a torus partition function by itself cannot reveal the coupling shift. At genus zero it supplies the reciprocal power required by the sphere term. This argument uses the higher-genus circle measure and its holonomy treatment. In the bosonic theory the summed partition function has a tachyon divergence, so this

formal comparison should not be silently promoted to a convergent nonperturbative sum.

As a complete finite example, set $\alpha' = 4$, $R = 3$, $g_{\rm s} = 3/2$ and $(n, w) = (2, -1)$. The original and transformed data are

$$(p_L, p_R) = \left(\frac{2}{3} - \frac{3}{4}, \frac{2}{3} + \frac{3}{4}\right) = \left(-\frac{1}{12}, \frac{17}{12}\right), \quad (R', n', w', g'_{\rm s}) = \left(\frac{4}{3}, -1, 2, 1\right). \tag{II.9.10}$$

Checking the transformed momenta directly gives

$$p'_L = \frac{-1}{4/3} + \frac{2(4/3)}{4} = -\frac{3}{4} + \frac{2}{3} = -\frac{1}{12}, \qquad p'_R = -\frac{3}{4} - \frac{2}{3} = -\frac{17}{12}. \tag{II.9.11}$$

The product $nw = -2$ is also preserved, since $n'w' = (-1)2 = -2$. The transformation has transported these zero-mode data from a radius larger than $\ell_s = 2$ to one smaller than ℓ_s, while the two zero-mode shell contributions remain the same. The data alone do not specify a physical state without oscillator and projection information. Figure II.9.2 fixes the orientation used in this example.

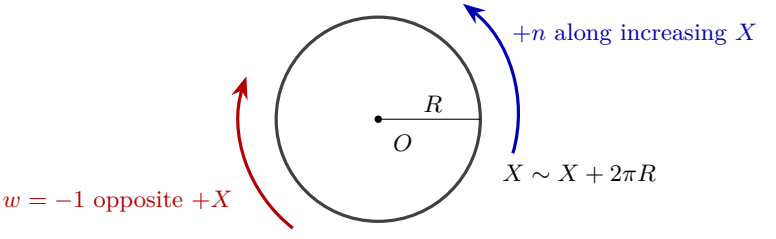


Figure II.9.2: A positively oriented physical circle of radius R with a chosen increasing coordinate X. The blue arrow follows increasing X for $n = 2$; the red arrow traverses the opposite direction for $w = -1$. T-duality interchanges the signed integers and sends R to α'/R. Arrow positions are separated to keep the circumference continuous.

An irrational-coupling round trip tests a feature that a rational example hides. Take $\alpha' = 4$, $R = 3$, and $g_{\rm s} = \sqrt{2}$. The first coupling is $g'_{\rm s} = 2\sqrt{2}/3$. On the dual circle $R' = 4/3$, a second application gives

$$g''_{\rm s} = \frac{2\sqrt{2}}{3}\frac{2}{4/3} = \sqrt{2}, \qquad R'' = \frac{4}{4/3} = 3. \tag{II.9.12}$$

No rational approximation is needed. The map is algebraically involutive for any positive exact coupling, while its physical use still rests on the specified isometry and measure premise. In later chapters, a brane wrapped on a dual circle has additional boundary conditions. One should use the open-string brane dictionary there, not infer it solely from (II.9.1).

II.9.3 IIB charge doublets

What is transported when a Type IIB S transformation is applied to a charged object? An electric string and a fivebrane each admit an ordered pair of integral charges, but their axes and orientations serve different source conventions. For the local electric-string calculation, let $q = (q_F, q_D)^T$ be an oriented (F1, D1) column. On this particular column take

$$S_e = \begin{pmatrix} 0 & -1 \\ 1 & 0 \end{pmatrix}, \qquad T_e = \begin{pmatrix} 1 & 1 \\ 0 & 1 \end{pmatrix}, \qquad \det S_e = \det T_e = 1. \tag{II.9.13}$$

These matrices give an integral exercise basis. They are not the transformation matrix for the book's outward fivebrane column, nor are they sevenbrane branch-cut matrices. The physical assertion that the full Type IIB theory realizes the required $SL(2,\mathbb{Z})$ transformations is a nonperturbative premise. We can nevertheless calculate precisely what an assumed integral action would preserve.

First consider a primitive charge vector, one whose two components have greatest common divisor one. If $A \in SL(2,\mathbb{Z})$, then A^{-1} has integral entries. Each component of Aq is an integral combination of those of q, so $\gcd(q)$ divides $\gcd(Aq)$. Applying the same statement to A^{-1} gives the reverse divisibility. Hence

$$\gcd\big((Aq)_1, (Aq)_2\big) = \gcd(q_1, q_2), \qquad A \in SL(2,\mathbb{Z}). \tag{II.9.14}$$

For two charge columns q and q', define their oriented pairing by $\langle q, q' \rangle = \det(q, q')$. Matrix multiplication gives

$$\langle Aq, Aq' \rangle = \det(Aq, Aq') = \det A \, \det(q, q') = \langle q, q' \rangle. \tag{II.9.15}$$

The pairing calculation concerns a free rank-two integral lattice. A physical Dirac–Schwinger–Zwanziger lattice interpretation requires actual compatible charged sectors, including appropriate magnetic sectors. The determinant identity cannot populate those sectors.

Temporal order matters. With $q = (2,1)^T$, apply T_e first and S_e second. Then

$$T_e q = \begin{pmatrix} 3 \\ 1 \end{pmatrix}, \qquad S_e T_e = \begin{pmatrix} 0 & -1 \\ 1 & 1 \end{pmatrix}, \qquad S_e T_e q = \begin{pmatrix} -1 \\ 3 \end{pmatrix}. \tag{II.9.16}$$

The final vector is primitive, and $\det(S_e T_e) = 1$. By contrast, $D = \mathrm{diag}(2,1)$ has determinant two and takes $(0,1)^T, (1,0)^T$, whose pairing is -1, to a pair with pairing -2. Its inverse is not integral. A matrix that happens to preserve the gcd of one selected vector is not enough to give a lattice automorphism.

The tension comparison needs the source metric and charge frame. In Schwarz's electric-string frame, let χ be the asymptotic axion, $g_{\mathrm{s}} = e^{\phi} > 0$, and $\tau = \chi + i/g_{\mathrm{s}}$. The source uses an Einstein metric g and a string metric $G = e^{\phi/2} g$. Its scalar matrix and source charge column $q = (q_1, q_2)^T$ are

$$\mathcal{M} = \begin{pmatrix} g_{\mathrm{s}}\chi^2 + g_{\mathrm{s}}^{-1} & g_{\mathrm{s}}\chi \\ g_{\mathrm{s}}\chi & g_{\mathrm{s}} \end{pmatrix}, \qquad \det \mathcal{M} = 1. \tag{II.9.17}$$

Inverting this explicit two-by-two matrix yields the dimensionless Einstein-frame squared-tension factor

$$\Delta_q = q^T \mathcal{M}^{-1} q = g_{\rm s}(q_2\chi - q_1)^2 + \frac{q_2^2}{g_{\rm s}}. \tag{II.9.18}$$

The inverse is essential. Under the source convention $\mathcal{M} \mapsto \Lambda \mathcal{M} \Lambda^T$, the potential column transforms as $B \mapsto (\Lambda^T)^{-1} B$. Its electric charge column transforms as $q \mapsto \Lambda q$. Consequently

$$(\Lambda q)^T (\Lambda \mathcal{M} \Lambda^T)^{-1} (\Lambda q) = q^T \mathcal{M}^{-1} q. \tag{II.9.19}$$

This is covariance of the source expression when both scalars and charges move. It does not equate tensions at fixed τ for arbitrarily different charges. Figure II.9.3 keeps the electric and magnetic-facing book axes separate.

For a fixed-source comparison, take $\chi = 0$ and $g_{\rm s} = 2$. The matrix and its inverse are diagonal, so three primitive charge columns give

$$\mathcal{M} = \begin{pmatrix} 1/2 & 0 \\ 0 & 2 \end{pmatrix}, \quad \mathcal{M}^{-1} = \begin{pmatrix} 2 & 0 \\ 0 & 1/2 \end{pmatrix}, \quad (\Delta_{(1,0)}, \Delta_{(0,1)}, \Delta_{(1,1)}) = \left(2, \frac{1}{2}, \frac{5}{2}\right). \tag{II.9.20}$$

The mixed vector has a squared-tension factor equal to the sum of the two axis factors at this particular χ. This is not an additivity law for tensions, since physical tensions are proportional to $\sqrt{\Delta_q}$ in this Einstein frame. If the axion is nonzero, the off-diagonal entries of $\mathcal{M}^{-1}$ also change the mixed factor. The example shows why the charge column, scalar matrix, and frame must be specified together.

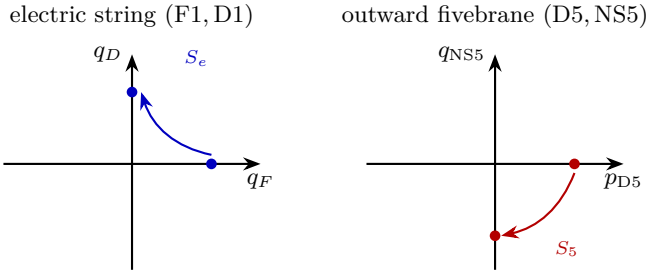


Figure II.9.3: Separate oriented integral charge planes. Left: the local electric string basis $q = (\mathrm{F1}, \mathrm{D1})$ uses $S_e(1,0)^T = (0,1)^T$. Right: the book's outward fivebrane basis is $Q_5 = (\mathrm{D5}, \mathrm{NS5})$, with $S_5(1,0)^T = (0,-1)^T$. The vertical arrows deliberately differ. No arrow identifies a source electric charge with a fivebrane charge.

For the outward fivebrane convention used in the later web chapters, write $Q_5 = (p,q)^T = (\mathrm{D5}, \mathrm{NS5})^T$. Its adopted S operation is

$$S_5 = \begin{pmatrix} 0 & 1 \\ -1 & 0 \end{pmatrix} = S_e^{-1}, \qquad S_5 \begin{pmatrix} 1 \\ 0 \end{pmatrix} = \begin{pmatrix} 0 \\ -1 \end{pmatrix}. \tag{II.9.21}$$

Thus an outward D5 maps to an oppositely oriented NS5 in this house basis. Dropping the minus sign would change the orientation relevant to a finite Hanany–Witten con-

figuration. Chapter 10 treats the NS5 object; later sevenbrane discussions have still another cut convention.

A source-local tension check illustrates why literal formulas take priority over a nearby sentence. At $\chi = -1/2$, equation (II.9.18) gives $\Delta_{(1,0)} = g_{\mathrm{s}}$ and $\Delta_{(1,1)} = 9g_{\mathrm{s}}/4 + 1/g_{\mathrm{s}}$. Therefore

$$\Delta_{(1,1)} - \Delta_{(1,0)} = \frac{5}{4} g_{\mathrm{s}} + \frac{1}{g_{\mathrm{s}}} > 0. \tag{II.9.22}$$

This is a statement about the displayed source formula in its own frame. It does not alter the house fivebrane S operation. The printed source claim of degeneracy at this axion value conflicts with that formula; the discrepancy is recorded in the chapter-end source notes. Neither equality of a self-overlap nor a charge diagram establishes the complete spectrum or a nonperturbative equivalence.

II.9.4 The IIA/M circle

Why does the Type IIA D0 tower suggest momentum in one more direction? Begin with a physical length frame, rather than a dimensionless source metric. Let $\alpha' = \ell_s^2$ and $g_{\mathrm{s}} > 0$ be measured in an unwarped asymptotic IIA string frame. The proposed M circle has physical radius R_{10} and angular coordinate θ_{10}, with

$$X^{10} = R_{10}\theta_{10}, \qquad \theta_{10} \sim \theta_{10} + 2\pi, \qquad R_{10} = g_{\mathrm{s}}\ell_s. \tag{II.9.23}$$

The coordinate X^{10} consequently has period $2\pi R_{10}$. The angular coordinate has no length units. This distinction is important when a membrane wraps the circle or a ten-dimensional coupling is obtained by integrating over it.

The IIA/M dictionary supplies the eleven-dimensional Planck length and minimal membrane tension in the same length convention:

$$\ell_p^3 = R_{10}\alpha' = g_{\mathrm{s}}\ell_s^3, \qquad T_{\mathrm{M2}} = \frac{1}{(2\pi)^2\ell_p^3}, \qquad T_{\mathrm{F1}} = \frac{1}{2\pi\alpha'}. \tag{II.9.24}$$

These are sourced physical unit premises. They are not obtained by declaring a new coordinate in ten dimensions. Chapter 8 used the same absolute units in reducing the bulk action. Here they let us make two independent numerical comparisons.

First, the unit D0 BPS mass in this convention is $M_{\mathrm{D0}} = 1/(g_{\mathrm{s}}\ell_s)$. A free unit Kaluza–Klein momentum on the physical circle has magnitude $1/R_{10}$. Substituting (II.9.23) gives

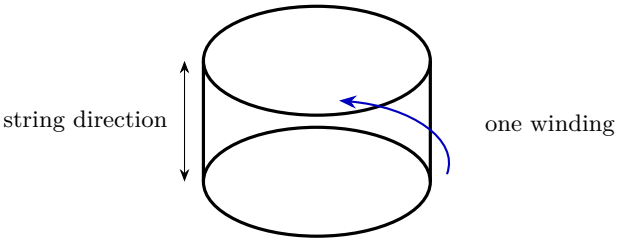
$$M_{\mathrm{D0}} = \frac{1}{g_{\mathrm{s}}\ell_s} = \frac{1}{R_{10}} = M_{\mathrm{KK},1}, \qquad M_{\mathrm{KK},k} = \frac{|k|}{R_{10}}. \tag{II.9.25}$$

The last expression is the circle momentum spectrum for an integer k, assuming the modes exist. The D0 charge is proposed to supply those sectors in the strong-coupling completion. Equal masses are a compatibility condition for that proposal. They do not construct the higher-charge bound states or prove the completion.

Second, a membrane wrapped once around the full physical circumference has an effective string tension equal to area tension times length. Keeping the 2π factors gives

$$T_{\text{wrapped M2}} = (2\pi R_{10})T_{\mathrm{M2}} = \frac{2\pi R_{10}}{(2\pi)^2\ell_p^3} = \frac{1}{2\pi\alpha'} = T_{\mathrm{F1}}. \tag{II.9.26}$$

If one had used R_{10} rather than $2\pi R_{10}$, the result would be short by 2π. If the membrane wraps m times without changing orientation, its classical area contribution is $|m|$ times this unit tension. Whether all such sectors are stable or independent requires more than this area calculation. Figure II.9.4 shows the angular and physical descriptions of the same circle.



$$\theta_{10} \sim \theta_{10} + 2\pi$$

$$X^{10} = R_{10}\theta_{10}, \text{ circumference } 2\pi R_{10}$$

Figure II.9.4: The same M circle in an angular coordinate θ_{10} of period 2π and a physical coordinate $X^{10} = R_{10}\theta_{10}$ of period $2\pi R_{10}$. A membrane strip wraps the entire circumference once and extends along one noncompact spatial direction. Its effective string tension uses the full length $2\pi R_{10}$.

At the values $\alpha' = 4$ and $g_s = 3/2$ used earlier, $\ell_s = 2$. The two lengths and the unit masses are

$$R_{10} = \frac{3}{2}\,2 = 3, \qquad \ell_p^3 = 3 \cdot 4 = 12, \qquad M_{\mathrm{D0}} = \frac{1}{(3/2)2} = \frac{1}{3} = M_{\mathrm{KK},1}. \tag{II.9.27}$$

The membrane comparison can be checked without decimal approximations. At these values $T_{\mathrm{M2}} = 1/(48\pi^2)$, so

$$T_{\text{wrapped M2}} = 6\pi\frac{1}{48\pi^2} = \frac{1}{8\pi}, \qquad 2\pi T_{\text{wrapped M2}} = \frac{1}{4} = 2\pi T_{\mathrm{F1}}. \tag{II.9.28}$$

The two comparisons use different quantities: a particle mass and a string tension. Agreement in both provides a tighter unit test than either alone, though it remains conditional on the sourced D0 and M2 units and the IIA/M identification.

There is a frame trap in reading the classic strong-coupling argument. Witten's source metric uses a circle radius that scales as $g_s^{2/3}$ in its chosen eleven-dimensional metric convention. That coordinate radius is not R_{10} in (II.9.23). Its physical PDF page 11 also describes radius and KK mass scaling in prose opposite to the implication of its following displayed equations. We use the equations after an explicit frame translation and the book's independently specified absolute units. Schwarz's wrapped-membrane comparison likewise uses a source eleven-dimensional radius r before a factor $e^{-2\phi_A/3}$ is included in comparing tensions. Neither source radius may be inserted into (II.9.26) as though it already measured the book's physical string-frame circumference.

The scaling translation can be performed in the source variables without identifying its coordinate radius with our physical one. If $r = e^{\gamma}$ and $e^{-2\phi} = e^{-3\gamma}$, then $\gamma = 2\phi/3$

and $r = e^{2\phi/3}$. Witten's ten-dimensional metric inherited from the source eleven-dimensional frame obeys $G^{10} = e^{-\gamma} g$, where g is the ten-dimensional string-frame metric in that comparison. Thus $ds_{G^{10}} = e^{-\gamma/2} ds_g$ at constant asymptotic dilaton. Equating the proper-time terms $m_{G^{10}} ds_{G^{10}} = m_g ds_g$ gives $m_g = e^{-\gamma/2} m_{G^{10}}$. Hence the source's KK scaling measured in g is

$$m_{\mathrm{KK}}^{(g)} \sim \frac{e^{-\gamma/2}}{r} = e^{-3\gamma/2} = e^{-\phi} = g_{\mathrm{s}}^{-1}. \tag{II.9.29}$$

This reproduces the coupling power of (II.9.25). Witten's schematic step does not fix the absolute ℓ_s coefficient; that comes from the physical unit premise in (II.9.23). Reading $r = e^{2\phi/3}$ as a string-frame radius would instead predict the wrong coupling power for a unit KK mass.

As g_{s} increases at fixed ℓ_s, equation (II.9.23) says the physical M circle grows. This suggests why an additional geometric direction is useful at strong IIA coupling. It does not turn a weak-coupling calculation into a theorem about every state. In Chapter 8 the bulk fields supplied the reduction interface. The later M5 construction uses a stronger lift and a protected low-energy continuation; its physical content cannot be deduced from the two equalities above.

II.9.5 Heterotic duality interfaces

What can be compared before declaring two theories equivalent? Low-energy actions and protected multiplets often give sharp constraints, yet they sample only part of a quantum spectrum. Two proposed nonperturbative links make this distinction concrete. One compares the $SO(32)$ heterotic string with Type I. The other compares heterotic string theory on T^4 with Type IIA on K3. Each link has its own hypotheses and state dictionary.

For the first link, start with the local gauge algebra $\mathfrak{so}(32)$. An antisymmetric 32×32 matrix has one independent entry for each unordered pair of distinct indices. Its dimension is therefore

$$\dim \mathfrak{so}(32) = \binom{32}{2} = \frac{32 \cdot 31}{2} = 496. \tag{II.9.30}$$

Both weakly coupled descriptions have this local gauge-algebra count in the relevant low-energy comparison. It does not fix the global gauge group, line operators, or all charged representations. In particular, spinor states seen on the heterotic side do not appear as elementary perturbative Type I strings. The proposed identification requires their nonperturbative realization on the Type I side.

The dilaton weights explain why a weak description on one side can face a strong description on the other. In schematic ten-dimensional string-frame normalization, the heterotic gauge and gravity terms carry the same closed-string factor $e^{-2\Phi_H}$, while Type I gravitational closed-string and open-string gauge terms carry different powers:

$$S_H \supset \int \sqrt{-g_H}\, e^{-2\Phi_H} \big(R_H + \cdots + \operatorname{tr} F_H^2 + \cdots \big), \tag{II.9.31}$$

$$S_I \supset \int \sqrt{-g_I}\big(e^{-2\Phi_I} R_I + \cdots + e^{-\Phi_I} \operatorname{tr} F_I^2 + \cdots\big). \tag{II.9.32}$$

The coupling powers can be followed through the source frame change. Write $g_H = e^{\Phi_H} g_I$ and $\Phi_I = -\Phi_H$. In ten dimensions, the metric determinant contributes five powers of e^{Φ_H}, while a two-form field strength contracts two inverse metrics. For the displayed curvature and gauge factors this gives

$$\begin{aligned} \sqrt{-g_H} &= e^{5\Phi_H}\sqrt{-g_I}, \qquad R_H = e^{-\Phi_H}(R_I + \text{dilaton derivative terms}), \\ \operatorname{tr} F_H^2 &= e^{-2\Phi_H} \operatorname{tr} F_I^2. \end{aligned} \tag{II.9.33}$$

Consequently the relative dilaton powers become

$$\begin{aligned} \sqrt{-g_H} e^{-2\Phi_H} R_H &\sim \sqrt{-g_I} e^{2\Phi_H} R_I = \sqrt{-g_I} e^{-2\Phi_I} R_I, \\ \sqrt{-g_H} e^{-2\Phi_H} \operatorname{tr} F_H^2 &= \sqrt{-g_I} e^{\Phi_H} \operatorname{tr} F_I^2 = \sqrt{-g_I} e^{-\Phi_I} \operatorname{tr} F_I^2. \end{aligned} \tag{II.9.34}$$

The curvature line isolates its leading R_I coefficient. The omitted derivatives must be combined with the transformed dilaton kinetic term to compare complete actions. The gauge line is a local Weyl-weight identity for the same field-strength components. Neither line constructs the missing Type I spinor states. The omitted dimensionful coefficients and field normalizations matter for an equality of complete actions. These displayed powers show why simply setting $\Phi_H = \Phi_I$ in the two string frames would not match the gauge and gravity terms. The proposed relation uses inverse couplings and a frame change. That is a low-energy interface, with the nonperturbative state problem still present.

For the second link, use a smooth K3 and a generic abelian point where the stated reduction of the IIA Ramond–Ramond fields applies. Its second Betti number is $b_2(K3) = 22$. The ten-dimensional one-form C_1 gives one six-dimensional vector. Expanding the three-form C_3 on a basis ω_I of harmonic two-forms gives twenty-two more:

$$C_3(x,y) = \sum_{I=1}^{22} A_1^I(x) \wedge \omega_I(y) + C_3^{(6)}(x) + \cdots, \qquad d\omega_I = 0. \tag{II.9.35}$$

Here x labels six-dimensional spacetime and y labels K3. The A_1^I are vectors in the uncompactified directions. The six-dimensional three-form $C_3^{(6)}$ has a four-form field strength. Let $V > 0$ denote the K3 volume in the reduced action's metric normalization. Its kinetic term carries a factor V. In the source dualization convention the four-form is related to a vector field strength by

$$F_4^{(6)} = dC_3^{(6)}, \qquad V F_4^{(6)} = *_6 F_2^{\mathrm{dual}}, \qquad F_2^{\mathrm{dual}} = dA_1^{\mathrm{dual}}. \tag{II.9.36}$$

Thus the dual vector's kinetic term has the reciprocal volume weight, $V^{-1}|F_2^{\mathrm{dual}}|^2$, up to the same common normalization. The V factor belongs to the source's reduced field convention; dropping it would change the coupling of this last vector even though the count stayed twenty-four. The resulting generic RR vector count is

$$N_{\mathrm{vec}}^{\mathrm{RR}} = 1 + b_2(K3) + 1 = 1 + 22 + 1 = 24. \tag{II.9.37}$$

The last one is easy to miss if C_3 is only expanded on internal cycles. It is not an extra harmonic two-form. The dualization assumes a suitable local six-dimensional field description; it does not, by itself, establish a global equality of charge lattices.

A concrete comparison puts the two counts side by side. At the generic abelian K3 point, list the twenty-four IIA RR vectors as $\{C_1, A_1^1, \ldots, A_1^{22}, A_1^{\mathrm{dual}}\}$. Separately, the local $SO(32)$ adjoint has 496 algebra generators and rank 16. The numbers answer different questions. The first counts six-dimensional RR vector fields on one compactification branch and can describe rank-24 abelian gauge data there; the second gives the dimension and rank of a ten-dimensional local algebra in a different proposed link. Neither the six-dimensional count nor the adjoint dimension fixes the global gauge-group quotient.

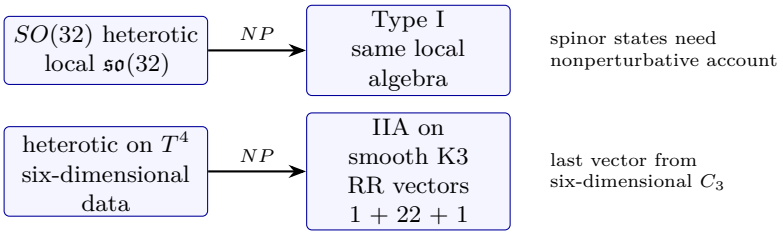


Figure II.9.5: Two distinct heterotic comparisons. The upper route relates $SO(32)$ heterotic and Type I low-energy gauge data; spinor states require a nonperturbative Type I account. The lower route compares heterotic T^4 with IIA on smooth K3. The IIA RR-vector count is $1 + 22 + 1 = 24$, with the last vector obtained by dualizing the six-dimensional three-form. Arrows denote proposed physical links rather than consequences of the field counts.

The K3 count is an interface to a proposed heterotic/IIA($K3$) equivalence. Matching low-energy fields and protected data can motivate that proposal and test particular sectors. It does not produce every massive state, a complete charge-lattice isomorphism, or the dynamics at a singular K3 point. Chapter 5 supplies the heterotic lattice background; the later K3 construction chapter will use the geometric side with its own assumptions. Figure II.9.5 avoids turning the two heterotic proposals into one undifferentiated arrow.

II.9.6 Chains and their conditionality

What remains to be assumed when individually meaningful links are joined into a brane construction? We will classify a step by the physical job it performs. A P step is a perturbative or kinematic operation, such as a coordinate relabelling in its specified setup. An NP step imports a nonperturbative duality generator. An A step names a physical assumption independent of duality about a brane motion, occupancy, or infrared continuation. An adiabatic step, when present, would need its own conditions; neither selected path below has such a separate step. The labels identify dependencies. They do not establish the operations for all configurations.

The first selected path starts with a finite linear Type IIB arrangement of D3-branes ending on oriented fivebranes. Its four operations are ordered. Type IIB S changes the fivebrane species, the signed coordinate rotation restores the comparison frame, a selected fivebrane motion invokes brane creation and occupancy, and a selected reconnection or deformation is continued to an infrared description. Write their dependency sets as

$$\begin{aligned} D_1 &= \{NP(\text{IIB S})\}, & D_2 &= \{P(\text{signed rotation})\}, \\ D_3 &= \{A(\text{creation/occupancy})\}, & D_4 &= \{A(\text{IR continuation})\}. \end{aligned} \tag{II.9.38}$$

The physical fivebrane S at the first step is the outward-column action in (II.9.21). The rotation in the second step is a signed coordinate and field reidentification, not a hidden T-duality. The third and fourth steps are specific to the selected finite path. In particular, conservation of the linking quantities used to track creation does not derive the microscopic occupancy rule or guarantee that the final deformation reaches the intended IR theory.

For this path, the exact union is

$$\begin{aligned} D_{\text{HW}} = \bigcup_{i=1}^{4} D_i = \{&NP(\text{IIB S}), P(\text{signed rotation}), \\ &A(\text{creation/occupancy}), A(\text{IR continuation})\}. \end{aligned} \tag{II.9.39}$$

This set is not compressed to "S-duality" because doing so would discard two independent brane premises. It is also not enlarged by a circle T transformation that the selected route does not use. Figure II.9.6 follows the actual order, with the endpoints of each arrow placed at the configuration to which that operation applies.

The dependency can be tested one operation at a time. After the selected motion but before the infrared continuation, the route has used only

$$\begin{aligned} D_{\text{HW}}^{(3)} &= D_1 \cup D_2 \cup D_3 \\ &= \{NP(\text{IIB S}), P(\text{signed rotation}), A(\text{creation/occupancy})\}. \end{aligned} \tag{II.9.40}$$

The desired comparison of final infrared descriptions needs one more premise. In this finite path its difference from the partial set is

$$D_{\text{HW}} \setminus D_{\text{HW}}^{(3)} = \{A(\text{IR continuation})\}. \tag{II.9.41}$$

This explicitly locates the step that cannot be discharged by calculating conserved linking quantities. One may verify an integer relation before and after motion while the infrared continuation remains an independent statement about dynamics.

The second path starts from a Type IIA D4–NS5 configuration and proposes a single lift to an M5 description. This step assumes the nonperturbative IIA/M lift $NP(\text{IIA/M lift})$:

$$D_{\text{M5}} = \{NP(\text{IIA/M lift})\}. \tag{II.9.42}$$

Comparing low-energy descriptions additionally assumes protected continuation along the chosen construction. This condition applies to the comparison of the low-energy

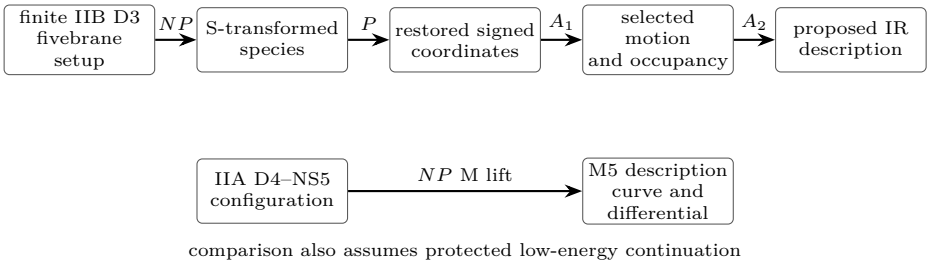


Figure II.9.6: Two selected construction paths with their dependency types. The upper finite linear Hanany–Witten route contains one nonperturbative IIB S step, one signed coordinate restoration, and two distinct physical brane premises. The lower path has a single specified IIA D4–NS5 to M5 lift. A protected low-energy continuation is an additional premise of comparing its descriptions. The diagram does not assert a circular-web generalization.

descriptions. The M5 curve by itself is insufficient data for this comparison. One also needs its distinguished differential and declared cycles or charge lattice. The actual derivation of that curve and the M5 dynamics belongs to the later construction chapter. Equations (II.9.25) and (II.9.26) fix units under the IIA/M premises; they do not prove the lift of an interacting D4–NS5 configuration or its protected continuation.

There is a useful failure test for both paths. Suppose a charge-conserving rearrangement is drawn between two configurations. An integer conservation equation can be satisfied even when no supersymmetric state realizes one intermediate configuration, or when a required deformation crosses a wall. Consequently

$$\text{charge conservation} \not\Rightarrow \text{populated spectrum or preserved IR theory.} \tag{II.9.43}$$

This implication is a logical boundary, not a claim that the selected path fails. Its selected occupancy and continuation premises must be supplied where they are used. Likewise, the existence of an integral matrix group acting on candidate charges does not supply a nonperturbative physical action on every state.

Hull and Townsend's proposed $E_7(\mathbb{Z})$ U-duality concerns Type II theory compactified on T^6 in its stated setting. The proposal organizes electric and magnetic charge data and includes transformations invisible to a purely perturbative description. For it to act as a physical duality, the required charged sectors must exist and the nonperturbative transformations must relate their dynamics. Algebraic group inclusion, or a formal symplectic action on a lattice, is therefore weaker than exact symmetry of the quantum theory. We will use a group name as a map of required comparisons, not as an automatic proof of them.

These paths use distinct inputs. The free circle tests zero modes and the measure. IIB S and the M lift import separate nonperturbative premises. Later Hanany–Witten and M5 chapters add dynamics to the unit and charge calculations here.

II.9.7 Exercises

Show the intermediate calculation and explain the physical interpretation in writing. Exercises 1–4 accept the exact JSON fields in the public companion. For public submissions, follow `benchmark/PROTOCOL.md`. Exercise 5 is assessed as a written argument.

1. For $\alpha' = 4$, $R = 3$, $g_{\mathrm{s}} = 3/2$ and $(n, w) = (2, -1)$, use (II.9.1), (II.9.2), and (II.9.6). Submit `dual_radius`, `dual_coupling`, `dual_p_left`, and `dual_p_right` as exact rational strings. Explain why the right-moving sign reverses and why the coupling does not follow from the mass shell.

2. On the oriented local $(\mathrm{F1}, \mathrm{D1})$ integer column $q = (2, 1)^T$, apply T_e first and then S_e from (II.9.13). Submit `matrix`, `charge`, `determinant`, and `primitive`. Show how an integral inverse enters the gcd proof. State separately what the house fivebrane S does to an outward D5.

3. Assume the IIA physical-circle units (II.9.23)–(II.9.24) and the D0 mass in (II.9.25). At $\alpha' = 4$ and $g_{\mathrm{s}} = 3/2$, compute R_{10}, ℓ_p^3, the D0 and unit KK masses, and 2π times each of the wrapped-M2 and F1 tensions. Submit the six exact rational fields named in the public question schema. Show the full circumference in the membrane calculation.

4. Compute the local $\mathfrak{so}(32)$ adjoint dimension and the generic smooth-K3 IIA RR vector count. Separate the contributions of C_1, C_3 on K3 two-cycles, and the dualized six-dimensional C_3. Submit the five integer fields named in the public question schema. Explain why the dualized vector is not a twenty-third K3 two-cycle.

5. For the selected finite linear D3/fivebrane route, label the ordered IIB S, signed coordinate rotation, creation/occupancy, and infrared reconnection/continuation as P, NP, or A. Give the union of required premises. Then analyze the single specified IIA D4–NS5 to M5 lift and its separately attached protected low-energy continuation. Explain why charge conservation and the D0/KK equality prove neither premise. State what additional physical content the original Type II on T^6 $E_7(\mathbb{Z})$ proposal needs.

II.9.8 Take-home message

Take-home message

On a free isometric circle, $R' = \alpha'/R$ with $(n', w') = (w, n)$ preserves p_L and reverses p_R; the coupling transformation also needs the worldsheet measure premise. Integral $SL(2, \mathbb{Z})$ matrices preserve primitive charges and oriented pairings, while physical IIB transport remains a nonperturbative input. In one physical IIA length frame, $R_{10} = g_{\mathrm{s}}\ell_s$ matches D0 and KK unit masses, and wrapping an M2 around $2\pi R_{10}$ matches the F1 tension. Heterotic low-energy counts and selected brane chains identify testable interfaces and their remaining assumptions. None of these finite calculations alone establishes the full quantum equivalences.

The reader can now calculate a circle image including its coupling, transport a specified integral charge, compare M-circle masses and tensions with all 2π factors, count the generic K3 RR vectors, and list the physical dependencies of a selected brane chain. The next chapter develops the NS5 object used in the fivebrane path. The later mirror and M5 construction chapters supply dynamics beyond the arithmetic and unit interfaces established here.

Status and sources

Section 9.1. The physical circle, tension and fivebrane conventions are stated above.
Section 9.2. The free-circle zero mode is [WS], from Giveon et al. (1994, sec. 2.2, physical PDF pp. 14–16). The radius and integer exchange at $R, \alpha' > 0$ are [MATH]. The gauged-circle measure and holonomy premise is [WS], from Giveon et al. (1994, sec. 2.3, physical PDF pp. 17–18, eqs. (2.3.9)–(2.3.11), sec. 4.1, physical PDF p. 89, eq. (4.1.10)). Density and genus-weight equalities and examples are [MATH] given the free-circle zero modes, measure and holonomy premises. Source momentum and curvature-dilaton normalizations are translated in the body; oscillator and projection sectors remain separate.
Section 9.3. The discussion takes full IIB $SL(2,\mathbb{Z})$ as a nonperturbative premise, not a worldsheet derivation; the source electric frame is Schwarz (1995, sec. 2, physical PDF pp. 3–6, eqs. (6)–(21)). The fivebrane action uses the outward-oriented charge column. The gcd and pairing preservation are [MATH] on a free integral lattice; compare Hull and Townsend (1995, sec. 2, physical PDF pp. 10–11, eqs. (2.6)–(2.9)). The macroscopic-string tension has source supergravity support [SUGRA]; inverse-matrix covariance and the example are conditional [MATH], not full IIB equivalence. Source electric axes differ from house fivebrane axes. The cited example transcribes Schwarz's $\chi = -1/2$ sentence, Schwarz (1995, physical PDF p. 6, eq. (17) and paragraph after eq. (21)); the nonzero difference in (II.9.22) is conditional [MATH], not an attributed source correction.
Section 9.4. The lift uses physical IIA/M circle and Planck units under the nonperturbative IIA/M lift and the stated absolute-unit normalization, translating Witten (1995, sec. 2.3, physical PDF pp. 11–13, eqs. (2.9)–(2.14)); this is not a worldsheet derivation. Source Weyl scaling, the D0/KK masses, and the full-circumference M2/F1 tensions are conditional [MATH]. Schwarz (1995, sec. 4, physical PDF p. 10, eqs. (31)–(32)) uses source r and $e^{-2\phi_A/3}$, not physical R_{10}. Witten's radius/KK prose conflicts with its equations, Witten (1995, physical PDF pp. 11–12, eqs. (2.13)–(2.14)); we translate the equations. No M5 tension is imported.
Section 9.5. The perturbative action powers and absence of elementary Type I spinors have source [WS] support, Witten (1995, sec. 5, physical PDF pp. 52–53, eqs. (5.1)–(5.2)); neither derives heterotic/Type I equivalence, a distinct nonperturbative premise. The local 496 count and Weyl weights are conditional [MATH]; global gauge form stays open. The generic smooth-K3 $1 + 22 + 1$ RR count is [MATH] under the source $VF_4 = *F_2$ convention, Witten (1995, sec. 4.5, physical PDF pp. 49–50, eqs. (4.32)–(4.34)). The heterotic T^4/IIA K3 equivalence is a distinct nonperturbative premise, Witten (1995, secs. 4.2–4.3, physical PDF pp. 34–36, eqs. (4.5)–(4.10)); low-energy and protected

matches support sectors, not the full equivalence or spectrum.
Section 9.6. Hull–Townsend's Type II on T^6 $E_7(\mathbb{Z})$ proposal, Hull and Townsend (1995, abstract and sec. 1, physical PDF pp. 1–4), is conditional on populated electric/magnetic sectors and nonperturbative transformations. The dependencies of the two finite paths are combined conditionally [MATH]. The Hanany–Witten path uses IIB S, signed coordinate restoration, brane creation and occupancy, and infrared continuation. The D4–NS5 path uses the nonperturbative IIA/M lift. The comparison of low-energy descriptions further assumes protected continuation. Charge conservation discharges neither generator nor continuation.
Sections 9.7–9.8. Exercises 1–4 request bounded consequences of the displayed premises; Exercise 5 requests written reasoning about the exact selected paths. The take-home message adds no stronger equivalence claim.

References

Giveon, A., M. Porrati, and E. Rabinovici (1994). "Target space duality in string theory". In: *Phys. Rept.* 244. Source edition v1, pp. 77–202. DOI: 10.1016/0370-1573(94)90070-1. arXiv: hep-th/9401139.

Hull, C. M. and P. K. Townsend (1995). "Unity of superstring dualities". In: *Nucl. Phys. B* 438. Source edition v2, pp. 109–137. DOI: 10.1016/0550-3213(94)00559-W. arXiv: hep-th/9410167.

Schwarz, J. H. (1995). "An SL(2,Z) multiplet of type IIB superstrings". In: *Phys. Lett. B* 360. Erratum: Phys. Lett. B 364, 252 (1995); exact local source version v5, pp. 13–18. DOI: 10.1016/0370-2693(95)01405-5. arXiv: hep-th/9508143.

Witten, E. (1995). "String theory dynamics in various dimensions". In: *Nucl. Phys. B* 443. Source edition v2, pp. 85–126. DOI: 10.1016/0550-3213(95)00158-O. arXiv: hep-th/9503124.

Chapter II.10

NS5-branes and other solitonic objects

II.10.1 A fivebrane seen from outside

A fundamental string couples electrically to the two-form B_2. A fivebrane can instead be detected by carrying a three-sphere around it and measuring the flux of $H_3 = dB_2$. This is the magnetic description of an NS5-brane. Its six-dimensional worldvolume occupies $x^{0,1,2,3,4,5}$, leaving the four coordinates $x^{6,7,8,9}$ transverse. We will first ask what an observer outside that worldvolume can calculate. The answer has a magnetic integer, a long radial throat, and a coupling that grows toward the core.

A second view replaces a transverse circle by a geometric fiber. There the same sort of integer appears as a Chern number, but only an isometric circle enters the elementary T-duality map. A third view wraps an NS5 on a holomorphic curve. The Newton boundary of that curve determines outward asymptotic directions. These three views will become useful in later brane constructions. Their relation is a physical dictionary with stated domains, not a consequence of comparing integers alone.

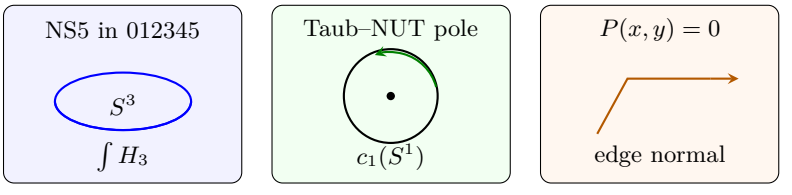


Figure II.10.1: Three exterior views used in this chapter. A transverse linking S^3 detects H_3 around an NS5; a circle fiber collapses at a coincident Taub–NUT pole; and a Newton edge controls an asymptotic arm of a holomorphic curve. The arrows indicate the local observables calculated below. They do not identify the full worldvolume theories.

Chapter 8 fixed the NS two-form and string-frame metric, and Chapter 9 supplied the

circle dictionary. We use those ingredients to calculate exterior quantities. Chapter III.10 will address worldvolume multiplets and dynamics.

II.10.2 NS charge and a fivebrane throat

What does it mean for a codimension-four object to be magnetic? Let $r > 0$ be the Euclidean radius in the transverse $\mathbb{R}^4$, and put $\ell_s^2 = \alpha' > 0$. In string frame, the sourced type-II NS5 ansatz for $N > 0$ coincident units is

$$ds^2_{\rm str} = \eta_{\mu\nu}dx^\mu dx^\nu + Z_5(r)\big(dr^2 + r^2 d\Omega_3^2\big), \qquad Z_5(r) = 1 + \frac{N\alpha'}{r^2}, \qquad e^{2\Phi} = g_s^2 Z_5(r), \tag{II.10.1}$$

where $\mu, \nu = 0, \dots, 5$ and $g_s = e^{\Phi(\infty)}$. The brane source and its basic magnetic charge are physical input to this ansatz. The field equations and supersymmetry of the full source are not derived by the radial manipulations that follow.

The flux sign requires an orientation. Parametrize the unit linking sphere by $0 \le \theta \le \pi/2$ and angles ϕ, ψ of period 2π. We choose the outward transverse orientation $dr \wedge \mathrm{vol}_{S^3_+}$, with

$$\mathrm{vol}_{S^3_+} = \sin\theta\cos\theta\, d\theta \wedge d\psi \wedge d\phi, \qquad \int_{S^3_+} \mathrm{vol}_{S^3_+} = (2\pi)^2 \int_0^{\pi/2} \sin\theta\cos\theta\, d\theta = 2\pi^2. \tag{II.10.2}$$

A convenient source-local angular potential is written in units $\ell_{\rm str} = 1$ as $B = n_5 \cos^2\theta\, d\phi \wedge d\psi$. The order of its angular differentials matters. Differentiating the coefficient and then exchanging $d\phi, d\psi$ gives

$$dB = -2n_5 \sin\theta\cos\theta\, d\theta \wedge d\phi \wedge d\psi = +2n_5 \sin\theta\cos\theta\, d\theta \wedge d\psi \wedge d\phi. \tag{II.10.3}$$

Thus the integral in those source units is $4\pi^2 n_5$. The same angular coordinate forms G and B acquire a factor α' when lengths are restored. With the chapter's physical identification $n_5 = N$ for N minimally charged sources, the book-unit form and oriented charge are

$$H_3 = 2N\alpha' \,\mathrm{vol}_{S^3_+}, \qquad \int_{S^3_+} H_3 = 4\pi^2\alpha' N, \qquad Q_{\rm NS5} := \frac{1}{4\pi^2\alpha'} \int_{S^3_+} H_3 = N. \tag{II.10.4}$$

The flux unit is consistent with the fundamental-string coupling $\frac{1}{2\pi\alpha'}\int B_2$: moving its worldsheet description across a gauge patch must leave its phase well defined. That normalization fixes a unit for the period. Calling one such unit one physical NS5 source uses the separately sourced minimal-charge premise. A D-brane Page-charge expression can also shift by this S^3 flux under a choice of filling; it is not an equality between D-brane and NS5 charges.

For a concrete sign check set $\alpha' = 2$ and $N = 3$. Equation (II.10.4) gives $\int_{S^3_+} H_3 = 24\pi^2$ and $Q_{\rm NS5} = 3$. Reversing the sphere orientation yields $-24\pi^2$ and oriented charge -3. The positive harmonic function Z_5 does not turn negative. Figure II.10.2 keeps the sphere and the two integration arrows visible: reversing an integration orientation

changes a signed integral, while changing the number of sources would change the background.

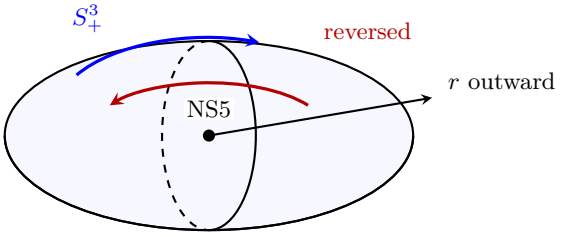


Figure II.10.2: An S^3 links an NS5 extending in directions 012345. The outward r arrow and blue angular arrow define $dr \wedge \mathrm{vol}_{S^3_+}$; the red arrow denotes the reversed integration orientation. The sphere contour remains continuous. The positive and negative integrals belong to the same local solution.

This flux is the magnetic use of Chapter 8's bulk field H_3. A nonzero integral is also a direct warning about potentials. If a single smooth B_2 existed over the whole linking S^3 with $H_3 = dB_2$ there, Stokes' theorem would give

$$\int_{S^3} H_3 = \int_{S^3} dB_2 = \int_{\partial S^3} B_2 = 0, \tag{II.10.5}$$

contrary to Equation (II.10.4). The displayed angular B is consequently a local gauge potential. Its apparent behavior where an angular circle degenerates calls for overlapping patches, not a globally smooth two-form on the sphere.

Why does the transverse harmonic factor contain r^{-2}? For a radial function $f(r)$ on punctured $\mathbb{R}^4$, the flat Laplacian is $r^{-3}\partial_r(r^3\partial_r f)$. Applying it to $f = r^{-2}$ gives

$$\partial_r r^{-2} = -2r^{-3}, \qquad \nabla_4^2 r^{-2} = \frac{1}{r^3}\partial_r(-2) = 0 \quad (r > 0). \tag{II.10.6}$$

A distributional extension has a delta term at the origin. One can see its mathematical coefficient by integrating over a ball with outward S^3 boundary:

$$\int_{B^4_\epsilon} \nabla_4^2 r^{-2}\, d^4x = \int_{S^3_\epsilon} \partial_r r^{-2}\, \epsilon^3 d\Omega_3 = (-2)(2\pi^2) = -4\pi^2. \tag{II.10.7}$$

Hence $\nabla_4^2 r^{-2} = -4\pi^2\delta^{(4)}(x)$ as a distribution with these Euclidean conventions. This identity checks the radial singularity. It does not derive the NS5 source action, the H_3 normalization, or the BPS property. In particular, a similarly named heterotic soliton charge defined with a gauge connection and a dimensionful H convention cannot be substituted for Q_{NS5}.

The metric already contains a geometric clue. Near $r = 0$, $Z_5 \simeq N\alpha'/r^2$, so the radial proper length between two positive radii is

$$L(r_1, r_2) = \int_{r_1}^{r_2} \sqrt{Z_5(r)}\, dr \simeq \sqrt{N\alpha'} \log \frac{r_2}{r_1} \quad (0 < r_1 < r_2 \ll \sqrt{N\alpha'}). \tag{II.10.8}$$

As $r_1 \to 0$, this string-frame distance diverges logarithmically while the angular S^3 approaches squared radius $N\alpha'$. A long throat follows from the sourced metric. It does not by itself certify a globally weak string expansion or an exact worldsheet theory.

The radial coordinate hides a simple product geometry in the leading metric. Define $\rho = \sqrt{N\alpha'}\log(r/r_0)$ for any reference radius r_0 inside the near-core range. Then $d\rho = \sqrt{N\alpha'}\,dr/r$, and the transverse line element becomes

$$ds_\perp^2 \simeq d\rho^2 + N\alpha' d\Omega_3^2, \qquad r = r_0 \exp\left(\frac{\rho}{\sqrt{N\alpha'}}\right). \tag{II.10.9}$$

The sphere remains finite while ρ extends toward $-\infty$ at the idealized source. In this approximation the dilaton is linear in ρ:

$$\Phi \simeq \log\left(\frac{g_s\sqrt{N\alpha'}}{r_0}\right) - \frac{\rho}{\sqrt{N\alpha'}}. \tag{II.10.10}$$

Its sign agrees with increasing coupling as one moves toward smaller r. This local leading form does not infer an exact conformal field theory from the supergravity metric.

II.10.3 Dilaton and near-source control

Can an asymptotically weakly coupled NS5 remain weakly coupled all the way down its throat? The local loop parameter is the exponential of the dilaton, not the asymptotic constant alone. From Equation (II.10.1),

$$g_{\rm loc}(r) := e^{\Phi(r)} = g_s\sqrt{1 + \frac{N\alpha'}{r^2}}, \qquad g_{\rm loc}^2(r) = g_s^2 + \frac{g_s^2 N\alpha'}{r^2}. \tag{II.10.11}$$

For $0 < g_s < 1$ this decreases monotonically as r increases. Its crossing of one therefore occurs at a unique positive radius. Solving $g_{\rm loc}^2 = 1$, without dropping the asymptotic 1 in Z_5, gives

$$1 = g_s^2\left(1 + \frac{N\alpha'}{r_*^2}\right), \qquad r_*^2 = \frac{N\alpha' g_s^2}{1 - g_s^2}. \tag{II.10.12}$$

The denominator explains the restriction $g_s < 1$. At $g_s = 1$ the coupling approaches one only at infinity and exceeds it at finite r; if $g_s > 1$ it is already greater than one asymptotically. There is no positive finite unity crossing in those cases.

The threshold partitions the positive radial line:

$$0 < r < r_* \implies g_{\rm loc} > 1, \qquad r > r_* \implies g_{\rm loc} < 1 \qquad (0 < g_s < 1). \tag{II.10.13}$$

It is the local loop expansion that changes character. A radius where curvature reaches the string scale need not coincide with r_*.

For example, choose $g_s = 1/4$ and $N\alpha' = 6$ in a fixed length unit. Substituting into Equation (II.10.12) yields

$$r_*^2 = \frac{6/16}{1 - 1/16} = \frac{6}{15} = \frac{2}{5}. \tag{II.10.14}$$

At $r^2 = 1/10$, the direct value is

$$g_{\rm loc}^2 = \frac{1}{16}\left(1 + \frac{6}{1/10}\right) = \frac{61}{16} > 1. \tag{II.10.15}$$

This radius is inside the crossing, as the monotonicity predicts. The arithmetic is useful because simply replacing Z_5 by its near-core term would miss the additive $1/16$. Figure II.10.3 places both radii on the same logarithmic axis.

Their squared ratio provides another check:

$$\frac{r_*^2}{r_{\rm probe}^2} = \frac{2/5}{1/10} = 4, \qquad r_{\rm probe} = \frac{r_*}{2}. \tag{II.10.16}$$

This comparison uses the same physical radial coordinate in both terms. Proper distance down the throat and the local coupling remain different observables.

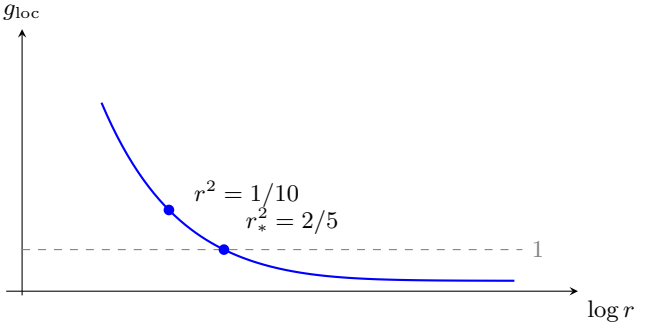


Figure II.10.3: The exact local coupling in the worked example, plotted against $\log r$ with $g_s = 1/4$ and $N\alpha' = 6$. The unity line meets the curve at $r_*^2 = 2/5$. The marked point $r^2 = 1/10$ has $g_{\rm loc}^2 = 61/16$. The curve diverges to the left even though its right asymptote is weak.

There are two distinct radial statements here. The proper distance to the idealized source diverges by Equation (II.10.8); the local loop parameter also diverges by Equation (II.10.11). A long distance in the string-frame metric is not an assurance that perturbation theory improves. Curvature and string-loop control are separate checks as well. The angular radius $\sqrt{N\alpha'}$ suggests that large N can make a local curvature scale large compared with ℓ_s, but the same N increases the coupling at a fixed r. A controlled region must satisfy the relevant conditions together, at the radius under discussion.

The nearby physical question is what degrees of freedom inhabit the core. These bulk equations do not answer it. Chapter III.10 treats worldvolume limits and multiplets; in the next section we first trade an isometric transverse circle for a geometric fibration. That trade requires explicit coordinates and orientations.

II.10.4 A circle transverse to the source

What becomes geometric when a transverse NS5 circle is dualized? A useful comparison is a coincident Taub–NUT pole. We use dimensionless source-local coordinates $\vec{r} \in \mathbb{R}^3$, $r = |\vec{r}|$, and a fiber angle ψ of period 4π. The parameter g in the following harmonic function is also source-local; it is neither the book's g_s nor a physical radius measured in units of α'. For $N > 0$ the metric and connection relation are

$$ds^2 = H(r)d\vec{r}\cdot d\vec{r} + \frac{1}{4}H(r)^{-1}(d\psi+\omega)^2, \qquad H(r) = \frac{1}{g^2} + \frac{N}{2r}, \qquad \nabla\times\vec{\omega} = 2\nabla H. \tag{II.10.17}$$

The one pole with coefficient $N/2$ describes coincident total charge. Separated centers would require a sum with their positions in its denominators. At large r the fiber has finite proper size, and at the pole the H^{-1} factor makes it shrink.

Let (ϑ, φ) be ordinary polar angles on the base, with $0 \le \vartheta \le \pi$ and φ of period 2π. They are distinct from the angle θ sometimes used for a transverse dual circle. Since $\nabla H = -N\hat{r}/(2r^2)$, a local choice $\omega = N\cos\vartheta\, d\varphi$ has $d\omega = -N\sin\vartheta\, d\vartheta\wedge d\varphi$, consistent with the curl equation. Put

$$\chi = \frac{\psi}{2} \quad (\chi \sim \chi + 2\pi), \qquad A = \frac{\omega}{2} = \frac{N}{2}\cos\vartheta\, d\varphi, \qquad d\psi + \omega = 2(d\chi + A). \tag{II.10.18}$$

This is the normalized circle connection.

The fiber part of the metric is now

$$\frac{1}{4}H^{-1}(d\psi+\omega)^2 = H^{-1}(d\chi + A)^2, \qquad \sqrt{G_{\chi\chi}} = H^{-1/2}. \tag{II.10.19}$$

Thus the increasing 2π-period coordinate χ has asymptotic proper radius g in these dimensionless units and shrinks as $r^{1/2}$ near a positive pole. Reading a radius directly from the coefficient of $d\psi^2$ would miss its 4π period. On the standard polar orientation $\sin\vartheta\, d\vartheta\wedge d\varphi > 0$, its curvature and Chern integral are

$$F_A = dA = -\frac{N}{2}\sin\vartheta\, d\vartheta\wedge d\varphi, \qquad \frac{1}{2\pi}\int_{S^2_{\text{polar}}} F_A = \frac{-N/2}{2\pi}(4\pi) = -N. \tag{II.10.20}$$

If we choose the opposite base orientation, with the increasing fiber χ held fixed, the same geometric fibration has the local number

$$\frac{1}{2\pi}\int_{S^2_{\text{opposite}}} F_A = +N. \tag{II.10.21}$$

Only the base orientation changed in this sentence. The linking S^3 orientation of the previous section is a separate choice. The local expression $A \propto \cos\vartheta\, d\varphi$ needs north and south patches, just as any connection with nonzero Chern number does. Figure II.10.4 separates the base orientation arrow from the increasing fiber arrow.

The patch transition displays the Chern magnitude. Choose $A_N = (N/2)(\cos\vartheta - 1)d\varphi$, regular at the north pole, and $A_S = (N/2)(\cos\vartheta + 1)d\varphi$, regular at the south pole. On the overlap,

$$A_S - A_N = N\, d\varphi. \tag{II.10.22}$$

Its integer winding around the equator agrees with the magnitude of the Chern integral. This geometric transition is not independently an NS5 flux measurement until the isometric duality premise is supplied.

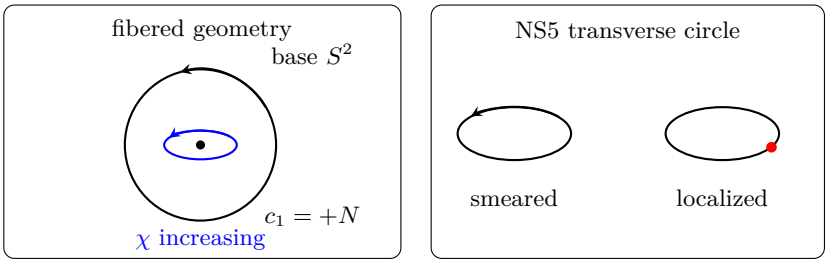


Figure II.10.4: Left: the S^1_χ fiber over a base S^2 surrounding the coincident pole. The blue fiber arrow fixes increasing χ; the black base arrow indicates the orientation opposite to the standard polar one, for which $c_1 = +N$. Right: an NS5 spread uniformly around a transverse dual circle has a shift isometry. The dot marked on the right-hand circle is a localized source; its position breaks that shift isometry. This schematic indicates the domain of the elementary Buscher step.

The behavior at the pole follows by an explicit radial coordinate change. In the limit $r \to 0$, discard $1/g^2$ only after noting it is subleading, set $R = \sqrt{2Nr}$, and define $\widetilde{\psi} = \psi/N$. Then $r = R^2/(2N)$ and $dr = (R/N)dR$. The two radial terms become

$$H\, dr^2 \simeq \frac{N}{2r}\frac{R^2}{N^2}dR^2 = dR^2, \qquad Hr^2 d\Omega_2^2 \simeq \frac{Nr}{2}d\Omega_2^2 = \frac{R^2}{4}d\Omega_2^2. \tag{II.10.23}$$

The fiber term becomes $\frac{R^2}{4}(d\widetilde{\psi} + \cos\vartheta\, d\varphi)^2$. Together these give

$$ds^2 \simeq dR^2 + \frac{R^2}{4}\left[d\vartheta^2 + \sin^2\vartheta\, d\varphi^2 + (d\widetilde{\psi} + \cos\vartheta\, d\varphi)^2\right], \quad \widetilde{\psi} \sim \widetilde{\psi} + \frac{4\pi}{N}. \tag{II.10.24}$$

The bracket is the usual Hopf presentation of a round three-sphere when $\widetilde{\psi}$ has period 4π. Therefore $N = 1$ has a smooth $\mathbb{R}^4$ core. For $N > 1$, the shortened period gives the local cone $\mathbb{C}^2/\mathbb{Z}_N$. For example, $N = 2$ makes the pole coefficient $N/2 = 1$, gives $c_1 = +2$ with the opposite base orientation, and leaves $\widetilde{\psi}$ with period 2π. The fiber collapses in both cases. The quotient is a statement about the coincident pole, not every arrangement of N centers.

The transverse duality statement has a precise domain. If an NS5 on $\mathbb{R}^3 \times S^1$ is uniformly smeared around its transverse circle, the fields are independent of its angular coordinate θ. The shift $\theta \mapsto \theta +$ constant is then an isometry. The elementary Buscher dictionary maps that isometric background to the circle-fiber geometry; schematically its exchanged data are

$$\text{isometric smeared NS5 on } \mathbb{R}^3 \times S^1_\theta \quad \xleftrightarrow[\text{circle isometry}]{\text{T-duality}} \quad \text{Taub–NUT with fiber } S^1_\psi. \tag{II.10.25}$$

The map exchanges the circle direction and uses the NS B data to produce the fiber connection. In the source-local description, the harmonic pole $N/(2r)$ and the fiber period 4π fix the Chern integer calculated above. A localized NS5 instead has a harmonic function that depends on θ. Its shift is not an isometry, so inserting that localized field into the elementary Buscher formulas is not licensed by Equation (II.10.25). This limitation does not say that a quantum T-duality is impossible. It specifies what the simple geometric step actually computes. Chapter 9's circle transformation and later suspension geometries use the same distinction.

The small S^3_+ of Section II.10.2 links a point source in local $\mathbb{R}^4$. It is a reference definition of the minimally charged localized NS5, not the Gaussian cycle of the isometric background in Equation (II.10.25). Smearing the same N source units around the transverse S^1_θ leaves an exterior with base $\mathbb{R}^3 \setminus \{0\}$, whose Gaussian cycle is $S^2 \times S^1_\theta$. We choose the transverse $\mathbb{R}^3$ orientation so that its boundary has the *opposite* polar orientation of Equation (II.10.21), then orient the product by that base followed by increasing θ of period 2π. The dual Taub–NUT fiber has increasing $\chi = \psi/2$ of period 2π.

The isometric source fields specify more than an equality of charges. In Tong's dimensionless coordinates the sigma-model torsion term fixes $B_{i\theta} = \omega_i/2 = A_i$ in the convention $\frac{1}{2}B_{ij}\epsilon^{\mu\nu}\partial_\mu X^i \partial_\nu X^j$. Locally, this is $B_{\mathrm{sm}} = A \wedge d\theta$, so $H_{\mathrm{sm}} = F_A \wedge d\theta$. Restoring the common sigma-model length unit multiplies these angular forms by α'; g and the source coordinates remain dimensionless and are not identified with g_s or a physical circle radius. Fiber integration now gives the signed relation

$$\frac{1}{2\pi\alpha'}\int_{S^1_\theta} H_{\mathrm{sm}} = F_A, \qquad Q_{\mathrm{smear}} := \frac{1}{4\pi^2\alpha'}\int_{S^2_{\mathrm{opposite}}\times S^1_\theta} H_{\mathrm{sm}} = \frac{1}{2\pi}\int_{S^2_{\mathrm{opposite}}} F_A = +N. \tag{II.10.26}$$

Indeed $F_A = -\frac{N}{2}\sin\vartheta\, d\vartheta \wedge d\varphi$ gives $-2\pi N$ on the standard polar base and $+2\pi N$ on the chosen opposite base; multiplying by the increasing circle period 2π gives $+4\pi^2\alpha' N$ for the restored product flux. Reversing the product orientation, for example by reversing only its base factor, changes that sign. The local S^3_+ integral also equals N in its separately sourced normalization, with the minimal physical charge identification supplied as an input. The isometric field relation connects the product flux to the Chern class; numerical agreement with the localized S^3 integral alone neither identifies their cycles nor derives a duality for an angle-dependent localized solution.

II.10.5 Fivebrane charges and holomorphic curves

How can a polynomial encode outward legs? In one brane-tiling construction an NS5 wraps a holomorphic curve $\Sigma = \{P(x, y) = 0\}$ in $(\mathbb{C}^*)^2$ while sharing four spacetime directions with the other branes. This physical realization is input. The polynomial calculation below concerns the asymptotic geometry of Σ; it does not establish a full brane duality.

Write a Laurent polynomial with finite support as $P(x, y) = \sum_{(m,n)\in S} c_{mn} x^m y^n$, where each listed $c_{mn} \neq 0$ and $x, y \in \mathbb{C}^*$. Its Newton polygon $\Delta(P)$ is the convex hull

of S in the exponent lattice. The real logarithmic map

$$\mathrm{Log} : (x, y) \longmapsto (X, Y) = (\log|x|, \log|y|) \tag{II.10.27}$$

projects the curve to its amoeba. An edge of $\Delta(P)$ can control an asymptotic branch of this image. The outward perpendicular to that edge gives its direction in (X, Y), with multiplicity set by lattice length when the relevant roots are simple.

Start with $P = 1 + x + y$. Its vertices in counterclockwise order are $v_0 = (0, 0)$, $v_1 = (1, 0)$, $v_2 = (0, 1)$. For a counterclockwise edge step $(\Delta m, \Delta n)$, the outward perpendicular is $(\Delta n, -\Delta m)$; divide its components by their greatest common divisor to get a primitive normal. The three steps and normals are

edge	$(\Delta m, \Delta n)$	u_{out}
v_0v_1	$(1, 0)$	$(0, -1)$
v_1v_2	$(-1, 1)$	$(1, 1)$
v_2v_0	$(0, -1)$	$(-1, 0)$

(II.10.28)

The vector sum is explicit:

$$(0, -1) + (1, 1) + (-1, 0) = (0, 0). \tag{II.10.29}$$

The shoelace sum gives twice the area 1, so this triangle has no hidden extra edge lattice points. In the outward $(D5, NS5)$ web drawing these normal pairs are the leg labels. The sum is an integer-geometric balance. Interpreting a physical junction requires the separate fivebrane construction and its allowed charge assignments.

Why is the perpendicular the right direction? Consider an edge exposed by an outward vector $u = (p, q)$, so all edge exponents maximize $pm + qn$ over the support. Scale $(|x|, |y|)$ along (e^{tp}, e^{tq}) with $t \to +\infty$. Each monomial $x^m y^n$ changes in magnitude by $e^{t(pm+qn)}$. Only the maximizing edge terms remain at the leading common exponential order. In logarithmic coordinates the escaping direction is u itself:

$$(X, Y) \mapsto (X, Y) + t(p, q), \qquad P(e^{tp}x, e^{tq}y) = e^{th}\big(P_E(x, y) + o(1)\big), \tag{II.10.30}$$

where $h = \max_{(m,n)\in S}(pm + qn)$ and P_E is the sum over *all* exponents on the exposed edge. This also explains why an outward normal, rather than an arbitrarily chosen perpendicular, is selected by the limit. The phase of x or y can change the location of an arm, while the normal fixes its asymptotic direction.

For the unit triangle, each edge has exactly two terms. The bottom-edge limit $y \to 0$ yields $1 + x = 0$, so $x = -1$ is a simple nonzero root. Along the left edge $x \to 0$ yields $1 + y = 0$. Along the slanted edge, x and y dominate the constant together, giving $x + y = 0$ or $y/x = -1$. Their leading cylinder descriptions may be written

$$\begin{aligned} x &= -1 \quad (Y \to -\infty), \\ y &= -1 \quad (X \to -\infty), \\ y/x &= -1 \quad (X, Y \to +\infty \text{ together}). \end{aligned} \tag{II.10.31}$$

These three limits realize the normals in Equation (II.10.28). Figure II.10.5 places the polygon and the logarithmic directions side by side, with separate spaces for the labels.

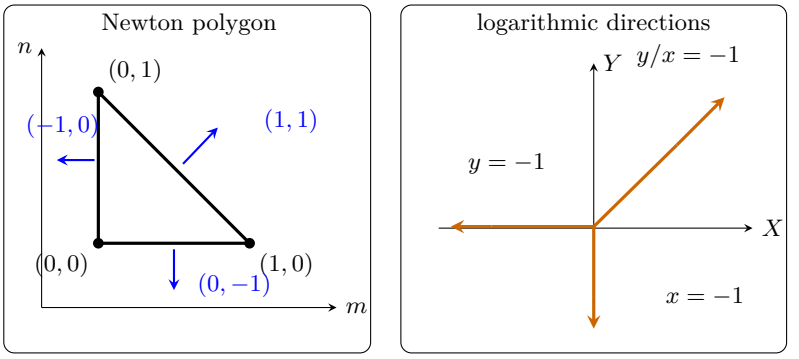


Figure II.10.5: Left: the counterclockwise Newton triangle of $1 + x + y$ with continuous edges and its primitive outward normals. Right: the three asymptotic directions in $(X, Y) = (\log|x|, \log|y|)$ space. The arrows encode leading behavior from edge polynomials; the thick center is schematic and does not supply a dimer equivalence.

A long edge needs its entire edge polynomial. Suppose an edge has endpoints (m_0, n_0) and $(m_0, n_0) + L(a, b)$, where (a, b) is primitive and L is its lattice length. Factoring a nonzero monomial leaves a one-variable polynomial in $z = x^a y^b$:

$$P_E(x, y) = x^{m_0} y^{n_0} f_E(z), \qquad f_E(z) = \sum_{j=0}^{L} c_j z^j, \qquad z = x^a y^b. \tag{II.10.32}$$

The endpoint coefficients are nonzero; some interior c_j may vanish, but every nonzero term on the edge remains at the same leading order in Equation (II.10.30). If f_E has L simple nonzero roots, each gives a distinct elementary asymptotic cylinder at the corresponding value of z. The normal gives their common direction, and the roots set transverse positions and phases. Without that simple-root hypothesis, lattice length alone does not assert L distinct simple ends. Even a long edge supported only at its two endpoints has $f_E = c_0 + c_L z^L$ with L distinct nonzero roots over $\mathbb{C}$, since $f_E' = L c_L z^{L-1}$ cannot vanish at a root. It therefore need not describe just one cylinder.

The simple-root condition has a local analytic explanation. In an integral coordinate basis adapted to an edge with primitive tangent (a, b), take $z = x^a y^b$ and a complementary monomial $w = x^c y^d$ with $ad - bc = 1$. Choose its sign so that $w \to 0$ toward the exposed boundary. After multiplying by a nonzero Laurent monomial, the nearby curve has the form $P(z, w) = f_E(z) + wG(z, w) = 0$, with G analytic near $w = 0$. Let $z_i \neq 0$ obey $f_E(z_i) = 0$ and $f_E'(z_i) \neq 0$. Set $z = z_i + \delta z$ and retain terms linear in w and δz:

$$0 = f_E'(z_i)\,\delta z + wG(z_i, 0) + O(w^2, w\delta z, \delta z^2), \qquad z(w) = z_i - \frac{G(z_i, 0)}{f_E'(z_i)} w + O(w^2). \tag{II.10.33}$$

The nonzero derivative permits a unique holomorphic branch for sufficiently small w by the local implicit-function theorem. The punctured parameter $0 < |w| \ll 1$ has a circle of phases and a radial logarithm, giving an elementary cylinder end. If $f_E'(z_i) = 0$, the

linear step cannot be divided by that derivative. Higher terms must be examined before counting separate ends.

Consider $P = 1 + 3x + x^2 + y$. Its bottom edge runs from $(0, 0)$ to $(2, 0)$, so $L = 2$ and $y \to 0$ retains three terms. The equation and roots are

$$f_E(x) = 1 + 3x + x^2 = 0, \qquad x_\pm = \frac{-3 \pm \sqrt{5}}{2}. \tag{II.10.34}$$

Both roots are nonzero and distinct. Their negative real values have different magnitudes, so the corresponding arms sit at different $X = \log |x_\pm|$ while both head toward $Y = -\infty$. Removing $3x$ by using endpoints only would produce the wrong positions. For $P = (1 + x)^2 + y$, the same edge length gives

$$f_E(x) = (1 + x)^2, \qquad x = -1 \text{ with multiplicity two.} \tag{II.10.35}$$

The repeated root does not justify two distinct simple cylinders in the leading limit. Subleading terms may resolve or ramify the local geometry, and the edge polynomial alone does not classify all such punctures.

Two supported terms can also occur on a long edge. For $P = 1 + x^2 + y$, the bottom edge still has length two, but its interior coefficient vanishes. The leading equation is

$$f_E(x) = 1 + x^2 = 0, \qquad x = +i \text{ or } x = -i. \tag{II.10.36}$$

The roots are simple and nonzero. Both arms have $X = \log |x| = 0$ at leading order, yet their phases differ by π. They are two elementary ends even though their logarithmic images can coincide. A picture in (X, Y) space can therefore hide distinct ends; the complex curve carries more information than its real projection.

For a nonunit direction, the arithmetic behind the outward-normal rule is equally concrete. Take a counterclockwise edge step $(\Delta m, \Delta n) = (4, 2)$. Its lattice length is $\gcd(4, 2) = 2$, its primitive tangent is $(2, 1)$, and its primitive outward normal is

$$u_{\text{out}} = \frac{(\Delta n, -\Delta m)}{\gcd(|\Delta m|, |\Delta n|)} = \frac{(2, -4)}{2} = (1, -2). \tag{II.10.37}$$

The edge contributes two copies of that primitive direction when two simple nonzero edge roots occur, not a single nonprimitive leg $(2, -4)$. To see a balanced closed example, take the counterclockwise triangle $(0, 0), (4, 2), (0, 2)$. Its other primitive outward normals and lengths are $(0, 1)$ with length 4, and $(-1, 0)$ with length 2. Their weighted sum is

$$2(1, -2) + 4(0, 1) + 2(-1, 0) = (0, 0). \tag{II.10.38}$$

This follows generally because multiplying each primitive outward normal by its edge lattice length restores the rotated edge step, and the steps of a closed polygon sum to zero. The computation establishes the polygon balance in the specified counterclockwise convention. It does not validate an arbitrary nonconvex polygon or prove that every drawn web is dynamically realized. The full toric-tiling story belongs in its later construction chapter.

II.10.6 Interfaces to six-dimensional theories

What does the exterior solution tell us before we quantize fields on the source? The type-II NS5 tension in the same α' and asymptotic-coupling conventions is

$$T_{\mathrm{NS5}} = \frac{1}{(2\pi)^5 \alpha'^3 g_s^2}. \tag{II.10.39}$$

This is a bulk source scale. It is not a count of massless worldvolume fields. Comparing it with the D5 tension in the same string-frame units makes the coupling distinction visible:

$$T_{\mathrm{D5}} = \frac{1}{(2\pi)^5 \alpha'^3 g_s}, \qquad \frac{T_{\mathrm{NS5}}}{T_{\mathrm{D5}}} = \frac{1}{g_s}. \tag{II.10.40}$$

At fixed α', replacing g_s by $g_s/2$ multiplies the NS5 tension by four and the D5 tension by two. The ratio doubles. Meanwhile Equation (II.10.12) moves the NS5 unity-coupling radius inward as g_s decreases. The source becomes heavier in asymptotic string units, yet its idealized local core still reaches strong coupling. These are compatible statements about different observables and regions.

Let $g_s' = g_s/2$ at fixed α' and N. Direct substitution gives

$$\frac{T_{\mathrm{NS5}}(g_s')}{T_{\mathrm{NS5}}(g_s)} = \left(\frac{g_s}{g_s'}\right)^2 = 4, \qquad \frac{T_{\mathrm{D5}}(g_s')}{T_{\mathrm{D5}}(g_s)} = \frac{g_s}{g_s'} = 2. \tag{II.10.41}$$

At every fixed positive radius the local coupling changes by the same factor as g_s, but the idealized core remains strong:

$$g'_{\mathrm{loc}}(r) = \frac{1}{2} g_{\mathrm{loc}}(r), \qquad \lim_{r\to 0} g'_{\mathrm{loc}}(r) = \infty. \tag{II.10.42}$$

Halving the asymptotic coupling postpones the strong-loop region; it does not remove it.

The scaling is visible at three sample asymptotic couplings if both tensions are divided by $C = [(2\pi)^5 \alpha'^3]^{-1}$. Each row follows from Equations (II.10.39) and (II.10.40):

g_s	T_{NS5}/C	T_{D5}/C
1	1	1
1/2	4	2
1/4	16	4

Table II.10.1: Bulk tension scaling at fixed α'. The entries compare source tensions, not six-dimensional spectra.

Table II.10.1 makes the different powers visible. It helps identify which object becomes heavy as the asymptotic coupling decreases, but it does not reveal the massless content on either brane.

The ordered fivebrane charge used by outward web legs is $(p, q) = (D5, NS5)$, so an NS5 is $(0, 1)$ and a D5 is $(1, 0)$. Charge labels track the junction legs. Neither Equation (II.10.39) nor the sum of Newton normals determines the BPS angle of a general (p, q) segment. That angle requires the Type IIB axiodilaton and a supersymmetry condition. Similarly, the exterior tension and flux cannot determine a six-dimensional multiplet or a little-string spectrum. Those questions need additional worldvolume and decoupling input in Chapter III.10. Chapter X.1 uses charged fivebranes to build a five-dimensional web; its finite-face dynamics uses more than the NS5 bulk ansatz here.

There is a useful boundary between three kinds of statement. The cited NS5 solution, the isometric duality, and the holomorphic NS5-curve construction are physical premises. The oriented integrals, radial threshold, Chern number, local quotient and edge normals are consequences calculated under those premises. An exact localized duality, full dimer equivalence, or six-dimensional dynamical theory would need further arguments. Keeping this boundary visible makes the exterior calculations useful without asking them to carry a theory they were not designed to derive.

II.10.7 Exercises

For Exercises 1–4, submit the stated exact fields using the public JSON schemas accompanying this chapter. Work the calculation on paper first; a sign, period or multiplicity is part of the answer. Exercise 5 is a written argument.

1. For $\alpha' = 2$, $N = 3$ and a linking S^3 with orientation reversed from the positive outward orientation, use $Q = (4\pi^2\alpha')^{-1} \int H_3$. Submit the coefficient of π^2 in the oriented integral and the oriented charge. Explain in one sentence why Z_5 is unchanged.

2. For $g_s = 1/4$ and $N\alpha' = 6$, solve exactly for the positive r^2 where $g_{\mathrm{loc}} = 1$. At $r^2 = 1/10$, compute g_{loc}^2 and decide whether it exceeds one. State why the asymptotic value alone does not decide the answer.

3. In the dimensionless coincident pole $H = 1/g^2 + N/(2r)$, set $N = 2$ and $\mathrm{period}(\psi) = 4\pi$. Use the base orientation giving positive Hopf Chern number. Submit the $1/r$ coefficient, signed Chern number, whether the fiber shrinks, and whether the transverse-circle shift is an isometry for a fully localized NS5 on $\mathbb{R}^3 \times S^1$. Explain the distinct roles of ψ and the dual-circle angle.

4. For $P = 1 + x + y$, order the Newton vertices $(0, 0), (1, 0), (0, 1)$ counterclockwise. Submit the primitive outward normals with multiplicity in lexicographic order, their vector sum, and twice the area. Derive each normal from an oriented edge step; then explain what changes for a length-two edge with a repeated edge root.

5. Explain which type-II NS5 bulk features follow from the local supergravity ansatz, why a localized source depending on the transverse angle does not enter the elementary isometric Buscher step, and which six-dimensional questions pass to Chapter III.10. Name the physical premises used by each part of your argument.

II.10.8 Take-home message

Take-home message

An NS5 has an oriented magnetic H_3 flux through a transverse linking sphere. Its string-frame exterior has an r^{-2} harmonic factor, a logarithmic radial throat and a local coupling that grows toward the core. A coincident Taub–NUT pole replaces an isometric transverse circle by a fiber with Chern number of magnitude N; the localized angle-dependent source lies beyond the elementary Buscher step. For a holomorphic NS5 curve, outward Newton normals give asymptotic directions, while the complete edge polynomial and its roots decide the simple-end count. These bulk and asymptotic calculations prepare brane constructions, but worldvolume dynamics requires separate input.

Status and sources

Opening. The three interfaces are organizational. The NS5 source, isometric circle correspondence and holomorphic curve are distinct sourced physical premises. The bulk-field normalizations and oriented axes are stated above.

NS charge and a fivebrane throat. The type-II string-frame ansatz and N basic magnetic units are in Johnson (2000, PDF p. 167, eq. (396)) [SUGRA]. The raw unit-length B is in Martinec et al. (2019, PDF p. 13, eq. (2.1)); the identification $H = dB$ and its displayed angular component occur on PDF pp. 17 and 24, eq. (4.8). Its $4\pi^2 n_5$ integral on PDF p. 43 follows a Page-charge ambiguity and is used only as a flux occurrence. The book-unit factor α' follows the entry-3 F1 phase convention. The minimal physical NS5 identification is an additional sourced premise [SUGRA]. Differentiation, oriented integration, Stokes' theorem, the punctured radial identity, distribution coefficient and logarithmic distance are conditional calculations [MATH]. The heterotic symmetric solution of Callan et al. (1991, PDF pp. 17–18, eqs. (6.2)–(6.6)) uses a dimensionful Q and a gauge connection; it supplies historical context, not this type-II flux normalization.

Dilaton and near-source control. The local coupling follows the sourced dilaton in Johnson (2000, PDF p. 167, eq. (396)) [SUGRA]. The unity radius and numerical example are algebraic [MATH]. No exact-CFT or uniform-curvature claim is inferred.

A circle transverse to the source. The coincident charge-N low-energy background metric, 4π fiber period and connection curl occur in Tong (2002, PDF p. 20, eqs. (A.32)–(A.33)) [SUGRA]. The classical isometric sigma-model dualization and field reconstruction are on PDF pp. 8–10, eqs. (2.11), (2.13) and Sec. 2.2 [WS]. This uses the elementary isometric T-duality, not a transfer of a QFT claim between frames. The overall action normalization is on PDF pp. 6–7, eq. (2.8) and its following explanation, and p. 9, eq. (2.13); together with the stated string-action convention it fixes the restoration $B_{\text{physical}} = \alpha' B_{\text{source}}$. The Chern signs, radial change of coordinates, product-cycle fiber integral and local quotient are conditional calculations with the declared orientations [MATH]. The small local S^3 and smeared $S^2 \times S^1$ are separate Gaussian cycles. Source g, r, ψ, θ are dimensionless, separate from book g_s, α' and a physical circle radius. A localized angle-dependent source is outside this elementary isometric map, without

ruling out quantum duality.

Fivebrane charges and holomorphic curves. The NS5–D5 holomorphic-curve setup is an imported geometry-to-quiver construction in Franco et al. (2006, PDF p. 6, Sec. 1) [GEO-E]. Newton-edge and amoeba asymptotics are in Feng et al. (2005, PDF pp. 33, 37, Secs. 6.1.1 and 7.1). The explicit normals, balances and edge-root examples are conditional polynomial calculations [MATH]. The simple nonzero-root hypothesis is required for distinct elementary ends. Entry 7 fixes the outward $(D5, NS5)$ axes. No general-polygon classifier or full coamoeba/dimer equivalence is claimed.

Interfaces to six-dimensional theories and exercises. The NS5 tension is in Johnson (2000, PDF pp. 167–168, eqs. (396)–(397)) [SUGRA]; the D5 comparison uses the stated D5 tension. Coupling rescaling and charge counts are conditional arithmetic [MATH]. Worldvolume multiplets, little-string dynamics and generic BPS junction angles are assigned to later chapters. Exercises 1–4 consume the displayed conventions; Exercise 5 requests written interpretation.

References

Callan Jr., C. G., J. A. Harvey, and A. Strominger (1991). *Supersymmetric String Solitons*. arXiv: hep-th/9112030v1.

Feng, B. et al. (2005). "Dimer Models from Mirror Symmetry and Quivering Amoebae". In: *Advances in Theoretical and Mathematical Physics* 12, pp. 489–545. arXiv: hep-th/0511287v1.

Franco, S. et al. (2006). "Brane Dimers and Quiver Gauge Theories". In: *JHEP* 01, p. 096. arXiv: hep-th/0504110v2.

Johnson, C. V. (2000). *D-Brane Primer*. arXiv: hep-th/0007170v3.

Martinec, E. J., S. Massai, and D. Turton (2019). "Little Strings, Long Strings, and Fuzzballs". In: *JHEP* 11, p. 019. arXiv: 1906.11473v2.

Tong, D. (2002). "NS5-Branes, T-Duality and Worldsheet Instantons". In: *JHEP* 07, p. 013. arXiv: hep-th/0204186v3.